1.0   2.8   2.5

3.2   2.2

3.6

1.1   2.0

1.8

1.25   1.4   1.6

MICROCOPY RESOLUTION TEST CHART
NATIONAL BUREAU OF STANDARDS

RADC-TR-77-244
Final Technical Report
July 1977

CROSS POLARIZATION TECHNIQUES INVESTIGATION

Harris Corporation

DDC
AUG 24 1977
C

Appproved for public release; distribution unlimited.

**ROME AIR DEVELOPMENT CENTER
AIR FORCE SYSTEMS COMMAND
GRIFFISS AIR FORCE BASE, NEW YORK 13441**

Some of the tables in this report are not of the highest printing quality but because of economical consideration, it was determined in the best interest of the government that they be used in this publication.

This report has been reviewed by the RADC Information Office (OI) and is releasable to the National Technical Information Services (NTIS). At NTIS it will be releasable to the general public, including foreign nations.

This report has been reviewed and approved for publication.

APPROVED: *Brian M. Hendrickson*

BRIAN M. HENDRICKSON
Project Engineer

APPROVED: *Fred I. Diamond*

FRED I. DIAMOND
Technical Director
Communications & Control Division

FOR THE COMMANDER: *John P. Huss*

JOHN P. HUSS
Acting Chief, Plans Office

REPORT DOCUMENTATION PAGE		READ INSTRUCTIONS BEFORE COMPLETING FORM
1. REPORT NUMBER RADC-TR-77-244	2. GOVT ACCESSION NO.	3. RECIPIENT'S CATALOG NUMBER
4. TITLE (and Subtitle) CROSS POLARIZATION TECHNIQUES INVESTIGATION		5. TYPE OF REPORT & PERIOD COVERED Final Technical Report 29 Sep 75 - 21 Jan 77
		6. PERFORMING ORG. REPORT NUMBER N/A
7. AUTHOR(s) C. A. Baird G. Pelchat		8. CONTRACT OR GRANT NUMBER(s) F30602-76-C-0041
9. PERFORMING ORGANIZATION NAME AND ADDRESS Harris Corporation/Electronic Systems Divsion P. O. Box 37 Melbourne FL 32901		10. PROGRAM ELEMENT, PROJECT, TASK AREA & WORK UNIT NUMBERS 62702F 45192105
11. CONTROLLING OFFICE NAME AND ADDRESS Rome Air Development Center (DCCT) Griffiss AFB NY 13441		12. REPORT DATE July 1977
		13. NUMBER OF PAGES 262
14. MONITORING AGENCY NAME & ADDRESS(if different from Controlling Office) Same		15. SECURITY CLASS. (of this report) UNCLASSIFIED
		15a. DECLASSIFICATION/DOWNGRADING SCHEDULE N/A

16. DISTRIBUTION STATEMENT (of this Report)

Approved for public release; distribution unlimited.

17. DISTRIBUTION STATEMENT (of the abstract entered in Block 20, if different from Report)
Same

18. SUPPLEMENTARY NOTES
RADC Project Engineer:
Brian M. Hendrickson (DCCT)

19. KEY WORDS (Continue on reverse side if necessary and identify by block number)
Dual polarization - orthogonally polarized channels - frequency interference correction - rain effects - dither type gradient control loops - link margin - circular and linear polarization pairs - frequency reuse.

20. ABSTRACT (Continue on reverse side if necessary and identify by block number)

The crosspolarization techniques investigation program had as its major objective the investigation of the use of crosspolarization to expand the bandwidth efficiency over line-of-sight (LOS) digital microwave links in the Defense Communications System (DCS) and to develop techniques which would improve crosspolarization utility.

The program resulted in development of an adaptive interference reduction design suitable for use with LOS microwave links. The design provides the

DD FORM
1 JAN 73 **1473**   EDITION OF 1 NOV 65 IS OBSOLETE   UNCLASSIFIED

capability of doubling the bandwidth efficiency of LOS microwave links, without requiring additional power margin (over the 3 dB necessary to provide the orthogonal channel) to overcome the crosspolar interference. This design featured the development of a special multi-tap correction network which not only offered increased bandwidth capabilities, but also gave unique controllability characteristics and a useful mathematical relationship between the weight settings and the physical nature of the crosspolar interference. The design also included a performance monitoring device and a simple dither-type gradient control method. The practicality of the design was verified by both the mathematical analysis and detailed computer simulations.

Based on the mathematical analysis and the extensive computer programs developed on this study, it is reasonable to assume that the adaptive interference reduction network designed will perform adequately and it was recommended that feasibility demonstration hardware be developed.

CONTENTS

CONTENTS (Continued)

CONTENTS (Continued)

CONTENTS (Continued)

APPENDICES (Continued)

APPENDICES (Continued)

ILLUSTRATIONS

ILLUSTRATIONS (Continued)

ILLUSTRATIONS (Continued)

ILLUSTRATIONS (Continued)

ILLUSTRATIONS (Continued)

ILLUSTRATIONS (Continued)

ILLUSTRATIONS (Continued)

TABLES

EVALUATION

Current plans indicate a continued evolution of military communication systems from primarily analog equipment to digital equipment. Increased use of digital communications will result in a significant increase in conjestion, particularly in the microwave frequency bands. In order to alleviate this congestion, bandwidth efficient modulation techniques are required. Several approaches have been taken to improve bandwidth efficiency (See RADC Research and Technology Plan, TPO 4B). One approach involves the use of cross polarization wherein independent data can be transmitted at one carrier frequency on orthogonal polarizations (either linear horizontal and vertical or circular right hand, left hand) thus doubling the amount of data that can be communicated in a given bandwidth.

The use of cross polarization is not without its technical problems. Rain, turbulence, and multipath can severely affect the separation between polarizations, particularly over long microwave links. These effects limit the the use of cross polarization because of the high availability requirements for LOS microwave, Typically 99.995%.

By the use of adaptive algorithms effects caused by the media can be counteracted. This will result in cross polarized transmission with high availability. The purpose of this program was to study and develop adaptive algorithms. The algorithm developed on this program has the potential of reducing cross polarized interference levels as high as 5 dB below the co-polar signal to 40 dB below the co-polar signal virtually eliminating the interference. A hardware follow-on program will implement the algorithm developed and documented in this report.

BRIAN M. HENDRICKSON
Project Engineer

1.0 INTRODUCTION

1.1 Objective

The major objective of the cross polarization techniques investigation was to investigate the use of cross polarization to expand the bandwidth efficiency over line-of-sight (LOS) digital microwave links in the Defense Communications System (DCS) and to develop techniques that will improve the cross polarization utility.

Cross polarization offers an additional approach, other than improved bandwidth efficient modulation techniques, to double bandwidth efficiency by transmitting independent information on orthogonal polarized channels which use identical frequency bands.

1.2 Approach

The program contained four main phases. During the first phase, the problems associated with the use of cross polarization, particularly the mechanisms for and effects of crosspolar interference were thoroughly investigated. In this investigation, the effects of rain, multipath, circuit dispersion, etc., on crosspolar links were considered. Physical and statistical models of the interference effects were developed. The second phase of the program selected adaptively controlled correction networks as the most feasible. Various trade-offs associated with this approach were developed and a specific design formulated for two alternative adjustable correction networks. This phase of the program also included the detailed mathematical analyses of the specific design as well as derivation of the general performance estimates for crosspole systems.

Phase 3 of the program was an extensive computer simulation activity. The results of the previous phases were modeled on a computer to verify the soundness of the design as well as the practicality of implementation. The final phase of the program involved developing a conceptual design plan for eventual feasibility hardware which is capable of demonstrating the results of this program.

1.3   Results

The major accomplishment of the program was the development of an adaptive interference reduction design suitable for use over long multipath corrupted microwave links such as would be encountered in the DCS. This design provides the capability of doubling the bandwidth efficiency of the links within the DCS without requiring additional power margin (over the 3 dB necessary to provide the orthogonal channel) to overcome the crosspolar interference.

This design features a special multi-tap correction network having unique controllability characteristics as well as a useful mathematical relationship between the weight settings and the physical nature of the crosspolar interferences.

1.4   Report Organization

The report is organized consistent with overall program plan and approach as discussed in Paragraph 1.2 above. Section 2.0 presents the discussion of the cross polarization problems and the development of the physical and statistical models. The trade-offs associated with adaptively controlled correction networks as well as selection of a specific design are presented in Section 3.0. The detailed mathematical analyses of the design are also provided in Section 3.0. Section 4.0 presents the results of the computer

simulation along with descriptions of the computer programs as well as tabulations of some of the more important computer runs. A conceptual hardware design approach, along with supporting diagrams are presented in Section 5.0. The final section, Section 6.0 provides concluding comments and recommendations.

2.0   CROSSPOLARIZATION PHENOMENA AND THEIR EFFECTS

Frequency reuse via orthogonally polarized channels can double the bandwidth efficiency of a communication system. Such systems transmit two different data signals of the same bandwidth using the same carrier frequency by using orthogonal field polarizations for the transmission of each signal. (These two polarizations will be termed polarization 1 and 2 with P_1 and P_2 representing the respective power levels.) For ideal antennas and ideal transmission media, the 3 dB bit rate (i.e., bandwidth) increase is accomplished with a corresponding 3 dB increase in total transmitted power. However, since neither antennas nor the transmission media are ideal, an additional power increment is required in order to maintain the same quality of communications achieved in the nonfrequency reuse system (hereafter termed the basic link). For the ideal cross-polarized frequency reuse links (termed crosspole links) the two polarizations remain orthogonal throughout, that is, there is no coupling of polarization 1 (P_1) into polarization 2 (P_2). (Power coupled into P_1 from P_2 is termed P_{12}, with P_{21} being the other coupling.) For these links the crosspole isolation defined as P_1/P_{12} and P_2/P_{21} is infinite, or similarly the crosspole coupling defined as P_{12}/P_1 and P_{21}/P_2 is zero.

Nonideal antennas and transmission media will be manifested as finite crosspolar isolation, with the corresponding coupling increasing the interference power (decreasing the S/N ratio) in the separate channels. For the basic link, when the S/N ratio is degraded (e.g., rain-induced fading), the quality of communications is reduced. However, the quality can be restored by the use of additional transmitter power, so that

if fading is expected, increased power, termed <u>system margin</u>, can be introduced to negate its effect. For crosspole links, the additional S/N degradation due to crosspole coupling can also be compensated for by increased power margin. Alternatively, various forms of decoupling networks can be introduced into the system which will restore the polarization orthogonality. The use of such networks are discussed in the latter sections of this report.

Many of the phenomena which introduce fading and crosscoupling are statistical in nature (e.g., rain, multipath, etc.), consequently their effects on the system will have a certain probability associated with them. A wide variety of data is available in the literature on various aspects of these phenomena, and in the following paragraphs such data is discussed. Specifically, the <u>link availability</u>, defined as the probability that a link of a specified quality (given S/N ratio, BER, etc.), is available as a function of the system margin, will be developed. This will be done for both the basic and crosspole links, with the effects of carrier frequency (8 GHz versus 15 GHz) and type of polarization (circular versus linear) also being considered.

2.1 Contributions to Crosspolarization Coupling

The primary contributions to polarization coupling in terrestrial microwave communications systems are antenna depolarization effects and coupling in the channel due to precipitation and multipath. For most well designed systems, the predominant effect will be coupling due to rain. Consequently, this phenomenon has received the

5

most widespread study, including both theoretical consideration in terms of the development of rain cross-coupling models and various experimental studies investigating the statistical and physical properties of rain crosspolarization.

2.1.1   Rain Effects

The two significant effects that rain has on microwave transmission are attenuation and crosspolarization coupling. The former is important on all microwave links while the latter is of importance only on crosspolar links. The levels of both at an instant of time on a particular link are functions of path length through the rain, rain rate and operating frequency. In addition, the level of crosspolarization coupling due to the rain is also a function of the polarization pair (circular versus linear) that is employed.

2.1.1.1   Statistical Rain Model

In order to develop link availability a statistical rain model must be postulated. Since Western Europe is a geographical area of special interest to this study, rain data for Slough, United Kingdom has been taken to be representative. Figure 2.1.1-1 is a plot taken from Norberry and White[1] giving the total time occurrence of point rain fall rates at Slough during the year 1970. For example, referring to the figure, it can be noted that rain rates equal to or exceeding 80 millimeters per hour occur with a probability of 1 in 10^5, or approximately 5 minutes a year. This data is

[1] Norberry, J. R., and W. J. K. White, "Point Rainfall Rate Measurements at Slough, U.K.," IEEE Conference Publication Number 98.
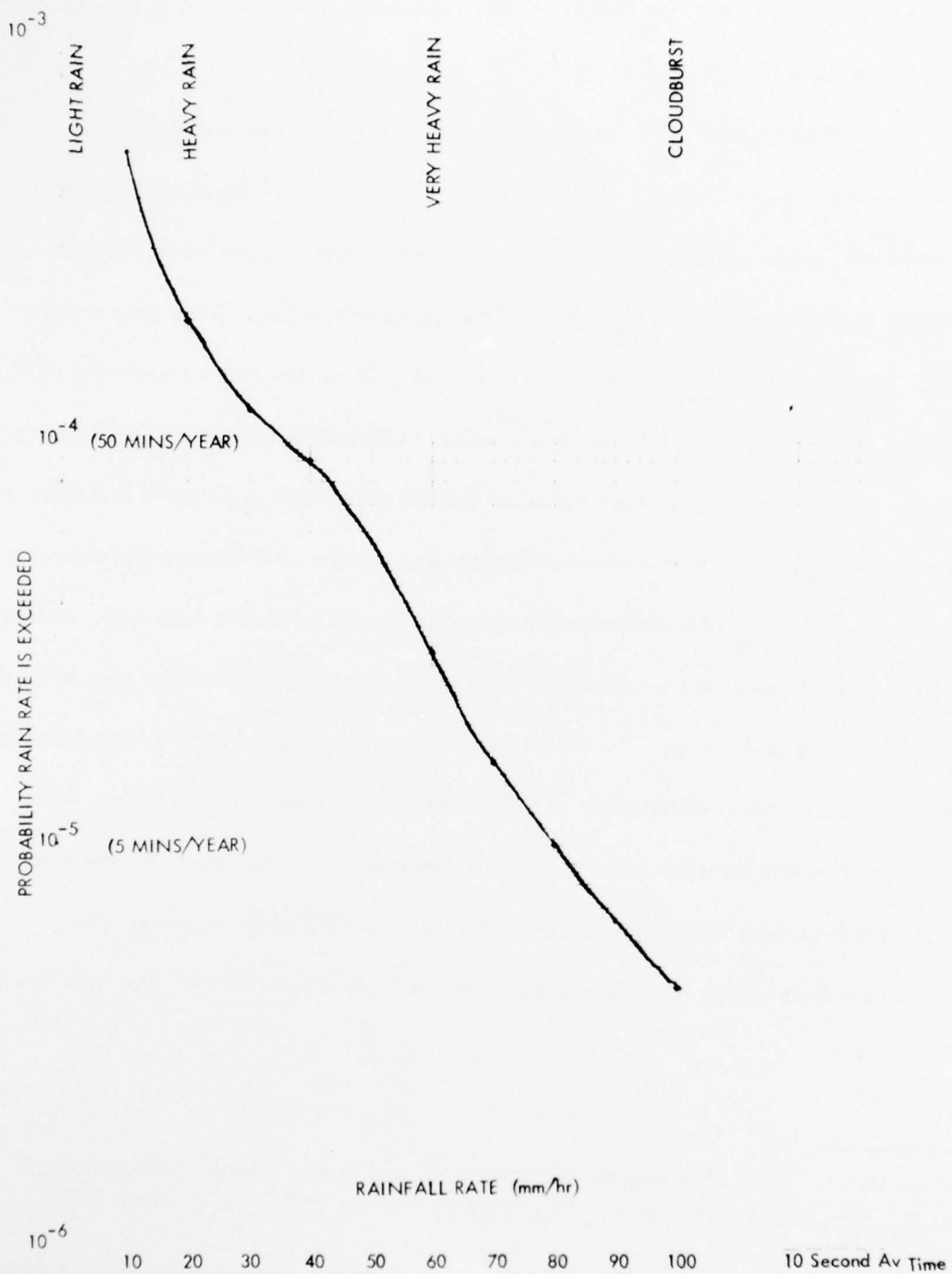
Figure 2.1.1-1   Point Rainfall Rate at Slough, United Kingdom Jan 70 - Dec 70

7

supported by data presented by Hogg[2] for rain rate measurements taken in Bedfordshire, England from July 1957 to August 1961.

Probabilities of point rain fall rates are insufficient for determining the desired availability prediction. What is required is the probability of path rain fall rates defined as the space average of the point rates along a path. Path rates, as such, are extremely difficult to observe (which explains the scarcity of published data on the topic). They must be inferred from point data and it is not obvious how rainfall statistics for a long path are related to those from a point. Obviously, point rates will not extend uniformly over a large area. Generally, it can be stated that point rates are related to path rates through such characteristics as storm size, shape, persistence and velocity of translation. In turn, these characteristics are intimately related to rain rate. Bussey[3] has made predictions based on empirical data of the relationship between path rainfall rates and point rainfall rates. He states that an annual distribution of 1 hour point rates approximates an annual distribution of instantaneous 50 kilometer path rates. This ergodic relationship between point and space averaged rain rates could be extrapolated to different time path length pairs, but in actuality is limited in its applicability to the specific data from which it was derived. A major limitation, assuming the hypothesis

---

[2] Hogg, D.C., "Path Diversity in Propagation of Millimeter Waves Through Rain," IEEE Transactions on Antennas and Propagation, Vol. AP-15, No. 3, May 1967, pp. 410-415.

[3] Bussey, H. E., "Microwave Attenuation Statistics Estimated from Rainfall and Water Vapor Statistics," Proceedings of the IRE, July 1950, pp. 781-785.

8

to be universally true (the supporting empirical data is derived from an extensive array of rain gauges covering a 90 mile diameter area in the Muskingum area of Ohio), is the limited availability of point rainfall data of the appropriate time intervals. However, Bussey's work does support the generally accepted principle that the greater the rain rate, the more concentrated the storm.

Using these ideas the following model for an approximate probability of path rainfall rates on a 16 km path can be postulated. The point rainfall rate probability is equivalent to the path rainfall rate probability for all rains of 25 mm per hour or less. For rain greater than 25 mm per hour, the path rain rate probability equals the point rain rate probability divided by the amount in mm/hour that the rain rate exceeds 25 mm per hour. Although this model was arbitrarily picked, it is representative of decreasing rain cell sizes with increasing rain rates as well as being consistent with limited data available from Norberry, White and Bussey. It is apparent that for one storm cell, as the path length increases, the probability for any specified average path rain rate decreases. Figure 2.1.1-2 is a plot of the resultant path rain rate probabilities for a 16 km path in Slough, United Kingdom.

2.1.1.2   Attenuation and Crosspolar Isolation

Having established a rain probability model, the effect of rain on both attenuation and cross coupling must be determined. Attenuation is considered initially.

9
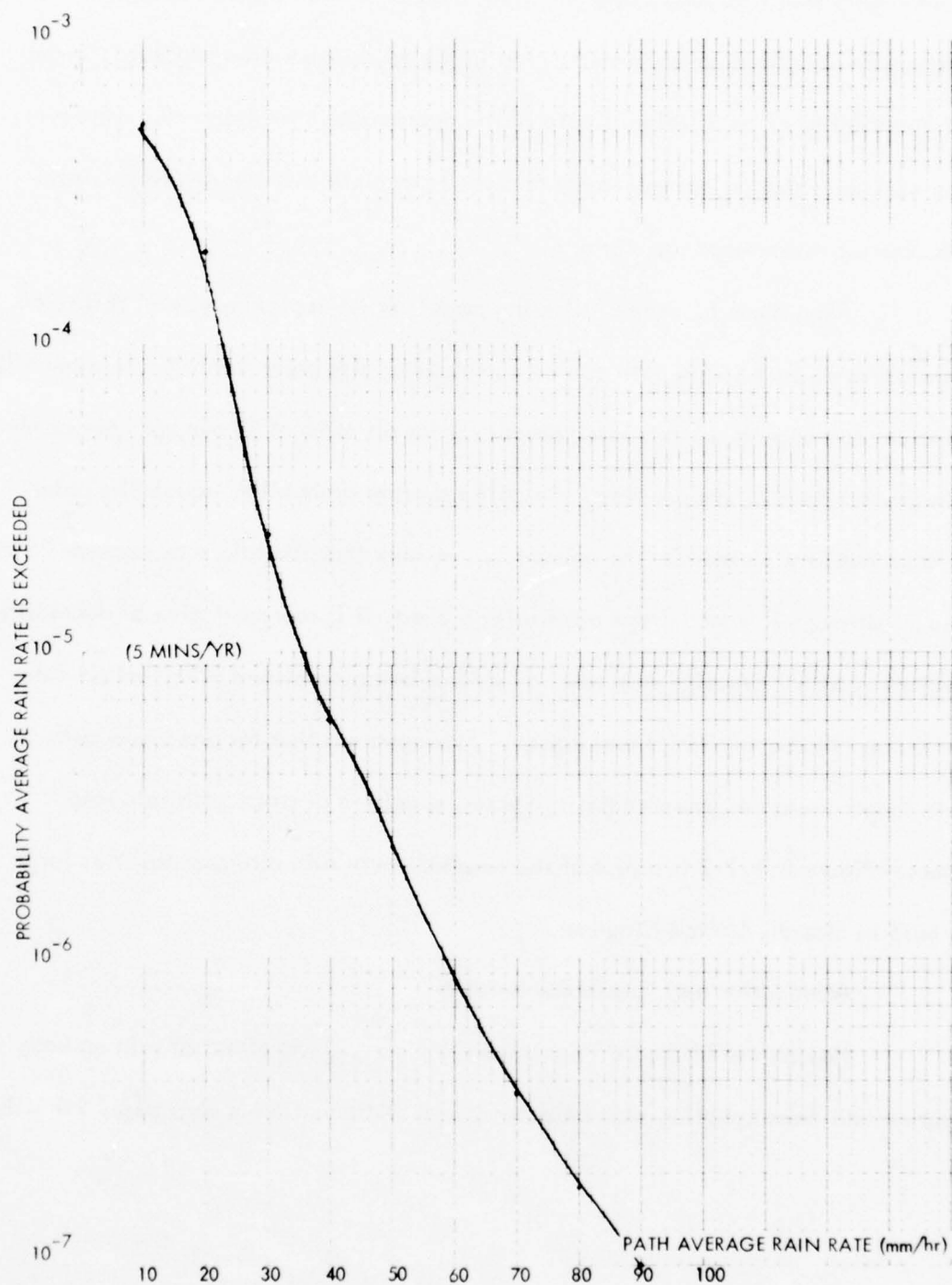
Figure 2.1.1-2   Estimated Rain Probability Over a 16 KM Path at Slough United Kingdom

Attenuation of microwaves by rain was considered in detail by Ryde and Ryde[4] in 1945, and the work was later confirmed and expanded by Medhurst.[5] Figure 2.1.1-3 presents graphs of path attenuation in dB's per kilometer versus rainfall rate in millimeters per hour as derived from the data of Medhurst. It is apparent from these curves that 15 GHz transmission suffers greater attenuation than 8 GHz. Furthermore, a doubling of path length through the rain will double the attenuation in dB's independent of frequency. The curves in Figure 2.1.1-3 have been experimentally supported by Blevis, et al.[6]

Crosspolarization coupling between spatially orthogonal channels has recently become a topic of much interest. This interest has been generated by a proliferation of systems proposing frequency reuse in efforts to conserve bandwidth. Since rain is a significant contributor to the level of cross coupling realized in microwave radio transmissions, it too has received recent interest. The coupling mechanism in rain is the differential phase shift and differential attenuation of electrical field components parallel and perpendicular to the main axis of oblate spheroidal raindrops. Figures 2.1.1-4 and 2.1.1-5 graph differential phase shift and differential attenuation versus rainfall rate for both 8 and 15 GHz transmissions. This data was taken from perturbation

_____

[4] Ryde, J. W., and D. Ryde, "Attenuation of Centimeter Waves by Rain, Hail, and Clouds," General Electric Co., Research Labs Report No. 8516, 8670, Wembley, England, August 1944, and May 1945.

[5] Medhurst, R. G., "Rainfall Attenuation of Centimeter Waves: Comparison of Theory and Measurements," IEEE Transactions on Antennas and Propagation, Vol. AP-13, No. 4, July 1965, pp. 550-564.

[6] Blevis, B. C., R. M. Dohoo, and K. S. McCormick, "Measurements of Rainfall Attenuation at 8 and 15 GHz," IEEE Transactions on Antennas and Propagation, Vol. AP-15, No. 3, May 1967, p 394.

11
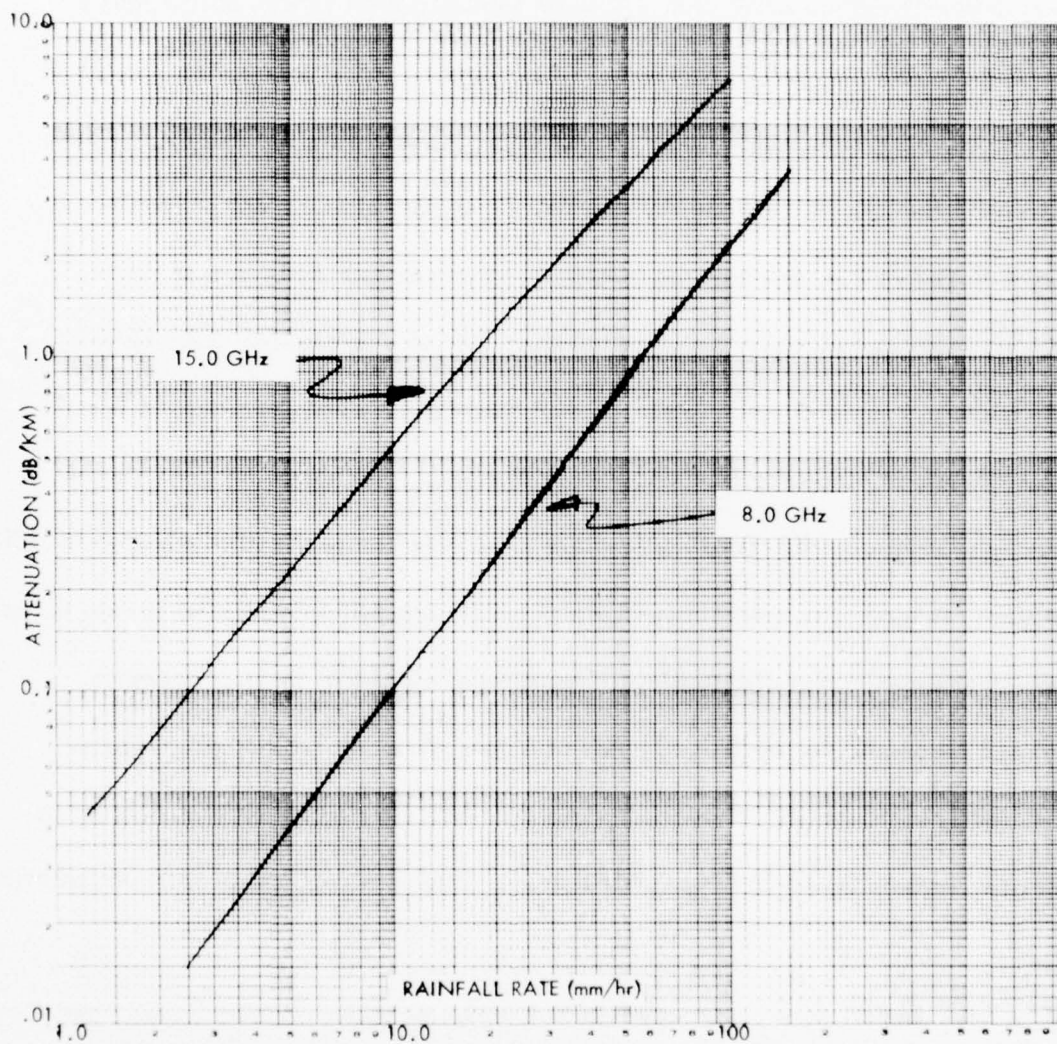
Figure 2.1.1-3. Attenuation by Rain

12
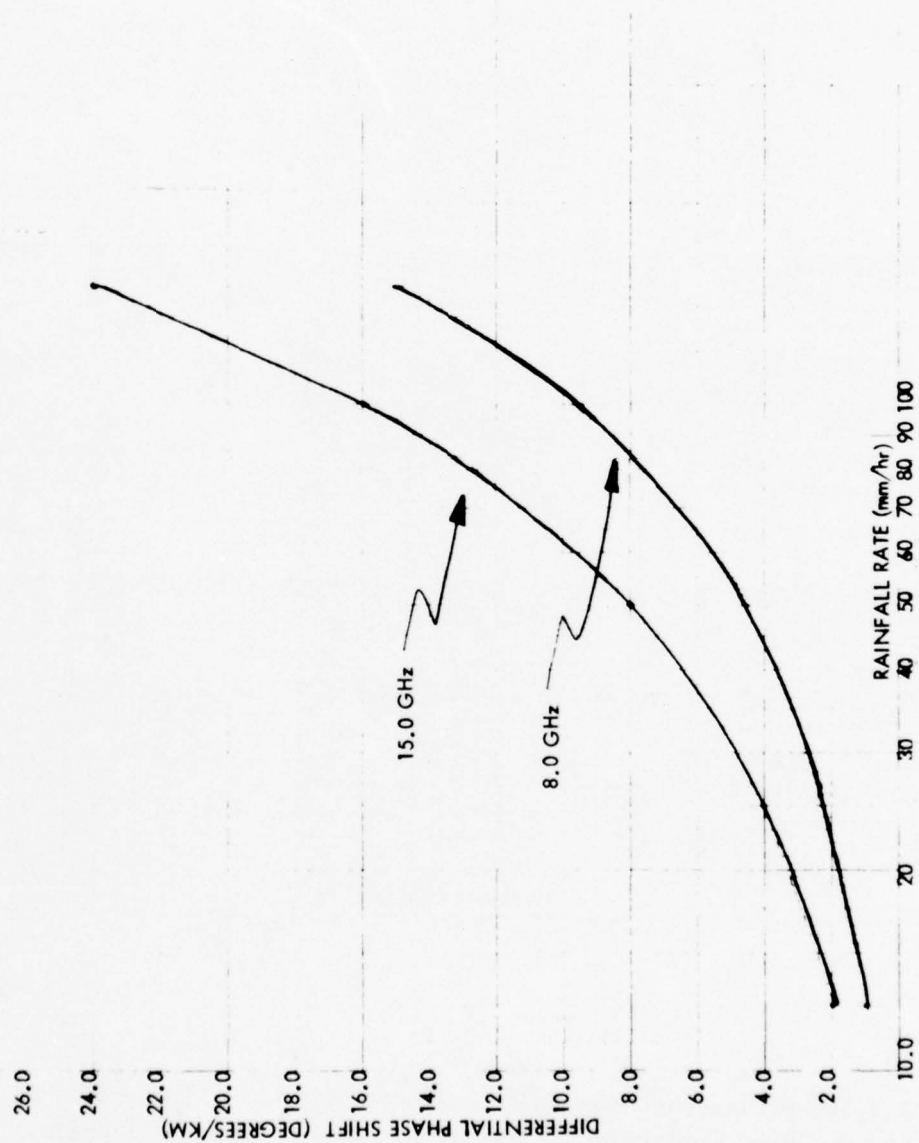
Figure 2.1.1-4 Differential Phase Shift In Planes
Parallel and Perpendicular to the Plane Containing the Axis of Symmetry of Oblate Raindrops
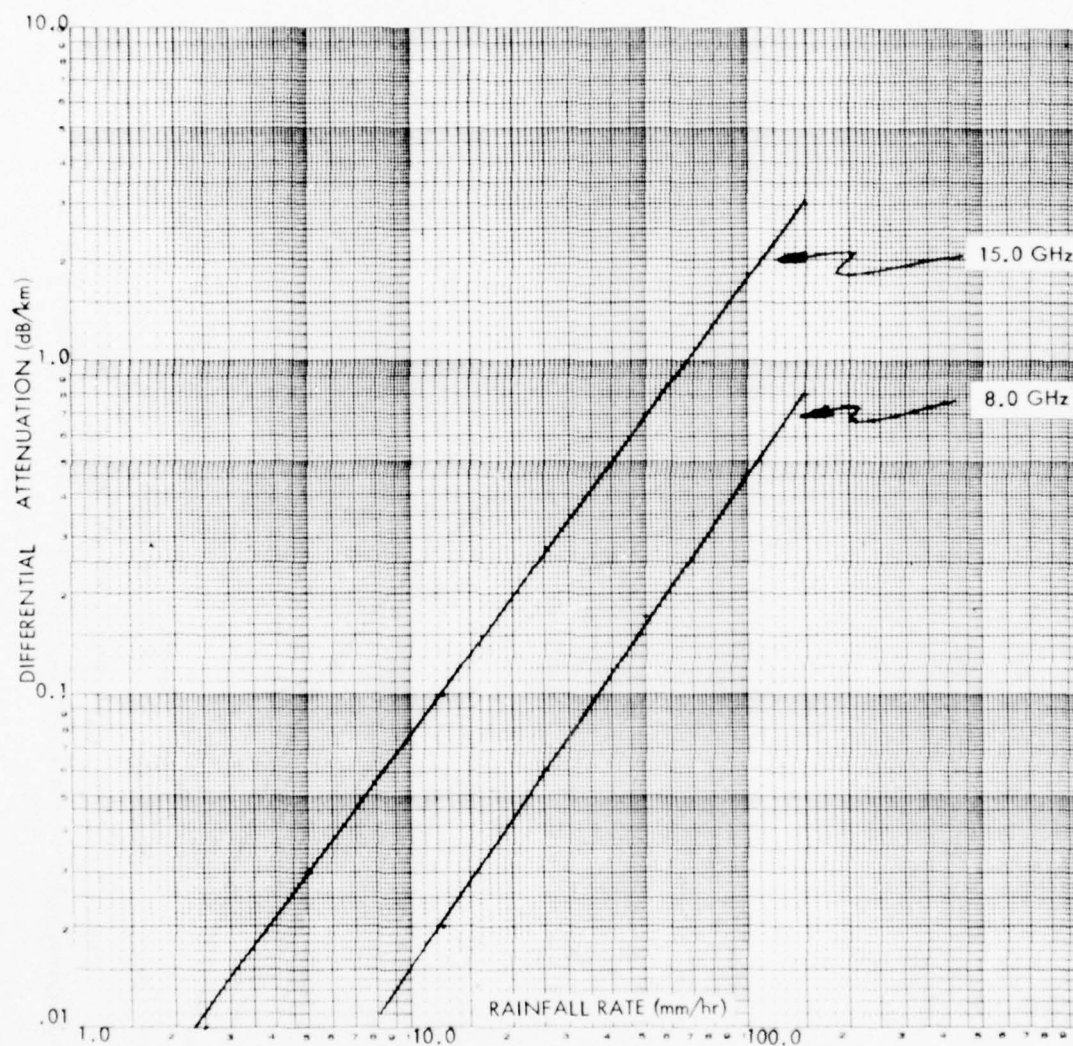
Figure 2.1.1-5 Differential Attenuation In Planes Parallel and Perpendicular to the Plane Containing the Axis of Symmetry of Oblate Raindrops

calculations done by Morrison and Chu.[7] As can be noted in these figures; both differential attenuation and differential phase shift depend strongly on frequency.

The differential attenuation and phase can be related to crosspolarization coupling via different expressions depending on the orthogonal polarization pair being used. For a circularly polarized system, the coupling C_c is given by

$$C_c = 20 \log \left| \frac{1 - e^{-\ell(\alpha + i\beta)}}{1 + e^{-\ell(\alpha + i\beta)}} \right| \qquad (2-1)$$

where α and β are the differential attenuation and differential phase shift per unit length as taken from Figures 2.1.1-4 and 2.1.1-5; and ℓ is the path length. If, on the other hand, the link employs linear polarization, an additional parameter, the raindrop canting angle, impacts crosspolarization coupling. The canting angle is the angle between the major axis of the image of an oblate spheroidal raindrop projected on the plane normal to the direction of propagation with respect to the horizontal. If the canting angle is denoted by θ, the crosspolarization coupling C_L is given by

$$C_L = 20 \log \left| \frac{1 - e^{-\ell(\alpha + i\beta)} \tan \theta}{1 + e^{-\ell(\alpha + i\beta)} \tan^2 \theta} \right| \qquad (2-2)$$

Examining the expressions for crosspolar coupling, it is apparent that the isolation between orthogonal circularly polarized waves will always be poorer than

---

[7] Morrison, J. A., and T. S. Chu, "Perturbation Calculations of Rain-Induced Differential Attenuation and Phase Shift at Microwave Frequencies," BSTJ, Vol. 52, No. 10, Dec. 1973, pp. 1907-1913.

between orthogonal linearly polarized waves, the only exception being for a 45° canting angle for which the two expressions are identical. In reality, there is no one canting angle for any particular rain, rather, there is a canting angle distribution. It is this distribution which determines the degree to which linear polarization isolation is superior to circular polarization isolation. It has been reported in the literature[8] that insufficient measurements of the distribution of raindrop canting angles are at present available to make precise predictions of the advantages of linear polarization. However, published estimates[9] which are supported by experimentation at particular frequencies suggest an approximately 10 dB improvement in isolation. Figures 2.1.1-6 and 2.1.1-7 incorporate this estimate in plots of crosspolar isolation versus rain rate for a 16 km link with operating frequencies of 8 and 15 GHz, respectively.

2.1.2   Nonrain-Induced Coupling

In addition to the rain induced crosspolar coupling discussed in the last section, coupling can result from various nonrain related fades and depolarization by the antennas. Relative to the rain related effects, much less work has been done on the effects of nonrain-induced fades on crosspolar coupling, and there is consequently less

[8]Watson, P. A., and M. Arbabi, "Rainfall Crosspolarization of Linearly and Circularly Polarized Waves at Microwave Frequencies," Electronic Letters, Vol. 8, No. 11, 1 June 1972, pp. 283-285.

[9]Semplak, R. A., "Simultaneous Measurements of Depolarization by Rain Using and Circular Polarizations at 18 GHz," BSTJ, Vol. 53, No. 2, Feb. 1974, pp. 400-404.
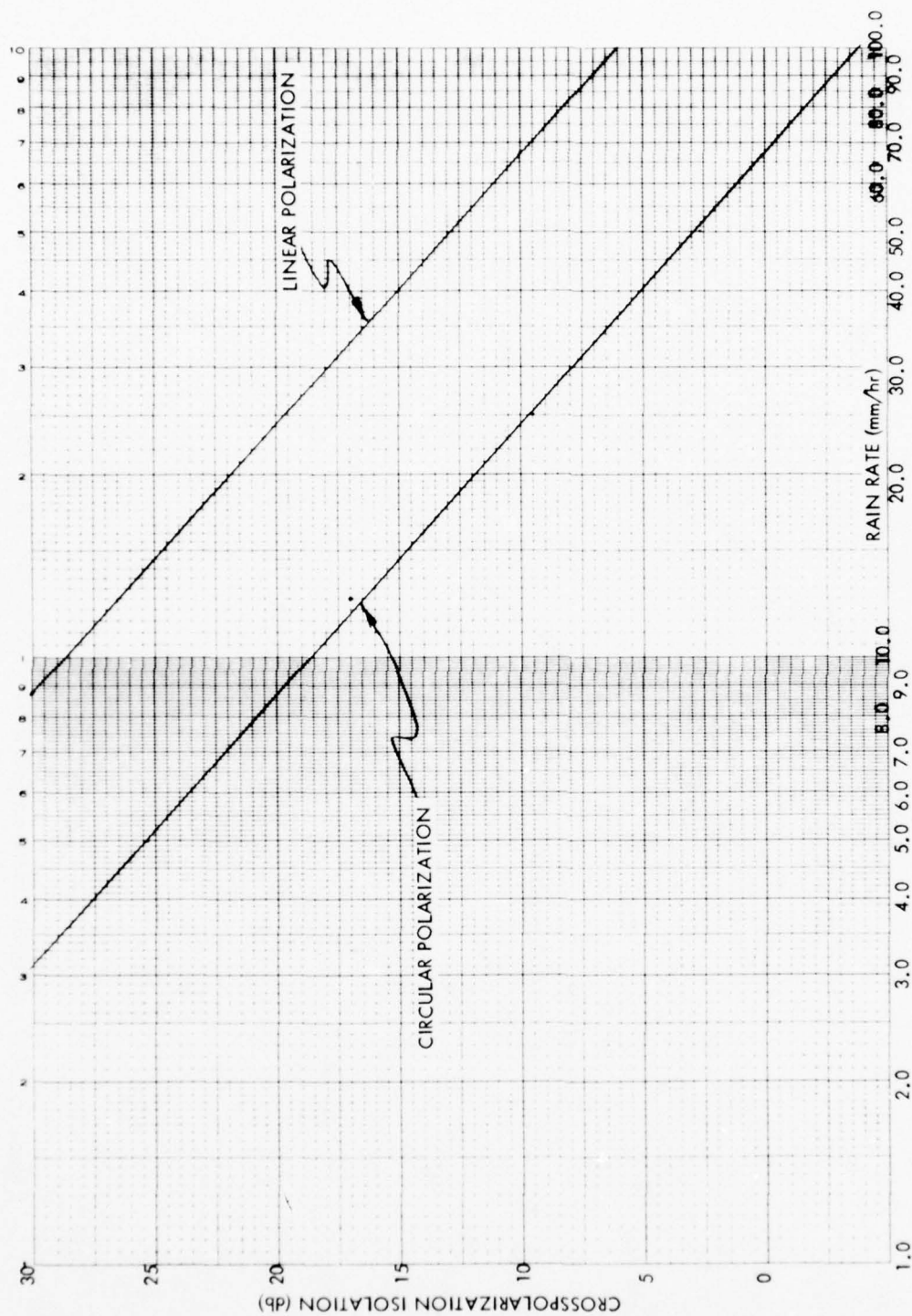
Figure 2.1.1-6   Crosspolarization Isolation Vs Rain Rate For an 8.0 GHz 16.0 KM Link

17
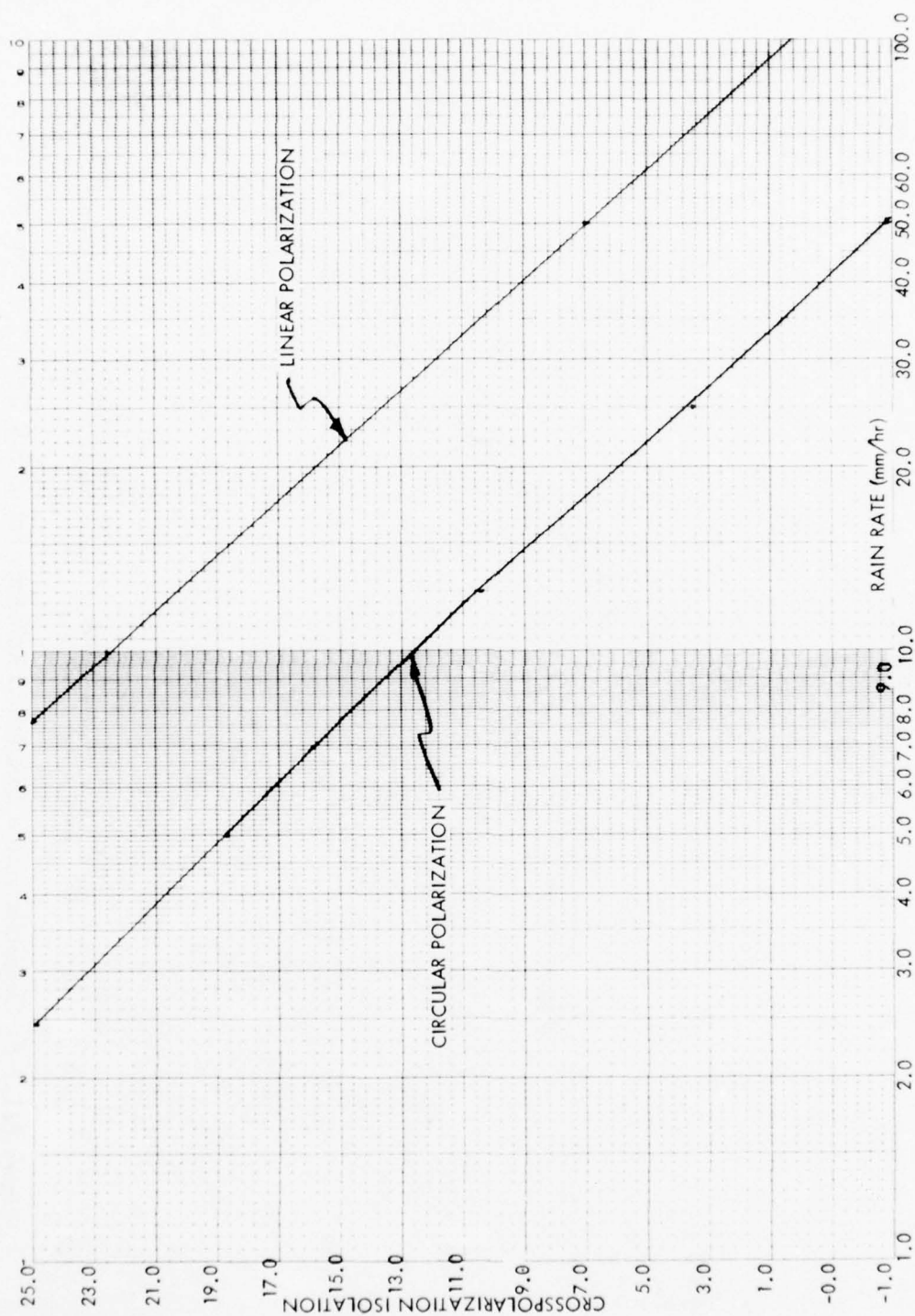
Figure 2.1.1-7   Crosspolarization Isolation Vs Rain Rate For a 15.0 GHz 16 KM Link

18

data available. Even so, some general conclusions can be discussed, particularly since

it is known that some of these effects can be polarization dependent and will therefore

introduce crosspolar coupling. For the antenna effects, crosspolar coupling is directly

introduced due to nonperfect isolation in the antenna and feed network as illustrated in

Figure 2.1.2-1a. As this isolation generally decreases at off-axis angles of arrival,

the antenna can have a secondary effect via the increased decoupling of multipath

signals which will arrive off axis.

Nonrain-induced fading is primarily a multipath phenomena and can

result from either diffraction, refraction, or reflection. Diffraction is caused by

obstructions in the path, refraction by variations in the atmospheric density, and

reflection from the radio waves striking reflecting surfaces. As reported by Barnett,[11]

multipath fades will directly introduce crosspolar coupling by the differential fading of

orthogonally polarized signals, often resulting in significant loss of crosspolar isolation.

Referring to Figure 2.1.2-1b this effect is illustrated by P_1 fading more than P_{12}. Also,

refraction can cause signals to arrive off-axis at the antenna, resulting in reduced

crosspole isolation as mentioned above.

A final mechanism for crosspolar coupling during fades results from

polarization selective fading and the resulting amplification of the depolarization in the

nonperfect antenna. Again referring to Figure 2.1.2-1a, if P_1 remains steady as P_2

---

[11] Barnett, W. T, "Deterioration of Crosspolarization Discrimination During Rain and Multipath Fading at 4 GHz," Proceedings ICC, 1974, pp. 12D-1 to 12D-4.
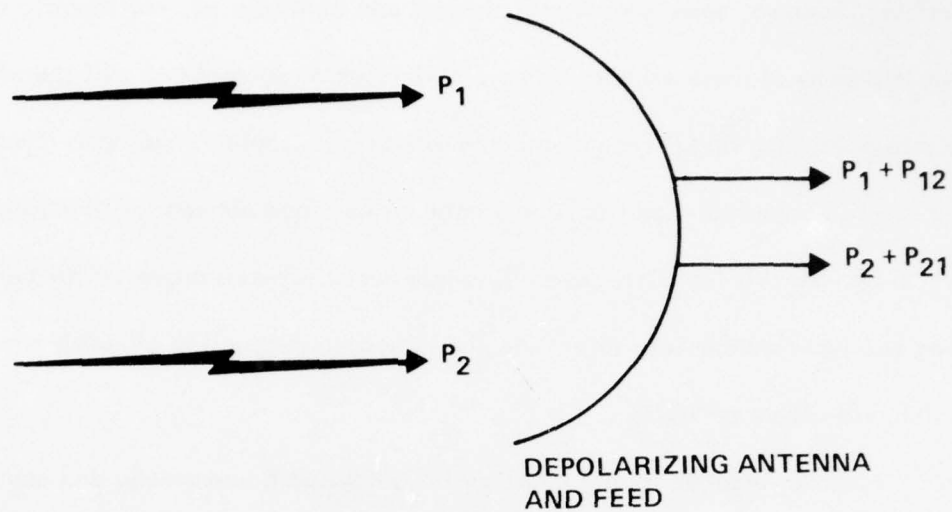
a. ANTENNA RELATED CROSSPOLAR COUPLING
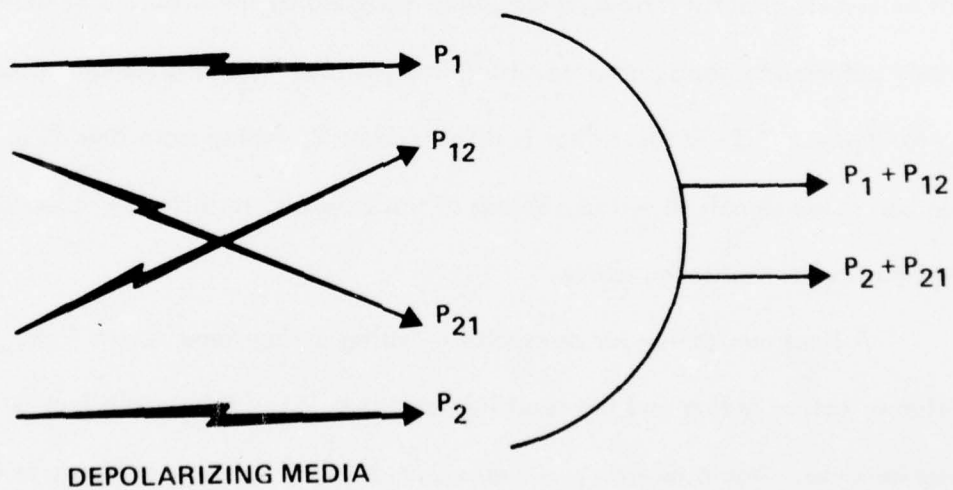
b. PATH RELATED CROSSPOLAR COUPLING

89631–19

Figure 2.1.2-1 Crosspolar Coupling in the Antenna and the Media

20

fades, then since P_{21} is also steady, P_2/P_{21} is degraded. This is said not to occur by Barnett; however, certain types of reflections are said to be polarization selective, and in fact, it is recommended that vertical polarization can be advantageous. On the other hand, the effect is most likely small, since polarization diversity is not really a widely accepted technique.

Quantitative evaluation of these nonrain-induced effects are quite dependent on the specific characteristics of individual links. However, a well designed link can avoid much of the adverse effects (e.g., good antennas, plenty of clearance from obstructions, etc.). Also, heavy rain will tend to reduce temperature variations in the atmosphere which can cause some of the multipath fades. Consequently, these effects will not generally be cumulative with respect to the rain induced crosspolar coupling. Also, it appears from the limited work available that these effects are of roughly the same order of magnitude as the coupling due to rain, indicating that a link designed to effectively combat rain will also perform satisfactorily against the nonrain-induced effects. However, such conclusions should be carefully examined in application to specific links.

2.2 Performance Degradation Due to Crosspolarization Coupling

The primary impact of crosspolar coupling on a dual polarization communications system will be a reduction in the received signal-to-interference ratio. To bound this effect for QPSK modulation, consider the phasor diagram shown in

21

Figure 2.2-1 where the four phase states are shown as vectors of magnitude A_s. The worst-case interference will correspond to a noise vector acting along a line between two adjacent phase states as shown by A_n. This corresponds to a case where the two channels have coincident symbol timing and carrier phases offset by 45°. As shown, the signal amplitude A_s is reduced to the effective signal amplitude $A_e = A_s - \sqrt{2} A_n$ which gives the worst-case degradation as $A_e / A_s = 1 - \sqrt{2} A_n / A_s$. This relates the crosspolar coupling A_n^2 / A_s^2 to the signal-to-noise degradation (or required margin to compensate for the crosspolar coupling) as shown in Figure 2.2-2.
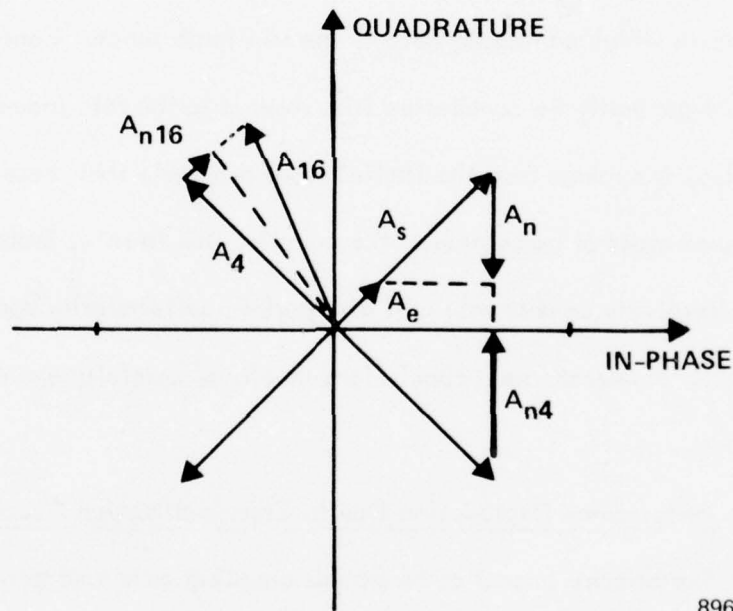
89631—14

Figure 2.2-1.   Illustration of Interference Effects for QPSK Signaling

22
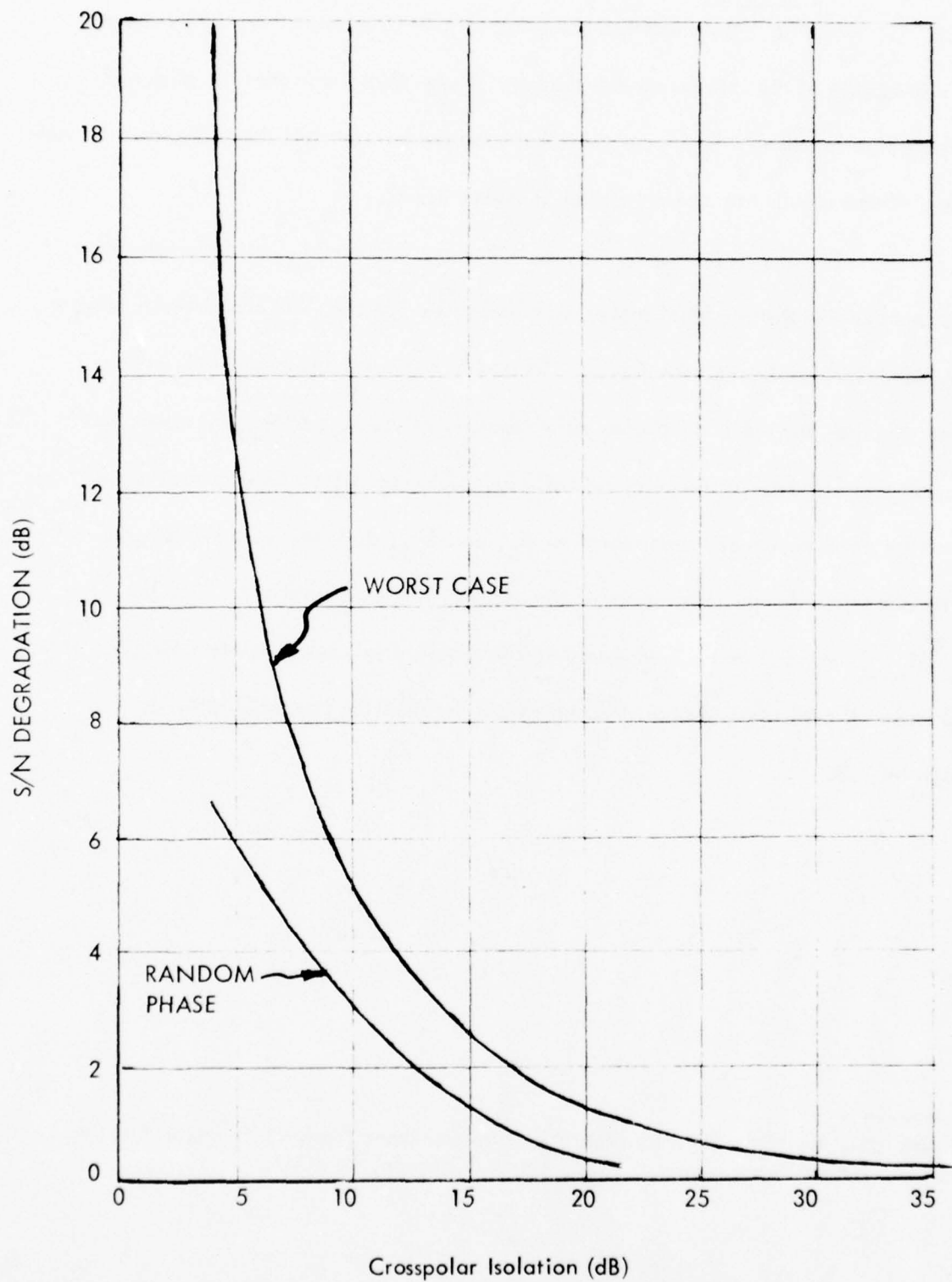
Figure 2.2-2.   Effect of Crosspolar Coupling On
Received S/N For QPSK Signaling

23

Prabhu[10] has presented the effect of CW interference on QPSK signals where the phase of the interference is random. These results describe the effect of crosspole interference with random phase between the two carriers and coincident symbol timing. These results are also presented in Figure 2.2-2.

The phasor diagram of Figure 2.2-1 can also be used to determine the increased system margin (signal power) required to double the system bandwidth using a more bandwidth-efficient modulation. To double the available bandwidth in this manner requires the use of 16 phases rather than 4, where A_4 and A_{16} represent two adjacent phase states for the 16 phase technique. Noise vectors having equivalent effects for each system are represented as A_{n4} and A_{n16} and their relative lengths will be the effective change in noise level when going from 4 to 16 phase. That is, $A_{n4}^2/A_{n16}^2 = 13.1$ or 11.2 dB would be the required increase in system margin. This information is presented, along with the margin required for crosspole links, in Paragraph 2.3.

---

[10] Prabhu, V. K. "Error Rate Considerations for Coherent Phase-Shift Keyed Systems with Co-Channel Interference," BSTJ, March 1969, pp. 743-767.

2.3 Link Margin and Availability

From the statistical rain models of Paragraph 2.1 and the analysis of the effect of crosspolar coupling in Paragraph 2.2, the required system gain margins and link availability for a given link can be calculated. These calculations can be performed for both frequency reuse and nonfrequency reuse links, thereby giving a quantitative comparison of the cost of doubling the bandwidth using a dual polarization system. For a given rain rate, Figure 2.1.1-3 gives the attenuation in dB's per kilometer, from which the required system margins for a 16-km link can be obtained. The cross polarization isolation associated with the given rain rate can also be obtained from Figures 2.1.1-6 and 2.1.1-7. Consequently, the crosspolar isolation that a dual polarized system would exhibit can be plotted versus the system margin that would be required by the basic link. This data is shown in Figures 2.3-1 and 2.3-2 and will be useful in constructing the comparisons to follow.

Another useful set of relationships can be derived using the probability of rain rate data of Figure 2.1.1-2 and the crosspolar isolation versus rain rate curves of Figures 2.1.1-6 and 2.1.1-7. Using these curves the probability of occurrence of a particular crosspolar isolation on the 16-km links can be obtained. These results are shown in Figure 2.3-3 for both 8- and 15-GHz links using linearly and circularly polarized transmissions. These curves indicate that the probability of occurrence of a given crosspolar isolation for a 15-GHz transmission is substantially higher than for an

25
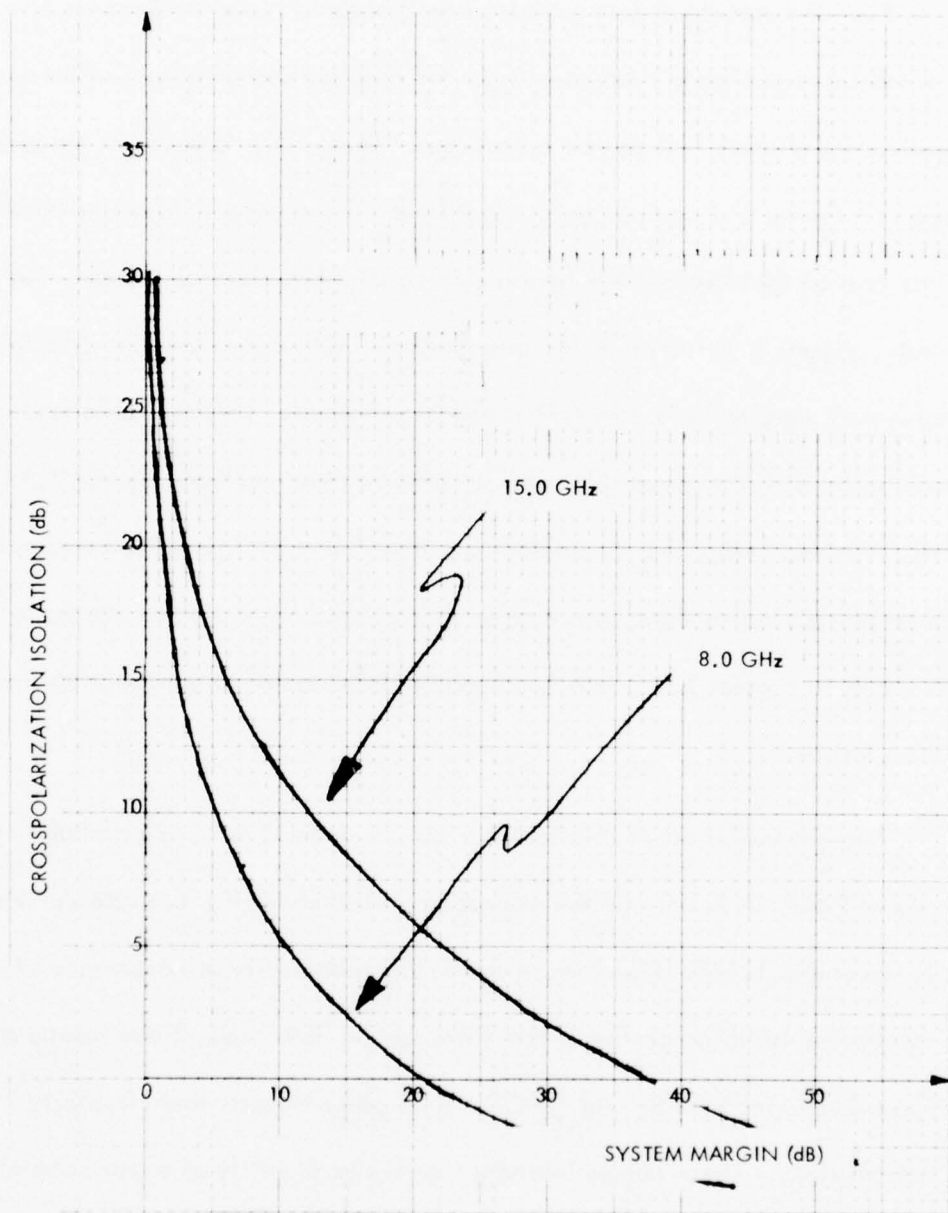
Figure 2.3-1   Crosspolarization Isolation Vs Required System Margin
For Circularly Polarized Transmission on a 16.0 KM Path With Varying Rain Rates
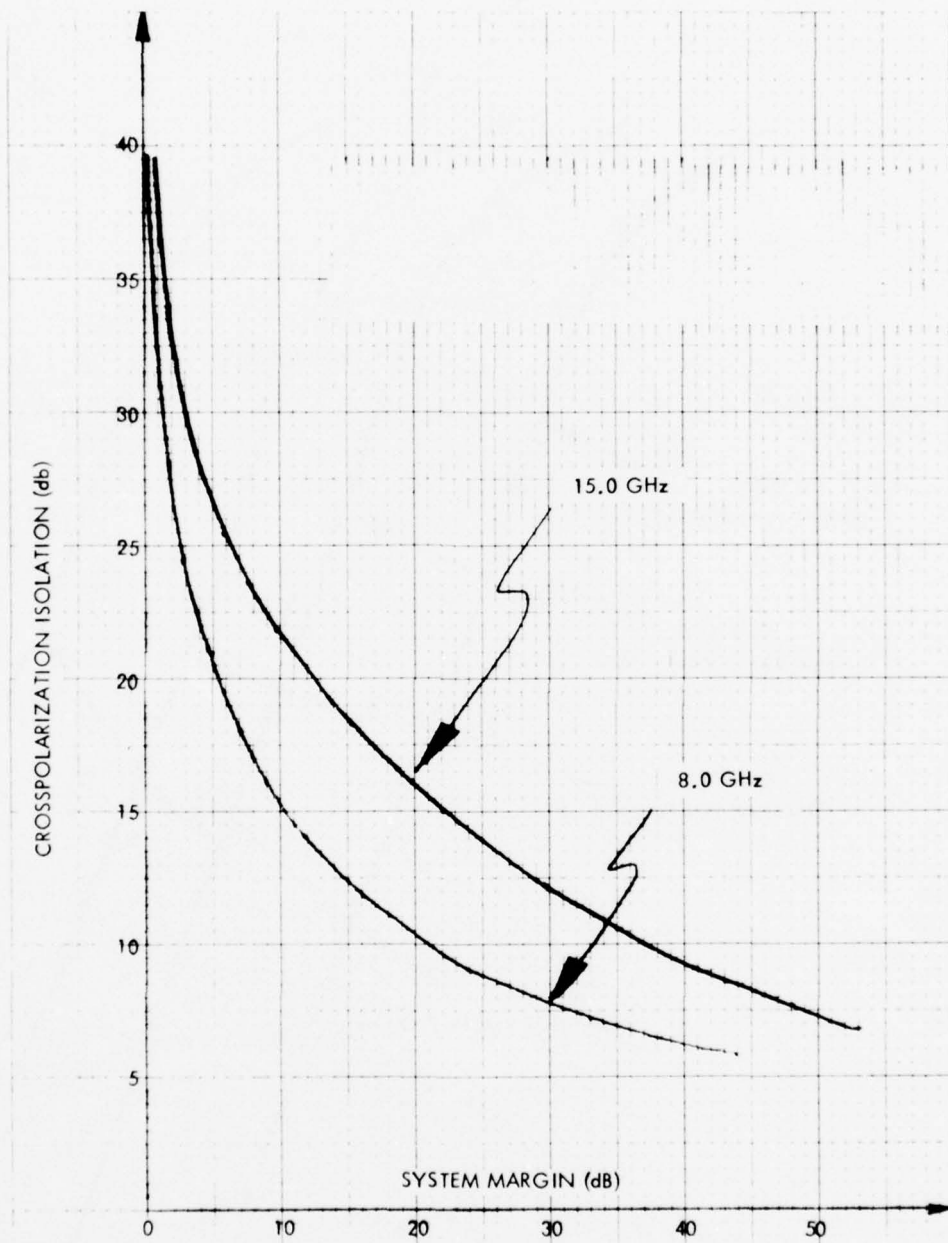
Figure 2.3-2   Crosspolarization Isolation Vs Required System Margin
For Linearly Polarized Transmission on a 16.0 KM Path With Varying Rain Rates

27

10^{-3}

10^{-4}

10 db

10 db

8.0 GHz
LINEAR POLARIZATION

15.0 GHz
LINEAR POLARIZATION

PROBABILITY COUPLING IS ATTAINED

10^{-5}

8.0 GHz
CIRCULAR POLARIZATION

10^{-6}

15.0 GHz
CIRCULAR POLARIZATION

10^{-7}

CROSSPOLARIZATION COUPLING (db)

-35   -30   -25   -20   -15   -10   -5   0
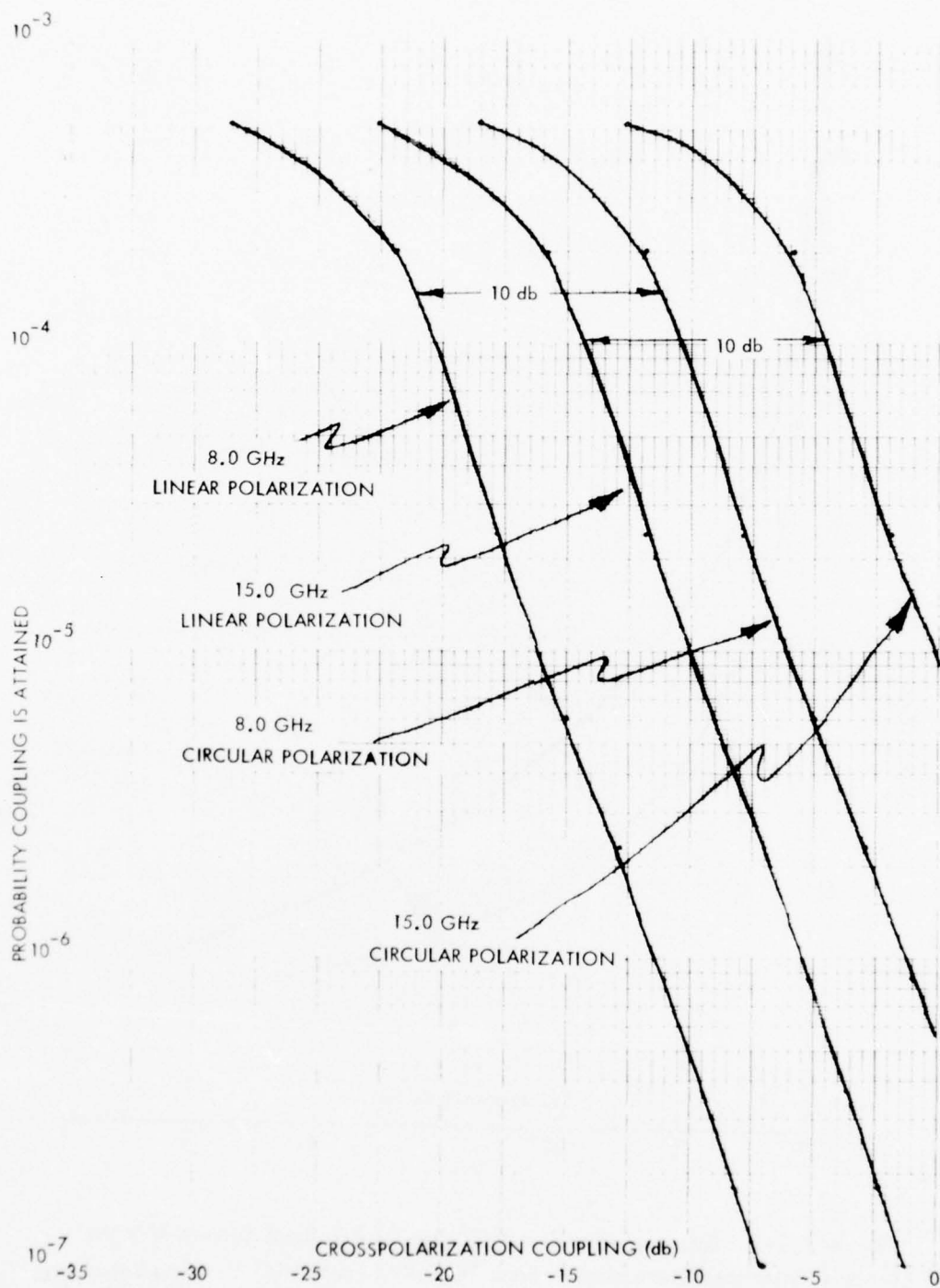
Figure 2 .3-3 Probability of Cross Coupling On A 16.0 KM Link

8 GHz transmission. Also, the assumed 10 dB differential between circular and linear polarizations are apparent in the plots.

Using the plots presented in this section, and Figure 2.2-2 giving the effect of crosspolar interference, link availability predictions based on the system rain margins can be graphed. Using the worst-case interference model of Paragraph 2.2 these plots are presented in Figures 2.3-4 and 2.3-5 for 15 GHz and 8 GHz links, respectively. In each case, the curves are for a 16-km link. The four curves on each figure are: a) the basic link where frequency reuse is not employed and the system margin must compensate for direct attenuation only; b) crosspolar links employing dual linearly polarized waves; c) crosspolar links employing dual circularly polarized waves; and d) links where bandwidth is doubled using 16 rather than 4-phase modulation. These curves indicate the reduction in availability for a fixed link margin (and similarly, the increased system margin required for a fixed availability) resulting from frequency reuse links and nonfrequency reuse links. Note that the use of a polarization correction technique will reduce the cross polarization coupling, effectively moving the dual polarization curves on each figure toward the lower one. It is worth reiterating that the predictions presented in Figures 2.3-4 and 2.3-5 are for the specific 16-km link. It is apparent as longer links are considered, the family of curves on each figure must rise indicating an increased probability of a given amount of rain on the link. As mentioned above, due to the limited amount of path rain data available in the literature, quantitative estimates of such increases are difficult.

29
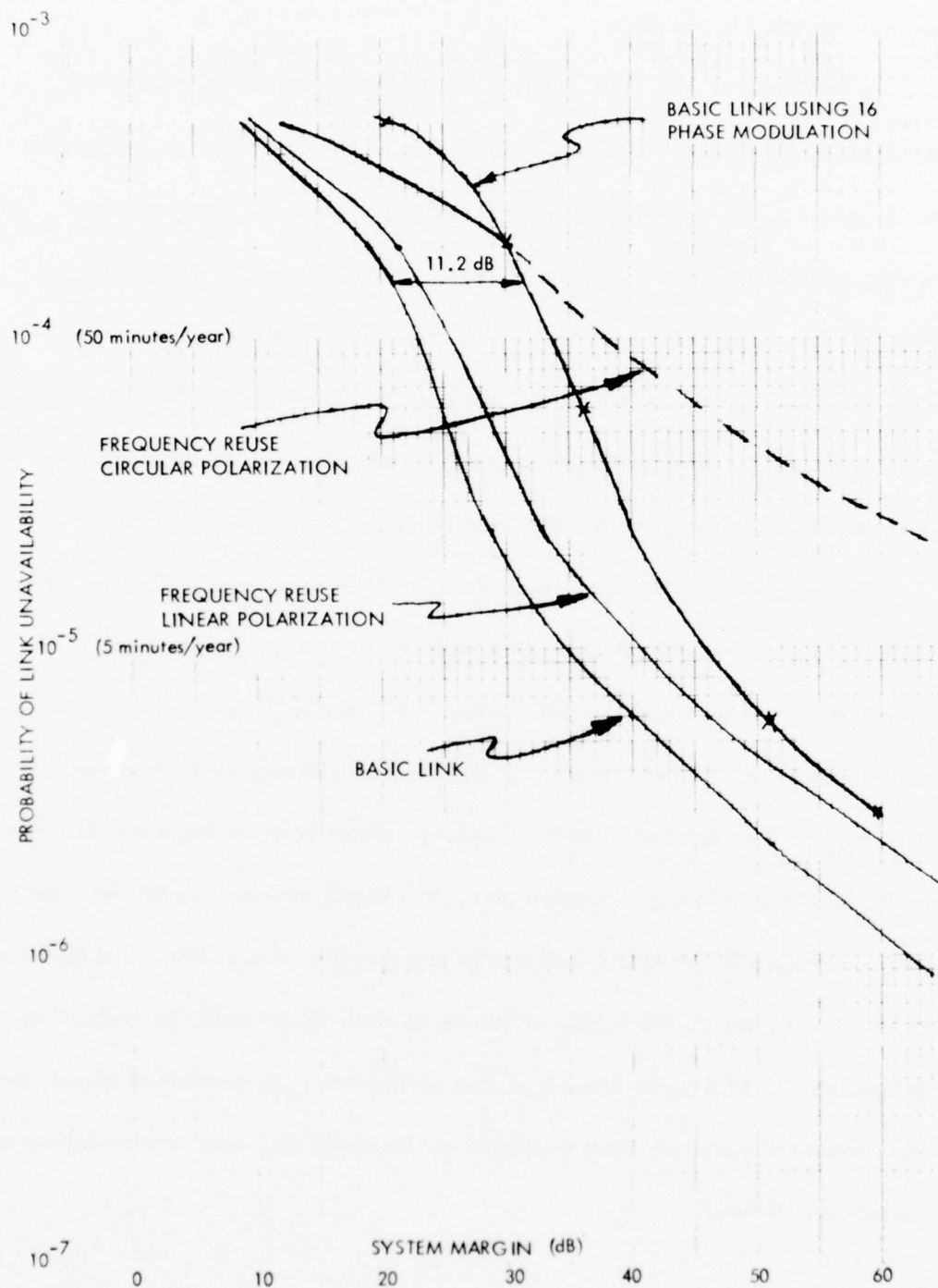
Figure 2.3-4 15.0 GHz Link Availability Vs System Margin

30
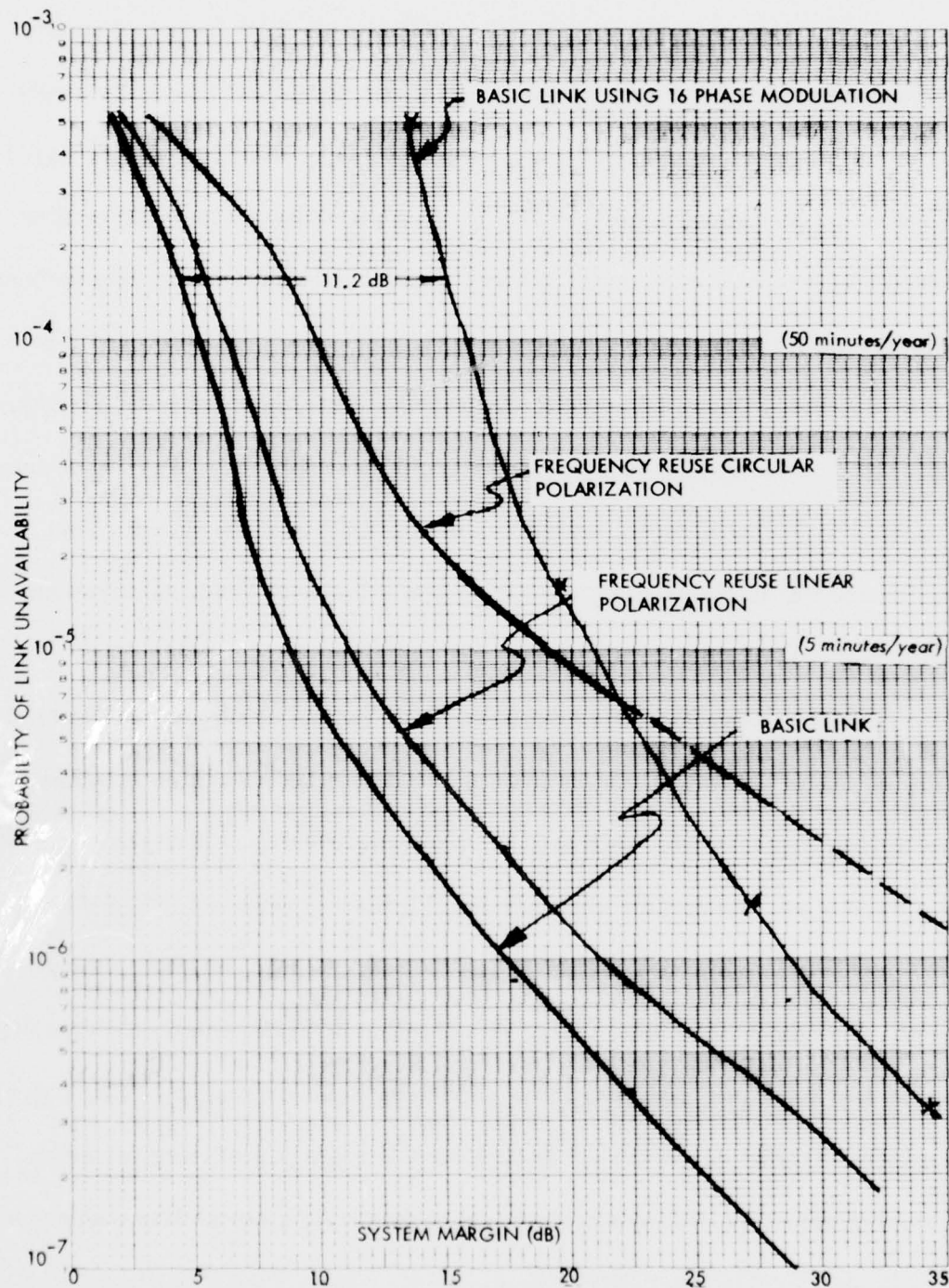
Figure 2.3-5   8.0 GHz Link Availability Vs System Margin

31

2.4   Discussion

In the preceding sections the link availability for both basic and cross-polar communication links have been developed for a specific 16-km link. To develop this data certain assumptions, such as the relationship between point and path averaged rainfall rates, were required. Consequently, this data should not be regarded as absolutely accurate or generally extendable. More important than the specific data derived is the technique developed. Using this technique more accurate predictions could be made in specific cases if the required data is available. By using such results the cost, in terms of increased margin, of frequency reuse could be established. Whether or not this cost is worth paying will depend on the required reliability of the specific links. A more definite result of this work is the conclusion that orthogonal linear polarizations are better suited for dual polarization systems than are circular polarizations.

An alternative to increased system margin for maintaining a specified link availability in crosspolar links would be the use of polarization correction networks. Fixed depolarization phenomena, such as certain antenna effects, could be compensated for by using a fixed correction network configuration. However, since the rain and multipath effects are functions of time, the correction networks must be adjusted as these effects vary. This suggests the use of adaptive correction networks which automatically sense the induced crosspolar coupling and adjust the networks accordingly. The cost of these adaptive correction networks must be compared with the cost of using increased system margin or any other available alternatives to determine their relative advantage.

The design of these correction networks will be discussed in the following sections. In addition to these considerations, the indirect cost of losing the ability to use crosspole isolation to separate adjacent channels must also be considered. Finally, an alternative to the above methods would be the use of path diversity, which in certain systems would be readily available. The utility of this technique is indicated by the fact that the more severe the rain (and therefore, crosspolar coupling), the more concentrated it is, and therefore the more likely a separate link would not be degraded. However, such considerations must be made relative to a specific system design.

3.0 DESIGN CONSIDERATIONS FOR ADAPTIVE INTERFERENCE REDUCTION

If crosspolar links are to be employed, additional link margin is required for each crosspole channel to perform on a par (maintain same availability) with a single polarization (basic) link. This is necessitated by the additional interference introduced by crosspole coupling. This interference, and the need for additional power margin, can be avoided by the use of adaptive interference reduction circuits. Alternative techniques such as path diversity or more efficient modulation schemes can also be utilized; however, the use of adaptive correction networks appears to be a promising approach. In order to make a meaningful assessment of the relative costs and complexities of the alternative methods, a detailed understanding of how they are designed is required. This section discusses the trade-offs involved in designing the adaptive correction circuitry and selects a particular technique which appears most suitable for the problem being addressed. An analysis of the performance of the selected method is presented, giving a further feeling for its cost and practicality.

3.1 Design Trade-Offs

As illustrated in Figure 3.1-1, an adaptive crosspole interference correction network consists of three basic components: the adjustable correction network, the performance measurement device, and the controller. .Associated with each of these components are a number of design considerations and trade-offs which are discussed in this section. (Also, see Appendix C.) These discussions will lead to a selected approach, the details of which are discussed in the remaining sections of this report.

34

$P_1' = P_1 + \epsilon P_{12}$

$P_2' = P_2 + \epsilon P_{21}$

ADJUSTABLE CORRECTION NETWORK

TO DEMODS

CONTROLLER

PERFORMANCE MEASUREMENT DEVICE

89631–13
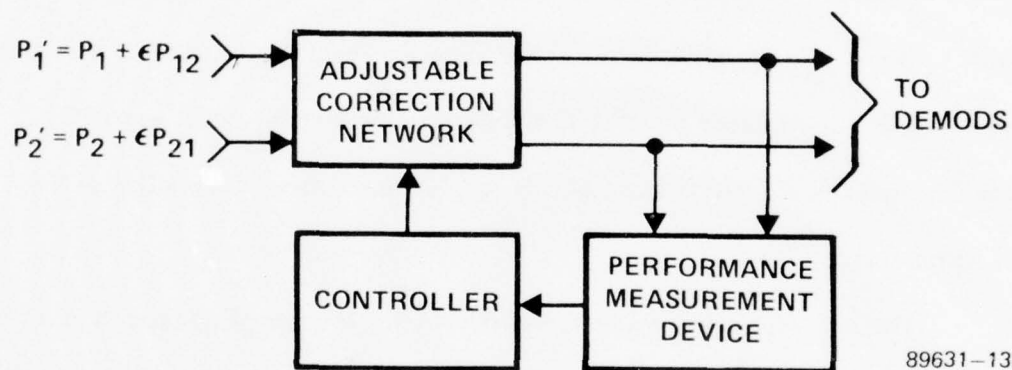
Figure 3.1-1 Adaptive Interference Reduction Network

3.1.1   Correction Network

The purpose of the correction network is to undo the coupling (deorthogo-
nalization) of the two polarizations which has occurred in the media and other parts of
the system. The primary considerations in its design are where it is placed in the system
and the type of network to be used. These considerations reduce to trade-offs of band-
width versus S/N loss and simplicity. The decoupling is accomplished by coupling the
signal from one channel, properly weighting it, and adding it back into the other
channel to undo the media induced coupling. If the coupling is caused by rotations or
pure differential phase shift, then the decoupling can be ideally accomplished losslessly
with phase shifters. On the other hand, if the coupling involves differential attenuation
(as is the case for rain induced coupling), the decoupling process must necessarily
introduce additional loss. The amount of this loss is a measure of the quality of the
decoupling network.

The magnitude of the loss associated with the decoupling process is a func-
tion of the amount of differential attenuation experienced in the coupling or deorthogo-
nalization process. As shown in a Harris report,[12] the correlation $\rho (\rho \leq 1)$ between the
received signals P_1' and P_2' is a measure of their orthogonality and the minimum loss
possible for any decoupling circuit can be calculated as a function of ρ. Since the major
noise source in the receiver is at the front end, best performance in terms of S/N degrada-
tion is obtained if lossy corrections are placed after the RF sections of the receiver. For
decoupling at the antenna outputs this minimum loss is $1 - \rho$, while for IF methods it becomes

---

[12] Rassweiler, et al., "Adaptive Polarization Separation Experiments," Final Report NASA
AAFE Contract NAS 1-13942, Harris ESD, Melbourne, Florida, August 1976.

36

$1 - \rho^2$. (These results are derived in Appendix B.) For relatively short links (5 km), ρ is small and this difference will be important only for very marginal systems. (See Appendix E for typical ρ values.) For longer links, ρ large implies a correspondingly large amount of attenuation, which will most likely be the limiting factor rather than the crosspolar coupling.

While IF decoupling is preferred for loss considerations, decoupling at RF has the advantage that the components (generally waveguide devices) are inherently less dispersive since the percent bandwidth for a given IF bandwidth is smaller. Also, the corrections are accomplished before the downconverters and associated filters and amplifiers have introduced additional dispersive effects. On the other hand, these RF techniques have the disadvantage that the hardware is more complex, where the adjustability requirement dictates the use of cumbersome electromechanical components. This also implies a more complex interface with existing hardware if the crosspole correction is to be a retrofit to existing equipment.

The less complex IF correction networks require the implementation of complex (in-phase and quadrature channels) weights which can be accomplished using any of several well developed techniques. Generally, these weights are constructed to work at a single center frequency and are useful for relatively narrow bandwidths. Additional effort is required to extend their application to wide bandwidths using tapped delay lines or other multitap configurations. Such devices are discussed in more detail in Paragraph 3.2. Another alternative to provide better bandwidth and low-loss would be the use of a hybrid network incorporating both RF and IF corrections. (See Appendix C.) The RF section would use only phase shifting elements, correcting for rotations and differential phase shifts at wider bandwidths and ideally introducing no loss, while the

37

lossy decoupling using attenuation would be done at IF. Again, the major disadvantage is hardware complexity.

3.1.2   Performance Measurement Technique

An important element of any adaptive system is the performance measuring device. In order to control the adjustable correction networks, some manner of determining whether one adjustment is better than another is necessary. Such techniques are generally application dependent, often requiring a good deal of ingenuity and special consideration about the specific system and parameters to be controlled. Nevertheless, certain general classifications can be considered. Generally, these techniques can be classified as either the direct methods that directly measure the performance parameters of interest (e.g., S/N, BER, etc.), or the indirect methods which evaluate the performance by monitoring a secondary parameter.

Examples of direct methods of interest to the crosspole problem being considered are techniques which measure the signal-to-noise ratio or the bit error rate. An important advantage of these methods is that they directly measure the performance over the entire bandwidth of interest. The use of bit error rate has the inherent disadvantage that it is very insensitive, particularly at high signal-to-noise ratios where it takes a long time to accumulate a significant number of errors. On the other hand, the signal-to-noise ratio would be a more satisfactory measure, provided a practical technique is available to make the measurement and that it did not impose difficult interface requirements on the demodulating equipment. A possible disadvantage of the direct methods

is their incompatibility with the popular LMS control technique discussed in the next section.

The indirect methods could also be termed the known signal format techniques. Generally, they require that each of the polarized signals have a separately measurable characteristic. The presence of this signal as an interference term in the crosspolar channel can then be measured. This generally requires that the signal format be modified, often an important disadvantage. For instance, if the data rate can be increased, a known bit pattern can be periodically transmitted on each channel. More simply, each channel could be alternated on and off for a small portion of the time, with the presence of a signal on the off channel indicating interference. An alternative to these methods would be to use different known pilot signals, added to each channel in such a manner as to not disturb *the data*. This could be tones offset from the data bandwidth, but such a scheme has the inherent disadvantage that it measures the interference only at the tone frequency. Consequently, it would not be useful against dispersive crosspolar interference. On the other hand, this technique is well suited for use with the LMS control algorithm.

3.1.3   Control Techniques

The controller utilizes the information from the performance measurement device to drive the correction network elements so as to optimize the system performance with respect to the measure being utilized. The control method used can be classified into two general categories, the gradient and the nongradient or search techniques.

39

The basic search methods are conceptually quite simple: they randomly select new correction network parameters, observe the performance measurement, and retain the parameters if the performance is improved. Since they must continually search for better parameters (necesary to track dynamics in the crosspole interference), they have the disadvantage that they introduce a "search noise" on the data signals, the magnitude of which is a function of the step size and update rate. This basic technique has been applied to a number of practical problems and a number of useful modifications have been developed. For instance, acceleration of the search can be accomplished by increasing the step size in successful directions, while deacceleration is used to back-track if a parameter overshoots and performance starts to degrade. Implementation is generally with special purpose logic, or dedicated microprocessors which readily accommodate such special functions.

The idea of using gradient information to determine optimal parameter values is widely used in both mathematical investigations and practical control circuitry, with many optimization procedures being based on this concept. The popular LMS technique is useful with the known signal performance measure formats, and coherently detects the presence of those signals to generate the required gradient and drives the controlled parameters in the correct direction. (See Appendix C for a more detailed discussion of this technique.) Derived gradient methods, on the other hand, are useful with any form of performance measure, and directly measure the gradient from several separate measurements using different parameter settings. This is the basis of the dither

method where the parameter values are alternately changed a small amount in each direction and the gradient is extracted with a detector. As with the search procedures, this process will also introduce a search noise in the output due to the parameter dithering.

While the LMS method introduces no search noise, it is restricted to the less convenient known signal performance measurements. Considering the analogy between the dither method and a conical scan type search radar, a monopulse type technique could be used to develop the gradient and avoid the search noise. This involves the use of additional hardware in the correction network to provide a separate channel with fixed offset parameter values (not in the data signal path) from which the gradient is measured. This is similar to the use of both sum and difference beams in the monopulse tracking antenna. In this manner, *if search noise is a problem, more hard-*ware can be introduced to avoid it, without the necessity to resort to the known signal formats.

3.2   Description of the Selected Approach

Given the basic design considerations presented in the last section, and the specific requirements of the desired crosspole system, a candidate system design can be developed. The basic design philosophy used is to propose what appears to be the most easily implemented design consistent with the specified requirements and analyze its performance. If this performance is acceptable, then the design is considered a success. This section will develop the proposed design and present a detailed mathematical description of the constituent parts.

3.2.1   Basic Block Diagram

The primary requirement of the desired crosspolarized system is that it be capable of providing high performance over long microwave links corrupted by multipath. The system was developed for application to microwave radios which use nonlinear amplifiers (e.g., travelling-wave tubes). The system, when implemented, should drive the crosspolarization interference well below thermal noise. That is, the link performance will be limited by thermal noise and not by crosspolar interference. The algorithm will be implemented at IF to simplify the hardware where precise cancellation of the interference over wide bandwidths can be accomplished using tapped delay line type networks. A technique for measuring the interference-to-signal ratio (inverse S/N ratio) is presented below. Finally, a control technique

based on the dither method of extracting the gradient is recommended, since it is easily implemented and it is demonstrated that the dither noise will not be a limiting factor. If multitap correction networks are used, the basic control logic will be time shared between the various tap weights.

The basic block diagram of this design is shown in Figure 3.2.1-1. Since the first chapter of this report determined that the vertical and horizontal polarization are preferred, the diagram shows the use of a vertical and horizontal channel with desired signals V and H. These signals are contaminated with crosspolar interference V_{xp} and H_{xp} and thermal noise n_v and n_h. In the next several sections the details of this diagram are presented.

3.2.2   Correction Network Description

To develop a general description of the correction networks, consider the mathematical description illustrated in Figure 3.2.2-1. In the figure, r_1 and r_2 represent the two orthogonally polarized transmitted signals while s_1 and s_2 are the received signals which have been coupled and distorted due to the transmission system. In general, this coupling and distortion can be modeled as frequency dependent transfer functions as shown where

$$r_1(\omega) = s_1(\omega) H_{11}(\omega) + s_2(\omega) H_{12}(\omega) \qquad (3-1)$$

$$r_2(\omega) = s_1(\omega) H_{21}(\omega) + s_2(\omega) H_{22}(\omega) \qquad (3-2)$$

Modeling the correction networks as transfer functions $w_{12}(\omega)$ and $w_{21}(\omega)$ as shown in the figure, the cross coupling can be removed by forming

43
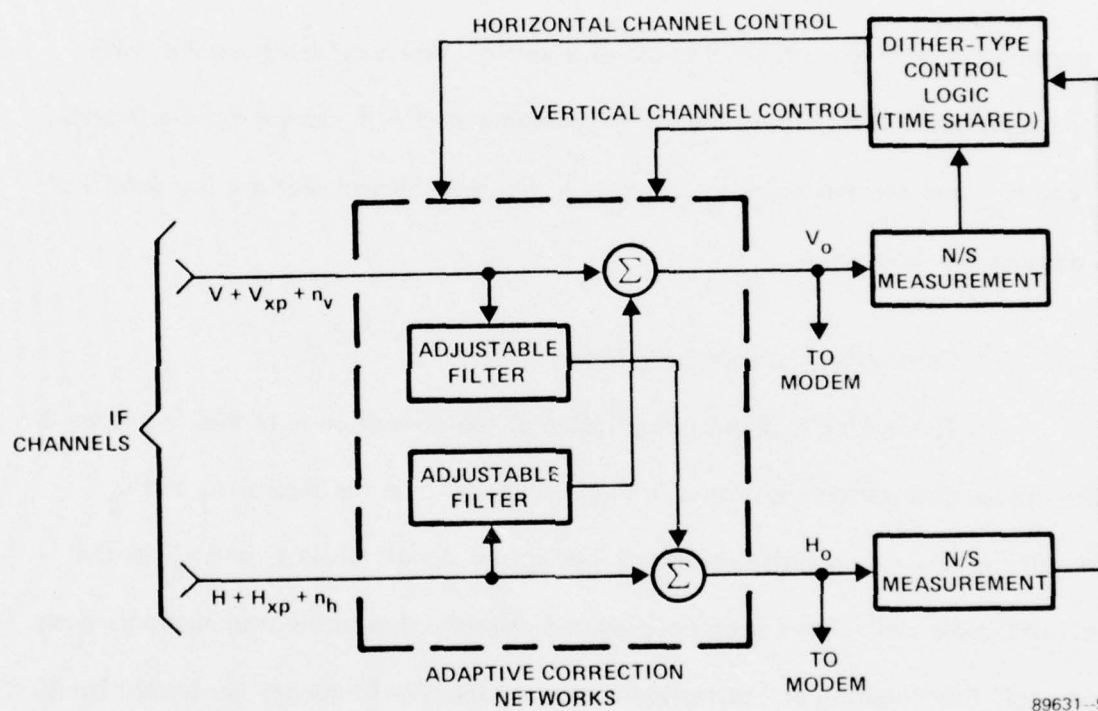
Figure 3.2.1-1 Basic Block Diagram

89631-9

44

$$W_{21}(\omega) = -\frac{H_{21}(\omega)}{H_{11}(\omega)}$$

$$W_{12}(\omega) = -\frac{H_{12}(\omega)}{H_{22}(\omega)}$$

CORRECTION NETWORK
MODEL

TRANSMISSION SYSTEM
TRANSFER CHARACTERISTICS
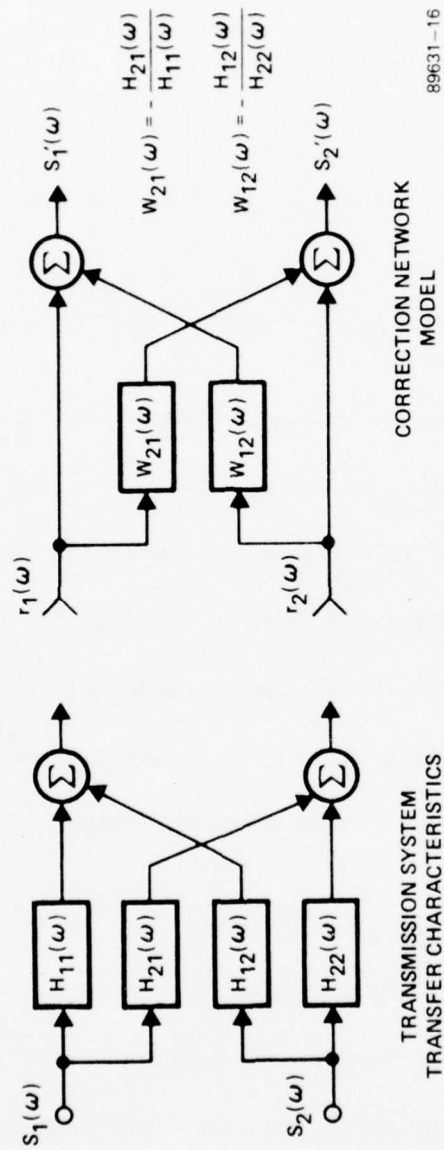
89631–16

Figure 3.2.2-1 Mathematical Description of Transmission and Correction Network Characteristics

45

$$s_1'(\omega) = r_1(\omega) - w_{21}(\omega) r_2(\omega) = r_1(\omega) - \frac{H_{12}(\omega)}{H_{22}(\omega)} r_2(\omega)$$

$$= s_1(\omega) \left[H_{11}(\omega) - \frac{H_{21}(\omega) H_{12}(\omega)}{H_{22}(\omega)} \right] \qquad (3-3)$$

and

$$s_2'(\omega) = r_2(\omega) - w_{12}(\omega) r_1(\omega) = r_2(\omega) - \frac{H_{21}(\omega)}{H_{11}(\omega)} r_1(\omega)$$

$$= s_2(\omega) \left[H_{22}(\omega) - \frac{H_{21}(\omega) H_{12}(\omega)}{H_{11}(\omega)} \right] \qquad (3-4)$$

As described above, the correction networks must provide the transfer functions $w_{12}(\omega) = -H_{12}(\omega)/H_{22}(\omega)$ and $w_{21}(\omega) = -H_{21}(\omega)/H_{11}(\omega)$. These transfer characteristics can quite generally be approximated by the conventional tapped delay line equalizer shown in Figure 3.2.2-2. In this figure the weights w_i are complex quantities with the length (number of taps) and time delay per tap depending on the specific transfer characteristics to be equalized. Several modifications of this form for the correction network are presented in the following sections.

3.2.2.1   Special Multitap Correction Network

As described in the last paragraph, the function of the correction network is to provide the required transfer characteristic to properly modify the received signal. This allows it to be used to cancel the interference it has induced in the crosspolar channel. Generally stated, it must be designed to synthesize a transfer function which can be represented in the Taylor series expansion
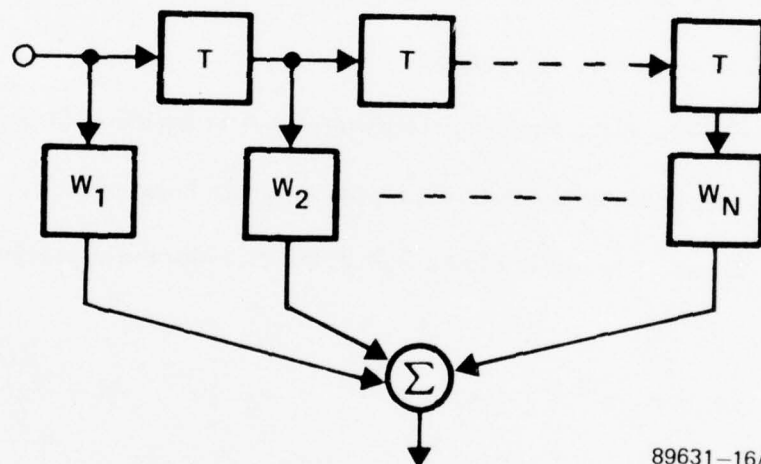
89631—16A

Figure 3.2.2-2 Conventional Tapped Delay Line Correction Network

47

$$w(\omega) = A + B\omega + C\omega^2 + \ldots \tag{3-5}$$

The conventional tapped delay line discussed above could be used, however, in this section a special correction network is developed which allows separate and uncoupled control of the constant (A), linear (B), and quadratic (C) terms in the frequency response. This device has the advantage of providing uncoupled control of each of these functions and allows the final setting of the network to be correlated with these specific characteristics of the transmission system. That is, when the adaptive control circuits have stabilized, the weight settings on this special correction network will indicate the form of the coupling that the system has caused.

To synthesize the frequency response shown in Equation (3-5), up to quadratic terms in ω, consider the building blocks shown in Figure 3.2.2.1-1. Combining these blocks as shown in Figure 3.2.2.1-2 provides the approximate transfer characteristic

$$
\begin{aligned}
w(\omega) &\approx w_1 \, e^{-j\omega T} + w_2 \, 2j e^{-j\omega T} + w_3 \left[e^{-j\omega T} \left(1 - \frac{\omega^2 T^2}{2} \right) \right] \\
&= e^{-j\omega T} \left[w_1 + (2\, j w_2\, T)\omega + \left(\frac{w_3 T^2}{2} \right) \omega^2 \right]
\end{aligned}
\tag{3-6}
$$

As illustrated by Equation (3-6), the block diagram of Figure 3.2.2.1-2 provides a transfer characteristic which approximates the general Taylor expansion up to quadratic terms in ω, where adjusting the complex weights w_1, w_2 and w_3 separately control the constant, linear and quadratic term in ω. A slight modification of this diagram (indicated on the diagram by moving w_1 to the output of the last summer) will

48

A

$$W_1(\omega) = e^{-j\omega T}$$

B
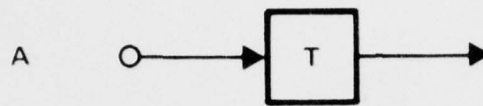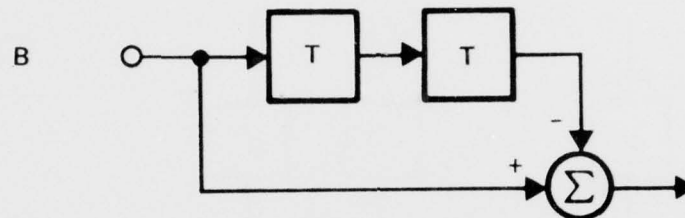
$$W_2(\omega) = 1 - e^{-j2\omega T} = e^{-j\omega T}\left[e^{j\omega T} - e^{-j\omega T}\right]$$

$$= -2j\,e^{-j\omega T}\sin\omega T \approx -2j\,e^{-j\omega T}\,\omega T$$

C
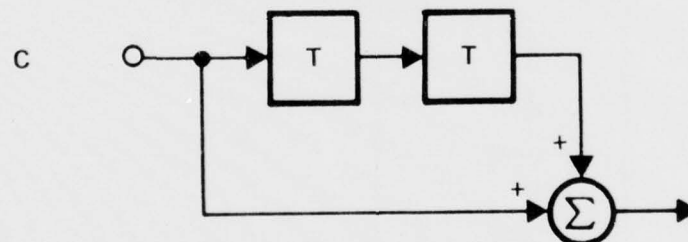
$$W_3(\omega) = 1 + e^{-j2\omega T} = e^{-j\omega T}\left[e^{j\omega T} + e^{-j\omega T}\right]$$

$$= 2\,e^{-j\omega T}\cos\omega T \approx 2\,e^{-j\omega T}\left[1 - \frac{\omega^2 T^2}{2}\right]$$

89631-17

Figure 3.2.2.1-1 Building Blocks for Special Multi-tap Correction Network
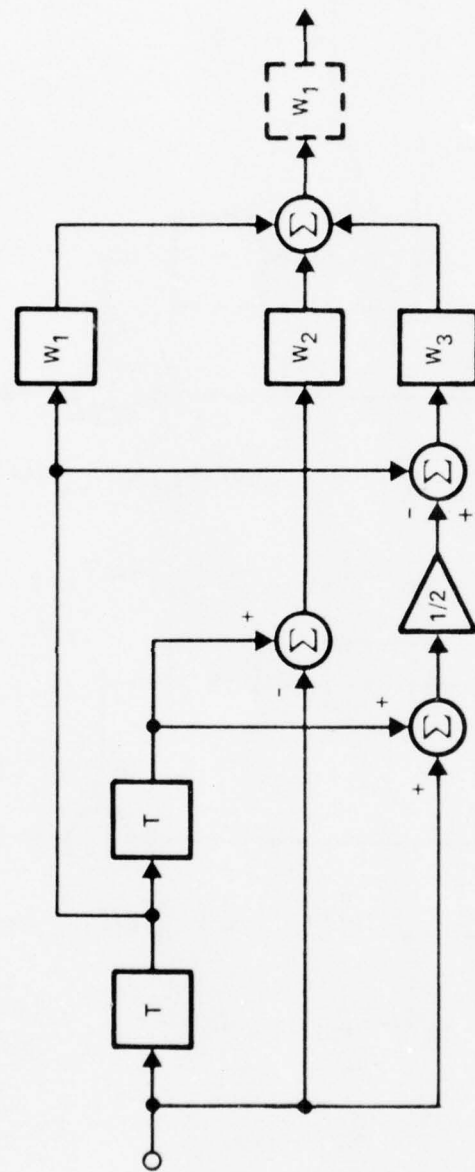
Figure 3.2.2.1-2 Special Multi-tap Correction Network

89631-10A

50

add the additional feature that the real and imaginary parts of these weights can be directly correlated with the amplitude and phase function of each of these terms. With this modification the frequency response of the network becomes

$$w(\omega) \approx e^{-j\omega T} w_1 \left[1 + 2j w_2 T\omega + \left(\frac{w_3 T^2}{2} \right) \omega^2 \right] \qquad (3-7)$$

To observe the effect of this modification consider the effect of the w_2 term in each case in terms of the phasor diagram shown below. Neglecting the 2jT term, this diagram shows that for fixed w_1, the impact of
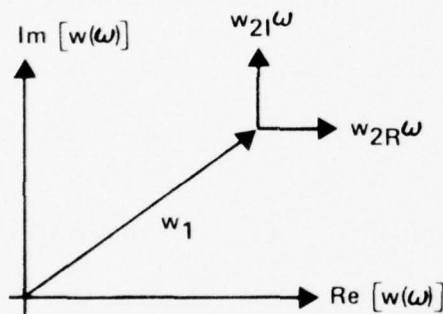
A. BEFORE MODIFICATION   B. AFTER MODIFICATION
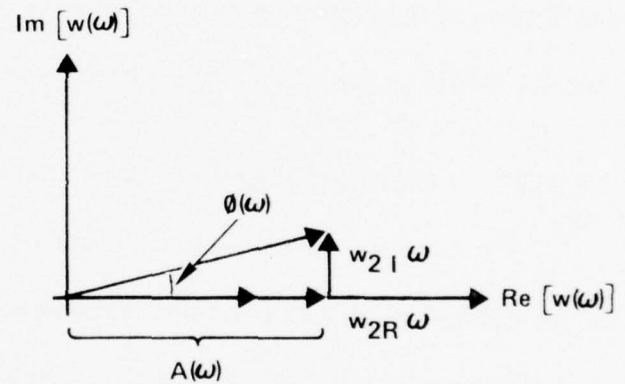
89631-22A

Phasor Diagram

w_2 now takes the form $1 + w_2\omega = 1 + w_{2R}\omega + jw_{2I}\omega$, rather than $w_1 + w_{2R}\omega + jw_{2I}\omega$. For small $w_{2R}\omega$ and $w_{2I}\omega$, Part B of the diagram shows that the magnitude of the real part of w_2 is directly related to the amplitude term $A(\omega)$ while the magnitude of the

imaginary part is independently related to $\emptyset\,(\omega)$. This would not be the case in part A.

The effect of w_3 will be added directly to the resultant vector in part B of the diagram,

where for $w_2\omega$ small this resultant is still approximately $(1 + j0)$ and the same argument

holds. That is, the real and imaginary parts of w_3 separately control the amplitude and

phase responses of the quadratic terms in ω.

For the above demonstration, it was assumed that $w_2\omega$ and $w_3\omega^2$ would

be small. This will be the case for relatively narrowband systems (where ω will represent

small deviations from a given center frequency) where the dispersion is not large (the B

and C terms of the expansion in Equation (3-5) are small). In most instances, it is felt

that this should be the case for the particular problem being addressed.

3.2.2.2   Simplified Single-Tap Correction Network

For the general case discussed in the last section, the weighting functions

for the correction network are functions of frequency, requiring that the correction

network be implemented as a frequency dependent device. If the bandwidth of the

system is small enough that the dispersive effects of the transmission media can be

neglected, then these weighting functions can be more simply implemented as adjustable

complex weights, independent of frequency. It will be useful to consider such an

implementation from two points of view. First, for some applications such simple networks

might, in fact, be adequate. (See Appendix A for a discussion of this relative to the

problem at hand.) More importantly, for the special multitap device (or conventional

tapped delay line) each of the three weights to be controlled are just complex weights,

52

and their control can be most simply implemented by time sharing the control circuitry between them. In this manner, the analysis and simulation of the system using the special multitap correction network is most easily developed as an extension of the work for the more simple single-tap device. In the following paragraphs, a mathematical model of the single-tap correction network will be developed, including a representation for the input and output signals assuming they are constant envelope signals in thermal noise.

Figure 3.2.2.2-1 illustrates the single-tap correction network and the signals in each channel. The horizontal and vertical desired signals (H and V) are assumed to be independent constant envelope signals (e.g., FM or PSK) which are modeled as $A_h \cos \omega t$ and $A_v \cos (\omega t + \theta)$, respectively, where the A's are the signal magnitudes and θ is a random process introduced to simply model the data modulation and the assumed statistical independence. The crosspolar coupling is given by the complex number $E_v \angle \emptyset_v$ and $E_h \angle \emptyset_h$, while the thermal noises are assumed to have equal power in their inphase and quadrature components such that the power on each channel is given by

$$N_h = \overline{n_h n_h^{\ *}} = \overline{\frac{x_h^2 + y_h^2}{2}} \text{ and } N_v = \overline{n_v n_v^{\ *}} = \overline{\frac{x_v^2 + y_v^2}{2}} \quad (3\text{-}8)$$

In terms of the more general model of Figure 3.2.2-1, $H_{11} = H_{22} = 1$, $H_{21} = E_h e^{i \emptyset h}$ and $H_{12} = E_v e^{i \emptyset v}$. Also, the weighting functions become $w_{12} = w_{hi} + j w_{hq}$ and $w_{21} = w_{vi} + j w_{vq}$. Since the vertical and horizontal channel corrections are uncoupled

53

$V + V_{xp} + n_v$

$= V_i = A_v \cos(\omega t + \theta) + E_v A_h \cos(\omega t + \phi_v) + x_v \cos \omega t + y_v \sin \omega t$

$H + H_{xp} + n_h$

$= H_i = A_h \cos \omega t + E_h A_v (\cos \omega t + \theta_i + \phi_h) + x_h \cos \omega t + y_h \sin \omega t$
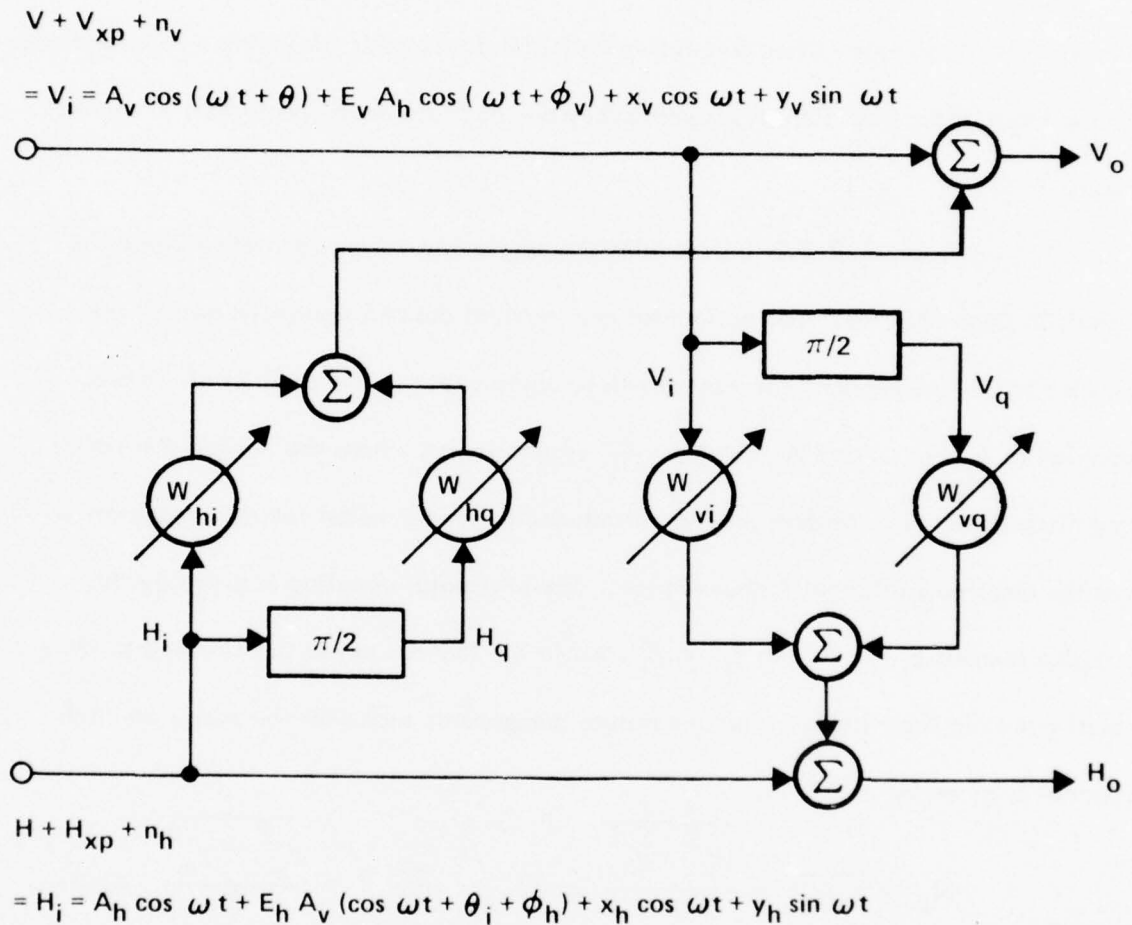
89631–3

Figure 3.2.2.2-1 Single-tap Correction Network Model

and the control techniques for each channel are identical and independent, only the correction of the horizontal channel will be analyzed.

Writing the input signals in terms of their inphase and quadrature components gives (using $\cos (a + b) = \cos a \cos b - \sin a \sin b$)

$$V_i = \left[A_v \cos \theta + E_v A_h \cos \phi_v + x_v \right] \cos \omega t$$
$$+ \left[y_v - A_v \sin \theta - E_v A_h \sin \phi_v \right] \sin \omega t \tag{3-9}$$

and

$$\bar{H}_i = \left[A_h + E_h A_v \cos (\theta + \phi_h) + x_h \right] \cos \omega t$$
$$+ \left[y_h - E_h A_v \sin (\theta + \phi_h) \right] \sin \omega t \tag{3-10}$$

Delaying the vertical channel signal by $\pi/2$ radians then gives the signal at the input to the quadrature weight as

$$V_q = \left[A_v \cos \theta + E_v A_h \cos \phi_v + x_v \right] \sin \omega t$$
$$- \left[y_v - A_v \sin \theta - E_v A_h \sin \phi_v \right] \cos \omega t \tag{3-11}$$

The horizontal channel output can now be written as (dropping the v subscript on the weights)

$$H_o = H_i + w_i V_i + w_q V_q = H_{oi} + H_{oq} \tag{3-12}$$

where H_{oi} is the component inphase with the desired horizontal channel signal ($A_h \cos \omega t$) and H_{oq} is the quadrature component. Using Equations (3-9 through 3-12) gives

$$H_{oi} = \left[A_h + E_h A_v \cos(\theta + \phi_h) + X_h + w_i A_v \cos\theta + w_i E_v A_h \cos\phi_v \right.$$
$$\left. + w_i x_v - w_q y_v + w_q A_v \sin\theta + w_q E_v A_h \sin\phi_v \right] \cos\omega t \qquad (3\text{-}13)$$

and

$$H_{oq} = \left[y_h - E_h A_v \sin(\theta + \phi_h) + w_i y_v - w_i A_v \sin\theta \right.$$
$$- w_i E_v A_h \sin\phi_v + w_q A_v \cos\theta + w_q E_v A_h \cos\phi_v \qquad (3\text{-}14)$$
$$\left. + w_q x_v \right] \sin\omega t$$

To simplify the above expressions the following assumptions will be

utilized

1. Horizontal and vertical desired signals are equal ($A_v = A_h \equiv A$).
    The thermal noise terms are also equal with $N_v = N_h \equiv N$.

2. Crosspole coupling is small (E_h and $E_v < A$) so that the required
    weights are also small and, therefore, terms involving the weights
    times the crosspole coupling are second order and can be neglected
    ($w \cdot E \ll A$).

3. Channel signal-to-thermal noise ratio is large, i.e., $\frac{A^2}{2} > N$ so
    that thermal noise components are small relative to the desired signal
    components.

The inphase component of the horizontal channel signal then becomes ($E \equiv E_v$ and

$\phi \equiv \phi_v$)

$$H_{oi} \approx \left[A + \left| A E \cos (\theta + \emptyset) + w_i A \cos \theta + w_q A \sin \theta \right. \right.$$

$$\left. \left. + x_h + w_i x_v - w_q y_v \right| \right] \cos \omega t \qquad (3\text{-}15)$$

$$\equiv \left[A + \epsilon_i \right] \cos \omega t$$

where ϵ_i is small relative to A since it consists of thermal noise terms and signal terms

attenuated by E and w. Note also that the quadrature components given by Equation (3-14)

are similarly composed so that H_{oq} can be defined as $\epsilon_q \sin \omega t \equiv H_{oq}$ and H_o becomes

$$H_o = H_{oi} + H_{oq} = (A + \epsilon_i) \cos \omega t + \epsilon_q \sin \omega t$$

$$\qquad (3\text{-}16)$$

$$= \left[(A + \epsilon_i) + j \epsilon_q \right] \cos \omega t$$

3.2.3   Performance Measurement Description

The performance measurement technique is a direct-type method based on

measuring the inverse of the signal-to-noise ratio. The network is designed to operate

with nominally constant envelope desired signal formats and measures the interference by

measuring the power in the envelope fluctuations. (Note that envelope fluctuations can

be tolerated, as long as the interference produces measurable envelope variations.) A

block diagram of this circuitry is shown in Figure 3.2.3-1. The variable gain amplifier,

magnitude detector and gain control keep the signal level at X constant so that fluctuations

in the desired signal level will not affect the interference measurement. The bandpass

filter then removes the dc terms due to the desired signal components. Finally, the square

law envelope detector (SLED) measures the average power level of the remaining noise terms.

If the gain of the variable gain amplifier is G, then using Equations (3-16)

gives the envelope X of the output of the magnitude detector as

57
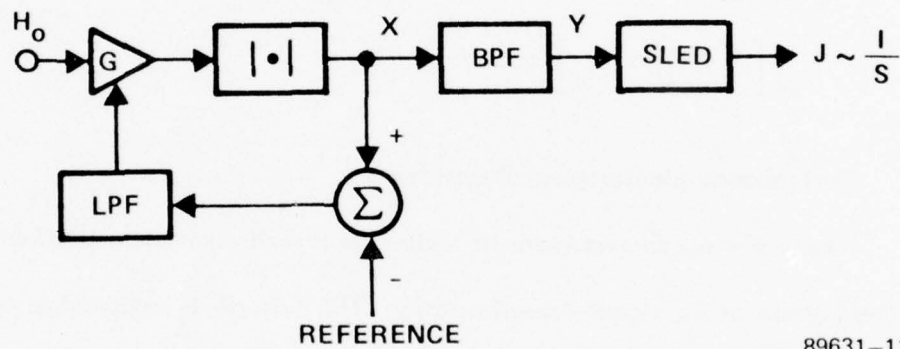
89631—11

Figure 3.2.3-1 Performance Measurement Device

58

$$\hat{X} = G\left[(A + \epsilon_i)^2 + \epsilon_q^2\right]^{1/2}$$

$$= G\left[A^2 + 2A\epsilon_i + \epsilon_i^2 + \epsilon_q^2\right]^{1/2} \tag{3-17}$$

$$\approx GA\left[1 + \frac{2\epsilon_i}{A}\right]^{1/2} \approx GA\left[1 + \frac{\epsilon_i}{A}\right]$$

If the reference voltage is set to unity and the LPF bandwidth is large enough to track the desired signal variations (but not too large that it removes the envelope fluctuations due to the interference), then with $GA \approx 1$, Equation (3-17) becomes

$$X = 1 + \frac{\epsilon_i}{A} = 1 + E\cos(\theta + \emptyset) + w_i\cos\theta + w_q\sin\theta \tag{3-18}$$

$$+ \frac{x_h + w_i x_v - w_q y_v}{A}$$

The ac coupling through the bandpass filter removes the dc terms due to the desired signal component and the envelope $\hat{Y}$ at the output of the BPF can be written as

$$\hat{Y} = (w_i + E\cos\emptyset)\cos\theta + (w_q - E\sin\emptyset)\sin\theta \tag{3-19}$$

$$+ \frac{x_h + w_i x_v - w_q y_v}{A}$$

Finally, the SLED squares and averages this to give

$$J = \frac{1}{2}\ \overline{\hat{Y}^2} = \frac{1}{2}\left[\frac{(w_i + E\cos\emptyset)^2}{2} + \frac{(w_q - E\sin\emptyset)^2}{2}\right. \tag{3-20}$$

$$\left. + \frac{(x_h + w_i x_v - w_q y_v)^2}{A^2}\right]$$

Since the separate thermal noise components are independent with $\overline{x_h^2} = \overline{x_v^2} = \overline{y_v^2} = N$, this expression becomes

59

$$J = \frac{1}{4} \left[(w_i + E \cos \emptyset)^2 + (w_q - E \sin \emptyset)^2 + \frac{1 + |w|^2}{\rho} \right] \quad (3\text{-}21)$$

where $\rho \equiv \frac{A^2}{2N}$ is the channel signal to thermal noise ratio.

Assuming that the input Y to the SLED is a zero mean gaussian random process, then the variance of the output is twice the mean of the output squared[13] and is given by

$$\sigma^2 = 2 J^2 \quad (3\text{-}22)$$

Consequently, the output of the interference measurement device is a random process with mean J and variance $2 J^2$, where J is given by Equation (3-21).

3.2.4 Control Logic Description

The circuitry described in the last section allows the measurement of the interference $J(w)$ and also provides the capability of measuring the gradient of the interference with respect to the correction network parameters, i.e., the weights w_i and w_q. This gradient information $\left(\frac{\partial J}{\partial w_i} \equiv \nabla J_i \text{ and } \frac{\partial J}{\partial w_q} \equiv \nabla J_q \right)$ can then be used to drive the weights to where the gradients are zero, the defining relations for the optimum weights. From Equation (3-21) the interference J is seen to be quadratic in the weights w_i and w_q, and therefore, the vanishing of the gradients will define unique weight settings which minimize the interference and thereby maximize the signal-to-interference ratio. Figure 3.2.4-1 illustrates the block diagram of a control technique which utilizes a dithering signal to develop the gradient of the interference with respect to the weights and the associated circuitry to drive the correction network weights to

60
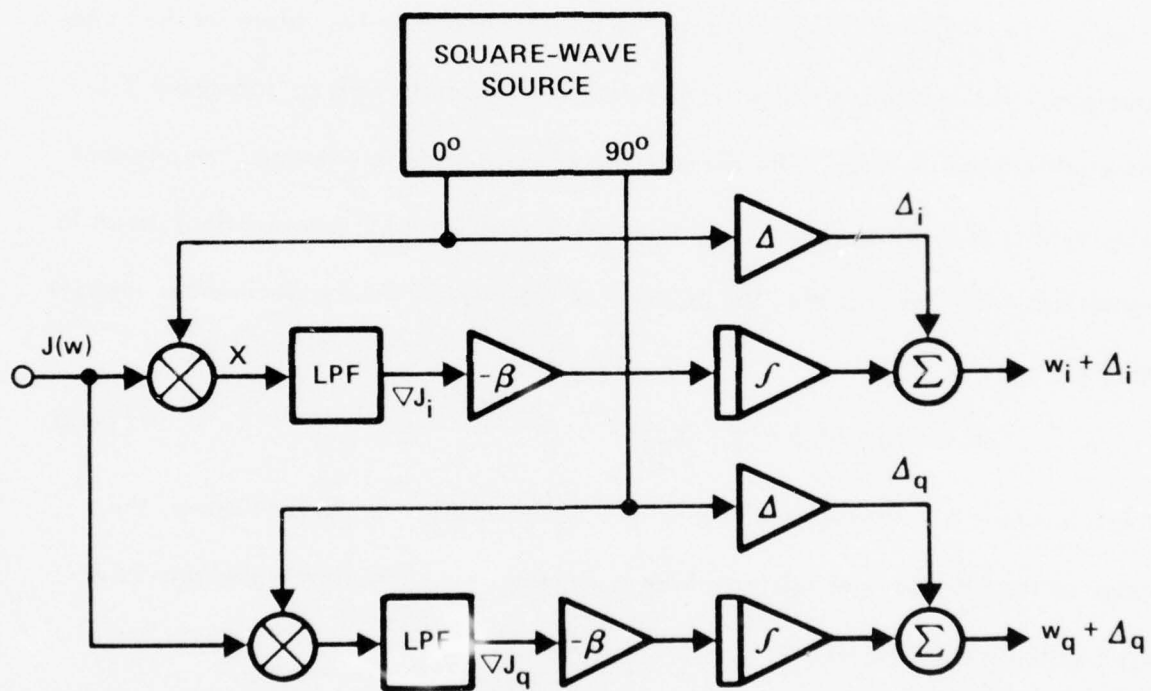
Figure 3.2.4-1 Block Diagram of Control Logic

89631—12

61

their optimum (zero gradient) values. For control of the special multitap correction network this control logic will be time shared between the three complex tap weights.

The circuitry illustrated in Figure 3.2.4-1 can be described in the following manner. The square wave source generates two orthogonal waveforms, each of which is used to dither one of the correction network weights by $\pm \Delta$, a square wave of magnitude Δ. In this manner the interference measurement network gives (for the inphase weight) $J(w_i + \Delta_i)$ and $J(w_i - \Delta_i)$ over the positive and negative values for the dither waveform. The quadrature weight is dithered simultaneously with an orthogonal (90° phase shifted) square wave, with the separate effects on the interference measurement being extracted with the synchronous detectors (multiplier – LPF combination) shown in Figure 3.2.4-1. For example, the output X of the inphase weight synchronous detector becomes

$$X = sgn(\Delta_i) J(w + \Delta_i) \tag{3-23}$$

which is $J(w + \Delta_i)$ when $\Delta_i > 0$ and $-J(w - \Delta_i)$ when $\Delta_i < 0$. Consequently, the output of the LPF averages this waveform to generate the approximate gradient ∇J of $J(w)$ with respect to w_i as

$$\nabla J(w_i) = \lim_{\Delta \to 0} \frac{J(w_i + \Delta_i) - J(w_i - \Delta_i)}{2\Delta_i} \tag{3-24}$$

$$\sim \overline{X} = \overline{J(w_i + \Delta_i) - J(w_i - \Delta_i)} \equiv \nabla J_i$$

As mentioned above, the interference J is quadratic in the weights, with an approximate sketch of this functional relationship being shown in Figure 3.2.4-2.

This figure illustrates that the minimum interference $J(w_{oi})$ corresponds to the point where $\nabla J_i = 0$ and the quadratic nature of this curve gives $\nabla J_i > 0$ if $w_i > w_{oi}$ and
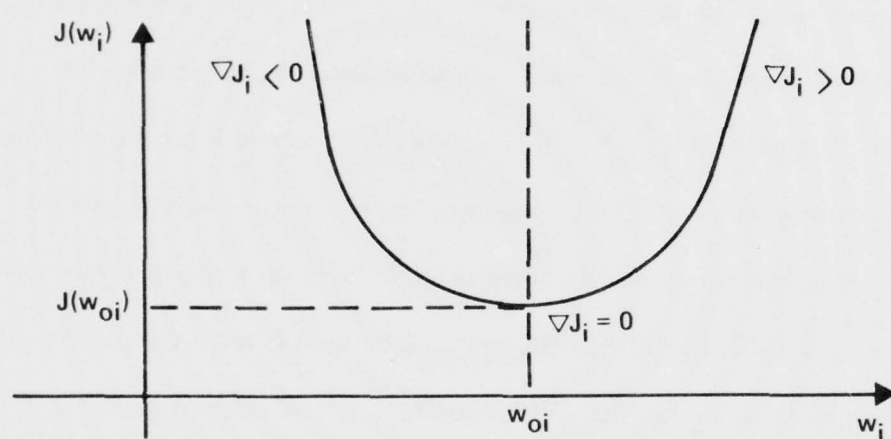
Figure 3.2.4-2. Approximate Sketch of Interference Versus Inphase Weight Setting

$\nabla J_i > 0$ if $w_i < w_{oi}$. These relationships allow the optimum weight to be found with a simple integration circuit as shown in Figure 3.2.4-1. That is,

$$\frac{dw_i}{dt} = -\beta \nabla J_i \tag{3-25}$$

where $\frac{dw_i}{dt}$ is zero when $\nabla J_i = 0$ and the weight remains constant, while nonzero ∇J_i tends to drive the weight toward the optimum (zero gradient) value. The quadrature

63

weight control is described similarly. More detail concerning gain settings (e.g., β value) and loop bandwidth is discussed in Paragraph 3.4 describing the control loop analysis.

As described above, the synchronous detectors include a low pass filter to average the output and form the required gradient. This averaging will remove the dither generated square wave due to the average or dc value of the performance measure at the particular operating point. For instance, at the optimum weight setting this square wave will be of magnitude $J(w_o)$. This quantity is computed in the next section. Since the control loop already contains an integrator, some averaging will be present and the additional LPF could cause stability problems. In fact, for high signal-to-noise ratios, the value of $J(w_o)$ will be quite small, and as long as it is small compared to the effect of the weight dither, its effect will be negligible. An alternative to the LPF after the synchronous detector is to remove the dc at the input to the detector with a high pass filter. This alternative is used in the simulations presented in Section 4.0.

3.3   Steady State Performance

This section discusses the performance of the adaptive crosspole correction circuitry in terms of its expected steady state performance with the correction network weights set at their optimum values. This discussion proceeds in two areas, one being a general discussion of optimum weight settings and performance, and the other being directed toward the specific circuitry and equations developed in the previous sections. The two fold purpose of this work is to present some general conclusions and also

64

facilitate the development of the analysis of the specific design. This analysis continues in the next section with the development of the dynamic performance analysis concerning the transient performance and weight jitter effects. The presentation will concentrate on the single-tap correction network, since general results using the special multitap network are more difficult. Since the analysis of the multitap network requires specific assumptions concerning the nature of the dispersive effects, it is therefore deferred until Section 4.0 where the simulations define specific dispersion models.

3.3.1 Optimum Weights for the Single-Tap Network

To further develop the mathematical analysis of the specific design considered in the last several sections, consider the steady state weight values that will be set by the control logic. These values are the optimum settings for the interference function of Equation (3-21) and as mentioned in the last section, they are defined by the vanishing of the gradient given by

$$\nabla J_i = \frac{1}{2} \left[w_i + E \cos \emptyset + \frac{w_i}{\rho} \right] = 0 \tag{3-26}$$

and

$$\nabla J_q = \frac{1}{2} \left[w_q - E \sin \emptyset + \frac{w_q}{\rho} \right] = 0 \tag{3-27}$$

These equations then give the optimum weight values as

$$w_{oi} = \frac{-\rho E \cos \emptyset}{1 + \rho} \tag{3-28}$$

and

$$w_{oq} = \frac{\rho E \sin \emptyset}{1 + \rho} \tag{3-29}$$

65

For large signal-to-thermal noise ratios ($\rho \gg 1$) these reduce to $w_{oi} \approx - E \cos \emptyset$ and $w_{oq} \approx E \sin \emptyset$, that is, the optimum weights can eliminate the crosspole completely without regard to the additional thermal noise which they introduce, since the thermal noise term is negligibly small. Note also that the approximate formulation of Equation (3-21) does not consider the additional effect of desired signal modification by the weighting circuits since this effect was assumed to be second order and was neglected to ease the analysis. For the computational work discussed in Section 4.0 the optimum weights are found numerically and include both the thermal noise and desired signal effects.

The value of the interference corresponding to the optimum weight settings can be obtained by substituting Equations (3-28) and (3-29) into Equation (3-21). This gives the minimum interference as

$$ J(w) \bigg|_{w = w_{opt}} = \frac{1}{4} \left[\frac{E^2}{(1 + \rho)} + \frac{1}{\rho} \right] \tag{3-30}$$

Note that as the ρ becomes large the minimum interference goes to zero, indicating complete crosspole cancellation and no additional thermal noise effects.

3.3.2 General Performance Results

To more easily describe the general steady state performance of the cross-pole correction circuitry, consider the simplified model and definitions for the single channel correction using one complex weight shown in Figure 3.3.2-1. In terms of these

$$V_i = V + \epsilon H + n_v$$

$$H_i = H + \epsilon V + n_h$$

$$H_o = (1 + \epsilon w) H + (w + \epsilon) V + n_h + wn_v$$
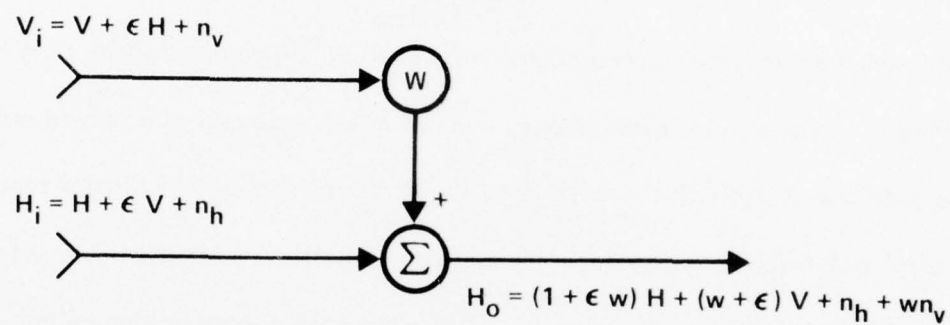
$$\epsilon \equiv \text{CROSSPOLAR VOLTAGE COUPLING} = \frac{V_{xp}}{V} = \frac{H_{xp}}{H}$$

$$S_i = P_v = \overline{VV}^* = P_h = \overline{HH}^*$$

$$N_i = \overline{n_v n_v}^* = \overline{n_h n_h}^*$$

$$\rho = S_i / N_i$$

89631−15

Figure 3.3.2-1 Simplified Circuit Model and Definitions

67

definitions the output signal-to-noise ratio (where noise includes both thermal noise and crosspolar interference) is given by

$$S_o/N_o = \frac{|(1 + \epsilon w) H|^2}{|(w + \epsilon) V + n_h + w n_v|^2}$$

$$= \frac{|1 + w \epsilon|^2}{|w + \epsilon|^2 + \dfrac{1 + |w|^2}{\rho}}$$

(3-31)

The term in the numerator represents the effect on signal power resulting from the weight coupling in the crosspole signal power, and has been neglected as a second order effect in the previous analysis (i.e., $w \epsilon \ll 1$). The first term in the denominator represents the output noise due to crosspolar interference, while the second term is due to thermal noise and includes the additional noise coupled into the output by the weight. Setting $w = -\epsilon$ will completely eliminate the crosspolar interference, without regard to the thermal noise, and results in a signal-to-noise ratio of

$$S_o/N_o \bigg|_{w = -\epsilon} = \frac{\rho}{1 + |\epsilon|^2}$$

(3-32)

where the signal power coupling is again assumed negligible. For reference purposes, if w is set to zero, Equation (3-31) will give the signal-to-noise ratio with no adaptive correction as

$$S_o/N_o \bigg|_{w = 0} = \frac{\rho}{1 + \rho |\epsilon|^2}$$

(3-33)

68

In the last section Equation (3-30) was derived as the output of the interference measurement device when the correction network weights were set at their optimum values. Recognizing this result as being proportional to the noise-to-signal ratio, where the factor of 1/4 is due to specific circuit gains, and $E^2 = \epsilon^2$ gives the optimum output signal-to-noise ratio as

$$\left. S_o/N_o \right|_{opt} = \frac{\rho(1+\rho)}{\rho|\epsilon|^2 + \rho + 1} \tag{3-34}$$

The equations of this section can now be used to develop several interesting comparisons. First, Equations (3-33) and (3-34) can be used to determine the improvement in signal-to-noise ratio due to the adaptive correction circuitry as

$$\frac{\left. S_o/N_o \right|_{opt}}{\left. S_o/N_o \right|_{w=0}} = 1 + \frac{\rho^2|\epsilon|^2}{\rho|\epsilon|^2 + \rho + 1} \tag{3-35}$$

This equation is plotted in Figure 3.3.2-2 for various values of crosspolar interference. Secondly, Equations (3-32) and (3-34) can be used to find the improvement in signal-to-noise ratio due to incomplete decoupling as (see also Appendix B for an analysis of this effect)

$$\frac{\left. S_o/N_o \right|_{opt}}{\left. S_o/N_o \right|_{w=-\epsilon}} = 1 + \frac{|\epsilon|^2}{\rho|\epsilon|^2 + \rho + 1} \tag{3-36}$$

This equation is plotted in Figure 3.3.2-3 for various values of crosspolar interference.
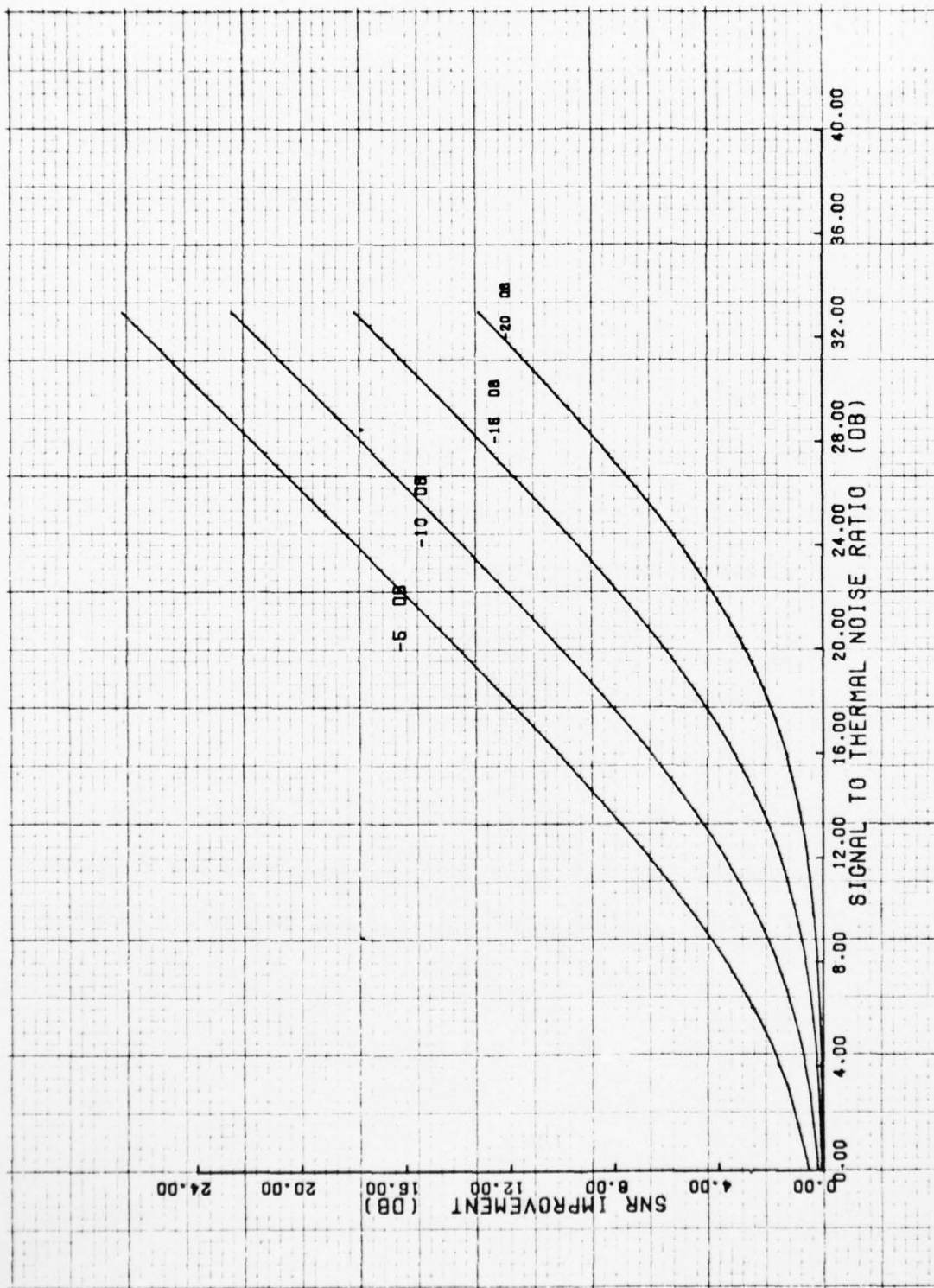
Figure 3.3.2-2 Improvement in S/N Due to Adaptive Corrective Circuitry

70
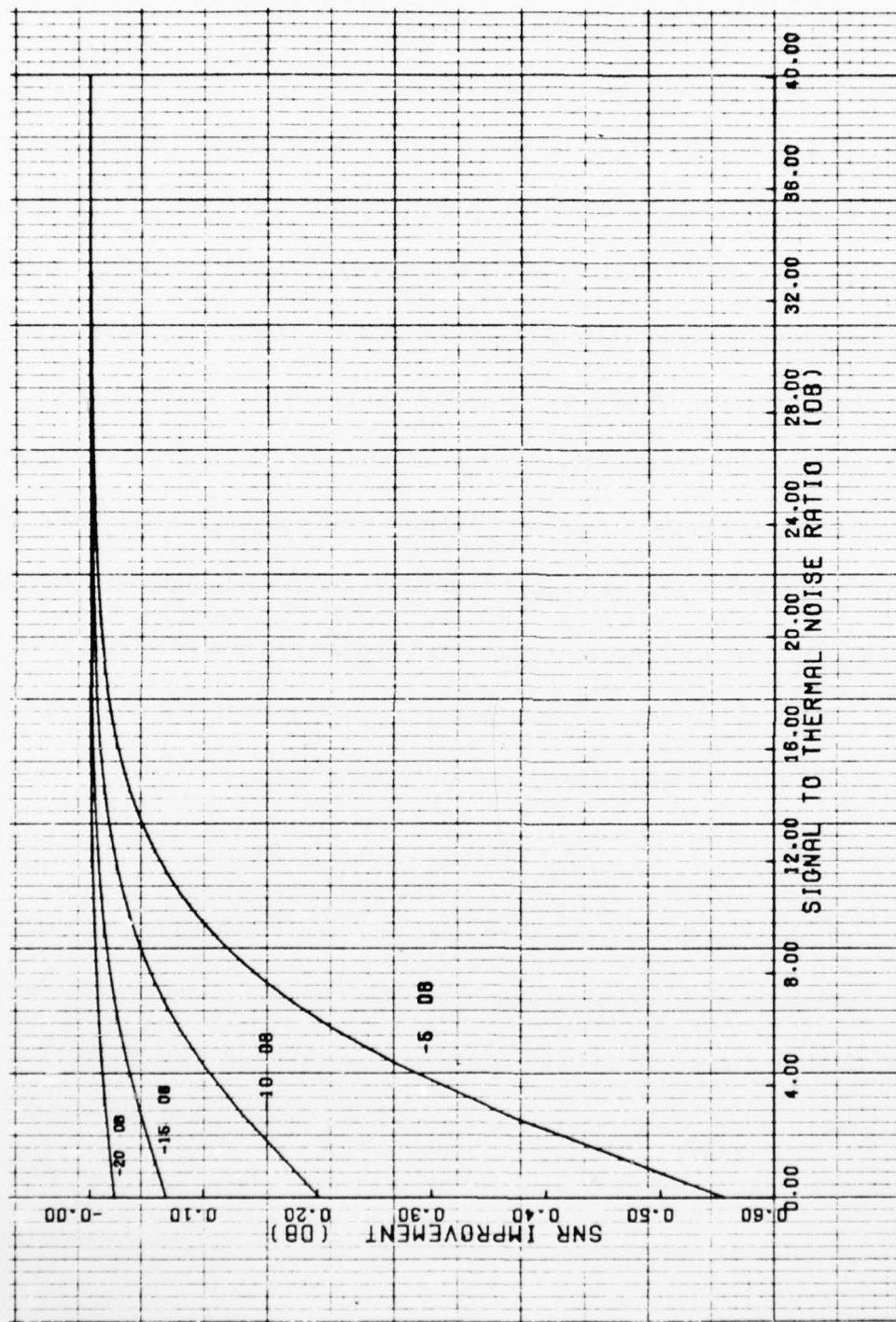
Figure 3.3.2-3   Improvement in SNR Using Incomplete Decoupling

71

3.4 Dynamic Performance Analysis and Parameter Selection

In the last section the steady-state performance of the adaptive correction circuitry was discussed. This work gives an indication of how good the circuitry can perform if it is well designed. However, if it is to perform well in a dynamic environment, the circuit parameters (loop gain and BW, dither size, filter BW's, etc.) must be carefully chosen. To accomplish this the dynamic performance of the circuitry (transient response, tracking rate, weight jitter, etc.) must be analyzed. This analysis will proceed by linearizing the circuit equations and developing an approximate linear model. Using this linear model, approximate transient response and steady-state weight jitter can be derived as a function of the circuit parameters. From these functional relationships the parameter values that yield good tracking performance and small degradation due to weight jitter can be derived. This work uses the equations developed for the single-tap correction network, but also discusses the extension to the multi-tap network.

3.4.1 Linear Control Loop Analysis

In the previous sections the various components of the adaptive crosspole correction device have been described. These can be functionally represented by the block diagram shown in Figure 3.4.1-1A. In their most general form the mathematical relationships between w, $J(w)$ and $\nabla J(w)$ would yield a nonlinear control loop and it would be difficult to analyze the performance of the complete system. However, the approximate formulation developed in the last several sections can be configured as the

72
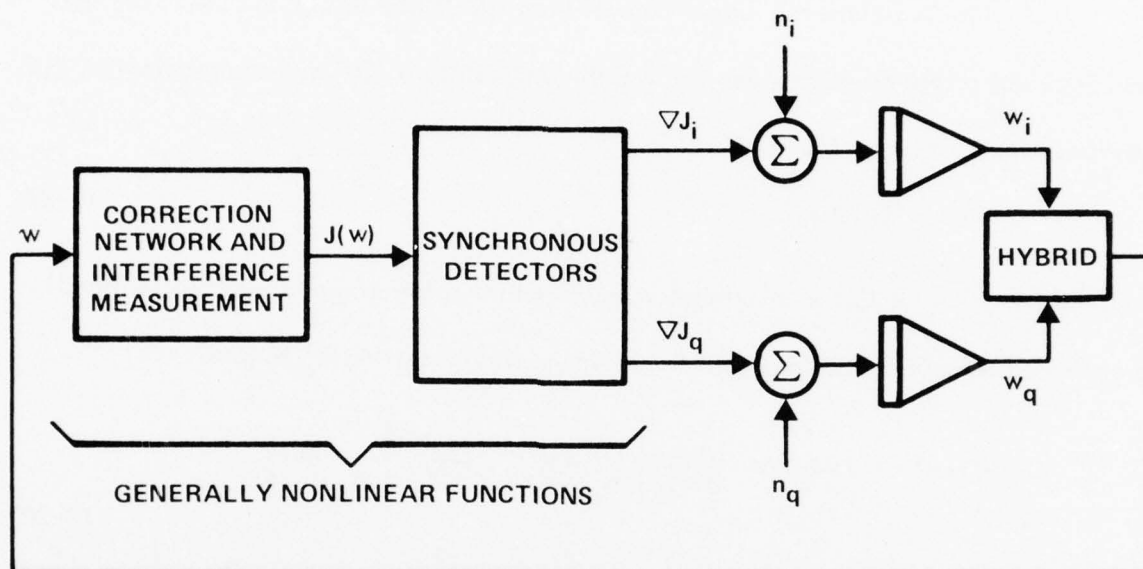
A. COMPLETE SYSTEM BLOCK DIAGRAM
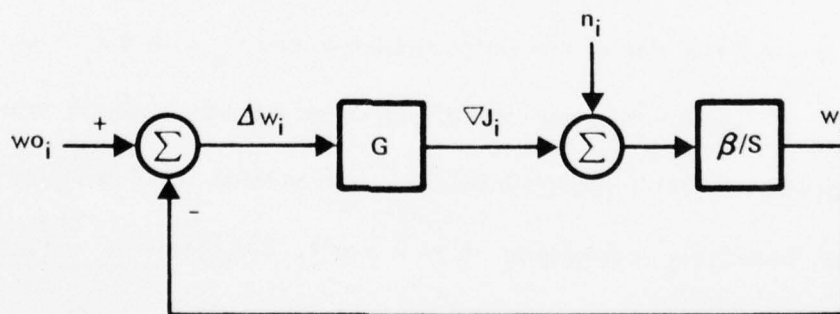
B. LINEAR CONTROL LOOP FOR APPROXIMATE ANALYSIS

89631-8

Figure 3.4.1-1 Control Loop Block Diagram

73

linear control loop shown in Figure 3.4.1-1B, where only the in-phase weight control is considered since the quadrature control will proceed in an identical manner.

To formulate the linear control loop illustrated in Figure 3.4.1-1B, the mathematical relationship between the weight perturbations Δw_i and the gradient of the interference ∇J must be found, as

$$\nabla J = G \, \Delta w_i \tag{3-37}$$

To obtain a value for G the interference measurement relation given by Equation (3-21) is expanded as a Taylor series about the optimum weight setting w_o to give

$$J(w) = J(w_o) + \frac{\partial J}{\partial w_i}\bigg|_{w_o} \delta w_i + \frac{\partial J}{\partial w_q}\bigg|_{w_o} \delta w_q$$

$$+ 1/2 \frac{\partial^2 J}{\partial w_i^2}\bigg|_{w_o} (\delta w_i)^2 + 1/2 \frac{\partial^2 J}{\partial w_q^2}\bigg|_{w_o} (\delta w_q)^2 + 0\left[(\delta w)^3\right] \tag{3-38}$$

where $J(w)$ is a real function of the real variables w_i and w_q with $\delta w_i = w_i - w_{oi}$ and $\delta w_q = w_q - w_{oq}$ representing the total displacement from the optimum values. Note that since Equation (3-21) is quadratic the higher order terms $0\left[(\delta w)^3\right]$ are zero and the expansion through the second order terms is exact. The gradients $\frac{\partial J}{\partial w_i}$ and $\frac{\partial J}{\partial w_q}$ are zero at $w = w_o$ and differentiating Equation (3-26) and (3-27) gives

$$\frac{\partial^2 J}{\partial w_i^2} = \frac{\partial^2 J}{\partial w_q^2} = 1/2 \left[1 + \frac{1}{\rho}\right] \tag{3-39}$$

Therefore, (Equation 3-38) gives the relationship

$$J(w) = J(w_o) + \frac{1}{4}\left(1 + \frac{1}{\rho}\right)\left[(\delta w_i)^2 + (\delta w_q)^2\right]$$

$$= J(w_o) + \frac{1}{4}\left(1 + \frac{1}{\rho}\right)\left|\delta w\right|^2 \tag{3-40}$$

Recognizing that δw consists of both the operating point offsets Δw_i and Δw_q and the dither Δ_i and Δ_q, and expressing the synchronous detector output as the average over one dither cycle gives

$$\nabla J(w) = J(w_o + \Delta w + \Delta) - J(w_o + \Delta w - \Delta) \tag{3-41}$$

Substituting into this expression from (Equation 3-40) then gives

$$\nabla J(w) = J(w_o) + \frac{1}{4}\left(1 + \frac{1}{\rho}\right)\left\{(\Delta w_i + \Delta_i)^2 + (\Delta w_q + \Delta_q)^2\right\}$$
$$- J(w_o) + \frac{1}{4}\left(1 + \frac{1}{\rho}\right)\left\{(\Delta w_i - \Delta_i)^2 + (\Delta w_q - \Delta_q)^2\right\} \tag{3-42}$$

which reduces to

$$\nabla J(w) = \left(1 + \frac{1}{\rho}\right)\left(\Delta w_i \Delta_i + \Delta w_q \Delta_q\right) \tag{3-43}$$

Consequently, the gain term G for the in-phase weight control is

$$G = \Delta\left(1 + \frac{1}{\rho}\right) \tag{3-44}$$

where $\Delta = \Delta_i = \Delta_q$ is the dither size. Note that the gain equations for the in-phase and quadrature control are identical as hypothesized above.

75

The derivation in the last paragraph defines the linear control loop illustrated in Figure 3.4.1-1B. From this the response time and the weight jitter performance can be determined. The transfer function from w_{oi} to w_i is

$$H(j\omega) = \frac{G\beta}{j\omega + G\beta} \tag{3-45}$$

with unit step function response

$$a(t) = \left[1 - e^{-G\beta t} \right] \tag{3-46}$$

Thus, the time constant of the control loop is

$$t_c = \frac{1}{G\beta} = \frac{\rho}{\Delta(\rho + 1)\beta} \tag{3-47}$$

where for $\rho >> 1$, $t_c \approx \frac{1}{\Delta\beta}$.
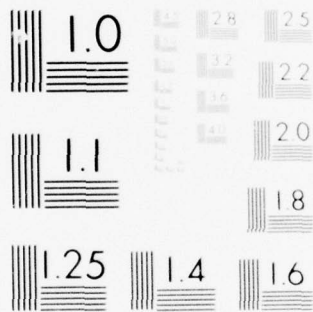
MICROCOPY RESOLUTION TEST CHART
NATIONAL BUREAU OF STANDARDS 1963 A

3.4.2   Weight Jitter Analysis

To compute the weight jitter $\overline{\Delta w_i^2}$ the transfer function $H_2(j\omega)$ from ∇J_i to Δw_i must be determined. This transfer function is given by

$$H_2(j\omega) = \frac{-\beta}{j\omega + G\beta} \tag{3-48}$$

and weight jitter is then defined by

$$\overline{\Delta w_i^2} = \frac{1}{2\pi} \int_{-\infty}^{\infty} \left| H_2(j\omega) \right|^2 N_i(\omega) \, d\omega \tag{3-49}$$

where $N_i(\omega)$ is the power spectral density of the noise n_i at the output of the synchronous detectors. The variance of $J(w)$ is given by Equation (3-22) as σ^2 and using Equation (3-41) to relate ∇J to J, the variance of n_i is also seen to be σ^2. Assuming the input to the SLED is zero mean Gaussian noise that is flat over the IF bandwidth B, with variance σ_y^2, then the variance of the output can be expressed $\sigma^2 = 2(1/2)^2 \sigma_y^4$. Consequently the power spectral density $N_i(\omega)$ evaluated at $\omega = 0$ can be evaluated in terms of the input variance as [14]

$$N_i(0) = 2\left(\frac{1}{2}\right)^2 \int_{-B}^{B} \left[\frac{\sigma_y^2}{2B}\right]^2 df = \frac{\sigma_y^4}{4B} = \frac{\sigma^2}{2B} \tag{3-50}$$

where $\qquad \sigma^2 = 2\left(\frac{1}{2}\right)^2 \sigma_y^4 = \frac{\sigma_y^4}{2}$.

Since the control loop bandwidth is small compared to the IF bandwidth, then $N_i(\omega)$ will be essentially constant at its $\omega = 0$ value over all values where $H_2(j\omega)$ has significant magnitude. In this case the integral in Equation (3-49) becomes

---

[14] Davenport, W.B. and W. L. Root, "An Introduction to the Theory of Random Signals and Noise," McGraw-Hill, N. Y., 1958 (pp 256-257).

77

$$\overline{\Delta w_i^2} = \frac{\sigma^2}{4\pi B} \int_{-\infty}^{\infty} \frac{\beta^2 \, d\omega}{\omega^2 + G^2 \beta^2} = \frac{\sigma^2 \beta}{4BG} \tag{3-51}$$

Substituting from Equations (3-22), (3-30) and (3-44) for σ^2 and G at the optimum weight settings gives

$$\overline{\Delta w_i^2}\,\Bigg|_{w=w_{opt}} = \frac{\rho \left[\dfrac{E^2}{(1+\rho)^2} + \dfrac{1}{\rho}\right]^2 \beta}{32 B \Delta (\rho + 1)} \tag{3-52}$$

If crosspole is limited to 10 dB and $\rho > 1$, this reduces to

$$\overline{\Delta w_i^2}\,\Bigg|_{w=w_{opt}} \approx \frac{\beta}{32 B \Delta \rho^2} \tag{3-53}$$

In the next section it is shown that for good tracking performance $\beta \cong \dfrac{2000}{\Delta}$. Using this in Equation (3-53) and assuming B = 14 MHz gives

$$\overline{\Delta w_i} = \frac{2.1 \times 10^{-3}}{\Delta \rho} \tag{3-54}$$

This expression is plotted in Figure 3.4.2-1 for several values of dither size in the range most likely to be utilized (see Paragraph 3.4.3).

3.4.3   Control Loop Parameter Selection

The analysis in the last several sections provides the rationale for the selection of the control loop parameters. The primary parameter is the loop bandwidth which is a function of the dither size (the gain G) and the integrator gain β. (See Equation (3-47).) This loop bandwidth will be selected to allow the loop to track a given cross pole rate of change with a specified accuracy while maintaining a good
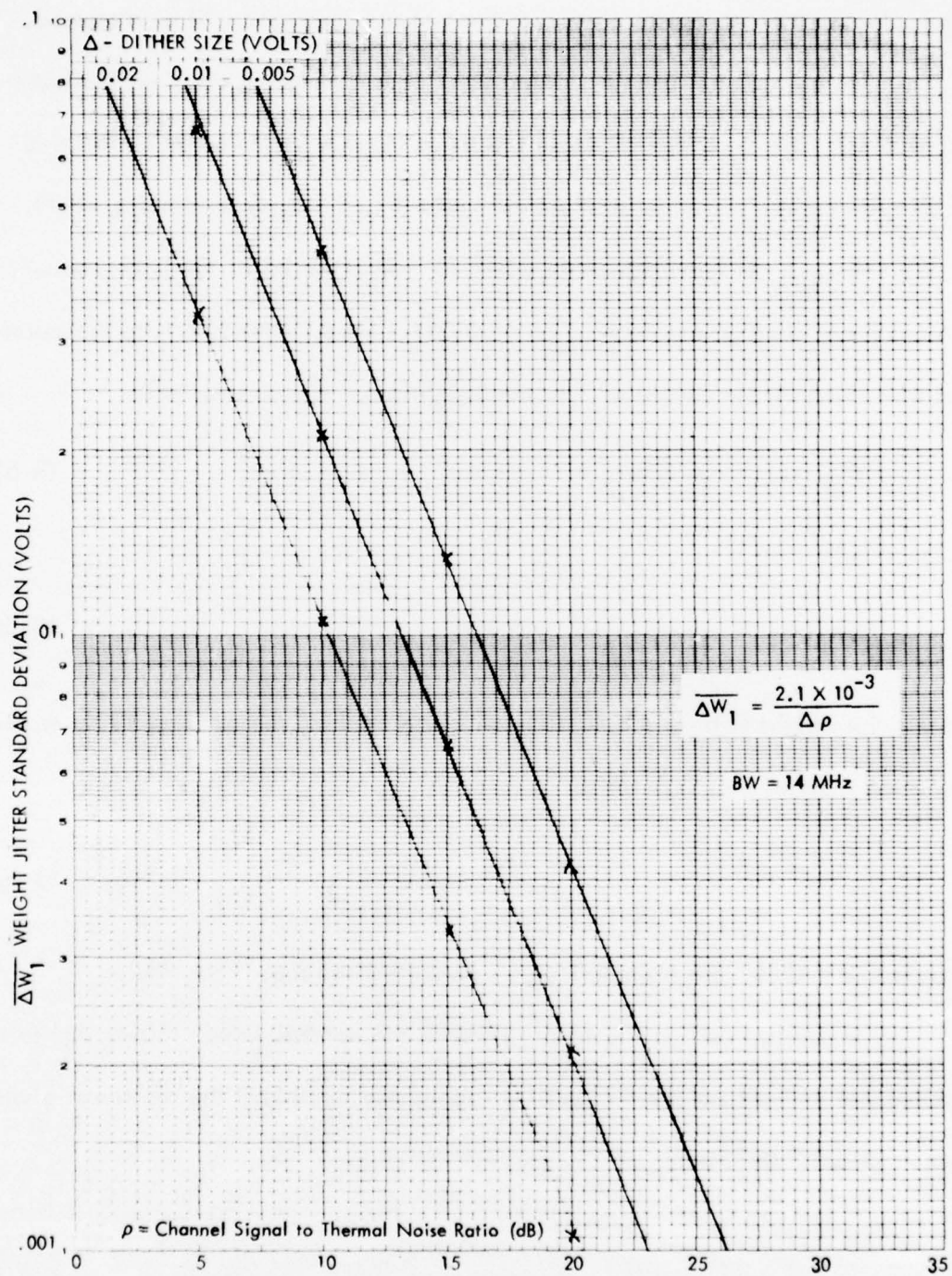
Figure 3.4.2-1 Standard Deviation of Weight Jitter

79

relationship between the weight jitter due to the interference and the weight dither. Also, the selection of dither rate relative to the system bandwidths will be discussed.

Data which has been collected on various communication links indicates that the maximum rate of change of crosspolar coupling due to atmospheric effects is limited to a few hertz. Assuming a sinusoidal variation, the optimum weights would behave as $w_o = w_{max} \cos \omega t$ where an $\omega = 2\pi 10 = 62.8$ should certainly be a worst-case rate. Also, for a 10 dB crosspole $|w_{max}| = 0.316$. From Figure 3.4.1-1B the transfer function from the optimum weight w_{o_i} to the weight error Δw_i is seen to be

$$H_3(j\omega) = \frac{j\omega}{j\omega + G\beta} \tag{3-55}$$

so that the weight error is

$$\Delta w_i(\omega) = \frac{j\omega}{j\omega + G\beta} \, w_{o_i}(\omega) \tag{3-56}$$

To maintain the weight error at the 40 dB level while tracking the assumed 10-Hz crosspole variation requires that $G\beta$ satisfy

$$\Delta \omega_i^2 (\omega) \bigg|_{\omega = 62.8} = 10^{-4} = \frac{\omega^2}{\omega^2 + (G\beta)^2} \bigg|_{\omega = 62.8} (.316)^2 \tag{3-57}$$

which gives $G\beta = 1986$. For high SNR ($\rho >> 1$), $G \approx \Delta$ so that $\beta\Delta \approx 2000$.

In the last section the weight jitter at the optimal weight setting due to the interference was derived, where for small crosspole and large SNR the result was given in Equation (3-53). Defining

$$\alpha = \frac{\beta}{32B\rho^2} \quad \text{gives} \quad \overline{\Delta w_i^2} \bigg| w = w_{opt} = \frac{\alpha}{\Delta}$$

Also, the weight jitter due to the dithering is Δ^2, so that the total weight jitter δ^2 is (since the dither and the interference are independent)

$$\delta^2 = \overline{\Delta w_i^2} + \Delta^2 = \frac{\alpha}{\Delta} + \Delta^2 \tag{3-58}$$

From this equation the optimum dither size, that is, the dither which results in the minimum total jitter δ can be found by differentiating this expression with respect to Δ and solving for the optimum dither size as

$$\frac{\partial \delta^2}{\partial \Delta} = \frac{-\alpha}{\Delta^2} + 2\Delta = 0 \tag{3-59}$$

This gives

$$\Delta \left(2 - \frac{\alpha}{\Delta^3}\right) = 0 \tag{3-60}$$

where the $\Delta = 0$ solution is a maximum, while $2 - \frac{\alpha}{\Delta^3} = 0$ gives the minimum as

$$\Delta^3 = \frac{\alpha}{2} = \frac{\beta}{64B\rho^2} \tag{3-61}$$

Since $\beta = \frac{2000}{\Delta}$ and substituting into Equation 3-60 with $\beta = 14$ MHz gives

$$\Delta^2 = \frac{1.494 \times 10^{-3}}{\rho} \tag{3-62}$$

Using Equation 3-62 the optimum dither size as a function of the channel signal-to-thermal noise ratio is plotted in Figure 3.4.3-1. This plot shows the dither size required to track a maximum 10-Hz crosspole rate of change with weight errors constrained to the 40 dB level, while maintaining the total weight jitter at its minimum value. From Equation 3-61, $\alpha = 2 \Delta^3$ and substituting this into Equation 3-58 gives the total jitter $\delta^2 = 3 \Delta^2$. This could be thought of as the effective dither size δ_e where

$$\delta_e = \sqrt{3}\Delta = 1.73\Delta \tag{3-63}$$

That is, a dither size of Δ will create a total weight jitter of $\sqrt{3}\,\Delta$. This effective dither level is also displayed in Figure 3.4.3-1.

The primary detrimental effect of the dither will be to produce a dither generated crosspole interference in the correction network output. Assuming equal signal levels in each of the channels, the effective dither level illustrated in Figure 3.4.3-1 will produce a dither generated interference which is 23.6 dB below the channel thermal noise for all signal-to-noise ratios. In other words, the desired tracking accuracy can be maintained with a dither size that will have a very minor impact on the system performance. In fact, for high signal-to-noise ratios, this design specifies an unnecessarily small dither level. These small dither levels would make the gradient detection difficult with practical hardware implementation (see discussion at end of Paragraph 3.2.3). Consequently, it is recommended that the dither size be greater than 0.01 volts. At this level, the effective dither would produce a crosspole interference 35 dB below

82
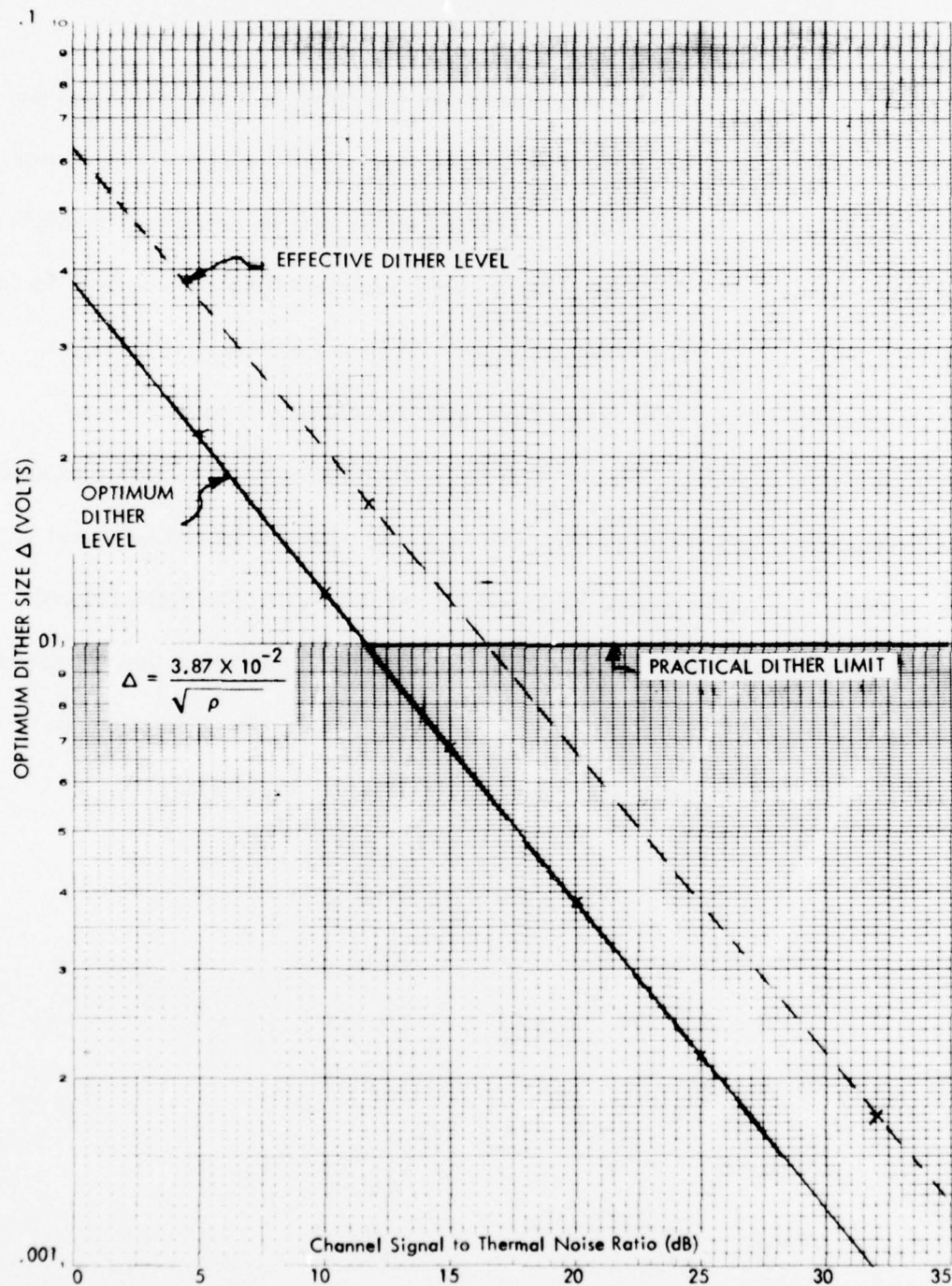
Figure 3.4.3.-1. Dither Level Required to Maintain Desired Tracking Accuracy

83

the desired signal. Recalling that the control loop integrator gain $\beta = \dfrac{2000}{\Delta}$, the recommended dither size and integrator gain are plotted in Figure 3.4.3-2.

The derivation presented above for the optimum dither size fixed the control loop response to be faster than the crosspole (and signal fading) rate of change so that such changes could be accurately tracked by the correction network. This defined the dither size and integrator gain and gives the time constant of the control loop (for ρ large) as $t_c \simeq 5$ ms. If the weights are not going to follow the dither (i.e., for the dither not to generate additional weight jitter), then the dither rate should be fast compared to this time constant. On the other hand, the dither should be slow compared to the AGC response time so that the AGC can track the variation in desired signal level due to the dither. The AGC response time must be fast relative to the desired signal fluctuations, but slow compared to the symbol rate since the interference due to crosspole is at this rate and the AGC must not track out this interference. These relations can be summarized in terms of the recommended bandwidths shown in Table 3.4.3-1.

Table 3.4.3-1. Relative Bandwidths

Signal Fluctuations	10 Hz
Control Loop BW	320 Hz
Dither Rate	$\sim 0.1\, B_{AGC}$
AGC BW	$B_{AGC} << B_{IF}$
IF BW	B_{IF}

84
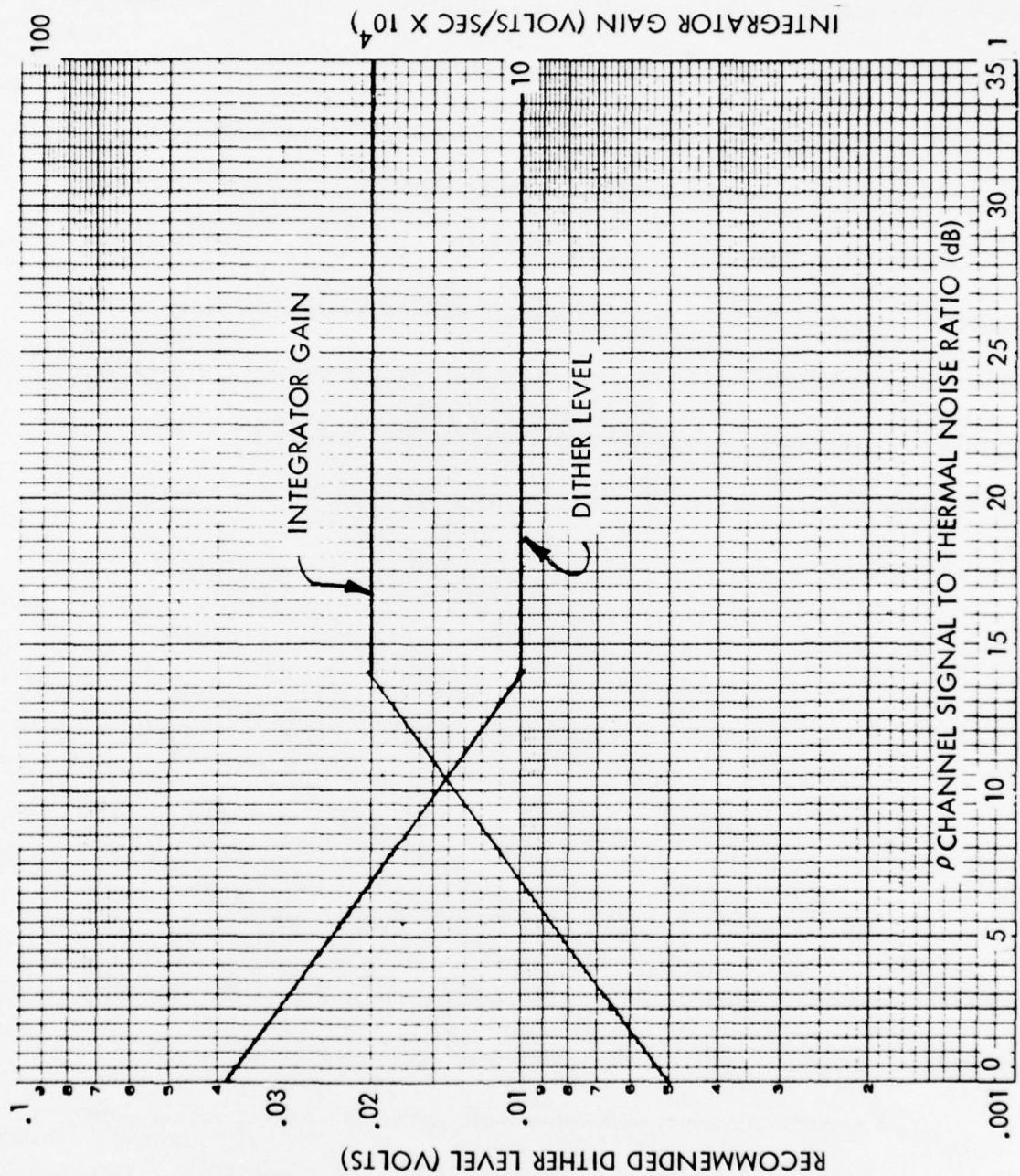
Figure 3.4.3-2. Recommended Dither Level and Integrator Gain

85

3.4.4   Extension to Multitap Control

The control technique and parameter values discussed in the preceeding paragraphs were derived for use with the single-tap correction network, however, the extension of this technique to the multitap case is straightforward. For the multitap case the control hardware designed above will be multiplexed between the three complex weights as illustrated in Figure 3.4.4-1. This technique utilizes the same control and interference measurement techniques, and the parameter values selected above will be the same, except that different control loop integrator gains (termed A_1, A_2 and A_3 in the figure) will be required. This is necessitated by the fact that the power levels into each of the three weights will be different. Referring to Figure 3.4.4-1 these power levels can be derived as

$$P_1 = E\left[x(t-T) \ x^*(t-T) \right] \approx R(0)$$

$$P_2 = E\left[\left\{ x(t) - x(t-2T) \right\} \left\{ x(t) - x(t-2T) \right\}^* \right] = 2\left[R(0) - R(2T) \right]$$

$$P_3 = E\left[\left\{ x(t-T) - \frac{x(t)}{2} - \frac{x(t-2T)}{2} \right\} \left\{ x(t-T) - \frac{x(t)}{2} \right. \right.$$

$$\left. \left. - \frac{x(t-2T)}{2} \right\}^* \right] = \frac{3}{2} R(0) - 2R(T) + \frac{R(2T)}{2}$$

where R is the correlation function of the channel signal $x(t)$. Given the time delay T and assumed expressions for $x(t)$, these power levels could be calculated.

An easier approach is to measure these power levels using the simulation in Section 4.0. These measurements give $P_1 = 0.90$, $P_2 = 0.12$ and $P_3 = 0.003$, and

Figure 3.4.4-1 Time Multiplexed Control of Special Multi-tap Network

87

can be used to select the gains A_1, A_2 and A_3. Note that the control of w_1 will be identical to the single tap case, since this weight still controls the frequency independent phase and amplitude level, which gives $A_1 = \beta$. Also, a possible disadvantage of moving w_1 outside the w_2 and w_3 weights is indicated by this discussion (see also Paragraph 3.2.2.1), since the level of w_2 will influence the gains in the w_2 and w_3 loop. This could require that the gains A_2 and A_3 be set as a function of w_1, but for the simulation used in Section 4.0, it was assumed that w_1 was constant at 0.2. This is a good assumption if w_1 is adjusted first and allowed to reach its approximate steady state value (in the simulations this was about -0.2) before w_2 and w_3 are adjusted. Consequently, to equalize the voltage gain in each loop

$$A_1 = \beta$$

$$A_2 = \frac{\sqrt{P_1}}{0.2\sqrt{P_2}}\,\beta \approx 15\beta$$

$$A_3 = \frac{\sqrt{P_1}}{0.2\sqrt{P_3}}\,\beta \approx 100\beta$$

4.0   COMPUTER SIMULATIONS

In the previous section the detailed design and analysis of an adaptive crosspole interference reduction technique was presented. The results of that section were a block diagram of a proposed system supported by analysis which defined the system parameter values which would give satisfactory performance. The purpose of this section is to present the results of computer simulations which confirm the design and analysis of that section. The first part of this section presents typical simulation results for the designed system using both the single and multi-tap correction networks. Results are presented to support the conclusions concerning the steady-state, optimal weight analysis and the dynamic transient performance of the system. The presentation of these results are followed by a detailed description of the various computer programs which were developed and a tabulation of additional computer runs.

4.1   Typical Simulation Results

4.1.1   Steady-State Performance

The utility of the computer simulation investigating the steady-state performance is twofold. First, it allows a confirmation of the steady-state performance analysis presented in Paragraph 3.3 and secondly, it develops the weight values which the dynamic simulation should approach, thereby providing a check on whether or not those programs are working correctly.

4.1.1.1   Single-Tap Network Results

For the single-tap network a computer program was developed which determined the optimal correction network weight values by using a random search optimization routine. This program was used to generate the curves presented in Figure 4.1.1.1-1. Part a. of the figure shows the output signal-to-thermal noise plus crosspole noise versus the input signal-to-thermal noise ratio, both with and without the use of the correction network, thereby indicating the gain to be had using the adaptive correction network. (Also see Figure 3.3.2-2). These curves are for equal crosspole coupling on each channel at 10 dB below the desired signal level ($E_v = E_n = .2236 + j.2236$). The optimal weights for the same crosspole interference are shown in part b where the real and imaginary parts are equal with magnitudes of 0.2236 for high S/N ratios where the crosspole interference is eliminated completely, but for low S/N the real part goes to zero. These specific weight values are due to the relative phase of the crosspole interference on each channel (in this case equal) and the particular compromise between crosspole interference elimination and the thermal noise and desired signal enhancement introduced by the correction network. Different crosspolar coupling would change part b of the figure, but the general characteristic that the weights approach constant values for high signal-to-noise ratio would be preserved.
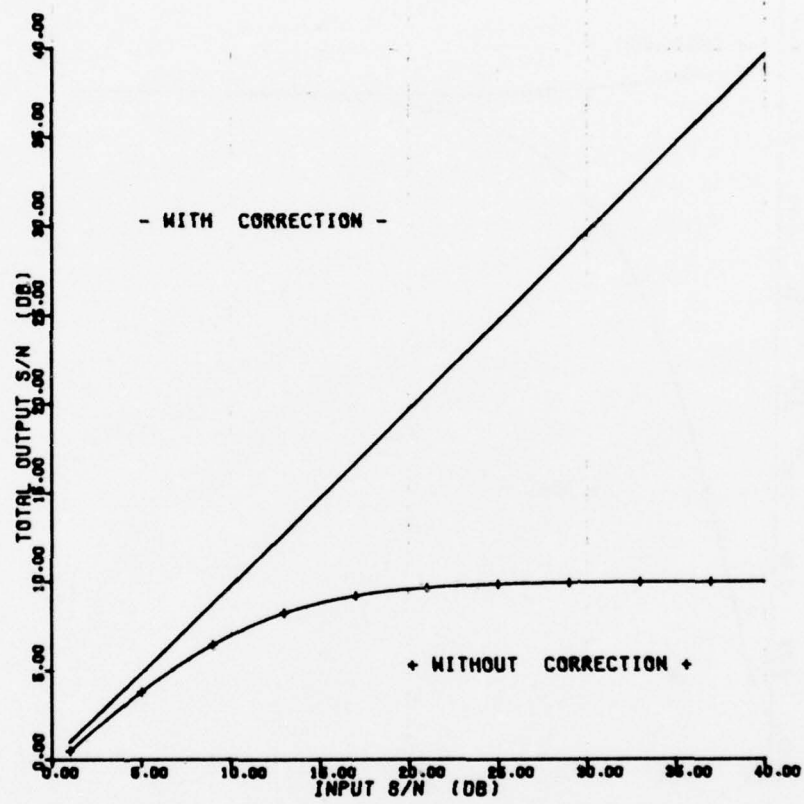
Figure 4.1.1.1-1 a   Output S/N

91
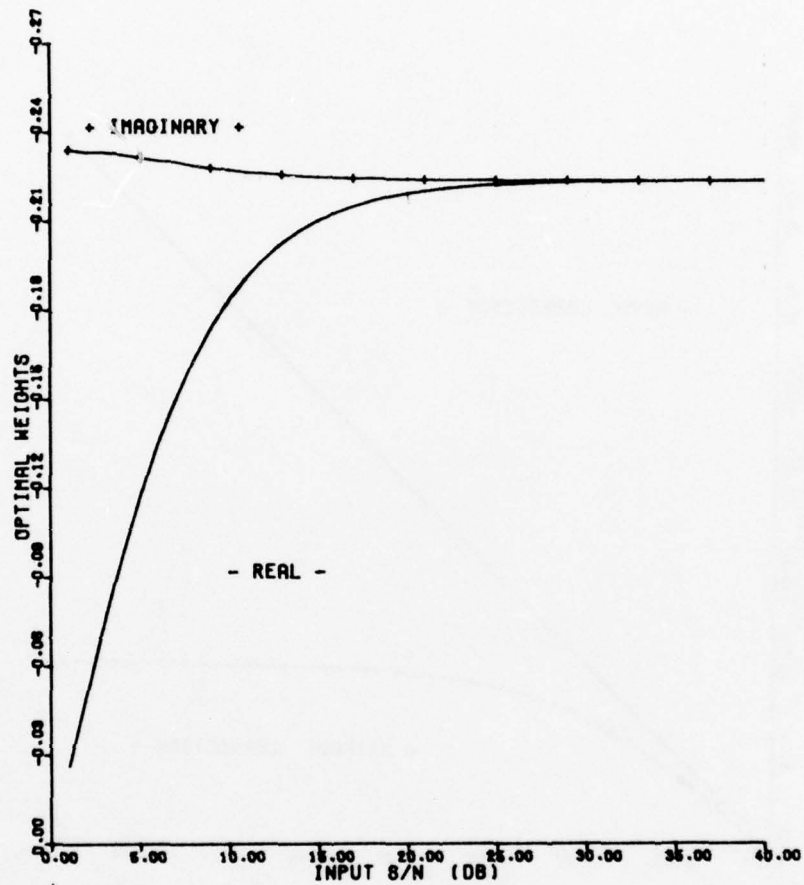
Figure 4.1.1.1-1 b   Optimal Weights vs Input S/N
for Crosspole Interference 10 dB below desired signal level
(ie, $E_v = E_h = .2236 + j .2236$)

92

4.1.1.2   Multi-Tap Network Results

For the special multi-tap network the derivation of the optimal weight values is more difficult and is dependent on a more complex interference scenario which must include the dispersive effects of the transmission media. However, if the model for this dispersive crosspole interference is specified, then the weights which give zero crosspole interference can be derived. As shown in Paragraph 3.3.2, for large channel signal-to-thermal noise ratios, zero crosspole interference and maximum output signal-to-noise ratio give very nearly the same performance. This result was for the single-tap network, but the principle is generally true. Consequently, the weights which give zero crosspole should indicate the best achievable output signal-to-noise ratio.

Referring to the model for the transmission media and correction network shown in Figure 3.2.2-1, the weights which eliminate the crosspolar coupling are given by

$$w_{21}(\omega) = - \frac{H_{21}(\omega)}{H_{11}(\omega)} \tag{4-1}$$

For the special multi-tap correction network the frequency response is given by (see Paragraph 3.2.2-1)

$$w_{21}(\omega) = \left[-w_1 w_2 - \frac{w_1 w_3}{2} \right] + \left[w_1 + w_1 w_3 \right] e^{-j\omega t} + \left[w_1 + w_2 - \frac{w_1 w_3}{2} \right] e^{-2j\omega t}$$

93

$$= \left[-w_1\, w_2\; -\; \frac{w_1\, w_3}{2} \right]\; +\; \left[w_1\; +\; w_1\, w_3 \right]\; Z^{-1} \qquad (4\text{-}2)$$

$$+\; \left[w_1\, w_2\; -\; \frac{w_1\, w_3}{2} \right]\; Z^{-2}$$

where $Z^{-1} = e^{-j\omega t}$. From Paragraph 4.2.1 the model for the input signal simulation specifies $H_{21}\,(\omega) = A = (.2236 + j\, .2236)$

and

$$H_{11}\,(Z) = \frac{\left(1 - \alpha_1\right)\,\left(1 - \alpha_2\right)}{1 - \left(\alpha_1 + \alpha_2\right)\; Z^{-1} + \alpha_1\, \alpha_2\; Z^{-2}} \qquad (4\text{-}3)$$

where $\alpha_1 = .5$ and $\alpha_2 = .5$. Using these expressions to form Equation 4-1 and equating like powers of Z gives a set of algebraic equations which can be solved for the optimum weight values. This solution gives

$$w_1 = -A = -.2236 - j\, .2236$$

$$w_2 = \frac{1 - \alpha_1\, \alpha_2}{2\,(1 - \alpha_1)\,(1 - \alpha_2)} = 1.611 + j0.$$

and

$$w_3 = \frac{-\,(1 + \alpha_1\, \alpha_2)}{(1 - \alpha_1)\,(1 - \alpha_2)} = -5.67 + j0.$$

94

Finally, referring to the computer model for the correction network in Paragraph 4.2.2 indicates that there are two sets of weights which the simulator will develop. For the case where the control loop gains are set such that $A_1 = \beta$, $A_2 = 15\beta$ and $A_3 = 100\beta$ (as prescribed in Paragraph 3.4.4)

$$w_1 = -.2236 - j\,.2236$$
$$w_2 = .107 + j0.$$

and

$$w_3 = -.0567 + j0.$$

Another case which was also used in some of the simulations was for $A_1 = \beta$, $A_2 = 5\beta$ and $A_3 = 10\beta$ giving

$$w_1 = -.2236 - j\,.2236$$
$$w_2 = .322 + j0.$$

and

$$w_3 = -.567 + j0.$$

To study the steady-state behavior of the special multi-tap network, the weights were initialized at their optimum values and the simulations were run. (The cases to be reported were for signal-to-thermal noise of 15 dB and signal-to-crosspole interference of 10 dB, with the dispersion model discussed in the last paragraph). First the control loops were left off so that the weights remained constant and the optimum output signal-to-noise was measured as 14.4 dB. In subsequent runs the control loops were turned on and

95

the weights allowed to seek their own levels. Figure 4.1.1.2-1 illustrates the resulting output signal-to-noise ratio, while Figures 4.1.1.2-2 and 4.1.1.2-3 shows the weight trajectories.

As shown on the figures, runs were made for cases with and without compensating delay. This refers to the use of delay in the channel to be corrected, before the output of the correction network is added in, to compensate for the time delay through the correction network. It might be expected that this would give improved performance, but this was not noticed in the simulations. The optimum weights were derived for the case without delay, and the figures indicate for that case the weights fluctuate around the optimum values. On the other hand, for the cases with the delay added, the weights seek slightly different values, but did not indicate better output signal-to-noise ratio.

Figures 4.1.1.2-4 shows a computer plot where the weights were again initiated at their optimum values, but a small dither level $\Lambda = 0.001$ was used, while the loop gains remained the same as in the last set of figures. It would be hoped that a small dither level would give better performance (less weight jitter), but this dither was too small, as the loops were unable to maintain a good output signal-to-noise ratio. The complete data output for this case is shown in Figure 4.3.2.2-1 where the weights can be seen to wander off the optimum values.

4.1.2   Dynamic Performance Results

To illustrate the dynamic performance of the simulated interference reduction techniques the correction network weights were set at zero and the resulting weight

96
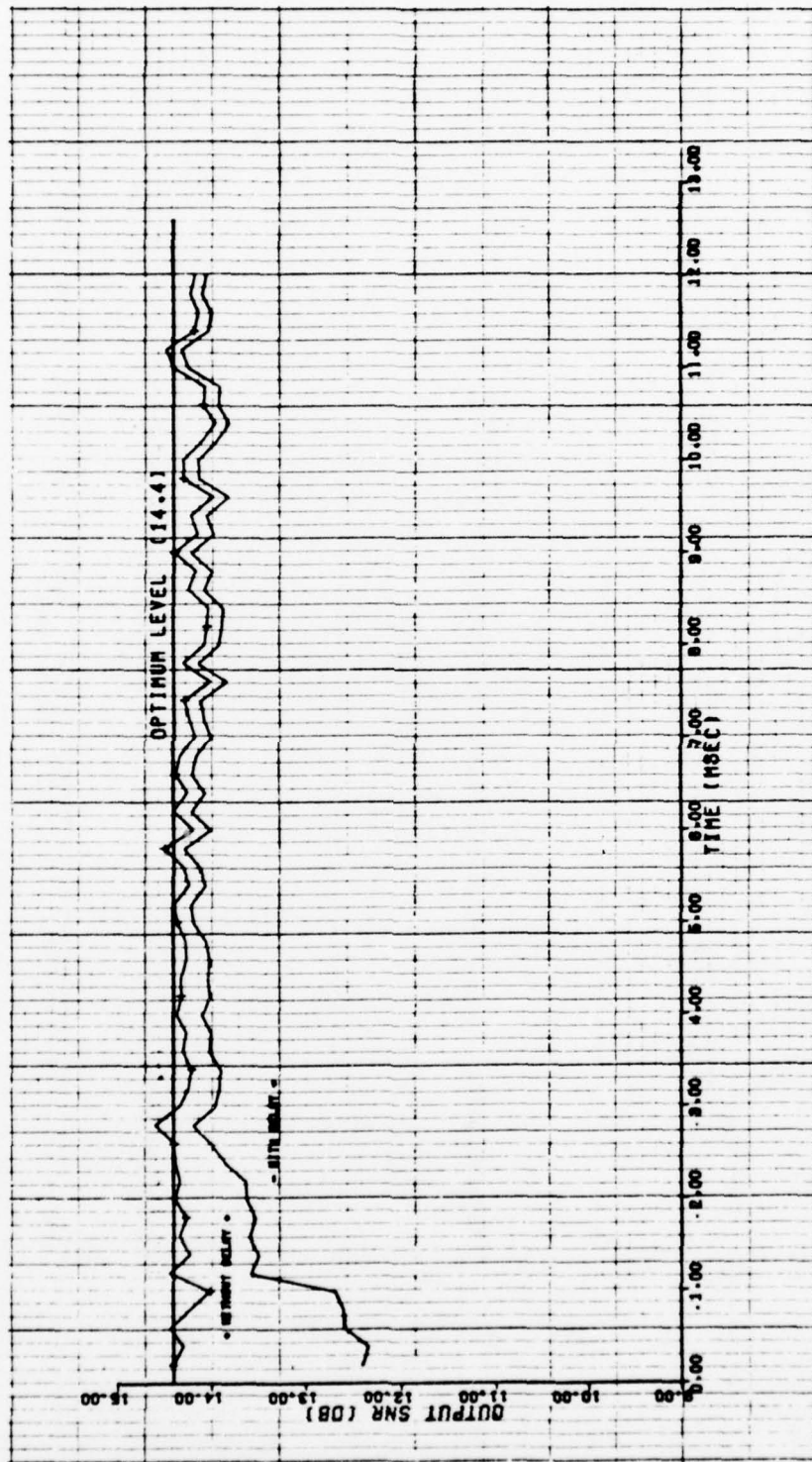
Figure 4.1.1.2-1 Steady State Performance of Special Multi-Tap Network. (With and Without Compensating Delay).
Control Loop Gains $A_1 = \beta$, A_2 15β and $A_3 = 100\beta$. $\Delta = .01$

97
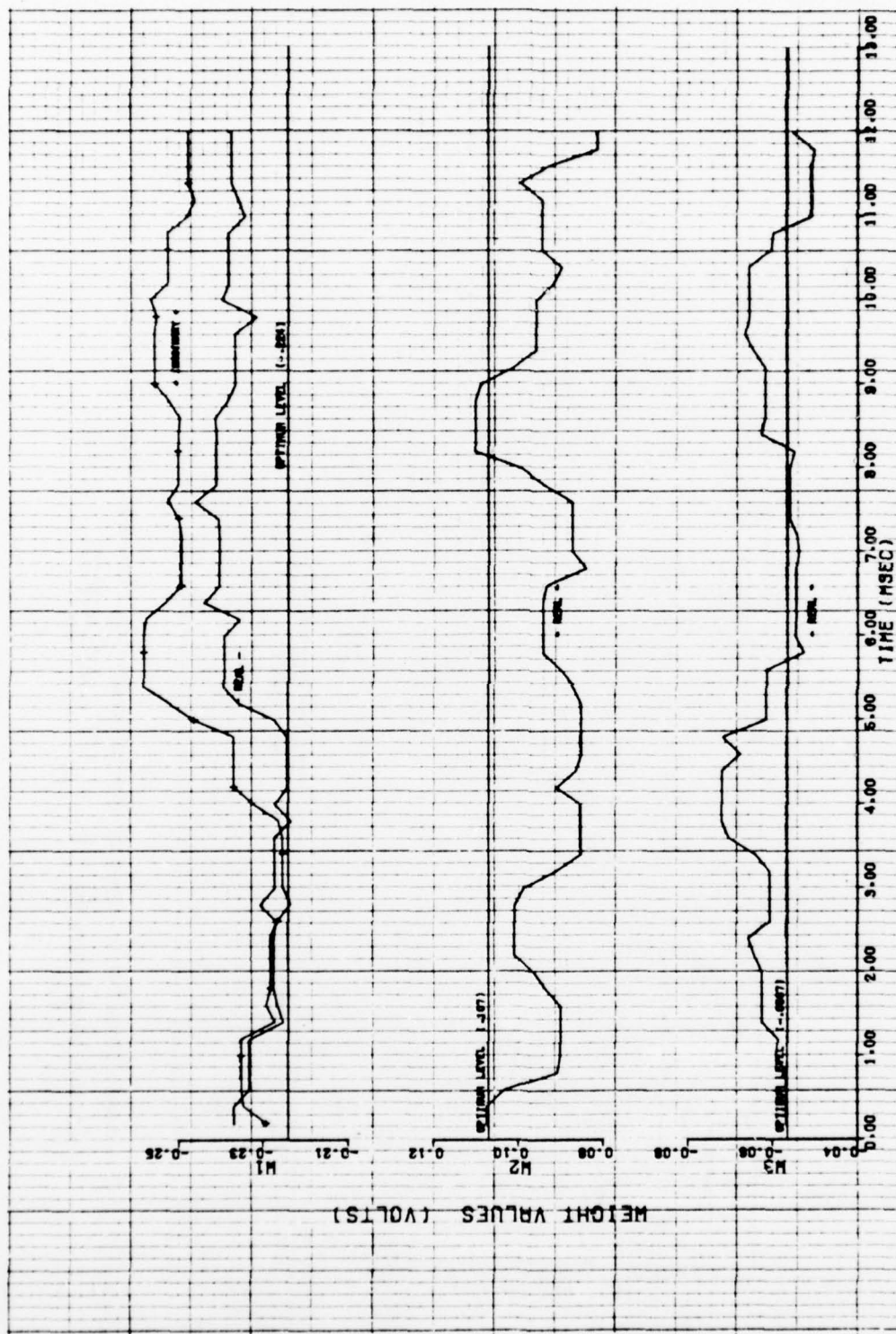
Figure 4.1.1.2-2 Steady State Weight Values for Special Multi-Tap Network (Without Compensating Delay).
Control Loop Gains $A_1 = \beta$ $A_2 = 15\beta$ and $A_3 = 100\beta$

98

Figure 4.1.2-3 Steady State Weight Values for Special Multi-Tap Network (With Compensating Dealy).
Control Loop Gains $A_1 = \beta$ $A_2 = 15\beta$ and $A_3 = 100\beta$

99

X - POLE TRANSIENT RESPONSE
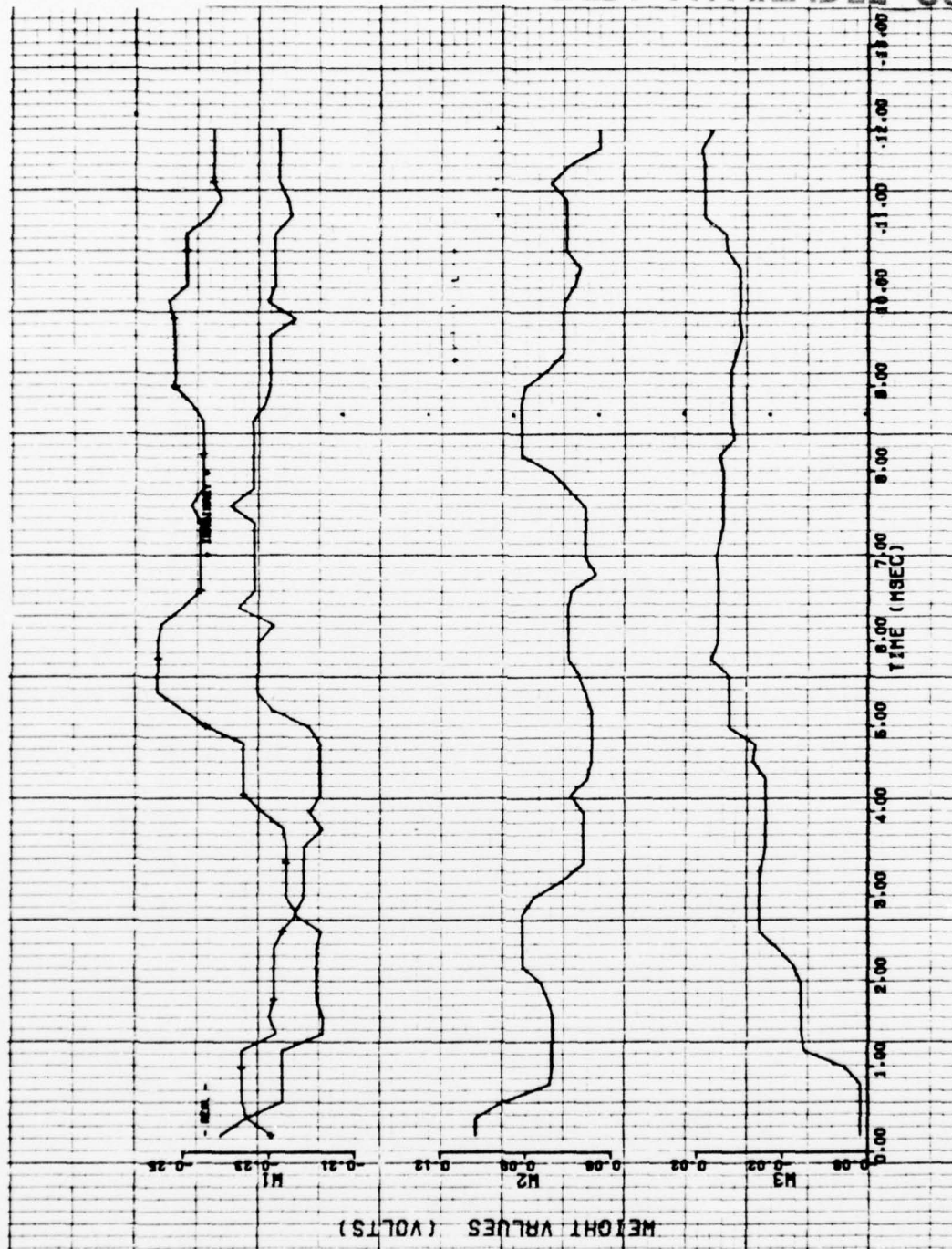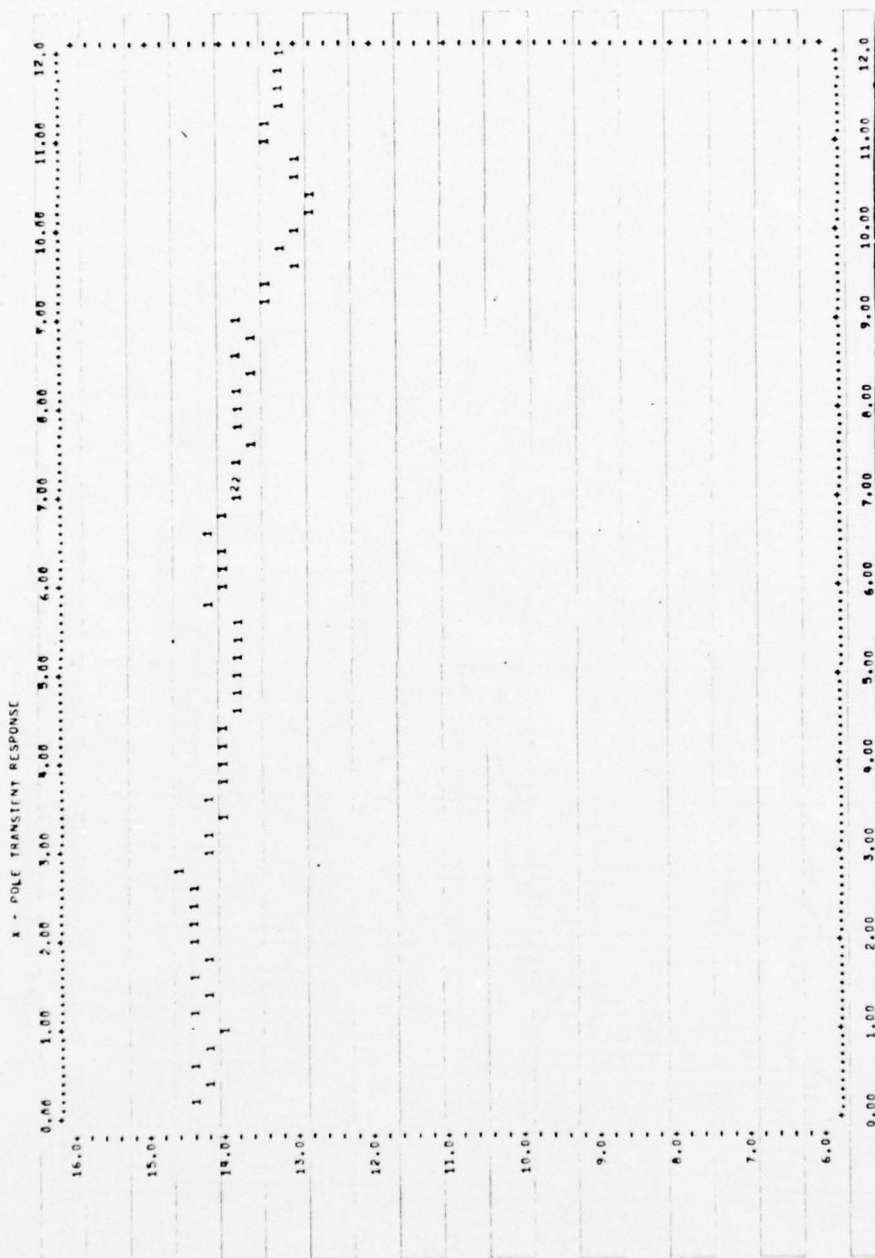
Figure 4.1.1.2-4 Output SNR (dB) vs time (msec) for Steady State Performance with Small Dither Level ($\Delta = .001$). $A_2 = 15\beta$ and $A_3 = 100\beta$.

100

trajectories and output signal-to-interference levels were recorded. Representative cases are reported in this section, and the data from a number of other simulation runs is also compiled in Paragraph 4.3.

4.1.2.1   Single-Tap Results

Transient performance simulations were run for a number of different crosspole powers and channel signal-to-thermal noise ratios. In each case close agreement with the analytical results and satisfactory performance were obtained. Typical results showing the weight trajectories for 14 Mb/s bit rate and SNR (ρ) of 15 dB are presented in Figures 4.1.2.1-1 and 4.1.2.1-2. Both these figures are for runs where the crosspole interference was 10 dB below the desired signal, the channel signal-to-thermal noise ratio was 15 dB (giving optimum weight values of $w_i = -.209$ and $w_2 = -.225$) and the weights were initially set at zero. Figure 4.1.2.1-1 illustrates a case where the optimum dither size of $\Lambda = 0.00688$ was used (see Figure 3.4.3-1), while Figure 4.1.2.1-2 uses a more practical dither size of $\Lambda = 0.026$ (see discussion in Paragraph 3.4.3). For both cases $\Lambda \beta = 2000$, as derived in Paragraph 3.4.3, which should give a time constant of 0.5 ms. That is, the weights should reach 63.2 percent of their final magnitude of about 0.21 (approximately 0.14) in .5 ms. The curves in Figure 4.1.2.1-2 are very close to this value. On the other hand, the results in Figure 4.1.2.1-1 are more erratic due to the unnecessarily small dither size. Detailed computer outputs for these cases are presented in Paragraph 4.3.1.2, Figures 4.3.1.2-1 and 4.3.1.2-2. These figures display the weight standard deviations which are in close agreement with the values plotted in Figure 3.4.2-1.

101
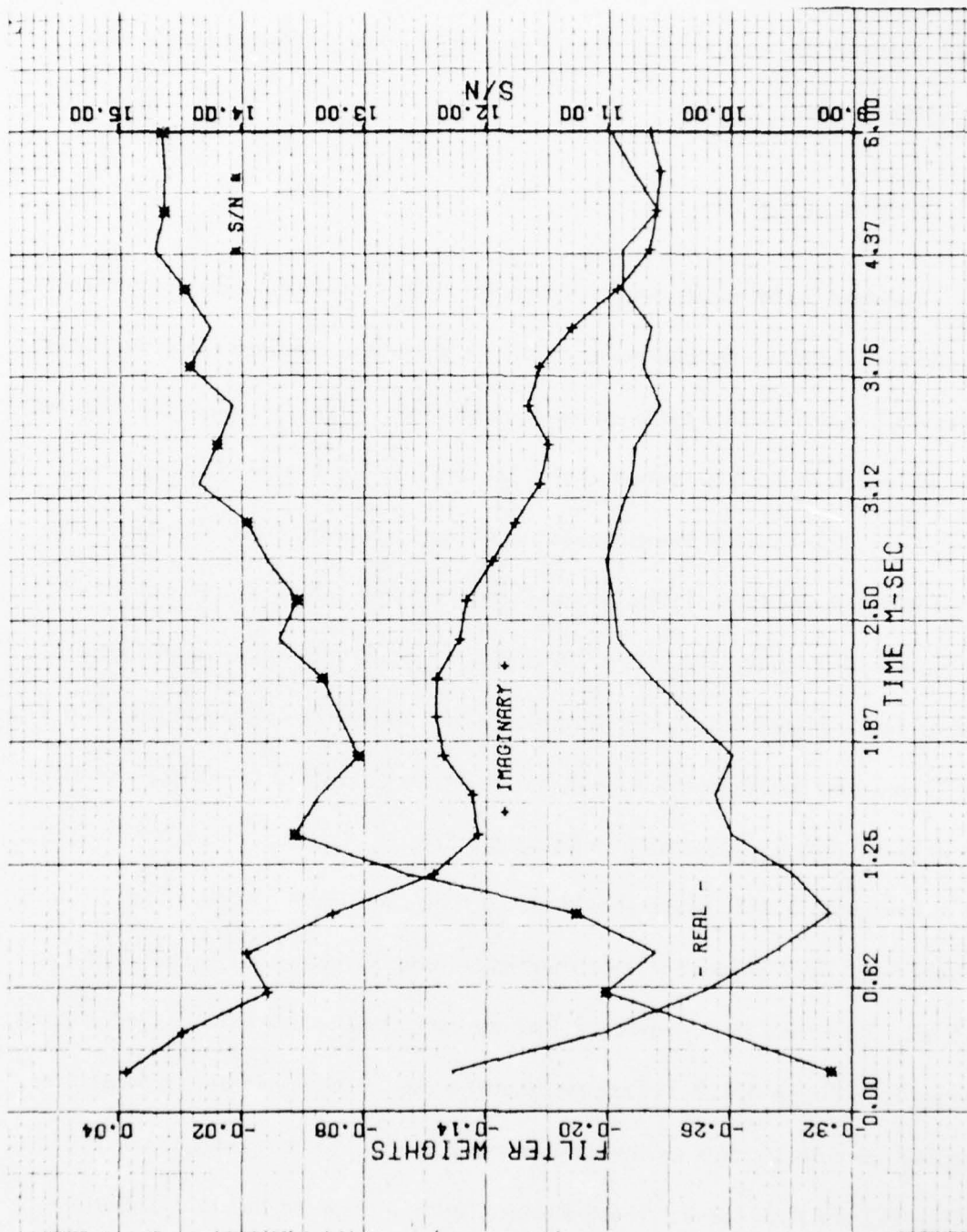
Figure 4.1.2.1-1 Weight Transients and Output S/N Ratio Using Optimum Dither Size ($\triangle = .00688$) for 10dB Crosspole and 15dB Channel SNR.

102
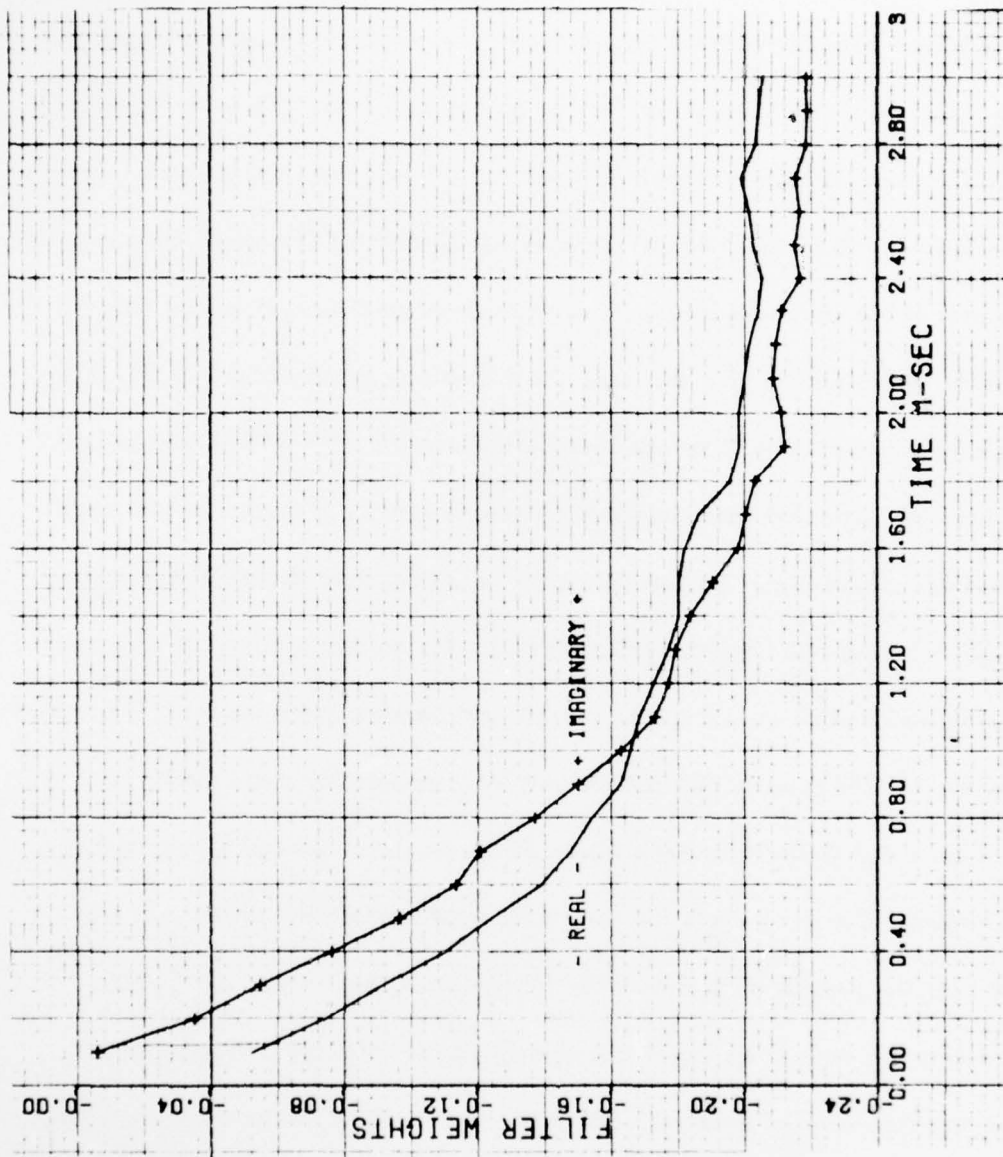
Figure 4.1.2.1-2 Weight Transient using more Practical Dither Size ($\Delta = .026$) for 10dB Crosspole and 15dB Channel SNR.

103

4.1.2.2   Multi-Tap Results

A number of transient performance simulations were also run using the time multiplexed control of both the conventional tapped delay line and the special multi-tap correction networks. A typical simulation for the special multi-tap case is presented in Figure 4.1.2.2-1 where the output signal-to-noise ratio versus time is displayed. Again, this simulation is for 15 dB channel signal-to-noise ratio, with 10 dB crosspole, where the dispersive features of the crosspole interference were developed using a second order filter as discussed in the next section. For this case the dither size was set at $\Delta = 0.01$, with each weight being adjusted for 4.2 ms and then held while the next weight was adjusted. This is larger than the expected time constant of approximately 0.5 ms and allows each weight to reach its optimum value before the next one is adjusted. Figure 4.1.2.2-2 shows the weight response and confirms that they reach the correct values. In this manner, the contribution of each weight to the overall performance improvement is illustrated since the network was designed so that the weights were essentially uncoupled.

Figure 4.1.2.2-3 is a compilation of the results of several other transient response simulations. Curve 1a shows the results for a case where the dither size was twice that used for the simulation presented in the last paragraph (i.e., $\Delta = 0.02$). (Curve 3 represents this case.) As expected, the signal-to-noise ratio improves more rapidly, however, the detailed data indicates poorer steady-state performance and more irregular weight trajectories (see Figure 4.3.2.2-2). Part b of curve 1 is for a case where the first weight is moved back within the second and third weight loops (see Figure 3.2.2.1-2) and as would be expected, the w_2 response is faster since the loop

104
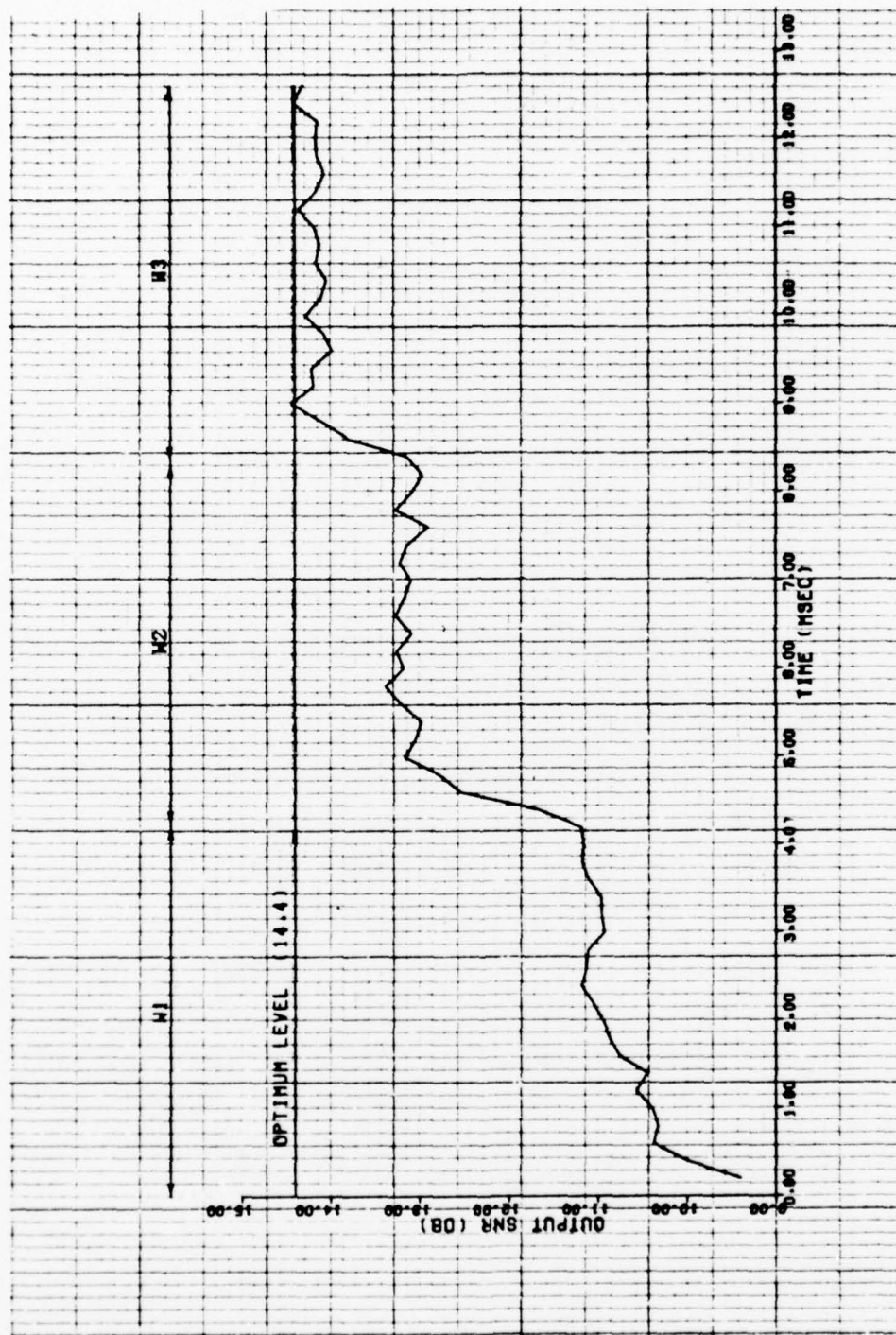
Figure 4.1.2.2-1 Transient Performance of Special Multi-Tap Network (Without Delay).

105
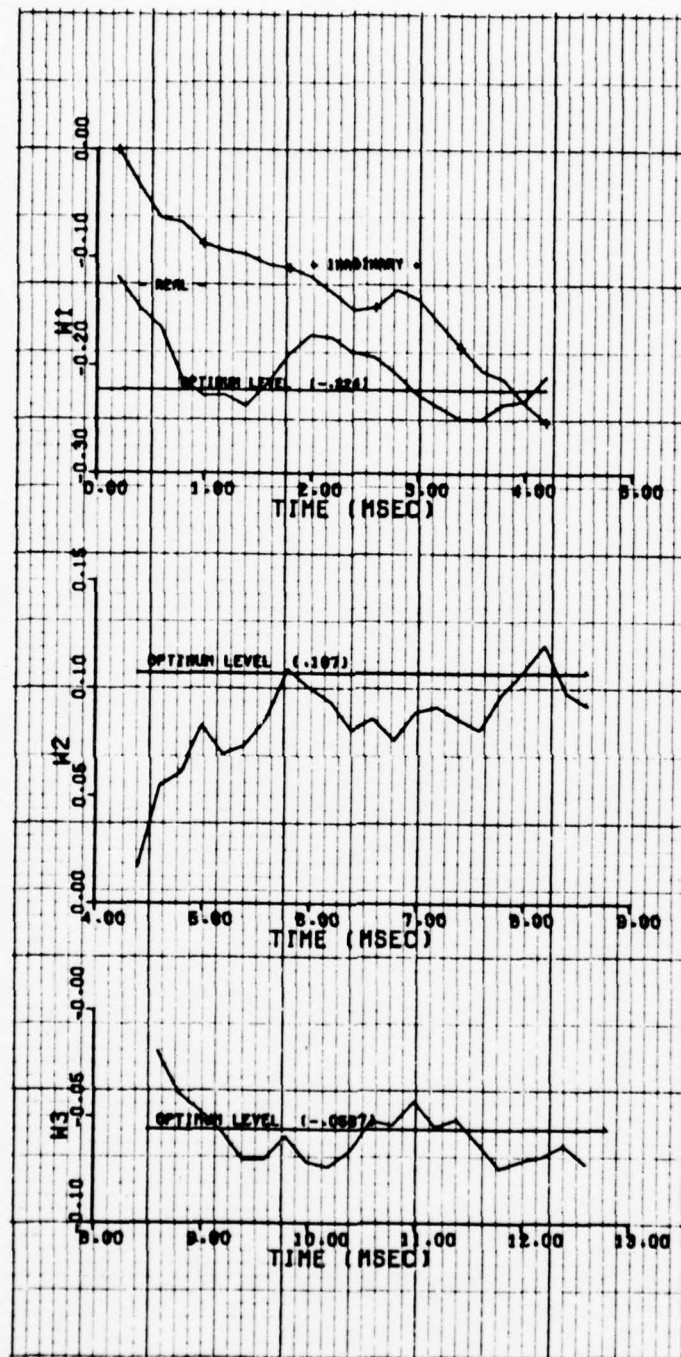
Figure 4.1.2.2-2   Transient Weight Values
for Special Multi-Tap Network (Without Delay).

106
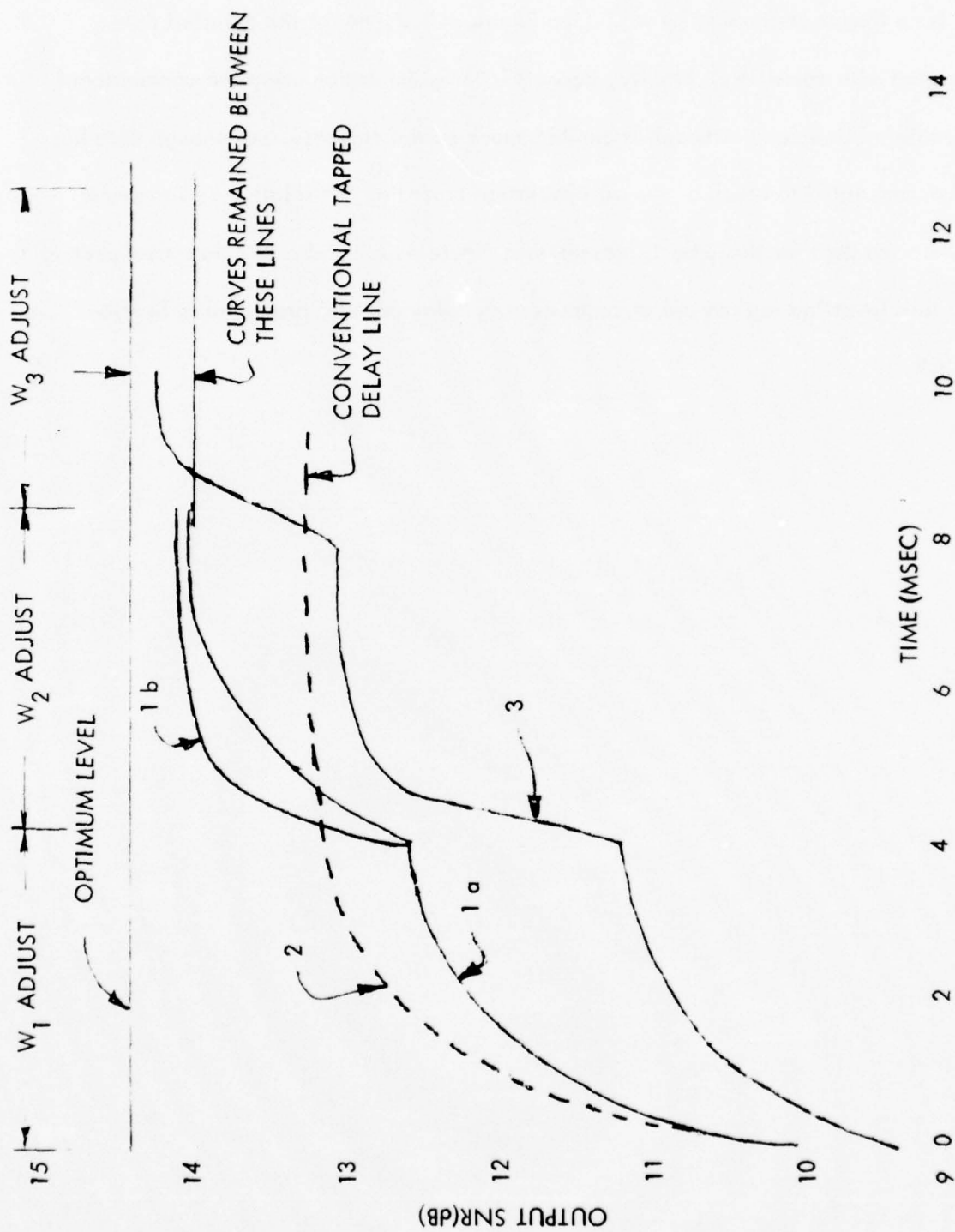
Figure 4.1.2.2-3 Representative Data From Several Multi-Tap Network Transient Performance Simulations

107

gain is no longer attenuated by w_1. (See Figure 4.3.2.2-4 for the detailed data associated with curve 1b.) Finally, curve 2 is for a simulation using the conventional tapped delay line, and although it exhibits much poorer response, not enough data has been accumulated to reach a general conclusion regarding the relative performance. The detailed data for this case is presented in Figure 4.3.2.2-5. The data from several other runs investigating the use of compensating delay are also presented in Section 4.3.2.2.

4.2 Computer Program Description

In this paragraph the computer programs used to generate the data presented in the last section are described in detail. Figure 4.2-1 is a block diagram of the computer program used for the single-tap network simulation. This diagram also formed the basis for the multitap network simulation, where the interference measurement and control network simulations were identical and time shared between the three complex weights. However, the input signals and correction networks themselves had to be modified as described below. Listings of the programs discussed in this section are shown in the next section, along with sample outputs.

4.2.1 Input Signal Simulation

Throughout the simulation the signals are modeled using complex numbers to represent their complex envelopes at baseband. For the single-tap network simulation, the desired signal on the horizontal channel (SH) is defined as unity while the vertical channel desired signal SV is $e^{i\theta}$ where θ is randomly selected at each iteration from $(0, \pi/2, \pi, 3\pi/2)$. This procedure simulates the quadraphase modulation with the required statistical independence between SH and SV. At each iteration 4 random numbers $TN(I)$, $I = 1, 4$ are generated from a normal distribution of zero mean and standard deviation ST (selected to give the specified signal-to-thermal noise ratio ρ), with the vertical channel thermal noise being given by $TNV = TN(1) + iTN(2)$ and the horizontal being $TNH = TN(3) + iTN(4)$. This defines the seconds per iteration (absolute time) since one of these independent noise samples is selected for each bit of data.
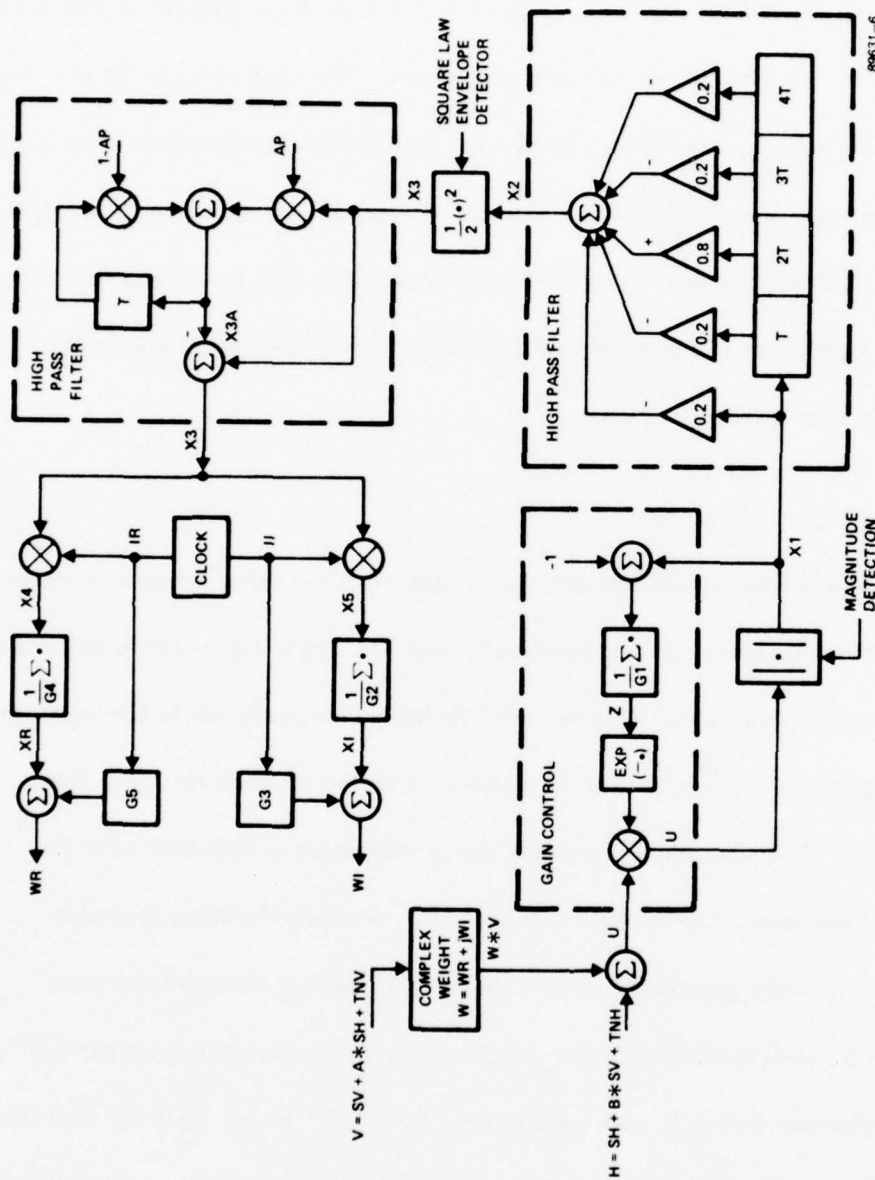
Figure 4.2-1 Computer Program Block Diagram for Single-Tap Network Simulation

110

Finally, the crosspole signals are computed as A * SH for the vertical channel and B * SV for the horizontal channel where A and B are complex coupling coefficients. Consequently, the total vertical channel signal is V = SV + A * SH + TNV while the horizontal is H = SH + B * SV + TNH.

For the multitap program the input signal simulation had to be completely changed. To simulate the differentially dispersive nature of the channel, the crosspole coupling signal had to have a frequency response different from the channel signal. Also, rather than using a single sample per bit, this required the use of 10 samples per bit, and the various accumulator gains had to be reduced by this factor to maintain the same relative parameter values. Figure 4.2.1-1 illustrates the resulting input signal simulation, where a second-order channel frequency response is simulated using two first-order recursive filters in series. To simulate thermal noise with the required correlation, independent random numbers were passed through a 10-sample aperture filter.

4.2.2   Correction Networks

Simulation of the single tap correction network is simply a complex number used to multiply the vertical channel signal before addition into the horizontal. Similarly, the conventional tapped delay line simulation is also trivial and is included in the subroutine CORTAP. The special multitap network simulation is shown in Figure 4.2.2-1. The gains A and B shown in the figure were used to adjust the gains for the entire loop. That is, the control loop integrator had gain β ($\frac{1}{G2}$ and $\frac{1}{G4}$ in the simulations), which was fixed; and changes in loop gain for each separate weight control
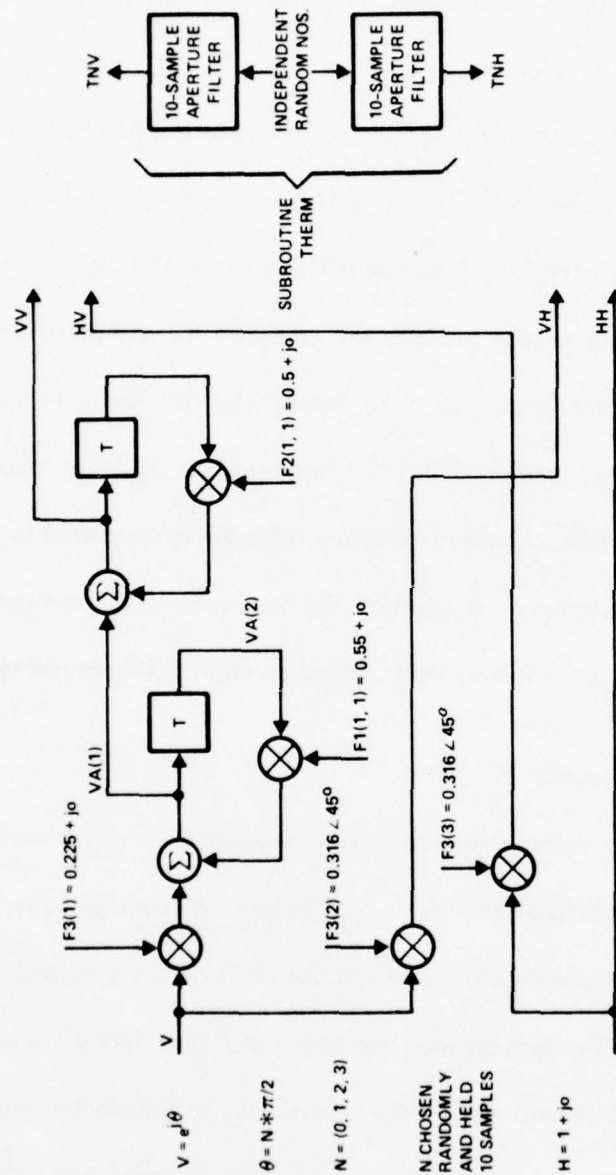
111

Figure 4.2.1-1 Input Signal Simulation

89631-1

112
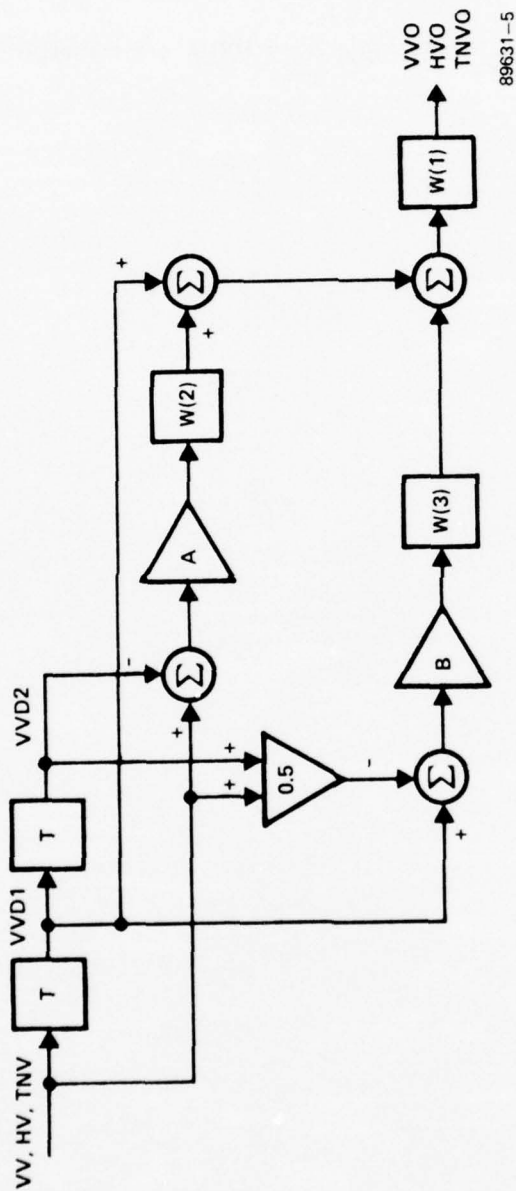
Figure 4.2.2-1 Special Multi-tap Network Simulation- Subroutine CORNET.

89631-5

113

were affected by setting A and B. For example, to change the control loop gains during

the multiplexed control of each separate weight, as described in Paragraph 3.4.4, A

was set to 15 and B was set to 100. These are relative to unity in the W_1 loop, and give

the control loop gain $A_1 = \beta$, $A_2 = 15\beta$ and $A_3 = 100\beta$ prescribed in Paragraph 3.4.4.

4.2.3   Interference Measurement

The interference measurement circuit was simulated for the single-tap program as shown in Figure 4.2-1. The gain control amplifier was modeled with gain $G = EXP(-Z)$ where Z was an average of the difference of the output $X1$ of the magnitude detector from unity. Thus, $X1$ tended to be of unit magnitude where the LPF for the averaging was modeled as an integrator. As mentioned in Paragraph 3.4.3, the AGC bandwidth should be much less than the IF BW, to avoid tracking out the fluctuations due to the interference which must be measured, so the gain of the integrator (accumulator) was set at 0.01 ($GI = 100$) which gives an AGC BW on the order of one percent of the IF BW. This is followed by the AC coupling filter which is simulated as a five-tap non-recursive low pass filter subtracted from unity to give a high pass characteristic. This filter should eliminate the DC term due to the desired signal at the output of the first detector, while passing most of the fluctuations due to the noise. The use of five-taps should pass a significant portion of the noise energy while eliminating the DC terms. Finally, the high pass filter output $X2$ is squared and multiplied by 1/2 to simulate the square law envelope detector with output $X3$.

The only modifications made for use with the multitap simulation are that the AC coupling filter is modeled with a recursive filter structure (as shown in the listing in Paragraph 3.3.2.1) and the accumulator gain $1/GI$ is reduced by a factor of 10 since there are 10 iterations per bit rather than one.

115

4.2.4 Control Logic

The output of the interference measurement device, X3 (J(w)) is used to generate a signal proportional to the gradient $\frac{\partial J}{\partial w}$. As discussed at the end of Paragraph 3.2.4, X3 is first passed through a high pass filter to suppress the dc level into the synchronous detectors. This filtering is simulated with a low pass recursive filter whose output X3 A is subtracted from X3. Since the DC level to be suppressed is already quite small, the high pass filter can have a low cut-off frequency, thereby passing most of the fluctuations defining J(w). Consequently, the recursive LPF bandwidth defined by AP = .9998 (gives a time constant of 5000 iterations) is .006 percent of the IFBW. The output of this HPF, again called X3, is then multiplied by the in-phase (IR) and quadrature (II) clock signals to simulate the synchronous detectors. The clock signals simulate the dither waveforms and are generated using a subroutine called CLOCK which outputs IR and II as two 90° out of phase sequences of + and – ones. The dither rate is defined by twice IS which defines the total number of iterations each sequence remains at each polarity. In keeping with the discussion in Paragraph 3.4.3 (Table 3.4.3-1), the dither period was selected as 1000 iterations (IS = 500) which defines the dither rate to be $\frac{1}{500}$ th of the IF BW. The outputs of the synchronous detectors associated with the real (X4) and imaginary (X5) parts of the weights then pass to accumulators to simulate the integrators of the control loop whose gains $\frac{1}{G2}$ and $\frac{1}{G4}$, both equal β. The dither amplitudes are G3 and G5 and are added to the outputs of the accumulators, XR and XI, to form the weights WR and WI. Use of this simulation with the multitap

116

program required only that the accumulator gains be reduced by a factor of 10, as discussed above.

4.2.5   Optimum Weight Computation

The optimum weight values WO for the single-tap network, are computed by a subroutine called OPTW. This subroutine utilizes a simple deterministic search optimization procedure which successively steps either up or down along the coordinates of the two dimensional space defined by the complex weight. (Thus four search directions are defined by DW(I), I = 1, 2, 3, 4). At each step the value S of the output SNR is computed by a separate subroutine called SSSN, with steps in successful directions (larger S) being continued with the step size DA being increased by A. (The initial step size A = .00001 is returned to after an unsuccessful step, with this quantity defining the granularity of the search.)

4.3   Program Listings and Auxilliary Data

This paragraph presents the computer program listings, along with some samples of the computer output. Also, some of the data plotted in Paragraph 4.1 is included in more complete form, together with additional data and computer plots not included in that section.

4.3.1   Single-Tap Simulation

4.3.1.1   Single-Tap Program Listing

```
C        ADAPTIVE CROSSPOLE CANCELLATION SIMULATION  -  SINGLE - TAP
         DIMENSION TN(4),Y(5)
         COMPLEX A,B,V,H,WO,W,SV,U,E,TNV,TNH,SHO,TNO
         CALL RANUP(1.)
         CALL RANVP(1.)
C        DEFINE PROGRAM CONTROL PARAMETERS
         IS = 250
         IPP = 1400
         IOS = 86800
         IR=1
         II=-1
         DR=57.2958
         PI=3.141593
         SR = 7.E6
         TT = 1000. / SR
C        DEFINE GAINS
         G1=100.
         G2 = 35.
         G3 = .01
         G4=G2
         G5=G3
         AP=.0002
         AP1=1.-AP
C        DEFINE INPUT S/N
C        DO 69 ISN=1,40
C        STDB = FLOAT(ISN)
C        STN(ISN) = STDB
         STDB=15.
         ST=10.**(-STDB/20.)
         ST=ST*.7071068
         SH=1.
C        DEFINE CROSS POLE PARAMETERS
         VXM=-10.
         VXP=45.
         HXP=45.
         HXM=-10.
      11 WRITE(6,456)
     456 FORMAT(" XPOLE PARAMETERS ARE")
         WRITE(6,3) VXM,VXP,HXM,HXP
       3 FORMAT(1H ,4F10.5)
         VXM=10.**(VXM/20.)
         HXM=10.**(HXM/20.)
         VXP=VXP/DR
         HXP=HXP/DR
         A=VXM*CMPLX(COS(VXP),SIN(VXP))
         B=HXM*CMPLX(COS(HXP),SIN(HXP))
C        COMPUTE OPTIMAL WEIGHTS AND S/N
         CALL OPTW(WO,SNO,A,B,STDB,AXP)
         WRITE(6,101)
     101 FORMAT(" OPTIMAL WEIGHTS AND OUTPUT S/N ARE")
C        PRINT SIMULATION PARAMETERS
         WRITE(6,511)
```

118

4.3.1.1   (Continued)

```
  511  FORMAT(" DITHER SIZE, GAIN AND S/N ARE")
       WRITE(6,3) G3,G4,STDB
  C       PLOT COMMANDS HAD BEEN USED HERE
       WRITE(6,500)
  500  FORMAT("   TIME(MS)    WRM      WRV      WIM      AIV       SO
      S         NO      XPMSE      S/NO    GAIN")
   10  IQ=IQ+1
       IP=IP+1
  C       COMPUTE INPUT SIGNALS
       DO 1 I=1,4
    1  TN(I)=RANN(0.,ST)
       TH=RANU(0.,4.)
       NTH=TH
       TH=NTH*PI*.5
       TNV=CMPLX(TN(1),TN(2))
       TNH=CMPLX(TN(3),TN(4))
       SV=CMPLX(COS(TH),SIN(TH))
       V=SV+A*SH+TNV
       H=SH+B*SV+TNH
  C       COMPUTE OUTPUT OF HORIZ CHANNEL
       U=H+W*V
       E=(B+W)*SV
       SHO=((1.,0.)+W*A)*SH
       TNO=TNH+W*TNV
       EDM=EDM+REAL(SHO*CONJG(SHO))
       EDV=EDV+REAL(TNO*CONJG(TNO))
       EP=REAL(E*CONJG(E))
       EPP=EPP+EP
  C      INTERFERENCE MEASURMENT
  C      MAGNITUDE DETECTOR - AGC
       U=EXP(-Z)*U
       X1=REAL(U*CONJG(U))**.5
       ZT=(X1-1.)/G1
       Z=Z+ZT
  C      AC COUPLING(BPF)
       DO 5 I=4,1,-1
    5  Y(I+1)=Y(I)
       Y(1)=X1
       X2=.8*Y(3)-.2*(Y(1)+Y(2)+Y(4)+Y(5))
  C       SLED
       X3=.5*X2*X2
       GJ=GJ+X3
  C      HIGH PASS FILTER
       X3A=AP*X3+AP1*X3D
       X3D=X3A
       X3=X3-X3A
  C      SYNCHRONOUS DETECTORS
       CALL CLOCK(IQ,IK,II,IS)
       X4=-X3*IK
       X5=-X3*II
  C      COMPUTE WEIGHT UPDATE
       XR=XR+X4/G4
```

119

4.3.1.1   (Continued)


```
        XI=XI+X5/G2
C       ADD DITHER SIGNAL
        CR=G5*IR
        CI=G3*II
        WR=CR+XR
        WI=CI+XI
        W=CMPLX(WR,WI)
        WRM=WRM+WR
        WIM=WIM+WI
        WRV=WRV+WR*WR
        WIV=WIV+WI*WI
        IF(IP.NE.IPP) GO TO 10
C       OUTPUT DATA
        GJ=GJ/IPP
        EPP=EPP/IPP
        WRM=WRM/IPP
        WIM=WIM/IPP
        WRV=WRV/IPP
        WIV=WIV/IPP
        EDV=EDV/IPP
        EDM=EDM/IPP
        WRV=WRV-WRM*WRM
        WIV=WIV-WIM*WIM
        WRV=SQRT(WRV)
        WIV=SQRT(WIV)
        S1=10.*ALOG10(EDM/(EDV+EPP))
        T=TT*IQ
926     WRITE(6,901) T,WRM,WRV,WIM,WIV,EDM,EDV,EPP,S1,GJ
901     FORMAT(1H ,10F10.5)
        GJ=0.
        IP=0
        EPP=0.
        WRM=0.
        WIM=0.
        WRV=0.
        WIV=0.
        EDM=0.
        EDV=0.
        IF(IQ.GT.IQS) GO TO 56
        GO TO 10
56      CONTINUE
        CALL EXIT
        END
```

4.3.1.1   (Continued)

```
       SUBROUTINE OPTW(W,SP,E,F,ST,AXP)
       COMPLEX DW(4),W,WT,E,F
       W=(0.,0.)
       ST=10.**(ST/10.)
       IT=1
       J=1
       SP=-1000000.
       A=.00001
       DA=A
       DW(1)=(1.,1.)
       DW(2)=(-1.,1.)
       DW(3)=(1.,-1.)
       DW(4)=(-1.,-1.)
   1   WT=W+DA*DW(J)
       CALL SSSN(WT,S,E,F,ST,AXP)
       IF(S.LT.SP) GO TO 10
       SF=S
       DA=DA+A
       W=WT
       GO TO 1
  10   DA=A
       J=J+1
       IT=IT+1
       IF(J.GT.4) J=1
       IF(IT.LT.12) GO TO 1
       SP=10.*ALOG10(SP)
       ST=10.*ALOG10(ST)
       RETURN
       END
```

4.3.1.1   (Continued)

```
SUBROUTINE SSSN(W,S,E,F,ST,AXP)
COMPLEX W,E,F,SNP,AN1,AN2
SNP=(1.,0.)+W*E
AN1=W
AN2=W+F
AXP = REAL(AN2 * CONJG(AN2))
AN = REAL(AN1 * CONJG(AN1)) + ST * AXP
AN=AN+1.
S=REAL(SNP*CONJG(SNP))
S=ST*S/AN
RETURN
END




SUBROUTINE CLOCK(I,IR,I1,IS)
ISO=IS/2
IM=I+ISO
IT1=MOD(I,IS)
IF(IT1.EQ.0) IR=-IR
IT2=MOD(IM,IS)
IF(IT2.EQ.0) II=-II
RETURN
END
```

4.3.1.2   Computer Outputs for Single-Tap Program

       The data associated with the curves presented in Paragraph 4.1.2.1 are shown

in Figures 4.3.1.2-1 and 4.3.1.2-2. In these figures WRM and WIM are the real and

imaginary weights averaged over the time between printouts, with WRV and WIV being

the respective standard deviations (without the dither signal). SO is output signal power,

NO is output thermal noise power, and XPMSE is the output crosspole interference power.

The column titled GAIN is the average value of the interference measurement output.

XPOLE PARAMETERS ARE

-10.00000 45.00000 -10.00000 45.00000

OPTIMAL WEIGHTS AND OUTPUT S/N ARE

-.20986 -.22502 14.65325

DITHER SIZE, GAIN AND S/N ARE

.02600 180.00000 15.00000

TIME (MS)	WRM	WRV	WIM	WIV	SO	NO	XPMSE	S/NO
.10000	-.05286	.01789	-.00639	.01564	.97969	.11114	.07979	9.45236
.20000	-.07458	.00831	-.03554	.00937	.98459	.09079	.05922	10.35196
.30000	-.09176	.00577	-.05503	.00414	.98571	.07936	.04655	10.94161
.40000	-.11050	.00428	-.07662	.00872	.98644	.06763	.03519	11.63942
.50000	-.12424	.00543	-.09716	.00703	.98890	.06050	.02749	12.13379
.60000	-.13936	.00522	-.11389	.00381	.99190	.05222	.02126	12.78620
.70000	-.14809	.00324	-.12120	.00222	.99298	.04982	.01762	12.99503
.80000	-.15448	.00336	-.13754	.00495	.99773	.04655	.01324	13.31061
.90000	-.16309	.00153	-.15050	.00462	.99911	.04418	.01008	13.54370
1.00000	-.16599	.00153	-.16319	.00250	1.00262	.04090	.00836	13.89419
1.10000	-.16870	.00213	-.17360	.00418	1.00807	.04059	.00727	13.95100
1.20000	-.17300	.00166	-.17755	.00192	1.00952	.04005	.00614	14.01568
1.30000	-.17746	.00106	-.17962	.00233	1.00837	.03914	.00526	14.11038
1.40000	-.18062	.00111	-.18415	.00204	1.00806	.03834	.00455	14.19813
1.50000	-.18078	.00127	-.19095	.00191	1.00995	.03747	.00423	14.30621
1.60000	-.13259	.00106	-.19843	.00245	1.01433	.03857	.00391	14.19981
1.70000	-.18655	.00267	-.20063	.00091	1.01515	.03733	00336	14.34502
1.80000	-.19601	.00298	-.20354	.00285	1.01240	.03592	.00243	14.50038
1.90000	-.19863	.00084	-.21241	.00247	1.01447	.03571	.00200	14.53398
2.00000	-.19859	.00099	-.21119	.00166	1.01253	.03717	.00206	14.35218
2.10000	-.19997	.00228	-.20868	.00097	1.01224	.03780	.00230	14.27829
2.20000	-.20159	.00118	-.20955	.00113	1.01333	.03659	.00209	14.42446
2.30000	-.20432	.00116	-.21126	.00246	1.01280	.03740	.00187	14.32657
2.40000	-.20572	.00100	-.21703	.00080	1.01385	.03597	.00165	14.49979
2.50000	-.20308	.00125	-.21542	.00254	1.01274	.03622	.00177	14.46598
2.60000	-.20174	.00145	-.21686	.00194	1.01551	.03654	.00198	14.43865
2.70000	-.19935	.00098	-.21575	.00097	1.01731	.03770	.00208	14.31165
2.80000	-.20370	.00079	-.21875	.00105	1.01673	.03654	.00175	14.44462
2.90000	-.20461	.00097	-.21908	.00115	1.01529	.03605	.00163	14.49659
3.00000	-.20581	.00062	-.21876	.00159	1.01330	.03653	.00165	14.43131
3.10000	-.20455	.00143	-.21773	.00210	1.01477	.03552	.00185	14.55873
3.20000	-.20750	.00187	-.21328	.00107	1.01280	.03645	.00176	14.43800
3.30000	-.20609	.00096	-.21402	.00165	1.01344	.03606	.00174	14.48778
3.40000	-.20576	.00118	-.21530	.00094	1.01296	.03609	.00166	14.48219
3.50000	-.20325	.00103	-.21432	.00203	1.01213	.03715	.00183	14.35284
3.60000	-.20174	.00095	-.21492	.00116	1.01457	.03558	.00201	14.55099
3.70000	-.20137	.00123	-.21722	.00095	1.01720	.03756	.00197	14.32731
3.80000	-.20521	.00215	-.21821	.00142	1.01583	.03661	.00169	14.43168
3.90000	-.20699	.00086	-.22023	.00155	1.01488	.03610	.00160	14.48875
4.00000	-.20883	.00099	-.21851	.00058	1.01195	.03501	.00156	14.60985

Figure 4.3.1.2-1   Data Associated With Figure 4.1.2.1-1.

XPOLE PARAMETERS ARE

-10.00000 45.00000 -10.00000 45.00000

OPTIMAL WEIGHTS AND OUTPUT S/N ARE

-.20992 -.22478 14.65325

DITHER SIZE, GAIN AND S/N ARE

.00608 48.30000 15.00000

TIME (MS)	WRM	WRV	WIM	WIV	SO	NO	XPMSE	S/NO	GAIN
.20000	-.23900	.08638	.00917	.05295	.89579	.03319	.06471	9.61408	.02013
.40000	-.32191	.01338	-.08712	.01816	.90617	.03521	.02880	11.50918	.01313
.60000	-.32718	.00967	-.11494	.01182	.91713	.03474	.02277	12.02676	.01160
.80000	-.30411	.01408	-.15390	.01690	.94448	.03454	.01183	13.08976	.01025
1.00000	-.27872	.00994	-.16164	.01147	.95804	.03481	.00711	13.58954	.00878
1.20000	-.25073	.01127	-.18474	.00846	.98020	.03327	.00245	14.38414	.00716
1.40000	-.23536	.00888	-.17862	.01123	.98339	.03455	.00237	14.25531	.00732
1.60000	-.22275	.00842	-.18174	.00989	.98994	.03393	.00192	14.41118	.00738
1.80000	-.22453	.01071	-.19214	.01084	.99426	.03474	.00122	14.41617	.00727
2.00000	-.20266	.01042	-.19859	.00761	1.00625	.03372	.00123	14.59217	.00693
2.20000	-.18903	.00736	-.20375	.00947	1.01432	.03422	.00173	14.50474	.00700
2.40000	-.18702	.00766	-.19821	.01036	1.01246	.03388	.00215	14.48674	.00694
2.60000	-.18390	.00815	-.18948	.00927	1.00948	.03402	.00289	14.36861	.00725
2.80000	-.18150	.00901	-.18920	.00875	1.01032	.03392	.00311	14.35886	.00693
3.00000	-.17137	.00717	-.19987	.00774	1.01969	.03307	.00340	14.46524	.00711
3.20000	-.16748	.00771	-.21611	.00913	1.02923	.03432	.00335	14.36476	.00705
3.40000	-.17583	.00870	-.21505	.01005	1.02528	.03392	.00253	14.49102	.00693
3.60000	-.20230	.01009	-.21714	.00989	1.01546	.03367	.00070	14.70558	.00652
3.80000	-.20331	.00777	-.24102	.01071	1.02683	.03404	.00089	14.68338	.00687
4.00000	-.19406	.00597	-.23231	.01041	1.02629	.03521	.00109	14.51362	.00707
4.20000	-.19489	.01142	-.21567	.00788	1.01777	.03545	.00108	14.45035	.00710
4.40000	-.19753	.00741	-.21557	.00854	1.01663	.03419	.00087	14.62351	.00707

Figure 4.3.1.2-2   Data Associated With Figure 4.1.2.1-2.

125

4.3.2   Multi-Tap Simulation

4.3.2.1   Multi-Tap Program Listing

```
C        ADAPTIVE CROSSPOLE CANCELLATION SIMULATION  -  MULTI - TAP
         DIMENSION TN(4),RP(3)
         COMPLEX VV,VH,HV,HH,TNH,TNV,VVO,HVO,TNVO,W(3),WM(3),F1,F2,F3,A,B,
        $U,E,VHO,HHO,TNHO,SHO,TNO,R(3)
         COMPLEX DL(10,3)
         CALL RANUP(2.)
         CALL RANVP(2.)
         NP = 60
         MP = 2
         XMAX = 12.0
         XMIN = 0.0
         YMAX = 16.
         YMIN = 6.
C        DEFINE PROGRAM CONTROL PARAMETERS
         IZQ=10
         IS=2000
         IPP=14000
         IDT=28000
         IF(IPP.LT.0) GO TO 56
         JJ=1
         JJ = 2
         IR=1
         II=-1
         DR=57.2958
         PI=3.141593
         SR=7.E6
         TT=1000./(10.*SR)
         TT=TT*IPP
C        DEFINE GAINS
C        CONTROL CIRCUIT GAINS
         G1=500.
         G2=700.
         G3=.01
         G4=G2
         G5=G3
         AP=.00004
         AP1=1.-AP
         BP1=.95
         BP1=.999
         BP=1.-BP1
C        SET INTIAL CONDITIONS
         X2D=1.
         W(1)=(-.2236,-.2236)
         W(2)=(0.,0.)
         W(3)=(-.02,0.)
C        INPUT SIMULATION GAINS
         F1=(.5,.866025)
         F2=CONJG(F1)
         F3=(1.-F1)*(1.-F2)
C        DEFINE INPUT S/N
         STDB=15.
         ST=10.**(-STDB/20.)
```

126

4.3.2.1   (Continued)

```
        ST=ST*2.52
C       DEFINE CROSS POLE PARAMETERS
        VXM=-10.
        VXP=45.
        HXM=-10.
        HXP=45.
 11     WRITE(6,74)
 74     FORMAT(1H1)
        WRITE(6,456)
456     FORMAT(" XPOLE PARAMETERS ARE")
        WRITE(6,3) VXM,VXP,HXM,HXP
  3     FORMAT(1H ,4F12.4)
        VXM=10.**(VXM/20.)
        HXM=10.**(HXM/20.)
        VXP=VXP/OR
        HXP=HXP/OR
        A=VXM*CMPLX(COS(VXP),SIN(VXP))
        B=HXM*CMPLX(COS(HXP),SIN(HXP))
C       PRINT SIMULATION PARAMETERS
        WRITE(6,511)
511     FORMAT(" DITHER SIZE, GAIN AND S/N ARE")
        WRITE(6,3) G3,G4,STDB
        WRITE(6,500)
500     FORMAT("  TIME(MS)   W1R     W1I      W2R      W2I      W3R
     $ W3I       SO      TNO     XPMSE   S/NO     J(W)     WRV     WI
     $IV")
 10     IP=IP+1
        IO=IO+1
        IG=IQ+1
C       COMPUTE INPUT SIGNALS
        CALL SIG(VV,VH,HH,HV,F1,F2,F3,A,B,IZQ)
        CALL THERM(TNV,TNH,ST)
C       COMPUTE OUTPUT OF HORIZ CHANNEL
        CALL CORNET(VV,HV,TNV,VVO,HVO,TNVO,W,R)
        HHO=HH
        VHO=VH
        TNHO=TNH
        U=VHO+HHO+TNHO+VVO+HVO+TNVO
        E=VHO+VVO
        SHO=HHO+HVO
        TNO=TNHO+TNVO
        EDM=EDM+REAL(SHO*CONJG(SHO))
        EDV=EDV+REAL(TNO*CONJG(TNO))
        EP=REAL(E*CONJG(E))
        EPP=EPP+EP
C       INTERFERENCE MEASUREMENT
C       MAGNITUDE DETECTOR - AGC
        U=EXP(-Z)*U
        X1=REAL(U*CONJG(U))
        X1=SQRT(X1)
        ZT=(X1-1.)/G1
        Z=Z+ZT
```

127

4.3.2.1   (Continued)

```
C       AC COUPLING(BPF)
        X2A=BP*X1+BP1*X2D
        X2D=X2A
        X2=X1-X2A
C        SLED
        X3=.5*X2*X2
C       HIGH PASS FILTER
        X3A=AP*X3+AP1*X3D
        X3D=X3A
        X3=X3-X3A
        GJ=GJ+X3
C       SYNCHRONOUS DETECTORS
C        FOR CONSTANT WEIGHTS PLACE " GO TO 973" CARD HERE
        CALL CLOCK(IQ,IR,II,IS)
        X4=-X3*IR
        X5=-X3*I1
C       COMPUTE WEIGHT UPDATE
        XR=XR+X4/G4
        XI=XI+X5/G2
C        ADD DITHER SIGNAL
        CR=G5*IR
        CI=G3*II
        WR=CR+XR
        WI=CI+XI
        WRV=WRV+WR*WR
        WIV=WIV+WI*WI
        W(JJ)=CMPLX(WR,WI)
  973   CONTINUE
        WM(JJ)=WM(JJ)+W(JJ)
        IF(IP.NE.IPP) GO TO 10
C        OUTPUT DATA
        GJ=GJ/IPP
        GJ=GJ*100.
        EPP=EPP/IPP
        WM(JJ)=WM(JJ)/IPP
        DO 778 I=1,3
        IF(I.EQ.JJ) GO TO 778
        WM(I)=W(1)
  778   CONTINUE
        WRM=REAL(WM(JJ))
        WIM=AIMAG(WM(JJ))
        WRV=SQRT(WRV/IPP-WRM*WRM)
        WIV=SQRT(WIV/IPP-WIM*WIM)
        EDV=EDV/IPP
        EDM=EDM/IPP
        S1=10.*ALOG10(EDM/(EDV+EPP))
        T=T+TT
        WRITE(6,901) T,WM(1),WM(2),WM(3),EDM,EDV,EPP,S1,GJ,WRV"WIV
  901   FORMAT(1H ,14F9.5)
        WRITE(6,   ) T,WM(1),WM(2),WM(3),EDM,EDV,EPP,S1,GJ,WRV"WIV
        IG = IG + 1
        IF(ID.LT.IDT) GO TO 783
```

4.3.2.1   (Continued)

```
       ID=0
       W(JJ)=CMPLX(XR,XI)
       JJ=JJ+1
       IF(JJ.GT.3)  JJ=1
       XR=REAL(W(JJ))
       XI=AIMAG(W(JJ))
 783   CONTINUE
       IP=0
       EPP=0.
       WRV=0.
       WIV=0.
       DO 779 I=1,3
 779   WM(I)=(0.,0.)
       GJ=0.
       EDM=0.
       EDV=0.
       IF(IG .EQ. 60) GO TO 57
       GO TO 10
  57   WRITE(6,101)
 101   FORMAT(1H1,30X,'X - POLE TRANSIENT RESPONSE')
       CALL GPLOTR(NO,AF,NP,MP,O,Q,XMAX,XMIN,YMAX,YMIN)
       IG=0
       XMIN=XMAX
       XMAX=XMIN+XMAX
       GO TO 10
  56   STOP
       END
```

4.3.2.1 (Continued)

```
      SUBROUTINE CORNET(V1,H1,T1,VVO,HVO,TNVO,W,X)
      COMPLEX VVO,HVO,TNVO,W(3),X(3),VV(3),HV(3),TNV(3),VT(3),HT(3)
      COMPLEX TNT(3)
      COMPLEX V1,H1,T1
      VV(1)=V1
      HV(1)=H1
      TNV(1)=T1
      A=15.
      B=100.
      VT(1)=VV(2)
      VT(2)=VV(1)-VV(3)
      VT(3)=VV(2)-.5*(VV(1)+VV(3))
      VVO=W(1)*(VT(1)+A*W(2)*VT(2)+B*W(3)*VT(3))
      HT(1)=HV(2)
      HT(2)=HV(1)-HV(3)
      HT(3)=HV(2)-.5*(HV(1)+HV(3))
      HVO=W(1)*(HT(1)+A*W(2)*HT(2)+B*W(3)*HT(3))
      TNT(1)=TNV(2)
      TNT(2)=TNV(1)-TNV(3)
      TNT(3)=TNV(2)-.5*(TNV(1)+TNV(3))
      TNVO=W(1)*(TNT(1)+A*W(2)*TNT(2)+B*W(3)*TNT(3))
      DO 1 I=3,2,-1
      VV(I)=VV(I-1)
      HV(I)=HV(I-1)
    1 TNV(I)=TNV(I-1)
      DO 2 I=1,3
    2 X(I)=VT(I)+HT(I)+TNT(I)
      RETURN
      END



      SUBROUTINE CORTAP(VV,HV,TNV,VVO,HVO,TNVO,W)
      COMPLEX VV,HV,TNV,VVO,HVO,TNVO,VVD1,HVD1,TNVD1,VVD2,HVD2,TNVD2,
     $W(3)
      VVO=W(1)*VV+W(2)*VVD1+W(3)*VVD2
      HVO=W(1)*HV+W(2)*HVD1+W(3)*HVD2
      TNVO=W(1)*TNV+W(2)*TNVD1+W(3)*TNVD2
      VVD2=VVD1
      HVD2=HVD1
      TNVD2=TNVD1
      VVD1=VV
      HVD1=HV
      TNVD1=TNV
      RETURN
      END
```

130

4.3.2.1   (Continued)

```
      SUBROUTINE SIG(VV,VH,HH,HV,F1,F2,F3,A,B,I)
      COMPLEX VV,VH,HV,HH,F1,F2,F3,A,B,VA(3),V
      DD=1.E-20
      H=1.
      I=I+1
      IF(I .LT. 10) GO TO 1
      I=0
      TH=RANU(0.,4.)
      NTH=TH
      TH=NTH*1.5707964
      V=CMPLX(COS(TH),SIN(TH))
1     VA(1)=F3*V+F1*VA(2)+CMPLX(DD,DD)
      VA(2)=VA(1)
      VV=VA(1)+F2*VA(3)+CMPLX(DD,DD)
      VA(3)=VV
      HV=A*H
      VH=B*V
      HH=CMPLX(H,0.)
      RETURN
      END




      SUBROUTINE THERM(TNV,TNH,ST)
      DIMENSION TN(4)
      COMPLEX TNV,TNH,TV(10),TH(10),FV(3),FH(3)
      A=.5
      B=.25
      DO 1 I=9,1,-1
      TV(I+1)=TV(I)
1     TH(I+1)=TH(I)
      DO 2 I=1,4
2     TN(I)=RANV(0.,ST)
      TV(1)=CMPLX(TN(1),TN(2))
      TH(1)=CMPLX(TN(3),TN(4))
      TNV=(0.,0.)
      TNH=(0.,0.)
      DO 3 I=1,10
      TNV=TNV+.1*TV(I)
3     TNH=TNH+.1*TH(I)
      FV(1)=B*TNV+A*FV(2)
      FV(2)=FV(1)
      TNV=FV(1)+A*FV(3)
      FV(3)=TNV
      FH(1)=B*TNH+A*FH(2)
      FH(2)=FH(1)
      TNH=FH(1)+A*FH(3)
      FH(3)=TNH
      RETURN
      END




      SUBROUTINE CLOCK(I,IR,II,IS)
      ISD=IS/2
      IM=I+ISD
      IT1=MOD(I,IS)
      IF(IT1.EQ.0) IR=-IR
      IT2=MOD(IM,IS)
      IF(IT2.EQ.0) II=-II
      RETURN
      END$
```

131

4.3.2.2   Computer Outputs for Multitap Program

The data associated with some of the curves presented in Paragraph 4.1.1.2

and 4.1.2.2 are presented in the following figures. Also, a number of additional computer

runs are included. In particular, Figure 4.3.2.2-1 is the data associated with Figure

4.1.1.2-4 showing the steady-state performance when the dither size is chosen too small.

Figure 4.3.2.2-2,-3,-4 and -5 support the curves sketched in Figure 4.1.2.2-3. The

remaining figures (4.3.2.2-6,-7,-8,-9) present the data from runs made to investigate

the use of compensating delay as discussed in Paragraph 4.1.

Figure 4.3.2.2-1. Data For Steady State Performance With Small Dither Level $(\Delta = .001)$. $A_2 = 15\beta$ and $A_3 = 100\beta$. (See Figure 4.1.1.2-4)

Figure 4.3.2.2-2. Data Associated With Simulation of Special Multi-Tap Network Without Compensating Delay. $A_2 = 5\beta$ and $A_3 = 10\beta$. (See Figure 4.1.2.2-3)

XPOLE PARAMETERS ARE
-10.0000   45.0000   -10.0000   45.0000
OTHER SIZE, GAIN AND S/N ARE   15.0000
.0200   -63.0000

Figure 4.3.2.2-3. Data Associated With Simulation of Special Multi-Tap Network With Compensating Delay. $A_2 = 5\beta$ and $A_3 = 10\beta$. (See Figure 4.1.2.2-3)

Figure 4.3.2.2-4. Data Associated With Simulation of the Modified Special Multi-Tap Network. $A_2 = 5\beta$ and $A_3 = 10\beta$ (See Figure 4.1.2.2-3)

136

Figure 4.3.2.2-5. Data for Simulation of Conventional Tapped Delay Line Correction Network. $A_1 = A_2 = A_3 = \beta$. (See Figure 4.1.2.2-3)

Figure 4.3.2.2-6. Output SNR (dB) vs Time (msec) For Special Multi-Tap Network With 2T Compensating Delay. $A_2 = 15\beta$ and $A_3 = 100\beta$.

138

Figure 4.3.2.2-7. Data Associated With Figure 4.3.2.2-6.

139
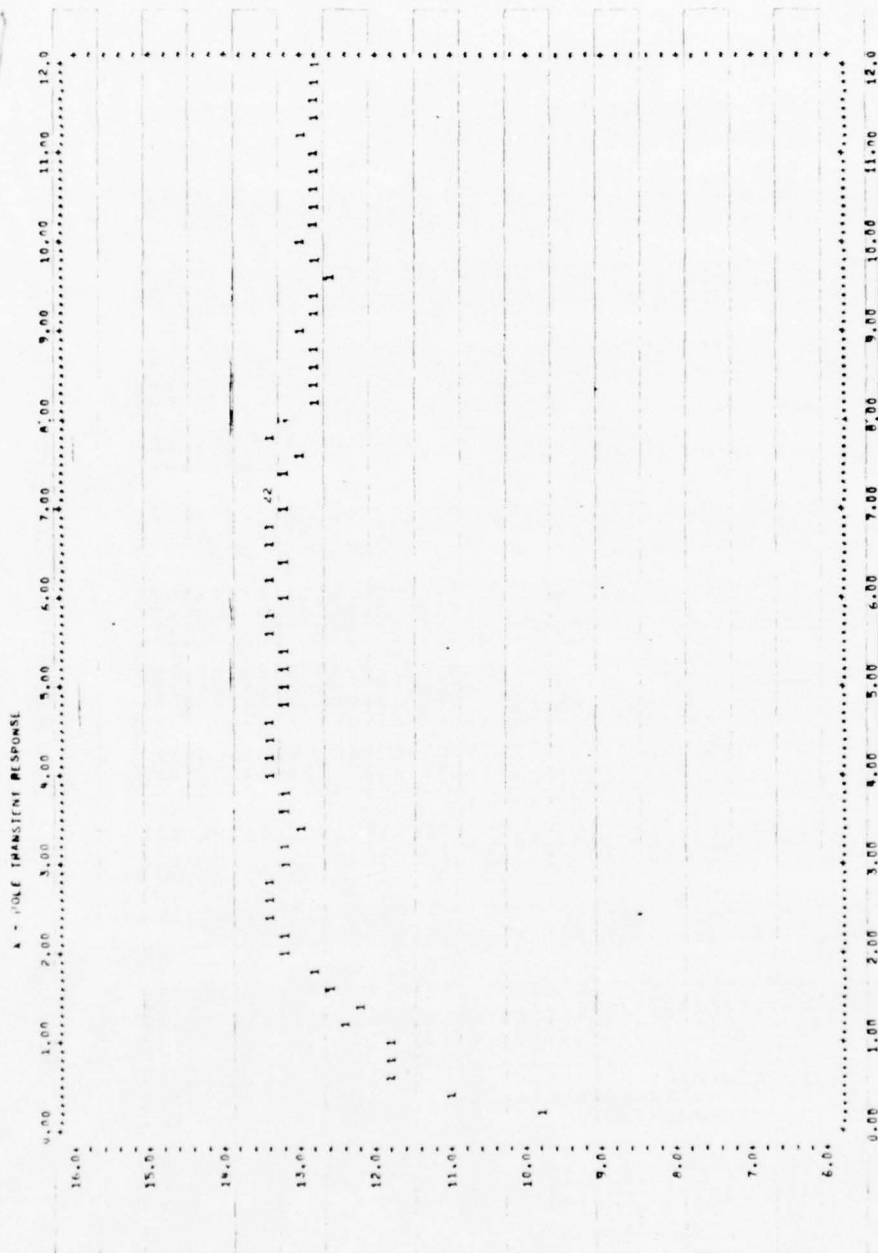
Figure 4.3.2.2-8. Output SNR (dB) vs Time (msec) For Special
Multi-Tap Network With 4T Compensating Delay.
$A_2 = 15\beta$ and $A_3 = 100\beta$

Figure 4.3.2.2-9. Data Associated With Figure 4.3.2.2-8.

141

5.0   IMPLEMENTATION CONSIDERATIONS

Although the study did not require hardware implementation, a conceptual design plan for adaptive crosspole correction hardware has been formulated. This design plan establishes an approach whereby demonstration hardware can be developed that is capable of implementing the correction techniques studied in the previous sections and proving their feasibility.

5.1   Implementation Goals

A major goal of the demonstration (and future) crosspole correction hardware is that it be able to be integrated into existing communication systems with a minimum of modifications to existing hardware; and further to be able to be used essentially independent of the existing modulation schemes.

The planned hardware has been conceptually designed to meet these goals and will operate with existing RADC QPSK modems as well as with the Broadband Modem (2 bits/Hz) presently under development by Harris ESD for RADC (Contract F30602-76-C-0434).

5.2   Generalized Crosspole Correction Circuitry

Figure 5.2-1 is a generalized block diagram depicting integration of the planned crosspole correction techniques in a typical communication system.

Ignoring for the moment the crosstalk corrector, the objective of the communication system is to transmit, over Link No. 1, previously modulated information from

142
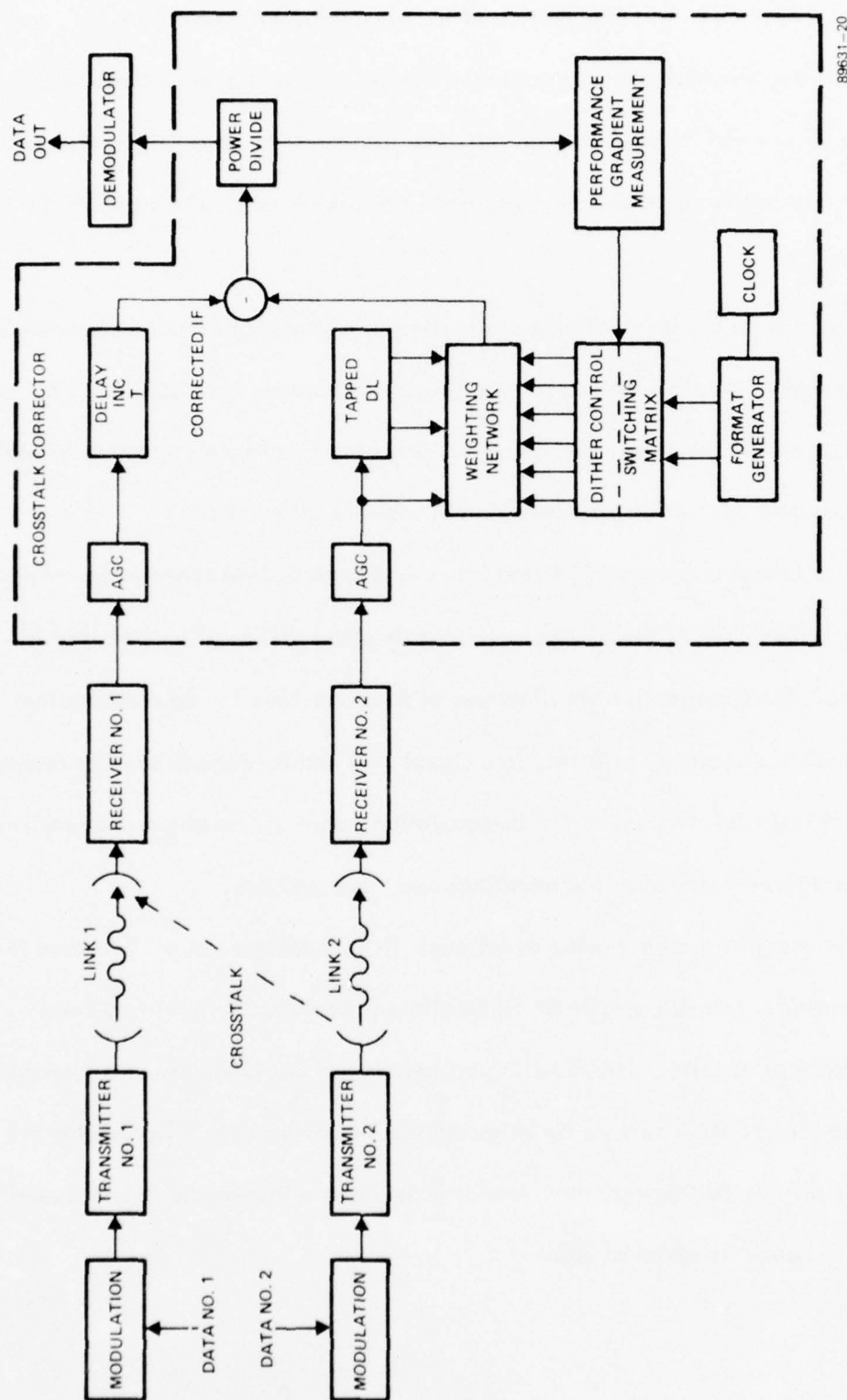
Figure 5.2-1 Generalized Communication System Block Diagram

143

Transmitter No. 1, receive this information at Receiver No. 1, demodulate the received signal and output the demodulated information. However, in a system utilizing cross polarization, a second link is operating on the same frequency at an orthogonal polarity resulting in some crosstalk being received (dashed line to Link No. 1) along with the desired signal.

In order to achieve optimum utilization of a cross polarized communications system, the interfering crosstalk between the orthogonal channels must be eliminated or reduced to a negligible level. The results of this study have indicated that it is feasible to implement crosspole correction hardware that is capable of doing this.

The crosspole corrector (dotted block in Figure 5.2-1) operates by taking a sample of the IF from Receiver No. 2 and adjusting its phase and amplitude so that it will cancel the crosstalk present at the IF output of Receiver No. 1. Subtracting the two signals cancels the crosstalk resulting in a signal that can be demodulated to reproduce the original input information at the demodulation output. The phase and amplitude are adjusted via a three-tap delay line equalizer and three weights.

The weights are controlled as follows: first, a measure of performance is derived by measuring bit-to-bit amplitude fluctuations (caused by the crosstalk) and averaging a number of samples. The resulting voltage is used as feedback in a loop which attempts to drive the crosstalk to zero by adjusting the weight values. The weights are adjusted sequentially by "dithering" them one at a time and allowing the "nondithered" control signal to assume its optimum value.

5.3   Detailed Crosstalk Corrector

A detailed block diagram at the planned crosstalk corrector is shown in Figure 5.3-1. Although correction for only one channel is shown, a second channel will also be required to fully demonstrate the feasibility of the approach.

The block diagram is relatively straightforward and depicts eight functional modules which are briefly described below.

Module 1 contains three identical AGC amplifiers and associated loop filters and detectors. Using AGC inputs allows the corrector to essentially operate independent of input levels.

The three-tap delay line equalizer is contained in Module 2. Isolation is provided via the hybrid dividers used at the taps. Coax cable will be used for delay in the demonstration hardware since it is relatively inexpensive, nondispersive over the bandwidth and easily tunable by adjusting its length.

Module 3 contains the signal dividing and combining circuits. For simplicity, the phase adjustment circuitry is shown in Inset 1.

The three voltage controlled weights are contained in Module 4. Again, for simplicity, the weight circuitry is shown in Inset 2. The weights, which feature dual gate FET's as gain control elements have been proven on other programs and appear to meet the dispersion requirements for this application.

Module 5 is essentially identical to Module 2 except that in this case it is used as a straight delay line.

145

146
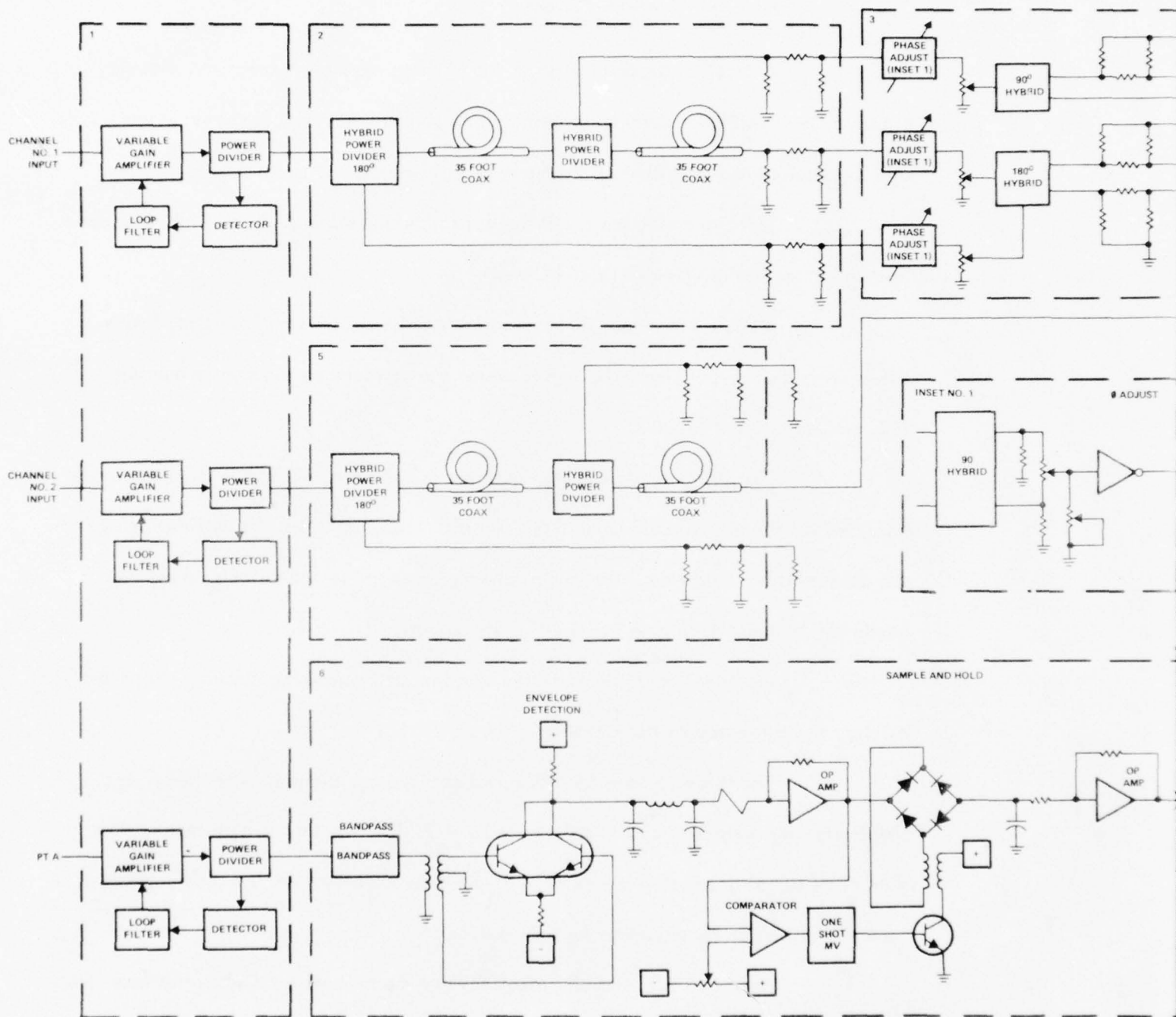
Figure 5.3-1 Crosstalk Corrector Detailed Block
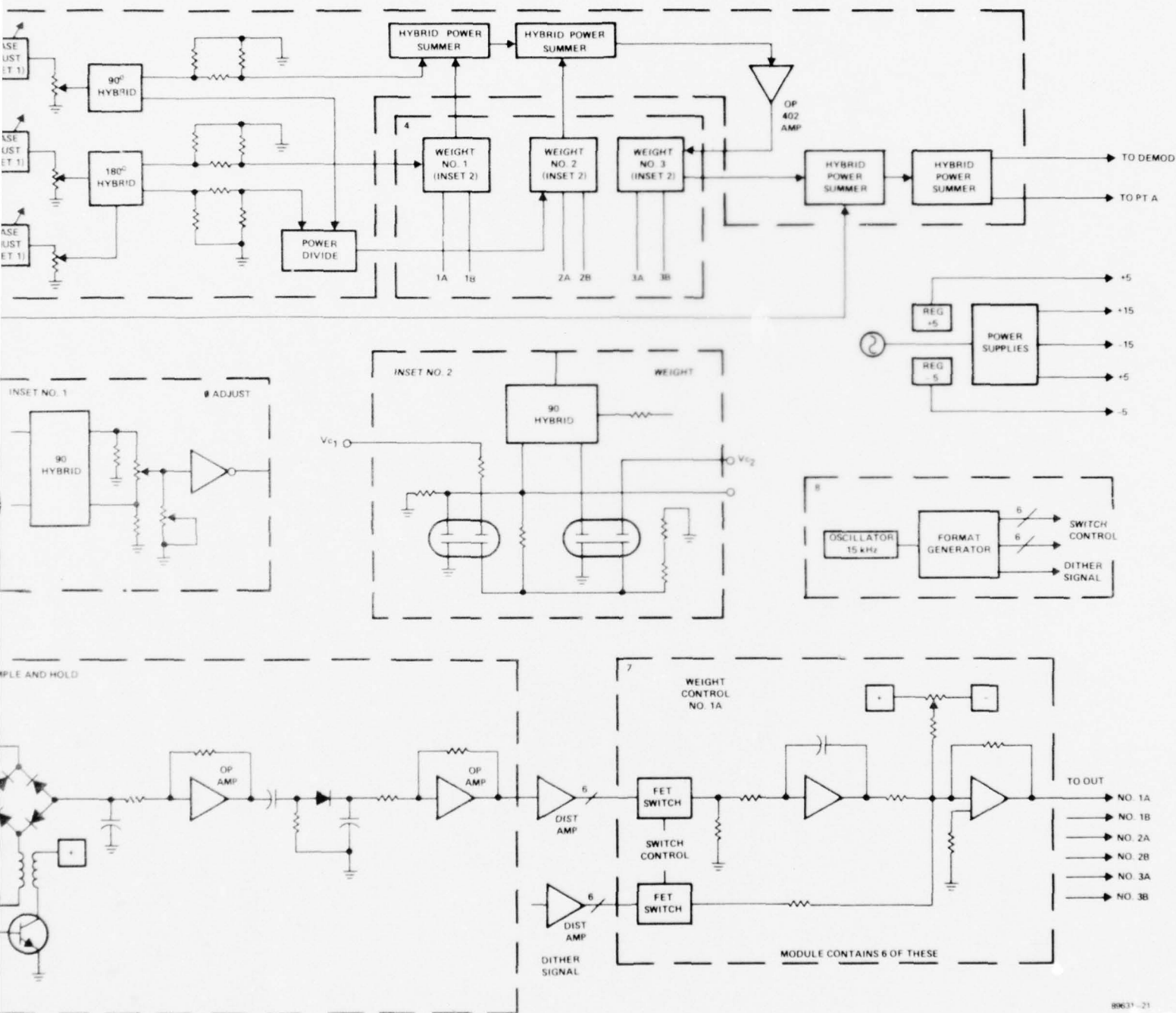
lk Corrector Detailed Block Diagram (One Channel)

Envelope detection and baseband processing required to generate the control signals is performed in Module 6.

Circuitry for distribution of the control signal and the dither signal to the six weight control inputs is contained in Module 7. It consists of six identical circuits as shown.

The master clock and format generator is included in Module 8. This module generates the digital control signals for the FET switches as well as the dither signal (square wave).

147

6.0   CONCLUSIONS AND RECOMMENDATIONS

This report has presented the design of an adaptive interference reduction device suitable for use over long LOS microwave links corrupted by multipath. The use of this device provides the capability of doubling the bandwidth efficiency of the links over LOS microwave links without requiring additional power margin (over the 3 dB necessary to provide the orthogonal channel) to overcome the crosspolar interference. A review of the physical and statistical properties of the crosspolar interference led to the development of a procedure to quantitatively define the interference problem and compare alternative interference reduction and bandwidth expanding techniques. Following this, a detailed discussion of the design trade-offs associated with the application of adaptive interference reduction resulted in the design of a specific system. The mathematical analysis of that design led to the development of both general performance estimates for dual polarized links and a system model through which specific component parameters could be chosen. This design featured the development of a special multitap correction network which not only offered increased bandwidth capabilities, but also gave unique controllability characteristics and a useful mathematical relationship between the weight settings and the physical nature of the crosspolar interference. Also featured in this design was the development of a performance monitoring device particularly well suited to approximately constant envelope signal formats and a simple dither-type gradient control method. The practicality of the design was verified by both the mathematical analysis and detailed computer simulations. The next step in the development of these techniques is the fabrication of the breadboard hardware suggested in the text.

148

A large amount of literature exists which discusses both the physical and statistical features of rain-induced fading and crosspolar interference. Utilizing data gathered from this literature, in conjunction with approximations which were developed relating crosspolar interference to degradation in signal-to-noise ratio, a procedure for computing the probability that a link of a given quality would be available was developed. These statistics were computed for links employing both circular and linear orthogonal polarizations, as well as for those which utilized modulation techniques to increase bandwidth efficiency, and were plotted as a function of the required power margin. In this manner, the relative costs (in terms of link power requirements) of these alternatives can be assessed. This excercise indicated that in all cases, dual linear polarization is less susceptible to rain-induced crosspolar interference than is circular polarization. Other generalizations from these results are limited by the relevance of the rain statistics used to the specific link being considered. That is, the procedure developed is a generally applicable method, but it requires that accurate rain statistics be compiled for the specific application being considered. Similarly, the effects of non-rain induced interference (e.g., multipath) are also very dependent upon applications and do not lead to easily generalized results. This examination of the literature also indicated that more information is required on the variation of crosspolar interference with frequency over the bandwidths which a given channel will occupy. This information is required to select the required transfer characteristics of the crosspole interference reduction networks.

149

The computations which determine the increased power margin required to compensate for crosspolar interference also indicate the relative importance of techniques which can be used to reduce that interference. Again, an absolute assessment would require data on specific links and exact specification of the desired link performance. However, this work does indicate that the use of adaptive interference reduction is an important design consideration, particularly for those links designed to yield high performance with minimum cost. The basic design philosophy used was to postulate what appears to be the most simple approach which is suitable to the problem and verify that its performance is adequate. For example, the dither-type gradient control method is quite simple to implement, but the injected dither can potentially limit the system performance. It was demonstrated that this was not a limitation. Also, the efficient use of this type of control requires the availability of an easily measured performance index. To accomplish this the technique to measure the interference induced envelope fluctuation was developed. The use of this was indicated by the fact that state of the art microwave radios use non-linear amplifiers and therefore require constant envelope signal formats, but its application requires only that the interference produce measurable envelope fluctuations. Synchronization of this measurement with the center of each bit can improve the performance of this technique, but again, the simple circuit developed has proven to be adequate. For the correction network implementation, the most simple procedure would be the use of the single complex weight, which will be adequate for relatively narrowband systems. However, since the radio characteristics examined in Appendix A indicate nonnegligible

150

dispersion between channels over the required bandwidth and insufficient data is available on the dispersive nature of the media, the more sophisticated special multitap network was also developed.

Based on the mathematical analysis and the extensive computer programs developed on this study, it is reasonable to assume that the adaptive interference reduction network designed will perform adequately. Consequently, it is recommended that breadboard hardware be developed to further investigate the performance and give a more realistic indication of the costs and problems associated with the construction of this type of device. Continued analysis and simulation could still resolve several points left unclear. For example, the question concerning the use of compensating delay and the fine tuning of the multiplexed control loops, particularly where W_1 is inside the W_2 and W_3 loops. Also, a better comparison of the conventional tapped delay line and special multitap correction network would be of interest. However, it would be more efficient to consider such questions in conjunction with the fabrication of the breadboard, when both the analysis and simulation, together with the hardware can be used to further understand these, as well as any additional questions that arise. This is particularly true since the computer simulations of the wideband circuitry are quite cumbersome, requiring 8-12 hours for a single run. Also, the implementation of the special multitap network will provide a means for obtaining more data on the dispersive structure of the crosspolar interference. Finally, it is of interest to consider the potential application of these techniques to other problem areas. For instance, hardware of this type could be used in

151

collection systems to identify the polarization properties of emitters, as a polarization tracker in single polarization systems, or in A-J systems to discriminate against jammers via their polarization structure. This last application could be a particularly useful addition to adaptive null-steering array capabilities where jammers on coincident angles of arrival with the desired signal can no longer be nulled using spatial filtering, but could be nulled using polarization discrimination.

APPENDIX A

DIFFERENTIAL PHASE AND AMPLITUDE RESPONSE IN MEASURED RADIO CHARACTERISTICS

A-1.0   INTRODUCTION

The use of crosspolar communication links requires a separate receiver for each of the channels. If a single-tap correction network is to be used (that is, frequency independent correction is to be used), then it is assumed that the two receiver paths do not have differential phase and amplitude responses across the bandwidth of the desired signals. This appendix analyzes some data recorded at RADC in order to determine if this is an acceptable assumption.

A-2.0   MEASURED RADIO CHARACTERISTICS

The receiver characteristics measured at RADC were analyzed in the following manner to give an estimate of the crosspole cancellation limitations to be expected. Figures A-2-1 and A-2-2 are the data measured by RADC and the curves for both $R_x(A)$ and $R_x(B)$ have been transferred onto the graph paper in Figures A-1a and A-1b. Figure A-1b represents the characteristics for $R_x(B)$, while Figure A-1a illustrates $R_x(A)$ and a comparison of $R_x(A)$ and $R_x(B)$ made by overlaying the $R_x(B)$ curves. The top curves in each of these figures represent the group delay measurements with the phase shift versus frequency (the middle curves) being obtained by graphical integration. The lower curves represent the amplitude response, which are traced directly from the measured data.

153

Rx (A)
UP CONVERTER (MLA)
.3 dB/Div. DELAY 1 ns/Div.
25 MHz IF FILTER #435
± 7 MHz SW

-1

Rx (B)
MLA UP CONVERTER
.3 dB/Div. DELAY 1 ns/Div.
25 MHz IF FILTER #295
± 7 MHz SW

-2

Figure A-2.   Measured Receiver Characteristics

Figure A-1 a

155

Figure A-1 b

156
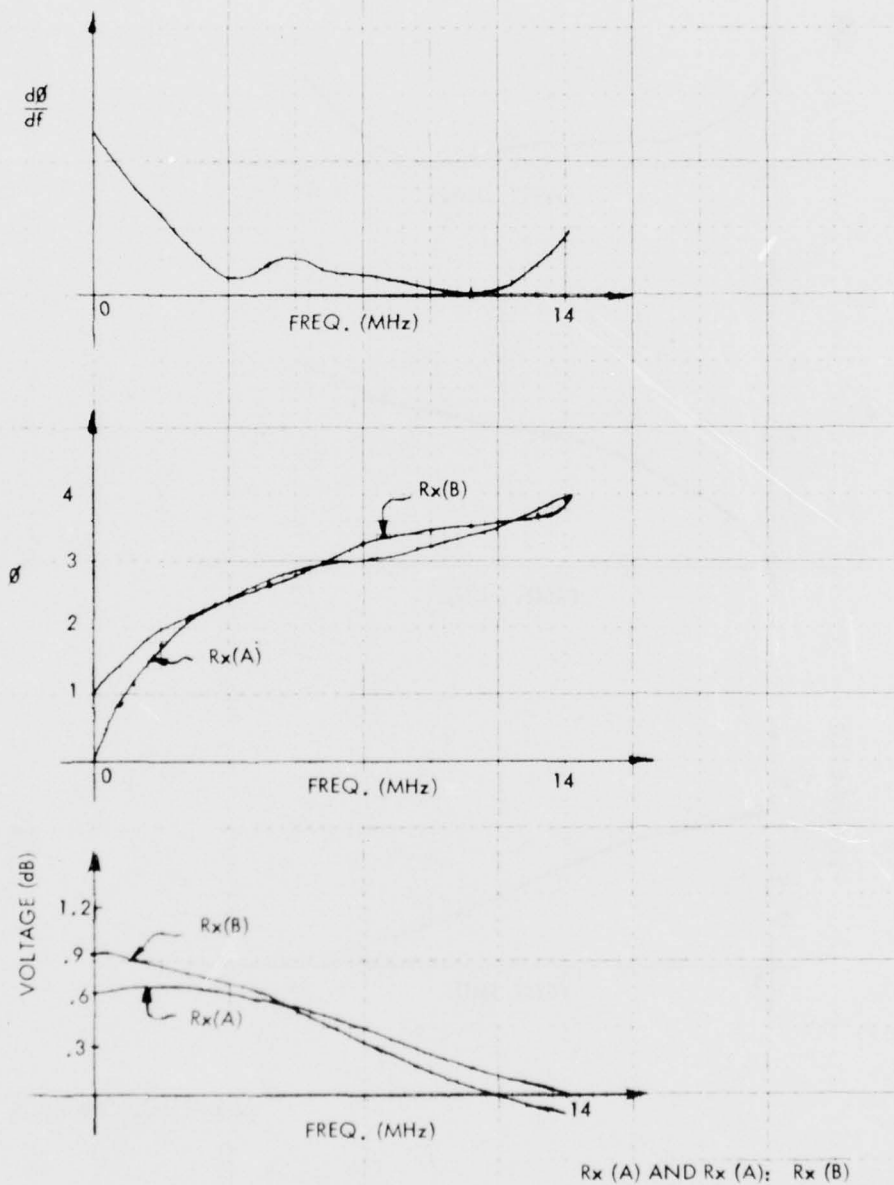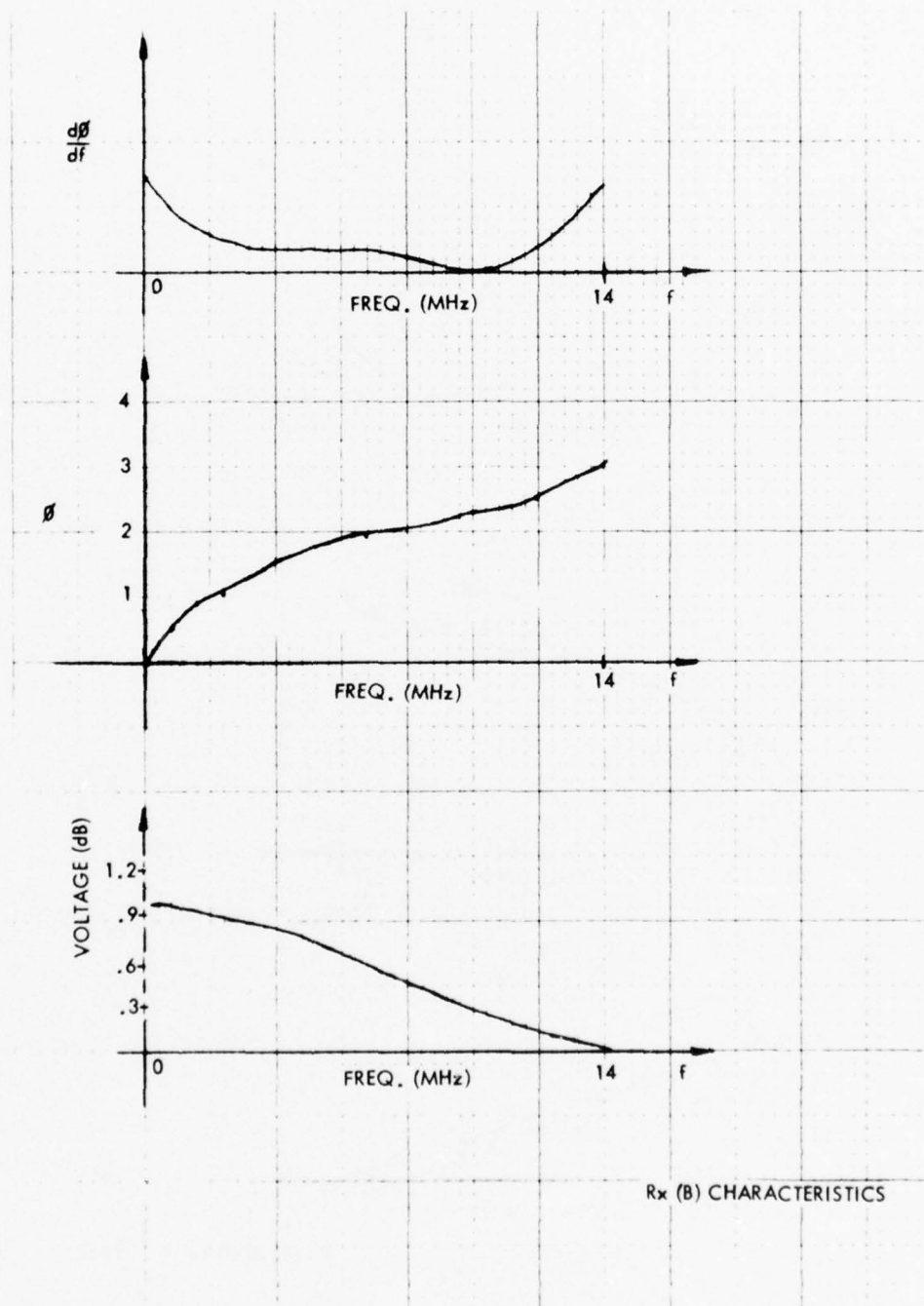
The phase shift and amplitude curves from Figure A-1b are traced on Figure A-1a, with the curves being lined up by eye to give the closest correspondence. From this, it is seen that the phase shift tracks with less than a degree of error, while the amplitude response tracks to about .2 dB.

A-3.0   EFFECT OF ERRORS ON CANCELLATION

To determine the effect of these errors on the obtainable cancellation, consider the case when the received signals x_1 and x_2 are orthogonal and the crosspolar coupling power is equal to the desired signal (these signals being represented are s_1 and s_2). This gives the received signals as

$$x_1 = s_1 + s_2$$

$$x_2 = s_1 - s_2$$

This situation might correspond to a 45° rotation of a linearly polarized antenna and should represent a worst-case for the effect of errors. Modeling the correction network with the flow diagram

157
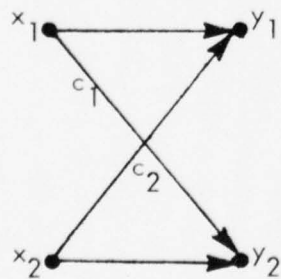
gives the outputs y as

$$y_1 = (1 - C_1) \, s_1 + (1 + C_1) \, s_2$$

$$y_2 = (1 + C_2) \, s_1 + (-1 + C_2) \, s_1$$

Ideally, $C_1 = -1$ and $C_2 = 1$ to completely eliminate the crosspole interference. The signal-to-interference ratio at the coupler output is then

$$\left(\frac{S}{I}\right)_o = \left| \frac{1 - C_1}{1 + C_1} \right|^2$$

and a similar equation applies for y_2. Suppose we have an amplitude error Δ such that $C_1 = -1 + \Delta$. Then

$$\left(\frac{S}{I}\right)_o = \left| \frac{2 - \Delta}{\Delta} \right|^2 \cong \frac{4}{\Delta^2} \, .$$

If we have a phase error θ such that $C_1 = -e^{i\theta}$

$$\left(\frac{S}{I}\right)_o = \left| \frac{1 + e^{i\theta}}{1 - e^{i\theta}} \right|^2 = \left(\frac{1}{\tan \theta/2} \right)^2 \simeq \frac{4}{\theta^2} \, .$$

Tabulated below are values of phase error and amplitude errors corresponding to various output signal-to-interference ratios.

158

$\left(\dfrac{S}{I}\right)_o$	Amplitude Error (dB)	Phase Error (Degrees)
40	0.172	1.15
35	0.304	2.04
30	0.533	3.62
25	0.926	6.44
20	1.584	11.4

Thus an output signal-to-interference ratio of 40 dB requires that the amplitude and phase errors be less than 0.17 dB and 1.15°. A reasonable budget for $(S/I)_o$ of 40 dB would allow

$$\text{Amplitude Error} = 0.707 \times 0.172 = 0.12 \text{ dB}$$

$$\text{Phase Error} = 0.707 \times 1.15 = 0.81^\circ$$

since both errors might be present at the same time. These errors can be thought of as errors in the coupling networks but the effect is the same if the medium or the receivers have amplitude or phase differentials. This indicates that the approximate 1° phase and .2 dB amplitude errors of the measured characteristics would limit the achievable $\left(\dfrac{S}{I}\right)_o$ to between 35 and 40 dB. If better performance is required, then frequency dependent multitap correction networks must be used.

APPENDIX B

ANALYSIS OF MINIMUM LOSS CIRCUITS

B-1.0   INTRODUCTION

It is the purpose of this appendix to relate the inherent loss of an optimum "minimum loss decoupling network" to a number, ρ, which measures the degree of non-orthogonality of the two polarizations. It is found that loss is at least $10 \log (1-\rho)$ for ideal orthogonalizing circuits preceding the low noise amplifiers and $10 \log (1-\rho^2)$ for orthogonalizing circuits following the low noise amplifiers. In addition, the effect of varying the transmitted polarization is analyzed, and the improvement in signal-to-noise ratio for incomplete decoupling is computed.

B-2.0   MINIMUM LOSS IN PASSIVE POLARIZATION DECOUPLING CIRCUITS

Figure B-1 shows a dual polarization communication system. Two independent data transmitters, operating on the same frequency, are connected to a dual polarization transmitting antenna. After propagation through the medium the two signals are received with a dual polarization antenna. It is assumed that the receiving antenna incorporates a matching network* such that the reflection coefficients at Terminals 1 and 2 are zero and the coupling coefficients between Terminals 1 and 2 are zero. With these assumptions, the power available from the antenna is simply the power incident on the polarization decoupling network.

---

* A matching network can be implemented with a lossless backward wave coupler, to eliminate coupling between the terminals, and followed by two conventional two-port matching circuits.
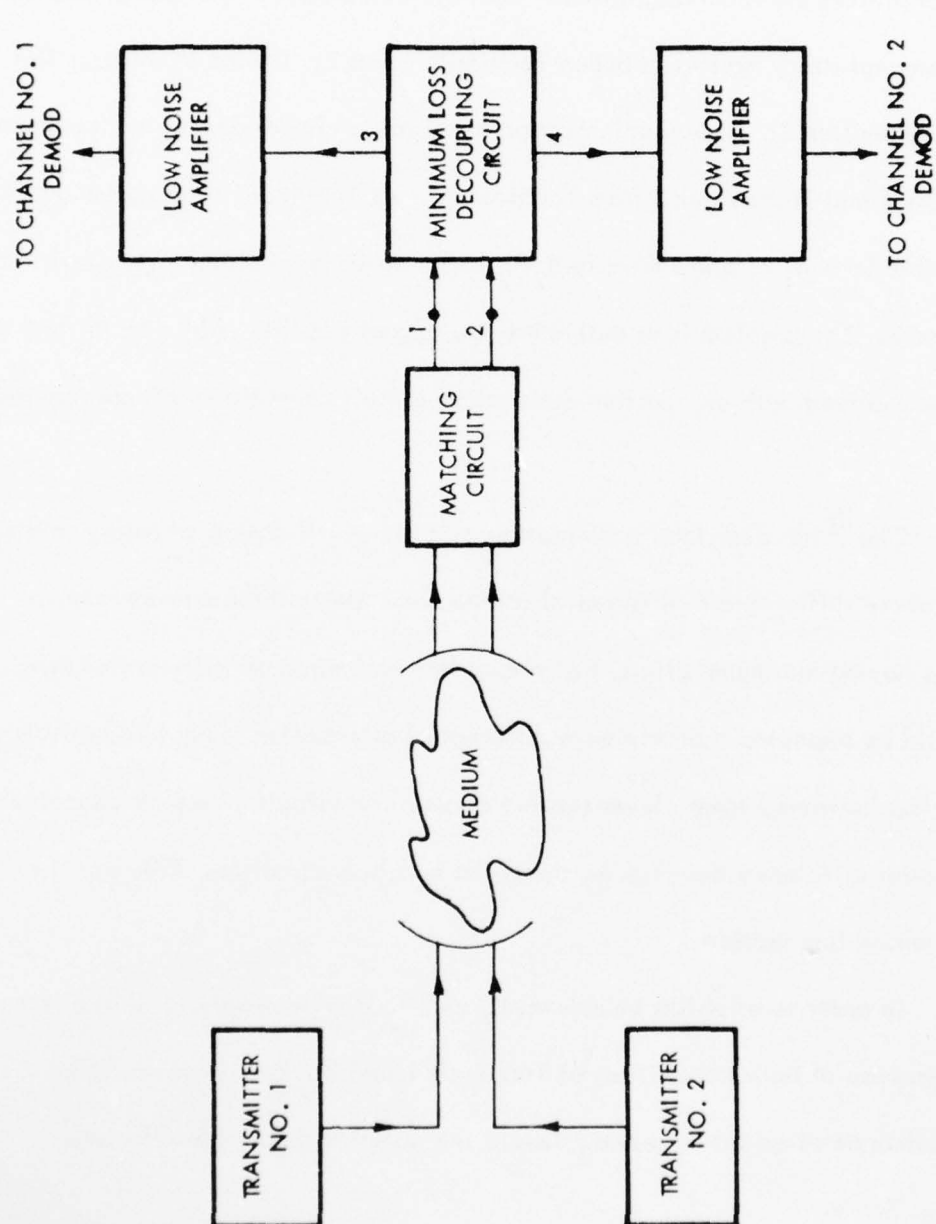
Figure B-1 Dual Polarization Radio Link with Decoupling Circuit Preceding the Low Noise Amplifiers.

The problem to be solved may be stated as follows: Let P_1 denote the power available from the receiving antenna due to Transmitter 1. This power can be divided in some arbitrary manner between Terminals 1 and 2. Define P_2 in a similar manner for Transmitter 2. Now a polarization decoupling circuit decouples Transmitter 1 from Terminals 4 and Transmitter 2 from Terminals 3. At Terminals 3 the power available from Transmitter 1_1 is $\eta_1 P_1$ and similarly $\eta_2 P_2$ is the power available at Terminals 4 due to Transmitter 2. The problem is to determine the largest possible values for η_1 and η_2 which can be realized with any passive decoupling circuit consistent with conservation of energy.

Chu[15] has described polarization circuits which consist of rotary joints, a differential phase shifter and a differential attenuator. Using these components, he gives designs having minimum differential phase shift and minimum differential attenuation. It could be expected that minimum differential attenuation is equivalent to maximum η_1 and η_2; however, some clever passive decoupling circuitry may be conceived with even better efficiency than can be achieved by Chu's circuitry. This was the motivation behind this section.

In order to establish bounds on η_1 and η_2 it is necessary to define in more detail the response of both transmitters at Terminals 1 and 2. Using conventional scattering matrix notation let a_1' and a_2' denote the complex amplitudes of wave

[15] T. S. Chu, "Restoring the Orthogonality of Two Polarizations in Radio Communication Systems," Part I, BSTJ, Vol. 50, No. 9, Nov. 1971, pp. 3063-3069, Part II, BSTJ, Vol. 52, No. 3., March 1973, pp. 319-327.

travelling to the right at Terminals 1 and 2, respectively, due to Transmitter 1. Similarly define a_1'' and a_2'' in a similar manner for Transmitter 2. The available received powers, defined earlier, can then be written

$$P_1 = \left|a_1'\right|^2 + \left|a_2'\right|^2 \; ; \; P_2 = \left|a_1''\right|^2 + \left|a_2''\right|^2 \quad . \tag{B-1}$$

As subsequent analysis will show, the parameter which determines the achievable values for η_1 and η_2 is given by

$$\rho = \left| \frac{a_1' (a_1'')^\star + a_2' (a_2'')^\star}{\sqrt{P_1 P_2}} \right| \quad . \tag{B-2}$$

Note that the total available power from both transmitters is

$$P_T = P_1 + P_2 + 2\rho\sqrt{P_1 P_2} \; e^{i\phi} \tag{B-3}$$

Where ϕ is a measure of the relative phase between the transmitters. Thus, if the phase is adjusted properly at the transmitting end, the maximum available received power is

$$P_{TM} = P_1 + P_2 + 2\rho\sqrt{P_1 P_2} \quad . \tag{B-4}$$

This suggests that ρ is a rather fundamental characterization of the received signals. In particular, ρ is independent of the exact form of the lossless matching circuit which follows the antenna; and the power transfer coefficients η_1 and η_2, for a minimum loss decoupling circuit, satisfy the relationship

$$(\eta_1 - 1)(\eta_2 - 1) = \rho^2 \tag{B-5}$$

Thus, if it is desired to receive only from Transmitter 1 set $\eta_2 = 0$, and the highest possible value of η_1 is

$$\eta_1 = 1 - \rho^2, \quad \eta_2 = 0 \tag{B-6}$$

Also, if the interest is in receiving from both transmitters, and $\eta_1 = \eta_2 = \eta$, then

$$\eta_1 = \eta = 1 - \rho \quad . \tag{B-7}$$

A decoupling circuit is a four-port device and its properties are specified, at one frequency, by a 4 x 4 matrix (16 complex numbers). Since the decoupling circuit is completely general, it may be assumed, without loss of generality, that it feeds matched loads. This assumption leads to considerable simplifications. Using conventional scattering matrix notation, and with the ports numbered as in Figure B-1, the operation of the decoupling circuit is described by

$$\begin{bmatrix} b_1 \\ b_2 \\ b_3 \\ b_4 \end{bmatrix} = \begin{bmatrix} S \end{bmatrix} \begin{bmatrix} a_1 \\ a_2 \\ 0 \\ 0 \end{bmatrix}$$

which gives the desired output as

$$b_3 = S_{31} a_1 + S_{32} a_2 \tag{B-8}$$

$$b_4 = S_{41} a_1 + S_{42} a_2 \tag{B-9}$$

Decoupling is achieved if b_4 is zero when a_1 and a_2 are due to Transmitter 1, and $b_3 = 0$, when a_1 and a_2 are due to Transmitter 2:

164

$$b_4' = S_{41} a_1' + S_{42} a_2' = 0,$$

$$b_3'' = S_{31} a_1'' + S_{32} a_2'' = 0,$$

or

$$S_{41} = - S_{42} \frac{a_2'}{a_1'} \triangleq - S_{42} \rho_1 \quad , \tag{B-10}$$

$$S_{32} = - S_{31} \frac{a_1''}{a_2''} \triangleq - S_{31} \rho_2 \quad , \tag{B-11}$$

In the last equations

$$r_1 e^{i\phi_1} = \rho_1 = a_2'/a_1' \tag{B-12}$$

and

$$r_2 e^{i\phi_2} = \rho_2 = a_1''/a_2'' \tag{B-13}$$

Substitution of (Equation B-11) in (Equation B-8) allows the output power due

to T_1 to be written as

$$P_0' = \left| S_{31} a_1 \right|^2 \left| (1 - \rho_1 \rho_2) \right|^2$$

and since the power available from Transmitter 1 is

$$P_1 = \left| a_1 \right|^2 + \left| a_2 \right|^2 = \left| a_1 \right|^2 \left[1 + r_1^2 \right]$$

then

$$\eta_1 = \frac{P_0'}{P_1} = \frac{\left| S_{31} \right|^2 \left| 1 - \rho_1 \rho_2 \right|^2}{1 + r_1^2} \quad . \tag{B-14}$$

Similarly

$$\eta_2 = \frac{\left| S_{42} \right|^2 \left| 1 - \rho_1 \rho_2 \right|^2}{1 + r_2^2} \quad . \tag{B-15}$$

165

The remaining problem is to find restrictions imposed on $\left|S_{31}\right|^2$ and $\left|S_{42}\right|^2$ by conservation of energy. For any input (a_1, a_2), the output of the decoupling circuit, (b_1, b_2), can be written as

$$\begin{bmatrix} b_1 \\ b_2 \end{bmatrix} = \begin{bmatrix} S_{31} & -\rho_2 S_{31} \\ -\rho_1 S_{42} & S_{42} \end{bmatrix} \begin{bmatrix} a_1 \\ a_2 \end{bmatrix} \quad , \tag{B-16}$$

or

$$\overline{b} = T \, \overline{a} \quad .$$

The total power in $\overline{b}$ is given by $\left|b_1\right|^2 + \left|b_2\right|^2$ and is related to the input by

$$(\overline{b})^+ b = (T\overline{a})^+ T a = a^+ (T^+ T) a$$

where the dagger denotes the conjugate transpose operation. It is well known from matrix algebra that the output power $b^+ b$, for a given input power $a^+ a$, is maximized by choosing a to be an eigenvector of the matrix $T^+ T$. Furthermore, the power gain is simply the largest eigenvalue of the matrix $T^+ T$. Thus, it is known that values of S_{42} and S_{31} which cause the largest eigenvalue of $T^+ T$ to be larger than unity, violate conservation of energy.

Direct computations of the matrix $T^+ T$ shows that it can be written as

$$T^+ T = \begin{bmatrix} A & B \\ B^* & D \end{bmatrix} =$$

166

where

$$A = |S_{31}|^2 + |\rho_1 S_{42}|^2 \quad ,$$

$$D = |S_{42}|^2 + |\rho_2 S_{31}|^2 \quad ,$$

$$B = -|S_{31}|^2 \rho_2 - |S_{42}|^2 \rho_1^* \quad . \tag{B-17}$$

Also, the eigenvalues of $T^+ T$ are given as the roots of $(A - \lambda)(D - \lambda) - |B|^2 = 0$

or

$$\lambda = \frac{A + D}{2} \pm \sqrt{|B|^2 + \left(\frac{A - D}{2}\right)^2} \quad .$$

Thus, the bounds on S_{31} and S_{42} are obtained by setting

$$1 = \frac{A + D}{2} + \sqrt{|B|^2 + \left(\frac{A - D}{2}\right)^2} \tag{B-18}$$

which reduces to

$$|B|^2 + A + D - AD - 1 = 0 \quad . \tag{B-19}$$

Substitution of definitions B-17, B-14, and B-15 into (Equation B-19) yields, after considerable algebraic manipulation, to the desired result

$$(\eta_1 - 1)(\eta_2 - 1) = \rho^2 \tag{B-5}$$

where ρ is as defined earlier by (Equation B-2) ρ is also given by

$$\rho = \frac{|\rho_1 + \rho_2^*|}{\left[(1 + r_1^2)(1 + r_2^2)\right]^{1/2}} \tag{B-20}$$

167

(Equation B-5) is the principal result of this section. It shows that loss is necessary to uncouple the two received signals unless $\rho = 0$. It also shows how the efficiencies can be traded between the two signals within the limits of $1 - \rho^2$ and 0. It is also seen that a circuit which obeys (Equation B-5) becomes lossless for a particular input excitation. It is expected, then, that a minimum loss decoupling circuit would introduce loss like a lossy card in a circular waveguide - i.e., the loss is zero for a polarization normal to the card.

B-3.0   A MINIMUM LOSS DECOUPLING CIRCUIT

In the previous section, bounds on the maximum achievable efficiency of polarization decoupling networks were obtained. In this section, is shown one realization of a decoupling network which achieves this bound. There are many other possible realizations. Chu's decoupling circuit can be shown to be minimum loss with $\eta_1 = \eta_2$.

The circuit to be described is shown in Figure B-2. Referring to this figure, let Transmitter 1 produce waves $1/\sqrt{1 + r_1^2}$ and $(r_1 e^{i\phi_1})/\sqrt{1 + r_1^2}$ into the coupling network at Terminals 1 and 2, respectively. Similarly, let Transmitter 2 produce waves $r_2 e^{i\phi_2}/\sqrt{1 + r_2^2}$ and $1/\sqrt{1 + r_2^2}$ at Terminals 1 and 2, respectively. The first operation is a differential phase shift $-\phi$, which gives in-phase responses* to Transmitter 1 at plane $a - a$. The second operation is equivalent to a coordinate rotation

---

* Terminals 1 and 2 can be viewed as vertical and horizontal polarizations in a circular guide. With this viewpoint, the phase shift $-\phi_1$ gives linear polarization for Transmitter 1.
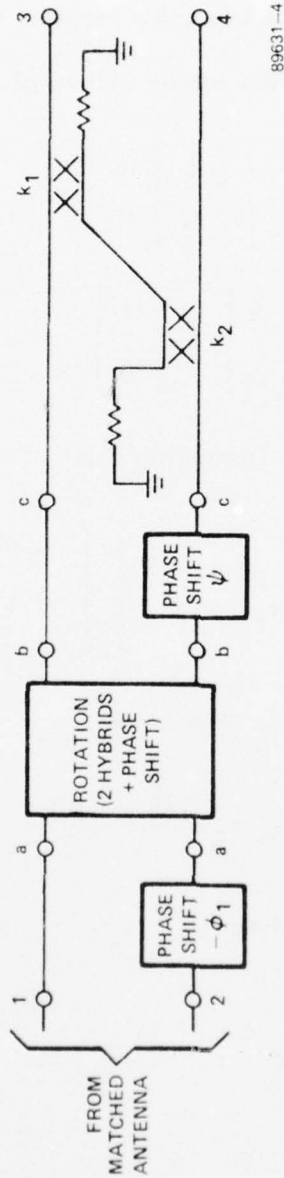
Figure B-2   One Realization of a Minimum Loss Polarization Decoupling Circuit.

through an angle θ where $\tan \theta = r_1$. Together with the phase shift $-\phi_1$, this rotation uncouples Transmitter 1 from the bottom line. So far, no loss has been introduced and the phase shift ϕ and θ are independent of the response to Transmitter 2. One method of implementing the rotation is shown in Figure B-3. Neglecting common phase shifts the outputs following the coordinate rotation can be written as:

$$- \frac{1}{\sqrt{1 + r_1^2}} \begin{bmatrix} \cos \theta & \sin \theta \\ -\sin \theta & \cos \theta \end{bmatrix} \begin{bmatrix} 1 \\ r_1 \end{bmatrix}$$

$$= \frac{1}{\sqrt{1 + r_1^2}} \begin{bmatrix} 1 & r_1 \\ -r_1 & 1 \end{bmatrix} \begin{bmatrix} 1 \\ r_1 \end{bmatrix} = \begin{bmatrix} 1 \\ 0 \end{bmatrix}$$

due to Transmitter 1. The response due to Transmitter 2 is

$$\frac{1}{\sqrt{(1 + r_1^2)(1 + r_2^2)}} \begin{bmatrix} 1 & r_1 \\ -r_1 & 1 \end{bmatrix} \begin{bmatrix} r_2 e^{i(\phi_1 + \phi_2)} \\ 1 \end{bmatrix}$$

$$= \frac{1}{\sqrt{(1 + r_1^2)(1 + r_2^2)}} \begin{bmatrix} r_2 e^{i(\phi_1 + \phi_2)} + r_1 \\ -r_1 r_2 e^{i(\phi_1 + \phi_2)} + 1 \end{bmatrix} = \begin{bmatrix} \rho e^{i\psi} \\ \sqrt{1 - \rho^2} \end{bmatrix} e^{i\alpha}.$$

In writing the last equation the fact is used that

$$\frac{\left| r_2 e^{i(\phi_1 + \phi_2)} + r_1 \right|}{\sqrt{(1 + r_1^2)(1 + r_2^2)}} = \rho \quad . \tag{B-21}$$

170

Figure B-3 Possible Implementation of Coordinate Rotation.
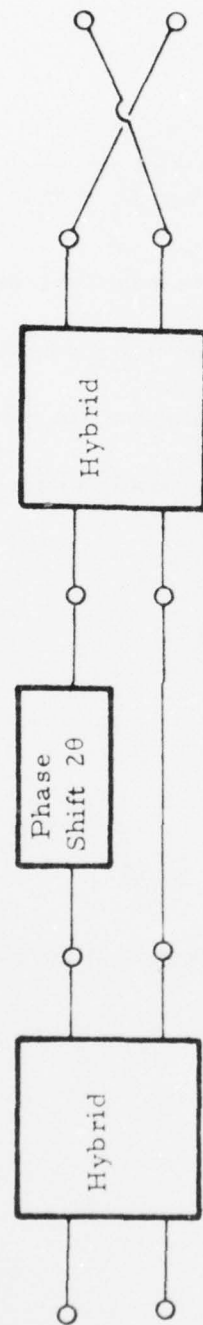
$$\frac{1}{\sqrt{2}} \begin{bmatrix} 1 & j \\ j & 1 \end{bmatrix} \qquad \begin{bmatrix} e^{-j2\theta} & 0 \\ 0 & 1 \end{bmatrix} \qquad \frac{1}{\sqrt{2}} \begin{bmatrix} 1 & j \\ j & 1 \end{bmatrix} \qquad \begin{bmatrix} 0 & 1 \\ 1 & 0 \end{bmatrix}$$

$$T = je^{j\theta} \begin{bmatrix} \cos\theta & \sin\theta \\ -\sin\theta & \cos\theta \end{bmatrix}$$

171

1.0

1.1

1.25   **1.4**   **1.6**

2.8   2.5

3.2   2.2

2.0

1.8
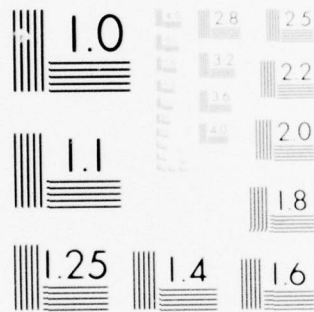
Also, ψ is defined as the angle between $x = r_2 e^{i(\phi_1 + \phi_2)} + r_1$ and $y = 1 - r_1 r_2 e^{i(\phi_1 + \phi_2)}$, i.e., ψ is the angle of xy^*.

$$\tan \psi = \frac{r_2 (1 + r_1^2) \sin (\phi_1 + \phi_2)}{r_1 (1 - r_2^2) + r_2 (1 - r_1^2) \cos (\phi_1 + \phi_2)} \quad . \qquad \text{(B-22)}$$

The common angle α is the angle of y and is unimportant for the present purpose. The next operation shown in Figure B-3 is to apply a differential phase shift ψ so that the responses due to T_2 are ρ and $\sqrt{1 - \rho^2}$, i.e., the responses are in-phase. The final operation employs a pair of directional couplers. The couplers have transfer matrices given by

$$\begin{bmatrix} k_i & i \sqrt{1 - k_i^2} \\ i\sqrt{1 - k_i^2} & k_i \end{bmatrix} \quad i = 1, 2 \quad .$$

Decoupling is then achieved if

$$\sqrt{1 - \rho^2} \ \sqrt{1 - k_2^2} \ \sqrt{1 - k_1^2} = k_1 \ \rho \qquad \text{(B-23)}$$

This equation does not specify k_1 and k_2 uniquely. Note that the efficiency for Transmitter 1 is

$$\eta_1 = k_1^2$$

and the efficiency for Transmitter 2 is

$$\eta_2 = (1 - \rho^2) k_2^2 \quad .$$

Substitution of the last two equations in (Equation B-23) gives

$$(\eta_1 - 1)(\eta_2 - 1) = \rho^2$$

which is the bounding relationship for η_1 and η_2 obtained in the previous section.

If $\eta_1 = \eta_2$ then

$$k_1^2 = \eta_1 = 1 - \rho$$

$$k_2^2 = \frac{\eta_2}{1 - \rho^2} = \frac{1}{1 + \rho} \qquad .$$

Since $1 - \rho \cong 1/1 + \rho$ for small ρ it is possible to make $k_1 = k_2$ for simplicity and end up with efficiencies that differ somewhat. For example if $\rho^2 = 0.1$ then, from (Equation B-23)

$$(1 - 0.1)(1 - k^2)^2 = 0.1 k^2$$

or

$$k^2 = 0.717624$$

Thus

$$\eta_1 = k^2 = 0.717624$$

$$\eta_2 = (1 - \rho^2) k^2 = 0.64586$$

compared to $\eta_1 = \eta_2 = 1 - \sqrt{0.1} = 6838$ when k_1 and k_2 are adjusted properly for equal efficiencies.

173

B-4.0 EFFECTS OF DECOUPLING CIRCUIT ON SIGNAL-TO-NOISE RATIO

Polarization decoupling circuits cause a reduction in the overall signal-to-noise ratio whose magnitude depends on

1. Degree of nonorthogonality ρ

2. Relative efficiencies η_1 / η_2

3. Location of lossy elements with respect to the low noise amplifiers (LNA's)

Case I - Decoupling Circuit After LNA

If the decoupling circuits follow the high gain LNA, noise generation within the circuit itself may be neglected. At the output of the LNA's, wave

$$x = s_1 + r_2 e^{i\phi_2} s_2 + n_1$$

on one line

and

$$y = s_2 + r_1 e^{i\phi_1} s_1 + n_2$$

on the other line. To eliminate s_2 from x add to it $- r_2 e^{i\phi_2} y$ to obtain

$$x^1 = s_1 (1 - r_1 r_2) + s_2 (r_2 - r_2) + n_1 - r_2 e^{i\phi_2} n_2 \quad .$$

Assuming n_1 and n_2 to be uncorrelated and to have the same variance N, write the output signal-to-noise ratio for Transmitter 1 as

$$'\left(\frac{S}{N}\right)_1 = \frac{s_1^2}{N} \frac{\left|1 - r_1 r_2\right|^2}{1 + r_2^2} \quad .$$

Now if s_2 were not present, add $r_1 e^{-i\phi_1} y$ to x (optimal diversity combiner) to obtain

$$x'' = s_1 (1 + r_1^2) + n_2 + r_1 e^{-i\phi_1} n_1$$

which gives a signal-to-noise ratio of

$$\left(\frac{S}{N}\right)''_1 = \frac{s_1^2}{N} (1 + r_1^2) \quad .$$

The degradation in signal-to-noise ratio due to removing s_2 is then

$$= \frac{\left(\dfrac{S}{N}\right)'_1}{\left(\dfrac{S}{N}\right)''_1} = \frac{\left| 1 - r_1 r_2 \right|^2}{(1 + r_1^2)(1 + r_2^2)} \quad .$$

Using (Equation B-21) for ρ the above equation can be put in the form

$$\frac{'(S/N)_1}{''(S/N)_1} = 1 - \rho^2 \quad .$$

It is possible to retrace the same steps and verify that (Equation B-24) also applies to the second signal.

Case II - Decoupling Circuit Before LNA

If the decoupling circuit is placed before the LNA's, the effective gain of the antenna will be reduced by the factors η_1 and η_2. Suppose it is desired to receive from Transmitter 1 only. In that case make $k_2 = 0$ in Figure B-2. With this arrangement, the pads in the coupling circuit radiate noise out of the antenna but not toward the LNA. Further, assuming equal and uncorrelated antenna noise from Terminals 1 and 2 (Figure B-1), it is readily argued that the antenna noise temperature is unchanged by

175

the decoupling network. Hence, the loss in signal-to-noise ratio is simply equal to the loss in signal which is $1 - \rho^2$.

Now, consider the case where both signals are to be received with equal efficiency: $\eta_1 = \eta_2 = \eta = 1 - \rho$. In this case the effective antenna gain is reduced by $1 - \rho$, but in addition, coupler k_2 in Figure B-2 radiates noise power $T_0 (1 - k_2^2)$ toward Terminals 4, and $T_0 k_2^2 (1 - k_1^2)$ toward Terminals 3; T_0 being the temperature of the couplers. As discussed in the previous section, equal efficiency is obtained with

$$k_1^2 = 1 - \rho$$

and

$$k_2^2 = \frac{1}{1 + \rho} \qquad .$$

Thus the couplers radiate

$$T_0 (1 - k_1^2) k_2^2 = \frac{T_0 \rho}{1 + \rho}$$

toward Terminals 3 and

$$T_0 (1 - k_2^2) = T_0 \frac{\rho}{1 + \rho}$$

toward Terminals 4. Also, the antenna noise as seen at Terminals 3 is

$$T_a (k_1^2 + (1 - k_2^2)(1 - k_1^2)) = \frac{T_a}{1 + \rho} \text{ and } T_a k_2^2 = \frac{T_a}{1 + \rho} \text{ at Terminals 4. Thus}$$

the system noise temperature referred to the LNA input as

$$T_s = \frac{T_a}{1 + \rho} + T_0 \frac{\rho}{1 + \rho} + T \text{ LNA} \qquad . \tag{B-25}$$

176

This results in a degradation given by

$$\frac{(1 - \rho)(T_a + T\,LNA)}{\dfrac{T_a}{1 + \rho} + T_o\,\dfrac{\rho}{1 + \rho} + T\,LNA} \quad . \tag{B-26}$$

This factor is $1 - \rho$ if the LNA's noise temperature dominates. It is $1 - \rho^2$ if the antenna noise dominates.

The preceding discussion is summarized as follows. The use of a polarization decoupling circuit preceding the LNA's reduces the overall signal-to-noise ratio by $10 \log (1 - \rho^2)$ when only one of the two received signals is extracted from the antenna. This neglects incidental losses present in the decoupling circuit. The same signal-to-noise ratio loss, $10 \log (1 - \rho^2)$, applies to polarization decoupling networks following the LNA, but in that case, both signals can be extracted with this loss. No bonus is to be had if only one signal is of interest. The use of a polarization decoupling circuit which delivers both signals with equal efficiency preceding the LNA's causes a signal loss of $10 \log (1 - \rho)$, and in addition, generates noise in the coupler. A simple formula giving the minimum degradation in that case is given by (Equation B-26). The loss can be as small as $10 \log (1 - \rho^2)$ when the antenna noise dominates, but can also be larger than $10 \log (1 - \rho)$ if the noise from the LNA's dominates.

B-5.0   EFFECT OF TRANSMITTED POLARIZATIONS ON SIGNAL-TO-NOISE RATIO

In the previous section, it was assumed the received polarizations were arbitrary but fixed. With this assumption, the complete system to the left of Terminals 1

177

and 2 in Figure B-1 was described by three real numbers: P_1, P_2 and ρ. In general, these three parameters depend on the transmitted polarizations. In this section, is investigated the dependence of the output signal-to-noise ratio on the choice of transmitted polarizations. The system to be considered is shown in Figure B-4.

The fixed portion of the system in Figure B-4 is a four-port network and generally requires a 4 x 4 matrix for its description at one frequency. However, it is assumed again that the antennas incorporate lossless matching networks such that the two ports of either antenna have zero mutual coupling and reflection coefficients. With this assumption, a 2 x 2 matrix is all that is required to describe the fixed portion of the system. For this purpose we can also describe the fixed portion of the system as a cascade of a lossless coupling circuit, a lossy uncoupled circuit, and another lossless coupling network as shown in Figure B-5*. The input lossless coupling circuit can be lumped into the variable coupling circuit at the transmitting end; also, the output lossless coupling network can be neglected, since, as discussed earlier, it has no effect on P_1, P_2 and ρ,

---

*The validity of the equivalent representation follows from the theory of matrices. An arbitrary square matrix. A can be written as

$$A = B \, \ell \, U \qquad .$$

U is a unitary matrix whose rows are the eigenvectors of the matrix $A^+ A$, ℓ is a diagonal matrix whose elements are the square roots of the eigenvalues of the matrix A^+A and B is a unitary matrix given by

$$B = A \, U^+ \ell^{-1} \qquad .$$

178
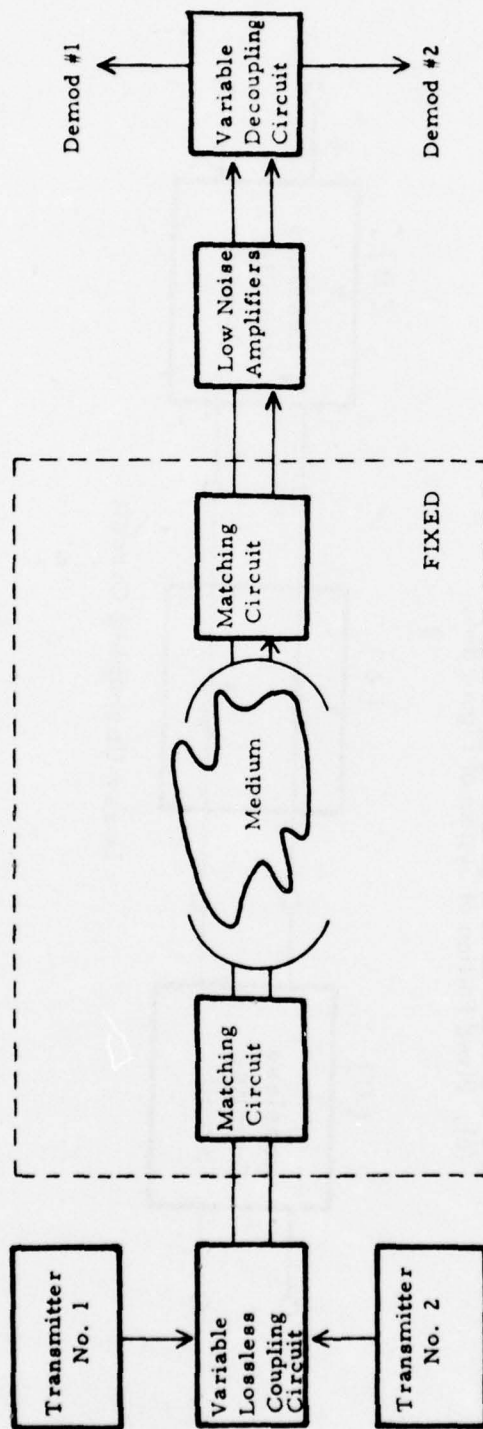
Figure B-4 Dual Polarization Radio Link With Variable Transmitted Polarizations.

179

[A]

Transmitting and Receiving
Antennas and Medium
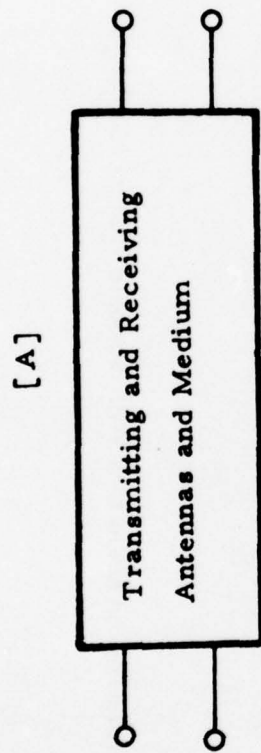
(a). Fixed Portion of System of Figure B-4.

[U]

Lossless
Coupling
Circuit

[ι]

l_1

l_2

[B]

Lossless
Coupling
Circuit

Lossy Uncoupled Circuit
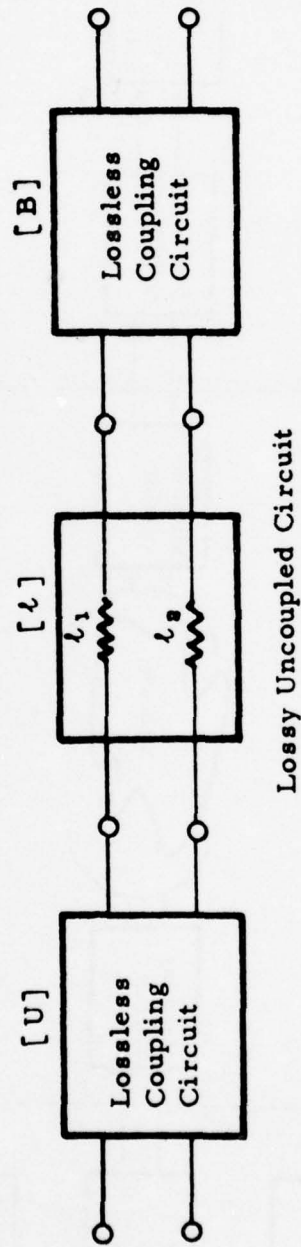
(b). Equivalent Representation of Circuit of Figure B-5A

Figure B-5

180

nor on the antenna noise characteristics*. Therefore, the system of Figure B-4 can be simplified to the equivalent system of Figure B-6. In Figure B-6, λ_1 is the power transfer coefficient for the polarization that propagates best (minimum loss) and λ_2 is the power transfer coefficient for the polarization that propagates the poorest. These two polarizations are always orthogonal (eigenvectors of the matrix A^+A are orthogonal). If $\lambda_1 = \lambda_2$ there is no preferred polarization from the present theoretical standpoint. But if $\lambda_1 > \lambda_2$, the output signal-to-noise ratios do depend on the choice of transmitted polarizations. If a single signal were to be transmitted use should be made of the polarization that propagates best and realize a power transfer coefficient λ_1. But with two signals to be transmitted, what constitutes a good choice of transmitted polarization?

Suppose that Transmitter 1 excites waves α_1 and β_1 at Terminals 1 and 2, respectively, in Figure B-2 and define α_2 and β_2 in a similar manner for Transmitter 2. Since the variable lossless coupling circuit has a transfer matrix equivalent to a rotation, it is necessary to have

$$
\left.
\begin{aligned}
\alpha_1 &= \sqrt{P_{T1}} \cos \theta \\
\alpha_2 &= \sqrt{P_{T2}} \sin \theta \\
\beta_1 &= \sqrt{P_{T1}} \sin \theta \, e^{i\phi} \\
\beta_2 &= \sqrt{P_{T2}} \cos \theta \, e^{i\phi}
\end{aligned}
\right\}
\tag{B-27}
$$

where θ and ϕ are arbitrary and P_{T_1} and P_{T_2} are the powers available

---

* Antenna noise voltage at Terminals 1 and 2, Figure B-2, are assumed to have equal variances and are uncorrelated. A lossless coupler preserves variance and lack of correlation.
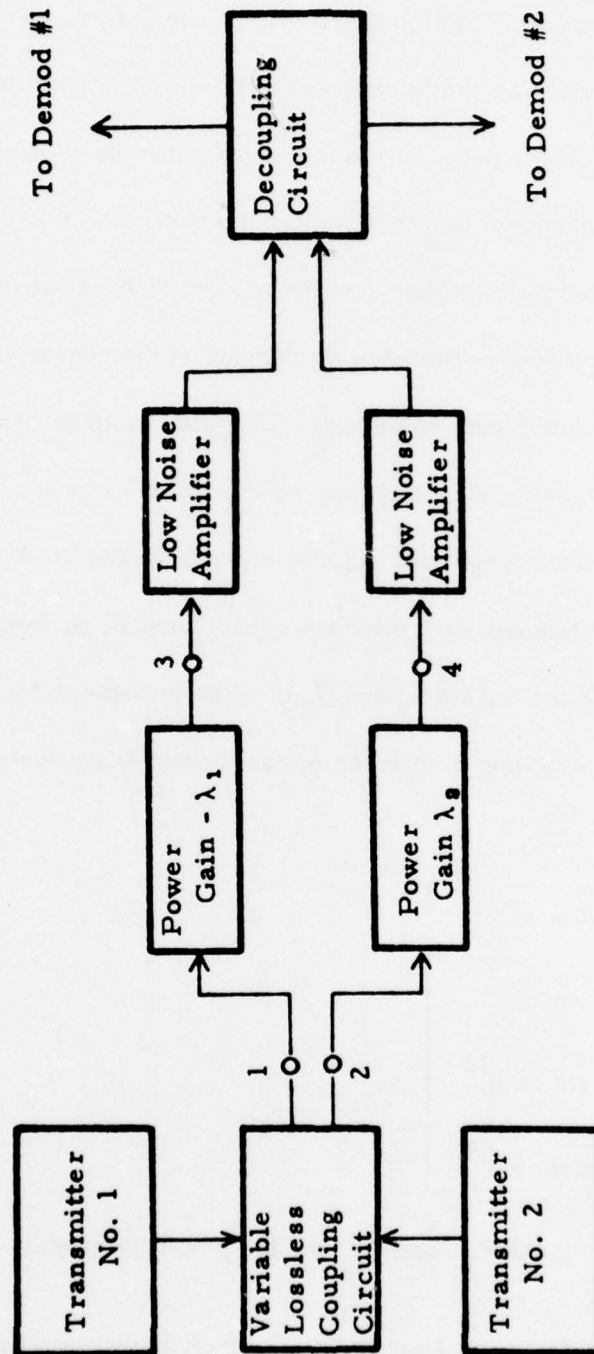
Figure B-6 Dual Polarization System Equivalent to System of Figure B-4 .

from Transmitters 1 and 2, respectively. The received power from Transmitter 1 is then

$$P_1 = P_{T1} (\lambda_1 \cos^2 \theta + \lambda_2 \sin^2 \theta) \qquad (B-28)$$

and, similarly,

$$P_2 = P_{T2} (\lambda_1 \sin^2 \theta + \lambda_2 \cos^2 \theta) \qquad (B-29)$$

Also, the correlation coefficient defined in Section B-2 is*

$$\rho = \frac{\left| \sin \theta \cdot \cos \theta (\lambda_1 - \lambda_2) \right|}{\sqrt{(\lambda_1 \cos^2 \theta + \lambda_2 \sin^2 \theta)(\lambda_1 \sin^2 \theta + \lambda_2 \cos^2 \theta)}} \qquad (B-30)$$

It is seen in Section B-4 that post LNA decoupling leads to an effective power loss of $1 - \rho^2$. Thus, the effective received power from Transmitter 1 is

$$P_{e1} = P_{T1} \frac{\lambda_1 \lambda_2}{\lambda_1 \sin^2 \theta + \lambda_2 \cos^2 \theta} = \frac{P_{T1}}{L_1} \qquad (B-31)$$

Similarly, we have

$$P_{e2} = P_{T2} \frac{\lambda_1 \lambda_2}{\lambda_1 \cos^2 \theta + \lambda_2 \sin^2 \theta} = \frac{P_{T2}}{L_2} \qquad (B-32)$$

Note that the transmission loss factors just defined are such that $L_1 + L_2 = \frac{1}{\lambda_1} + \frac{1}{\lambda_2}$, independent of θ.

---

*Note that the maximum value of $\rho = (\lambda_1 - \lambda_2)/(\lambda_1 + \lambda_2)$

183

Now suppose that the transmitted powers are equal and it is desired to have equal effective received signal powers (or output signal-to-noise ratios). Taking $\sin \theta = \cos \theta = 1/\sqrt{2}$, the effective received power is

$$\left. \begin{array}{l} P_e = P_T \; \dfrac{2\lambda_1 \lambda_2}{\lambda_1 + \lambda_2} \; , \\[2ex] P_e = P_{e1} = P_{e2} \\[2ex] P_T = P_{T1} = P_{T2} \end{array} \right\} \tag{B-33}$$

As a matter of interest, the same effective received powers are achieved if the total transmitted power is set

$$P_{T1} + P_{T2} = 2 P_T$$

and select $\theta = 0$ and adjust P_{T1} and P_{T2} such that equal powers are received, i.e.,

$$P_{T1} \lambda_1 = P_{T2} \lambda_2 \; .$$

The results of the preceding section may be summarized as follows. A transmission system consisting of dual polarized transmitting and receiving antennas with the intervening medium is equivalent to two uncoupled paths having power gains (much less than unity) λ_1 and λ_2. With post LNA decoupling circuits, the effective power gains depend on the transmitted polarizations in a manner given by Equations (B-31 and B-32) such that the sum of the effective power loss factors (reciprocal of power gain) is independent of the choice of orthogonal transmitted polarizations. With equal transmitter powers, the signal-to-noise ratios at the output of the decoupling circuits are equalized

184

from Transmitters 1 and 2, respectively. The received power from Transmitter 1 is
then

$$P_1 = P_{T1} \ (\lambda_1 \cos^2 \theta + \lambda_2 \sin^2 \theta) \tag{B-28}$$

and, similarly,

$$P_2 = P_{T2} \ (\lambda_1 \sin^2 \theta + \lambda_2 \cos^2 \theta) \tag{B-29}$$

Also, the correlation coefficient defined in Section B-2 is*

$$\rho = \frac{\left| \sin \theta \cdot \cos \theta \ (\lambda_1 - \lambda_2) \right|}{\sqrt{(\lambda_1 \cos^2 \theta + \lambda_2 \sin^2 \theta)(\lambda_1 \sin^2 \theta + \lambda_2 \cos^2 \theta)}} \tag{B-30}$$

It is seen in Section B-4 that post LNA decoupling leads to an effective power loss of
$1 - \rho^2$. Thus, the effective received power from Transmitter 1 is

$$P_{e1} = P_{T1} \ \frac{\lambda_1 \lambda_2}{\lambda_1 \sin^2 \theta + \lambda_2 \cos^2 \theta} = \frac{P_{T1}}{L_1} \tag{B-31}$$

Similarly, we have

$$P_{e2} = P_{T2} \ \frac{\lambda_1 \lambda_2}{\lambda_1 \cos^2 \theta + \lambda_2 \sin^2 \theta} = \frac{P_{T2}}{L_2} \tag{B-32}$$

Note that the transmission loss factors just defined are such that $L_1 + L_2 = \frac{1}{\lambda_1} + \frac{1}{\lambda_2}$,
independent of θ.

---

*Note that the maximum value of $\rho = (\lambda_1 - \lambda_2)/(\lambda_1 + \lambda_2)$

183

by having each transmitter divide its power equally between the maximum and minimum gain paths. If this 1:1 power split is not used, different signal-to-noise ratios will be achieved, one above and one below the value realized with the 1:1 power split. For example, if $\lambda_1 \neq \lambda_2$ because of the presence of oblate rain drops in the medium, use can be made of orthogonal circular polarizations or linear polarizations aligned $\pm 45^{\circ}$ from the major axis of the raindrops) to equalize the effective path loss for both transmitted signals. This statement applies only when a post LNA decoupling circuit is used. If the receiving system does not use polarization decoupling circuits the transmitted polarizations recommended above would result in maximum crosstalk.

B-6.0   IMPROVEMENT IN SIGNAL-TO-NOISE PLUS CROSSTALK RATIO WITH INCOMPLETE DECOUPLING

In Section B-4, it was shown that the presence of the cross polarization signal causes a degradation in the signal-to-noise ratio at the output of a post LNA decoupling circuit. The degradation factor was found to be $-\rho$ based on complete removal of the interfering signal. Figure B-7 shows an LNA decoupling circuit which optimizes signal-to-noise plus crosstalk power ratio. In Figure B-7, P_1 and P_2 denote signal powers, n_1 and n_2 are independent noise with the same variance N, and ρ is as defined earlier. The inputs to the decoupling circuits have been written in a form to simplify the computations to follow. These inputs could be written in apparently more general forms but the overall result would be the same.

185

$$\sqrt{P_1} + \rho\sqrt{P_2} + n_1 \qquad\qquad \sqrt{P_1} + \sqrt{P_2}\rho(1-g) + n_1 + \frac{g\rho}{\sqrt{1-\rho^2}}\, n_2$$

$$g =$$

$$\sqrt{(1-\rho^2)\, P_2} + n_2 \qquad\qquad \frac{\rho}{\sqrt{1-\rho^2}}$$
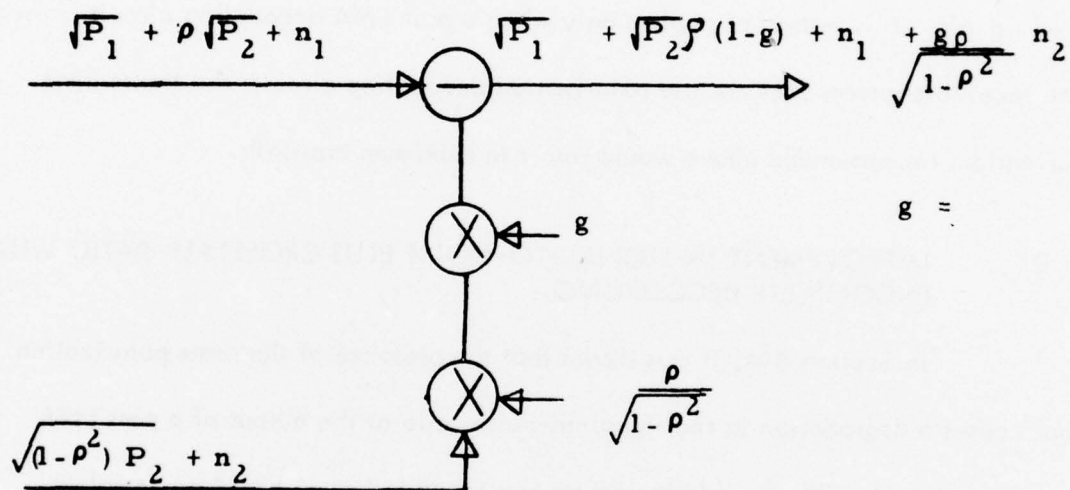
Figure B-7   Post LNA Decoupling Circuit Which Maximizes Signal-to-Noise Plus Crosstalk Power Ratio.

This circuit delivers a desired signal power P_1, crosstalk power X, where

$$X = P_2 \, \rho^2 \, (1-g)^2 \quad ,$$

and noise power

$$No = N \left(1 + \frac{g^2 \, \rho^2}{1 - \rho^2} \right)$$

The signal-to-noise plus crosstalk power ratio is then

$$\left(\frac{S}{N_T} \right) = \frac{P_1}{X + No} = \frac{P_1 \, (1 - \rho^2)}{P_2 \, \rho^2 \, (1 - \rho^2) \, (1 - g)^2 + N \, (1 - \rho^2 + g^2 \, \rho^2)} \quad . \text{(B-35)}$$

With $g = 1$ this equation reduces to

$$\left(\frac{S}{N_T} \right) = \frac{P_1 \, (1 - \rho^2)}{N}$$

in agreement with the results of Section B-4.

It is readily verified that $(S/N)_T$ can be maximized by choosing

$$g = g_o = \frac{P_2 \, (1 - \rho^2)}{N + P_2 \, (1 - \rho^2)} \tag{B-36}$$

Defining Y_1 and Y_2 as the signal-to-noise ratios, with $g = 1$ i.e.,

$$Y_1 = \frac{P_1 \, (1 - \rho^2)}{N} \quad ,$$

$$Y_2 = \frac{P_2 \, (1 - \rho^2)}{N} \quad ,$$

gives

$$g_o = \frac{Y_2}{1 + Y_2}$$

187

and substitution in (Equation B-35) gives

$$\left(\frac{S}{N}\right) = Y_1 \frac{(Y_2+1)}{(Y_2+1)-\rho^2}$$

$$= \frac{P_1}{N} \frac{1-\rho^2}{1-\frac{\rho^2}{Y_2+1}} \qquad\qquad (B-37)$$

Since Y_2 will generally be at least 10 it is concluded that the advantage resulting from the best setting of g is not very significant.

In summary, it is seen that a better signal-to-total noise power ratio can be realized by allowing some crosstalk power. With this noise, plus crosstalk power criterion for adjusting the decoupling circuits, the output signal-to-total noise power ratio is as given by (Equation B-37). Rather small improvements are realized with this new criterion unless the signal-to-noise ratios are very small.

188

APPENDIX C

ALTERNATIVE ADAPTIVE CROSS POLARIZATION CANCELLATION TECHNIQUES

C-1.0   INTRODUCTION

In this appendix a number of interference reduction techniques are discussed, some of which have been breadboarded.* These techniques include correction at RF, either before or after the low-noise amplifier (LNA), IF correction, and combinations of some of these schemes. In general, each of these techniques has a single common denominator; that is, each scheme must apply differential amplitude and phase correction to the interfering signals in a manner that will reduce the coupling between the signals. Hence, in order to implement working hardware, three elements are required. These are:

a. Correction (or "Weighting") Network

Amplitude and phase adjustments on each signal channel to enable cancelling the interfering signal in each.

b. Performance Measure

A measure of the performance of the weighting circuits, so that improvement can be made by the adaptive controller.

c. Controller

A control network which takes the performance measurement and adjusts the weights to improve performance.

---

*AAFE Contract NAS1-13942, Harris ESD, August 1976

C-1.1   Polarization Correction (Weighting) Networks

C-1.1.1   Trade-Offs of Loss Versus Location and System

The polarization correction network will cause some signal-to-thermal noise loss while minimizing the polarization crosstalk. Considerations of the location of the correction network for trading loss versus crosstalk minimization are;

     a. "Minimum" (or optimum) loss in S/N during polarization correction

     b. Resistive loss

     c. Obtainable crosstalk reduction, considering circuit dispersion

Cross polarizations of two signals can occur in two ways;

     a. Orthogonal polarizations (elliptical or rotated linear)

     b. Nonorthogonal polarizations

Chu[15] and others[16] have analyzed correction networks for such polarizations. It is known that orthogonal polarizations can be corrected using only lossless phase-shift networks, such as the first part of our RF correction network, and most other proposed RF correction networks. On the other hand, if the polarizations are nonorthogonal, some signal-to-noise loss will occur even in optimal correction networks; this loss will be called the "minimum loss." Most minimum-loss correction networks consist of a "lossless" phase-shift section, followed by an orthogonalizing circuit such as a coupler in the second part of our RF correction network. Appendix B analyzes this minimum loss in detail, using the inner product or correlation coefficient, ρ, as a measure of orthogonality of the two

15, 16 (See Reference Listing after Appendix E)

polarizations. The minimum loss varies according to where the low-noise amplifiers (LNA's) are placed, as will be discussed below. In addition, resistive loss contributes to noise temperature, depending upon the position of the LNA's.

On the other hand, correction circuit losses are not the only considerations for where to put the LNA's, since mismatch of the LNA's, if placed before the correction circuit, will limit the obtainable cross polarization cancellation. Several placements of correction network that have been studied are;

    a.   LNA before RF correction network

    b.   LNA after lossless RF correction, but before RF orthogonalization circuit

    c.   LNA after the RF correction network

    d.   IF correction network (after LNA, mixer, IF amplifier, etc.)

    e.   Hybrid correction network

        ●   RF lossless network

        ●   IF orthogonalization circuit

These alternatives are shown in Figure C-1 for RF correction, and Figure C-2 for IF and hybrid corrections.

C-1.1.1.1   LNA Before RF Correction (Figure C-1a)

This is the lowest noise configuration. "Minimum loss" is $(1 - \rho^2)$ from Appendix B. For a "worst-case" rain at 11 GHz, $\rho \cong 0.06$, from Appendix E. Thus, the "minimum loss" is 0.02 dB. Resistive loss does not add significantly to noise temperature
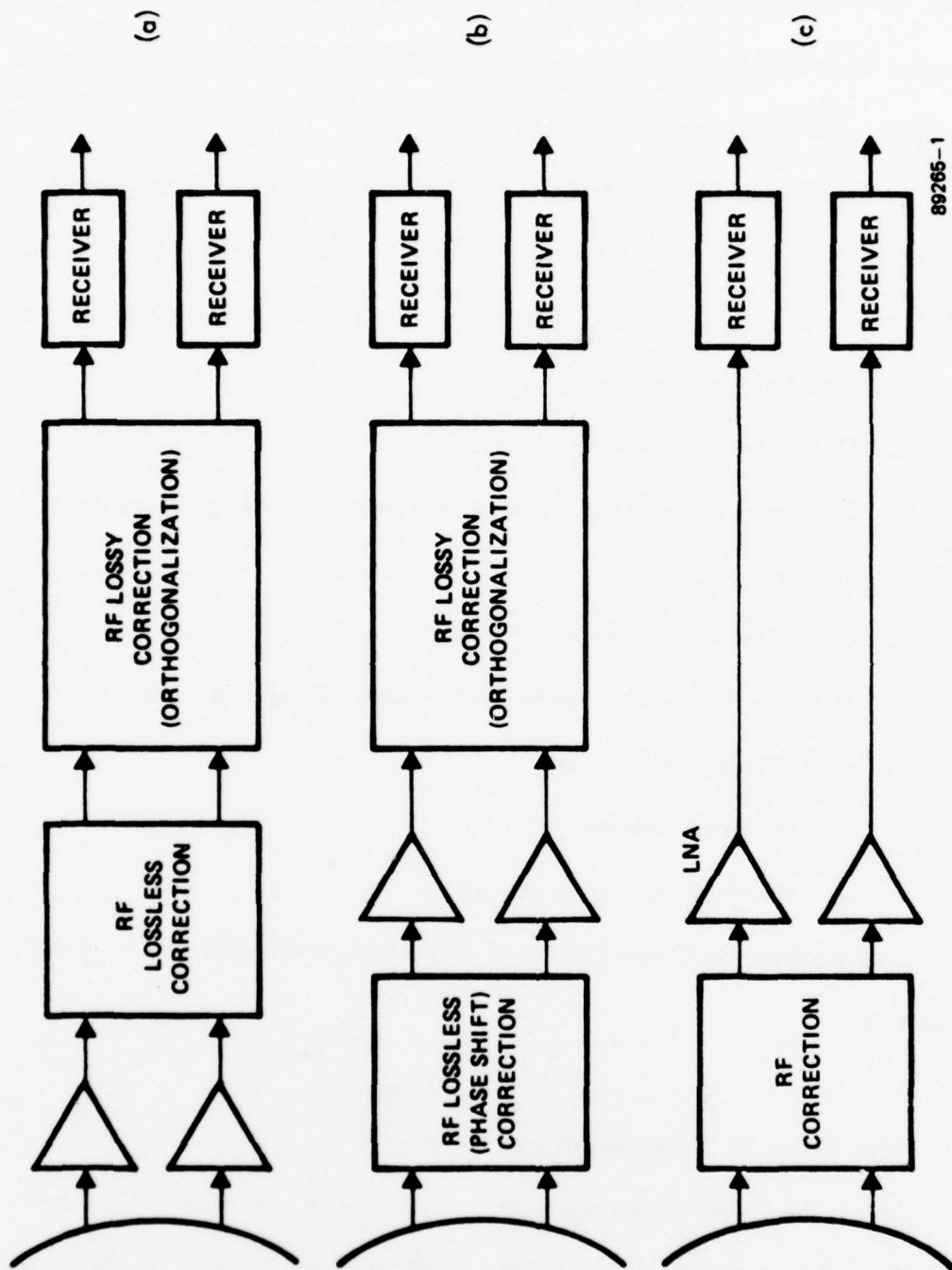
191

Figure C-1. Possible LNA Locations for RF Correction

89265-1

192
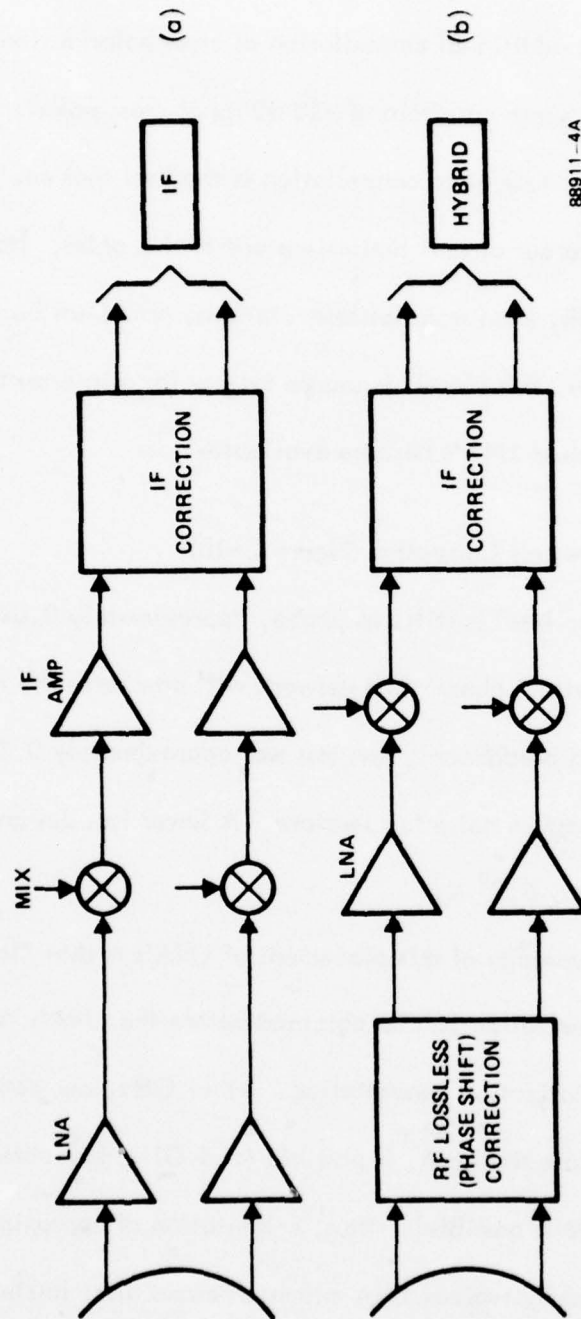
Figure C-2. IF and Hybrid Correction

88911-4A

193

because of LNA's. However, typical LNA mismatch (e.g., 0.5 dB and 10°) could cause limitation in the obtainable additional cancellation of cross polarization to approximately 15 dB. For example, for a worst-case rain of -20 dB input cross polarization, a limitation of approximately -35 dB crosstalk after cancellation is the best that could be obtained. This is not too serious, since our circuit limitations are of this order. However, input cross polarizations of -10 dB, even from lossless rotations, could not be corrected to better than -25 dB crosstalk. Thus, this circuit is usable mainly for rain cross polarization, unless extremely well-matched LNA's become available.

C-1.1.1.2   LNA After Lossless Correction (Figure C-1b)

The "minimum loss" is still, as above, approximately 0.02 dB. The resistive loss of the theoretical "lossless" phase-shift network will now raise the noise temperature. With the Harris Corporation breadboard, this loss was approximately 0.2 dB, causing approximately 13° K increase in noise temperature. A lower loss design, perhaps a 0.1 dB, would add approximately 6.7° K.

The main advantage of this placement of LNA's is that "lossless" phase-shift correction of the cross polarization can be obtained before the LNA's, with their mismatch errors which limit cross polarization cancellation. At 11 GHz, correction to -25 dB cross polarization or better, before the LNA, is possible (at 6 GHz, correction of typical rain cross polarization to -35 dB is possible). Thus, a limitation of approximately 15 dB additional cancellation imposed by typical LNA mismatch errors after lossless corrections

194

would still allow −40 dB crosstalk after both cancellation networks at 11 GHz. More importantly, arbitrary rotations, and other phase shift causes of higher input cross polarization, could also be corrected with similar performance.

C-1.1.1.3   LNA After RF Correction Network (Figure C-1c)

For the LNA after the correction network, the minimum loss is $(1 - \rho)$ from Appendix B, or 0.27 dB for a "worst-case" rain at 11 GHz with $\rho = 0.06$. In addition, resistive loss will contribute more to the noise temperature, since all loss occurs before the LNA's. For our breadboard, losses were approximately 0.7 dB for both parts of the correction network, adding approximately 43° K to the noise temperature. On the other hand, for systems where the ultimate noise temperature is not required, but maximum utilization of bandwidth is required, this configuration offers the maximum cross polarization cancellation to at least −35 dB to −40 dB crosstalk, as limited by waveguide circuit matching in our breadboard. Such residual crosstalk can be obtained even with very large input cross polarization, such as the −7 dB experiments with the NASA breadboard. Also, if only one channel is being received (e.g., as in a small single ground station receiving from a large dual polarization satellite), the minimum loss would be $(1 - \rho^2)$ from Appendix B, or 0.02 dB.

C-1.1.1.4   IF Cancellation (Figure C-2a)

In this case, the LNA's precede the correction network, yielding low-noise performance as in Section C-1.1.1.1. However, mismatch errors affecting cancellation depth include both LNA's and the RF/IF equipment. Typical mismatch budgets limit

additional cancellations to approximately 10-15 dB over a full 500 MHz bandwidth. Thus, a worst-case rain at 11 GHz of -20 dB cross polarization can be reduced to -30 to -35 dB crosstalk. However, much larger cross polarization cannot be corrected sufficiently. Of course, the greatest advantage of this network is the cheaper, simpler, all-electronic circuitry.

C-1.1.1.5   Hybrid Cancellation Network

This network would perform and have the advantages of the RF network with LNA's after the lossless portion of the RF correction network (see Paragraph C-1.1.1.2). Since the lossless correction is at RF before the LNA's, the large lossless corrections (e.g., rotations) could be performed. The orthogonalization circuit at IF would not have the correction capability of the RF orthogonalization circuit; nevertheless, for worst-case rains at 11 GHz, -25 dB crosstalk can be achieved by the first lossless phase-shift network, and -35 dB to -40 dB crosstalk can be achieved after the IF orthogonalization network. This circuit is quite simple, with two electromechanical axes forming the lossless correction network (which can also perform feed rotation, etc.), and an all-electronic orthogonalization network.

C-1.1.1.6   Summary of Performance Versus Location Trade-Offs

Table C-1 summarizes a comparison between RF techniques and IF polarization correction techniques. The advantages of the RF correction include the fundamental wideband nature of waveguide networks coming before most active device mismatch errors can limit cancellation depth. However, RF correction is usually done with electro-mechanical correction networks, with their associated control, wear, and inertia problems.

196

The advantages of the IF correction is mainly that it is all-electronic, thus considerably cheaper. In addition, it can be made flexible for various different RF frequencies without redesign, and can use lossy correction networks due to the IF amplification. Even better cancellation can be achieved with adaptive transversal equalizer approaches. Disadvantages of IF cancellation are that it is usually relatively narrowband for deep cancellations, and requires very careful front-end design. In addition, coherent local oscillators are needed; otherwise, complex frequency tracking cancellation circuits would be required.

Any of the above networks can correct the worst-case rain at 11 GHz to better than -30 dB crosstalk over 500 MHz, which is satisfactory for present QPSK and most video application. Thus, the simpler IF cancellation network is recommended. Future applications, using modulations requiring greater signal-to-crosstalk ratios or larger input cross polarizations may require the hybrid network, which can produce -35 dB to -40 dB crosstalk. This is also the limitation of our RF network, dur to slight waveguide mismatch perfections which must occur in any cancellation network. A 13° K to 43° K increase in noise temperature would be incurred with this hybrid network, depending on the position of the LNA's. For better crosstalk ratios, the RF correction network before LNA's could be used. Finally, for requirements of ultimate low-noise operation (deep space applications) and fairly low crosstalk, LNA's should be placed in front of the RF correction network, with very careful attenuation attention to matching the LNA's across the bandwidth.

197

Table C-1. IF/RF Correction Comparison

RF (Mechanical)	IF (Electronic)
Advantages	
1. Widest Bandwidth	1. All Electronic
2. Largest Cancellation	2. Lightweight Potential
3. Compatible with Existing Receivers	
Disadvantages	
1. Moving Parts	1. Less Cancellation and/or Less Bandwidth
2. Heaviest	
3. Higher Noise Figure (If Before LNA)	

For the NASA contract, both an RF and IF correction network were implemented. Although no low-noise amplifiers were used in the measurements, the second location of the low-noise amplifiers (before the orthogonalization network, but after the phase-shift network) is preferred for the RF approach; measurements were taken of the effect of mismatch errors for low-noise amplifiers at this location. Also, an IF technique was implemented in this contract, showing that a substantial wideband (500 MHz) cancellation is possible. The hybrid technique was also briefly tested, since both networks are available in cascade.

198

C-1.1.2   Specific Candidate RF Correction Networks

Several RF Correction Networks have been proposed and built. In this section, some of these are contrasted to the Harris ESD network, as already briefly described.

C-1.1.2.1   Chu's RF Correction Network

The possibility of using RF correction networks in waveguide has been discussed by Chu[15]. In this paper, Chu shows that by using differential waveguide phase shifters and differential attenuators, each properly oriented with respect to the incoming polarizations, it is possible to orthogonalize two arbitrary polarizations arriving from an antenna. In his article, he emphasized depolarizations due to rain, but the networks are general and capable of orthogonalizing depolarizations due to multipath or nonperfect antennas. A representation of a possible waveguide correction network is shown in Figure C-3. An antenna is depicted that has two focal plane feeds for vertical and horizontal polarization. The vertical and horizontal polarizations are then fed back into vertical and horizontal exciters in a circular waveguide via an orthomode transducer (OMT). In this waveguide, three rotating sections exist. Two of these sections have some mechanism to change phase shift or attenuation, such as depicted in the figure by a variable vane in the waveguide. The rotations, as well as the variations of the vanes, are controlled by electromechanical devices, such as motors. The section produces a differential phase shift between the horizontal and vertical polarizations. It is rotated in orientation (aspect) ratio, and can also produce variable phase shift, for example, as depicted by a rotating

<hr>

15 (See Reference Listing after Appendix E)
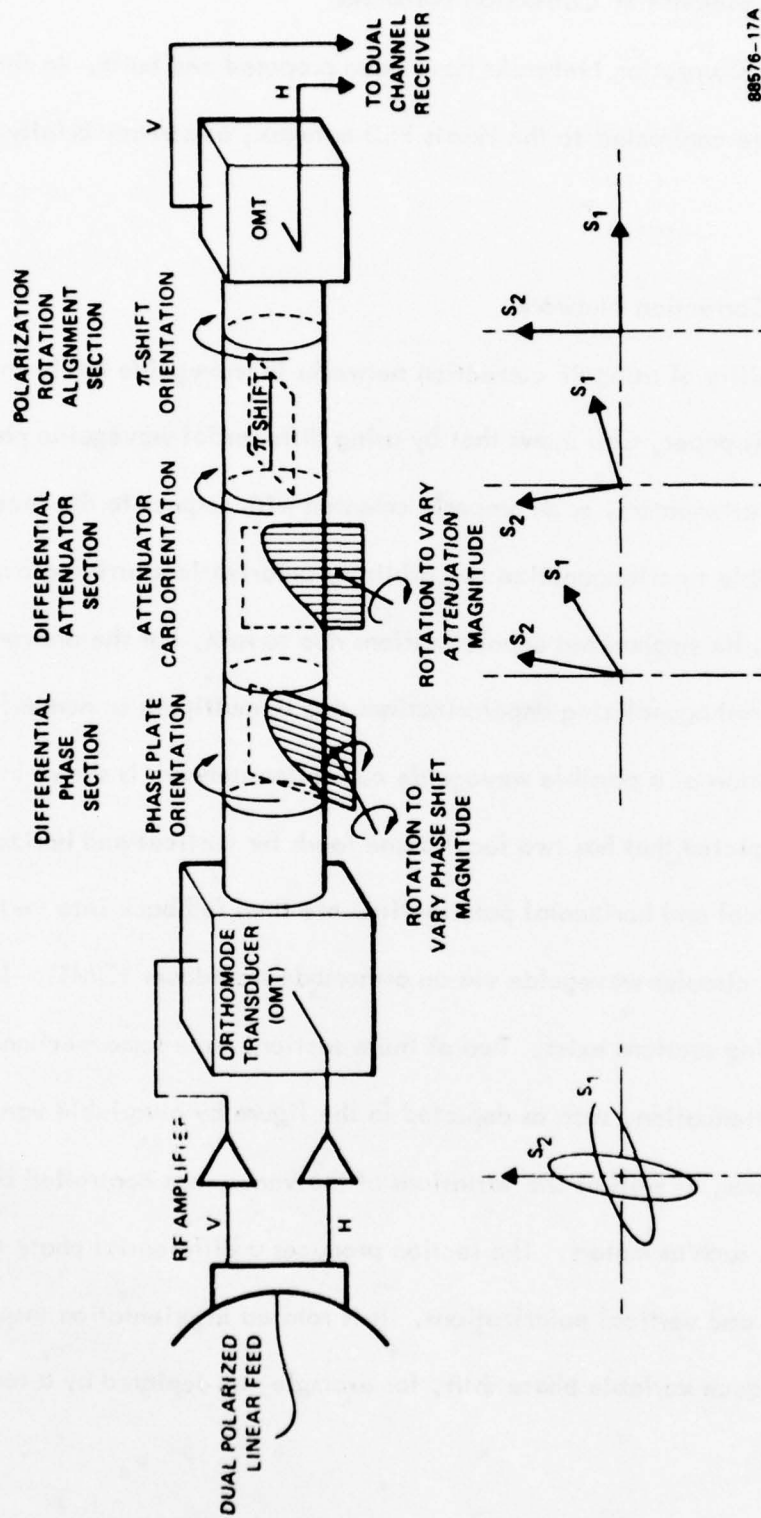
Figure C-3. Chu's RF Correction Network

88576-17A

200

vane varying in and out of the waveguide to achieve a variable phase shift (as well as a variable orientation) with respect to the two polarizations. This is the differential phase shifter, as required by Chu's correction technique, which linearizes incoming elliptic polarizations. The second rotating section can also be varied in orientation in the circular waveguide. It is depicted as a rotating attenuation vane (card) that can be inserted varying amounts depending on the amount of attenuation required. This is the differential attenuator, required by Chu's technique, which rotates the linearized polarization into spatial quadrature. Finally, a properly oriented phase shift vane rotates both polarizations together to match the vertical and horizontal probe pickups in the circular waveguide. Dual channel receivers would then follow, fed by the corrected, pure polarizations generated by the RF correction network.

Of course, there are many possible ways of actually implementing Chu's or other RF correction techniques. Specifically, the rotating vanes depicted in the previous example do not appear desirable, due to the required waveguide slots, VSWR, etc.

At least the first part of this network has been implemented by Rantec Corporation for Bell Telephone. Because of the low RF frequency of interest, 4-6 GHz, the range is essentially entirely corrected by the lossless differential phase shift operation.

The control of this network approach can be seen to be potentially difficult, and it is believed that it has not yet been done. Direct analog control of each axis appears too difficult, since any control of an axis would have to sense complex measures of an orthogonality and axis rotation.

C-1.1.2.2   Cross Coupling Technique

An alternative method for restoring orthogonality has been suggested by

Difonzo. [16c,d] The adaptive circuit employs couplers interconnected via series phase

shifters as shown in Figure C-4. It can readily be shown that a solution exists for the

coupler values (K) and the phase shifts (Ø) that will orthogonalize the two nonorthogonal

elliptically polarized input waves. The circuit operates by coupling a portion of each

signal channel into the other channel so that the interference is cancelled in each channel.

In order to effect an interference reduction, it is necessary to adjust the value of the K's

and Ø's so that the coefficients of the unwanted signal vanish at ports 1A and 1B. In prac-

tice all necessary phase shifts may be obtained with only $\emptyset_{14}$ and $\emptyset_{23}$ variable. In add-

tion the network may be simplified by making $K_2 = K_3$, $K_1 = K_4$, and $\emptyset_{12} = \emptyset_{34}$.

This network can be arranged for direct control of each axis, since each

coupling path corrects one of the two signals incident. Therefore, cross correlations of

the separate signals can independently control the respective cross-coupling path.

C-1.1.2.3   Marconi Network

The Marconi Corporation, under an INTELSAT contract, has designed the

network shown in Figure C-5. The first portion consists of a variable phase shifter that

also rotates about the waveguide axis with rotary joints like Chu's network. The objective

of this phase shifter is to linearize both polarizations simultaneously. Following that is a

rotary $180°$ (π plate) phase shifter, which rotates to the linear polarizations to angles

symmetrical to the horizontal and vertical polarization axes, as in the last part of the

[16c] DiFonzo, D, "Adaptive Antennas for Polarization Isolation in Frequency Reuse Systems,"
COMSAT Memorandum, TCLT/71-2085, July 15, 1971;

[16d] Difonzo, D.,"Interference Reduction Circuit," COMSAT Memorandum, TCLT/72-2018,
March 2, 1972.
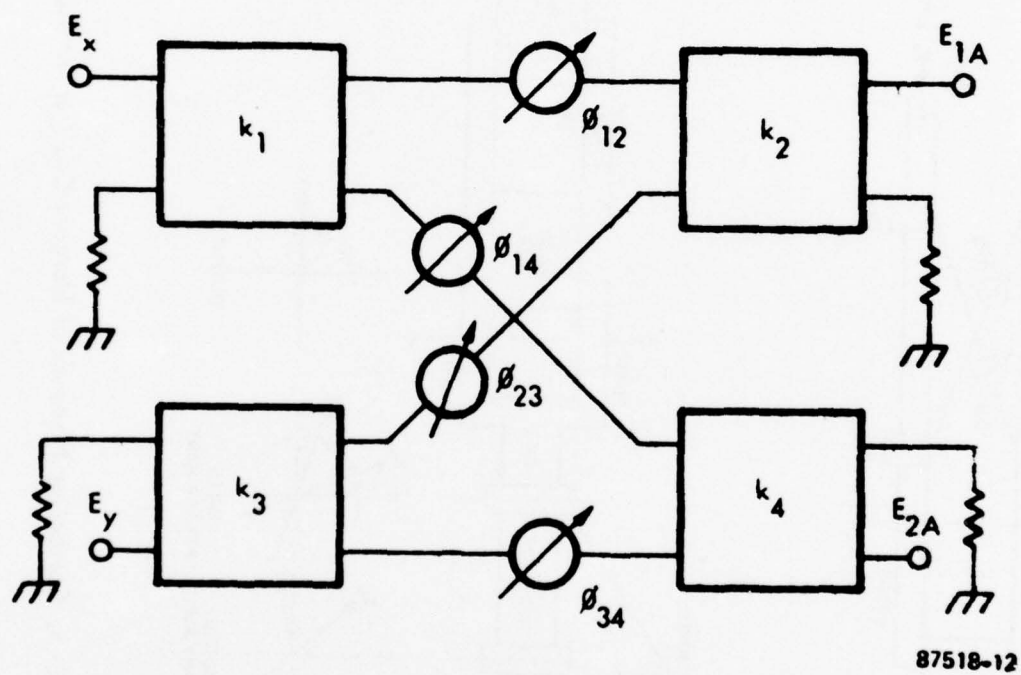
Figure C-4. Cross Coupling Interference Reduction Circuit
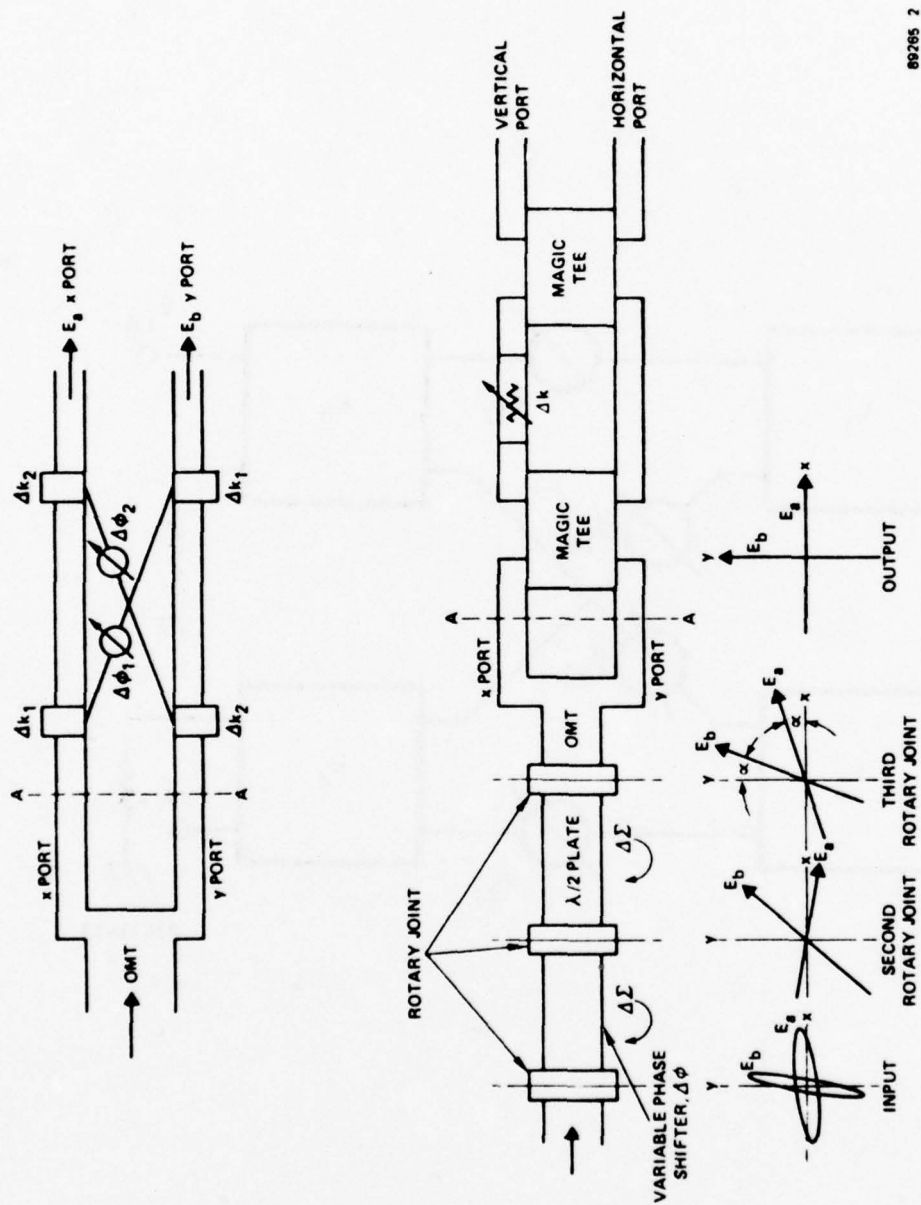
87518-12

Figure C-5. Correction Network of Marconi Co. (for Intelsat)

Chu network. Rather than using the variable rotating attenuator of the Chu approach, this network uses an OMT, and a dual cross-coupled network, which is actually implemented as shown by two magic tee networks, and a variable gain device. This device orthogonalizes the two linear polarizations simultaneously, since they are at equal angles, α, from the horizontal and vertical polarization axes.

Direct control of each axis in this network is also difficult, since the operations involve both polarizations simultaneously. Search optimization algorithms can be used.

C-1.1.2.4   Nippon Network

Nippon Corporation, in a contract from INTELSAT, developed a network[16a] shown in Figure C-6. Two fixed rotary phase shifters are used, similar to the Harris Corporation approach. However, the first phase shifter orthogonalizes the principal axis of the two polarizations, leaving both elliptical. The second rotary phase shifter (180°) rotates the two axes to vertical and horizontal polarizations, respectively, although both are still different elliptical polarizations. A cross-coupling network then completes the orthogonalization.

The key difference between the Nippon network and the Harris network is the way in which the components are used, i.e., the approach to orthogonalization. This network does not operate on one polarization at a time. Therefore, since direct control of each axis is difficult or impossible, search algorithms can be used.

_____

[16a] DiFonzo, D., Williams, A., and Tracktman, W., "Adaptive Polarization Control for Satellite Frequency Reuse Systems, "Internal Memo, COMSAT Laboratories," Clarksburg, Maryland, 1976.

205
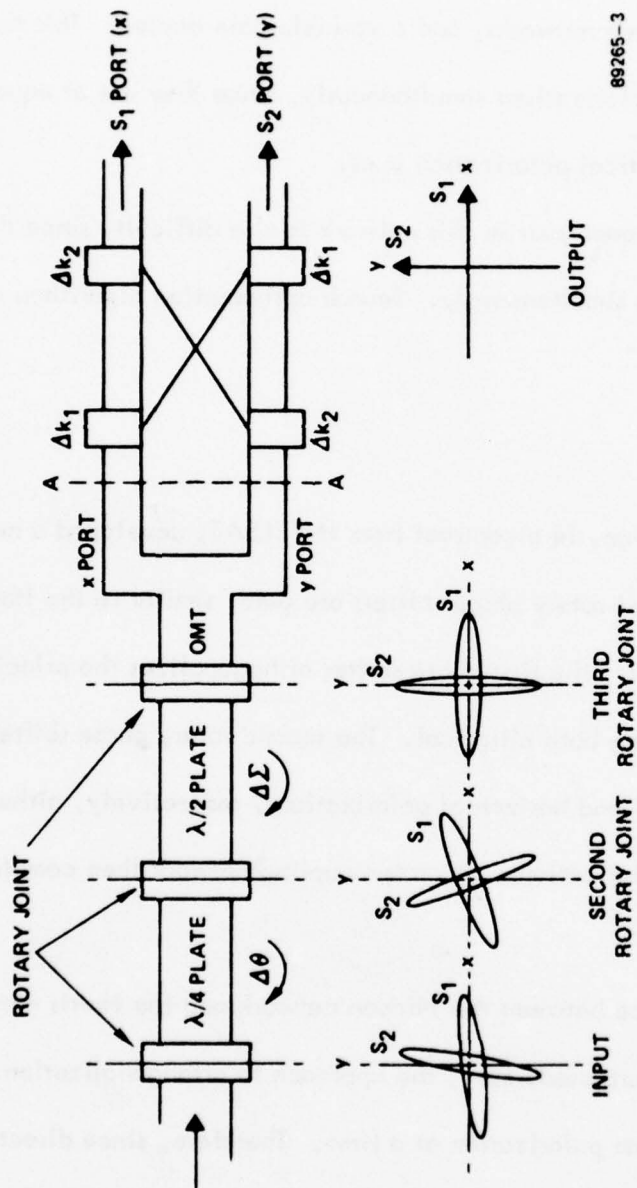
Figure C-6. Correction Circuit of Nippon Co. (for COMSAT)

89265-3

C-1.1.3   Specific IF Correction Networks

The Harris approach for IF polarization cancellation has been briefly discussed in Section 1. It operates by a cross-coupling from each channel to cancel cross polarization-caused crosstalk in the other channel. The variable cross coupling is performed by electronically variable PIN diode attenuation of in-phase and quadrature-phase (I-Q) components. In contrast, JPL[17] has developed the cross polarization cancellation network shown in Figure C-7. The cancellation for only one channel is shown. Another similar network, with additional front end mixers, is required for the other channel.

The principal discriminants for each polarization are two assumed carriers, at least slightly separated in frequency. The phase-locked loop at the left, using a reference CW carrier frequency, tracks the carrier, $\cos \omega_0 T$, for the "LCP" channel shown on the left. The cross polarization $A \cos (\omega_0 T + \theta)$ exists in the RF channel that is to be cancelled. This is done by phase-shifting the RCP channel via the variable phase shifter, ϕ, in the local oscillator line, and applying variable gain, G, so as to satisfy the equation:

$$\cos (\omega T) - G A \cos (\omega T + \theta - \phi) = 0$$

The control for the adaptive phase shifter is driven by a quadrature-phase detector that detects and minimizes a quadrature component of the output residual cross polarization. A variable gain device is driven from the in-phase detector of the residual cross polarization. Thus, both in-phase and quadrature-phase components of the residual cross polarization are driven to zero by the feedback circuit, in a manner similar to "LMS" control

---

[17] "System for Interference Signal Nulling by Polarization Adjustment," U.S. Patent 3,883,872 (to NASA), May 13, 1975.

207

Figure C-7. The JPL IF Adaptive Polarization Correction
(One Channel Shown at IF $\cong$ 10 MHz).

208

(as discussed in Paragraph C-1.3.1). In contrast to the Harris IF cancellation circuit, this circuit was constructed at 10 MHz IF for convenience, and did not demonstrate a significant cancellation bandwidth. The Harris circuit was built mainly to demonstrate performance over a large bandwidth, and used a high IF (2.3 GHz) to assure this. In addition, this circuit does not require separate sets of mixers for each channel; but the above approach does require these because the adaptive phase-shift is applied via the local oscillator. Nevertheless, the above circuit has the potential advantage that this mixer phase-shift approach is inherently very broadband. Also, the gain-loss coupling circuit does not inherently have a large loss, as does the Harris I-Q PIN diode weighting circuit, thus requiring less amplification.

Another possible IF cancellation circuit is adaptive delay line coupling shown in Figure C-8. This circuit has the advantage of being able to null as many frequencies as there are taps, and thus achieves broader bandwidth cancellations than a single-couple-line approach. This circuit can compensate not only for a circuit mismatch across a bandwidth, but nonflat media effects such as multi-path. Such effects can cause cross polarization to vary over frequency, preventing correction with a single coupled-line approach. The cost is the obvious complexity of this circuit. However, for ground-to-grounds links, or other applications with strong potential multi-path, the approach has promise.
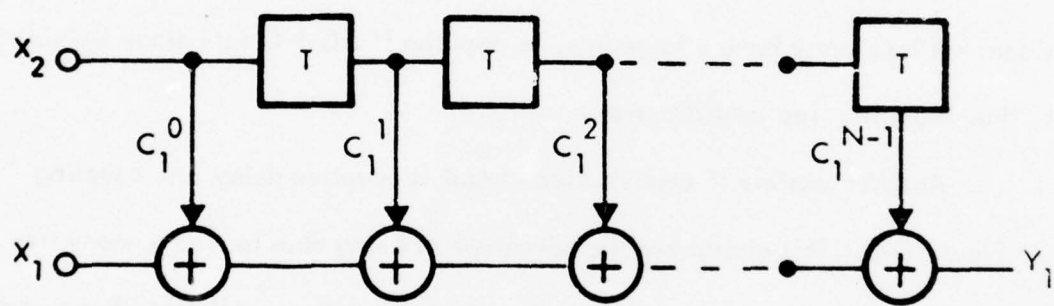
88576-22

Figure C-8. Tapped Delay Line Frequency Dependent Coupling Network

C-1.2   Performance Index Measurement Techniques

In an adaptive polarization correction system, performance must be monitored periodically or continuously to allow the coupling network to be adjusted for best performance. A number of different methods can be used to measure performance. Some possibilities are discussed below.

C-1.2.1   Pilot Signal Injection (used in the NASA breadboard)

A pilot signal can be added to each modulator output. Often these will be available, used for other purposes such as Doppler measurement, etc. The presence of Pilot 1 on the Signal 2 receive line is a measure of coupling. Of course, the pilot signals must be low in power so as not to require much power, and so as not to interfere with the desired signals. Furthermore, the two pilot signals should be orthogonal so as to be readily distinguished from one another. The pilot signals can be carriers modulated with different PN sequences or they can be tones at different frequencies. A tone system is simpler to implement but it measures coupling at a single frequency. In broadband systems, the tones can be placed at nulls in the data signal spectrum to alleviate the interference problems with the desired signal. Adaptive polarization correction systems, using pilot signals, have the advantage of a simple interface with the receiving system. It allows one or many demodulator channels, possibly of various types. Also important is the capability for coherent detection using pilot signals, allowing a direct gradient "LMS" optimization, rather than requiring a search optimization.

211

C-1.2.2   Carrier Offset Frequency

A very similar technique that would be usable with certain modulations is
to slightly offset the carrier in one polarization, and use this new frequency for the other
carrier. The two channel modems can then often provide these carriers. Additional
circuitry could detect the amount of cross polarized carrier in a given channel, thus
providing the performance measure without additional pilot signal generation and receivers.

However, most modulations have little or no carrier.

C-1.2.3   Known Pattern Injection

In systems where the data rate can be increased, it is possible to transmit
a fixed format on each signal to allow detection of the presence of coupling. The known
formats could be fixed bit sequences, but a simpler scheme can be obtained by alternately
blanking (turning off) each modulator output. The presence of S_1 on the Channel 2 receive
line, when S_2 is turned off, is a measure of coupling.

C-1.2.4   Bit-Error Rate

With a known bit sequence one might attempt to measure the bit-error rate
on the received sequence. However, when operating at low error rates, this technique
is very insensitive and would lead to slow response time. For example, error rates cannot
be used to sense a 30 dB signal-to-interference ratio. A more sensitive approach is to
measure signal-to-noise ratio continuously with unknown data as discussed below.

212

C-1.2.5   Decision Voltage or Signal-to-Noise Ratio (for digital modulations)

Under ideal conditions, the decision variable for digital modulations should take on a set of discrete values. For example, in a quadraphase system, the decision variable is a pair of voltages nominally equal to $\pm A$. However, the presence of thermal noise and other noises, including polarization coupling, will cause deviations in the values taken on by the decision variables. A suitable normalized variance of the decision variables. A suitable normalized variance of the decision variable can be taken as a measure of the system error rate. This approach to measuring error rate is much more sensitive than a direct measurement of error rate with a known format.

The signal-to-noise performance measure has the advantages that it will produce a higher average S/N over a wider bandwidth than pilot performance measures This is accomplished without wasting power and equipment on pilot tones.

The usual approach (e.g., Chu[15]) of:

a. Completely cancelling cross polarization

b. Equalizing loss in each channel

does not produce optimum S/N. Specifically:

a. Incomplete decoupling generally yields higher S/N than complete

decoupling because less signal loss occurs while still allowing the

residual cross polarization to be much smaller than the thermal noise;

however, the improvement is generally quite small. For example,

less than 10 percent improvement in the loss occurs for signal-to-noise

ratios as low as 10 dB, and less than 1 percent improvement in loss

occurs when signal-to-noise equals 20 dB.

213

b.   In general, since rain and other phenomena differentially attenuate

one channel with respect to another, it is preferable to have a cor-

rection circuit with less loss in the channel which has been most

attenuated by the media, and more loss in the other channel. The

solution for the minimum loss decoupling circuit in this case would

equalize the output signal-to-noise ratios, rather than equalizing the

losses incurred in the decoupling circuits. Thus S/N would appear to

be a preferable performance measure as in Chu's approach. Neverthe-

less, an adaptive control network would be required to measure signal-

to-noise ratio in the two channels, rather than more direct measures

like correlations of pilot cross polarizations.

A disadvantage of the S/N performance measure is that it is incoherently

detected (i.e., measures the performance, not the gradient of performance) and thus

cannot be used directly with a gradient (LMS) optimization approach. Nevertheless, a

search optimization technique can be used or gradients can be measured by modulating

the adaptive weights.

Another potential or disadvantage of this approach is that is usually requires

that the decision variables be made available at the demodulator output, a potential inter-

face problem especially with multiplexed signals.

Another possible disadvantage of the S/N performance measure is that it requires the amount of coupling be less than unity, when the system is turned on and during the operation of the system. Otherwise, the system could possible deliver a signal "one" in the place of signal "two," and vice versa, since the performance measure does not distinguish between the two signals, but only minimizes the amount of noise on each given signal. However, since the coupling is usually considerably less than unity, this feature should not represent an operational problem in most cases.

C-1.3   Control Algorithms

An important element of an adaptive polarization correction system is the technique employed to develop the drive signals for the variable coupling network. This problem is similar to the control problem found in adaptive antenna arrays, the main difference being that a single weight needs adjusting for the present problem, whereas many weights require adjustment in an adaptive phased array. Of course, this difference disappears if the coupler involves an N-tap delay line or other form of frequency response equalizer.

There are at least two major control approaches that can be used for the control of polarization correction networks:

a.   Gradient (LMS) algorithm (used in the Harris breadboard for both networks)

b.   Search algorithms

215

C-1.3.1   LMS Algorithm

The LMS algorithm[18,19] can be described as follows. Suppose that the two antenna ports, horizontal polarization and vertical polarization ports for example, carry signals with complex envelopes $x_1(t)$ and $x_2(t)$, and it is wished to form a linear combination of these two signals

$$y(t) = W_1(t) x_1(t) + W_2(t) x_2(t)$$

such that $y(t)$ approximates some known signal $y_d(t)$. It turns out that the mean square error between $y(t)$ and $y_d(t)$ is minimized if when

$$W_1(t) = \int^t x_1(\lambda) e(\lambda) d\lambda$$

$$W_2(t) = \int^t x_2(\lambda) e(\lambda) d\lambda$$

where $e(t)$ is the error $y(t) - y_d(t)$. Figure C-9 shows a block diagram of this control.*

The use of the LMS algorithm requires the knowledge of the "desired signal," $y_d(t)$, which it is wished to approximate, based on the performance measure to be used. The simplest desired signal is zero, i.e., $y_d(t) = 0$, so that the error signal is available immediately for minimization by the algorithm. For example:

a.   Pilot Signal (or offset carrier) Performance Measure. The "desired

signal" for each channel is the pilot transmitted on the orthogonally

polarized channel. This cross polarized pilot is desired to be zero for

each channel and is minimized by the LMS algorithm, as shown in

*For simplicity, complex operations are denoted by real operations.
[18,19] See Reference Listing (18a,b; 19a,b) after Appendix E

216
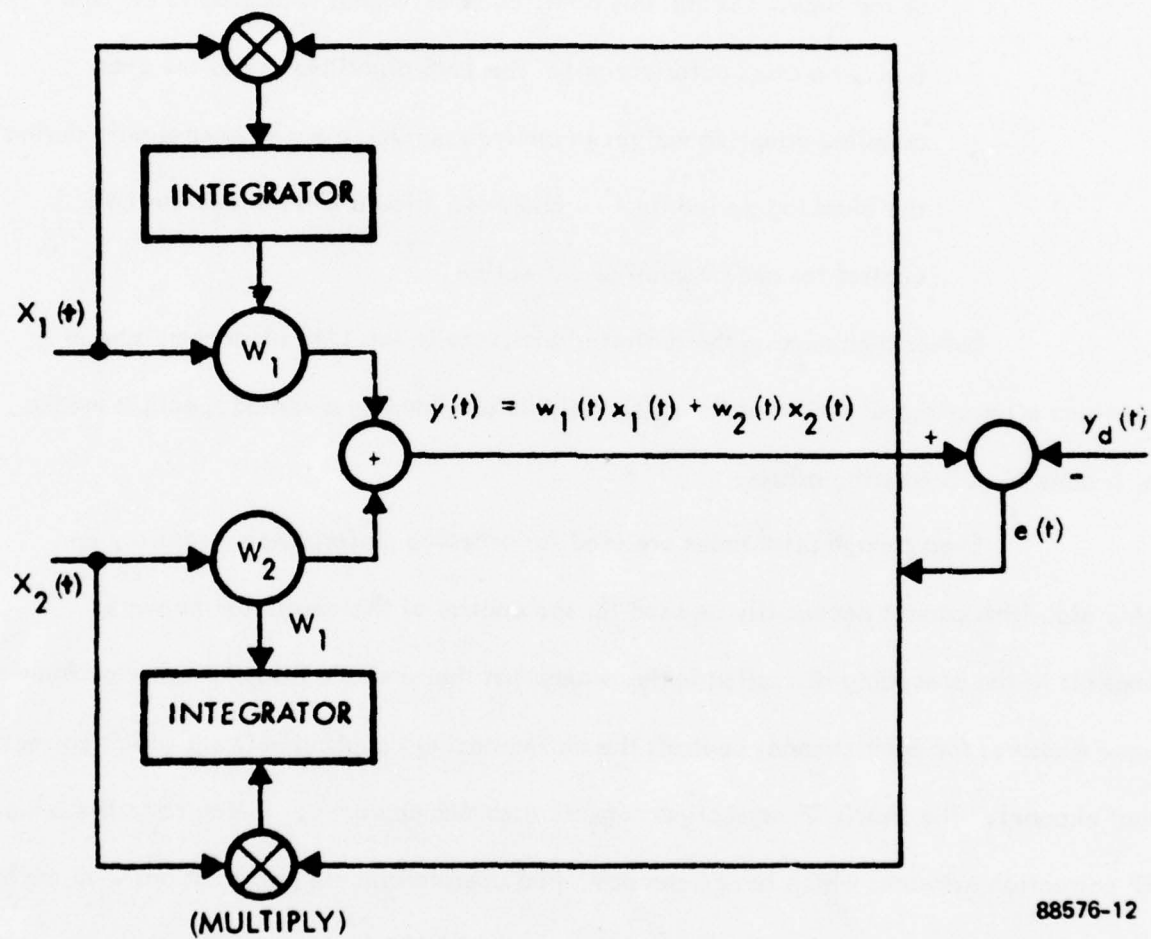
Figure C-9. The LMS Gradient Algorithm

88576-12

217

Figure C-10. The narrowband filters are needed to separate a correct pilot, in order to control each correction network.

b.   Known Blanking Pattern: Each signal is blanked for a small percentage of the time. During this time, channels signal is desired to be zero (i.e., no cross polarization). The LMS algorithm varies the cross coupling adaptive weight in order to minimize each channel only during the blanking period for that channel. Figure C-11 shows the LMS control for one channel of correction.

Rather than making the desired signal zero in the LMS algorithm, spread spectrum pilot or signal estimates for $y_d(t)$ could be provided by a spread spectrum modem, as is done in null steering arrays.

Even though pilot tones are used for adaptive performance measures, an LMS algorithm cannot necessarily be used for the control of the correction network. Implicit to the preceding discussion is the assumption that a single pilot (or other performance measure) for each channel controls the corresponding coupling network which corrects that channel. The Harris RF correction network uses this approach. In contrast, the other RF correction networks which have been described operate on both polarizations with each axis. Thus, direct control by simple analog control with the LMS algorithm appears difficult or impossible, although search optimization algorithms can be used.

C-1.3.2   Search Algorithm

A block diagram of an adaptive polarization correction circuit based on the search algorithm is shown in Figure C-12. In its simplest form, the search involves

NARROWBAND FILTER

INTEGRATOR

W_i

COMPLEX WEIGHT

$W_i = W_{real} + j W_{imag}$

NARROWBAND FILTER

TO MODEM
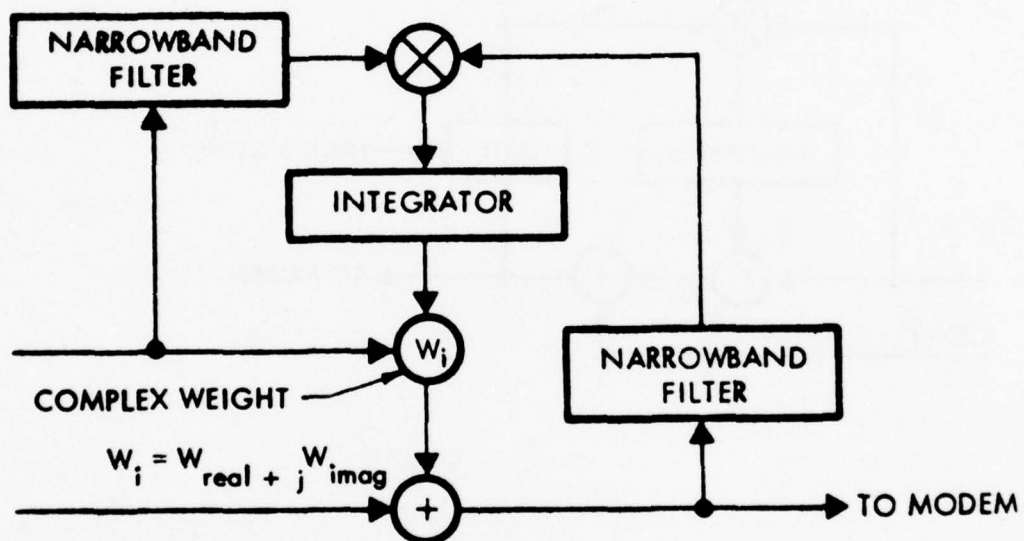
88576-8

Figure C-10. LMS Algorithm Used with Pilots (One Channel Correction Shown)

219
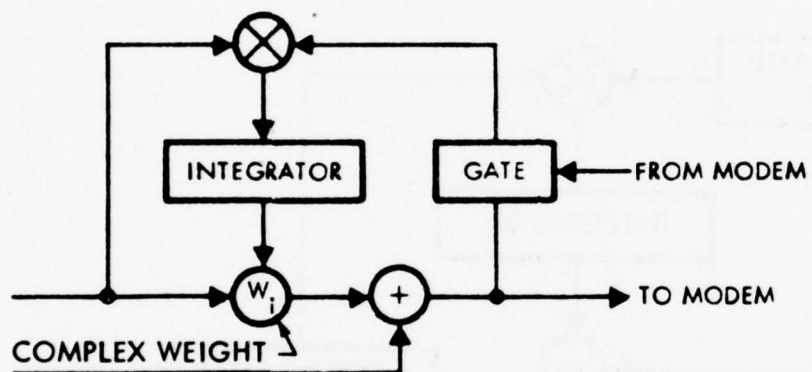
Figure C-11. LMS Algorithm with Alternately Gated Signals
(One Channel Correction Shown)
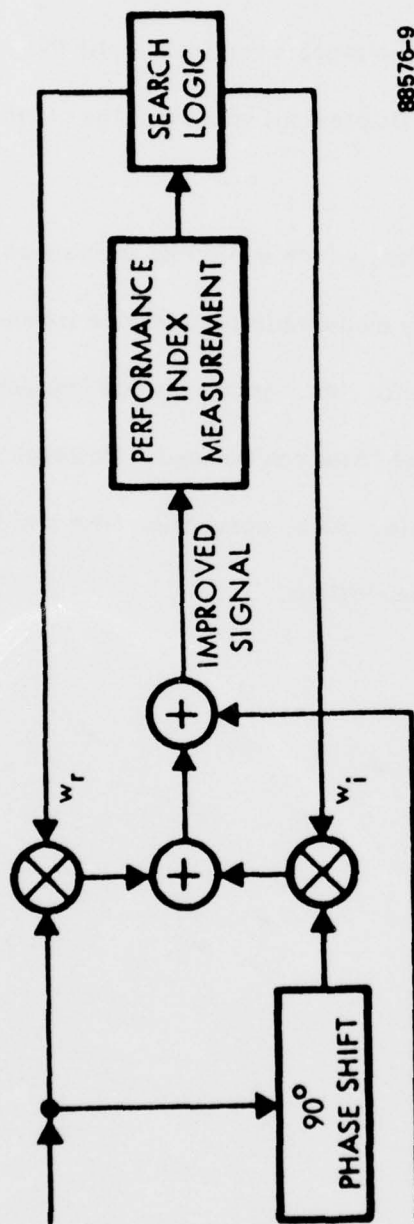
Figure C-12. Adaptive Polarization Correction Circuit Using Search Algorithm

88576-9

221

varying one weight at a time in small steps. After each step the performance index is measured. If the last step caused the performance index (PI) to increase, another step in the same direction is taken. The process continues until the PI decreases at which point the weight is returned to its previous value and the other weight is varied using the same procedure.

Unlike the LMS algorithm, which minimizes some mean square error, the search algorithm can be used with any measurable performance index such as decision voltage signal-to-noise ratio or bit error rate. It can also be implemented in systems where no special signal format or pilot tones can be used. However, some "search noise" degradation of the signals is inevitable. Also, acquisition time and tracking rate can be degraded from typical LMS implementations.

APPENDIX D

THE CROSS POLARIZATION PROBLEM IN A SATELLITE LINK

D-1.0   INTRODUCTION

This appendix discusses the cross polarization effects generally associated with a satellite to ground link.

D-1.1   Sources of Cross Polarization

There are several possible sources of cross polarization in a ground satellite link:

         a.   Weather, particularly rain

         b.   Antennas

         c.   Faraday rotation

         d.   Multi-path fading

Briefly, the last two effects are generally small for most satellite-to-ground links. Antenna depolarization is difficult to estimate; however, reasonably high performance satellites, with a high-gain stabilized antenna will have cross polarization down to at least -30 to -40 dB. Generally, rain can be shown to be the dominant effect.

D-1.1.1   Rain Cross Polarization

Rain cross polarization results from differential phase and differential attenuation of the electric field components parallel and perpendicular to the main axis of the

oblate raindrops. Polarization coupling levels depend upon frequency, rain rate, path length through the rain, type of polarization (linear or circular) and for linear polarization, raindrop canting angle. A good review of rain cross polarization effects on satellite communication has been given by Hogg and Chu.[19a] Appendix E reviews typical rain cross polarization calculations and data. A summary of this data for a typical 11 GHz satellite link is given below.

Chu[19] has shown that cross polarization can be expressed as a function of the total rain attenuation. This theory (supported by considerable data), is plotted in Figure D-1 for horizontal and vertical antenna polarization at 11 GHz, along with some very severe experimental data,[18] and theory from a worst-case "rain sheet" model by Oguchi. In this appendix, a 10 dB fade margin (i.e., maximum rain attenuation) was assumed. As can be seen, theory and data in the figure predicts that between -20 to -29 dB cross polarization results for a 10 dB rain attenuation.

Circular polarization is more severely depolarized by rain than vertical and horizontal polarizations at 11 GHz. Figure D-2 shows theoretical curves that predict a minimum of 7 dB worse cross polarization for circular rain polarization using the "rain sheet" model. Calculations by Chu[18,19] indicate greater than 10 dB difference. This strongly indicates advisability of horizontal and vertical polarizations at 11 GHz (Faraday rotation, discussed later, is negligible at 11 GHz).

———————
[19a]Hogg, D.D. and T. S. Chu, "The Role of Rain in Satellite Communications," Proc. IEEE, Vol. 63, No. 9, September 1975, pp. 1557-1579.
[18,19]See Reference Listing (18a,b;19a,b) after Appendix E.
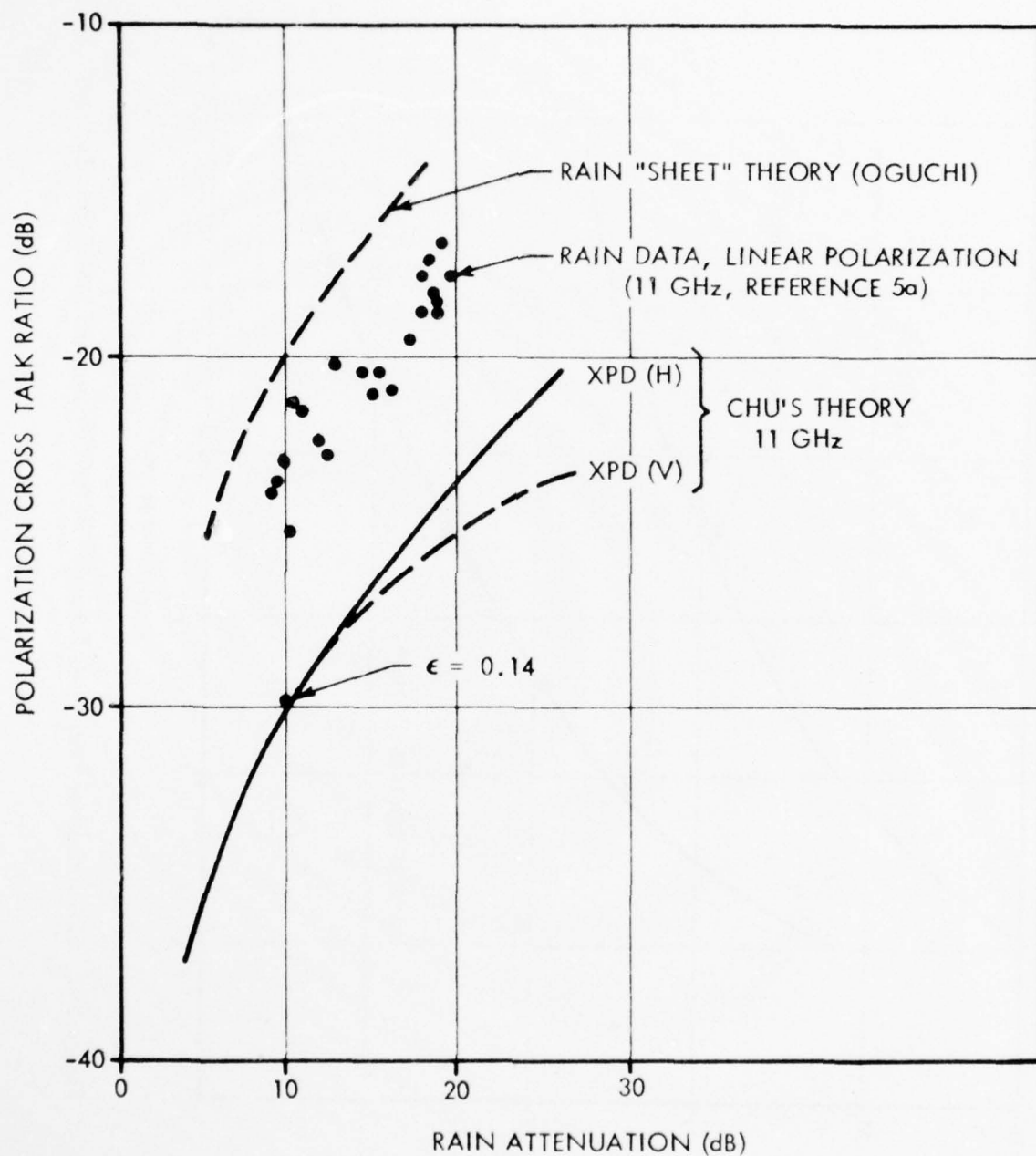
Figure D-1. Calculated vs Measured Cross Polarization
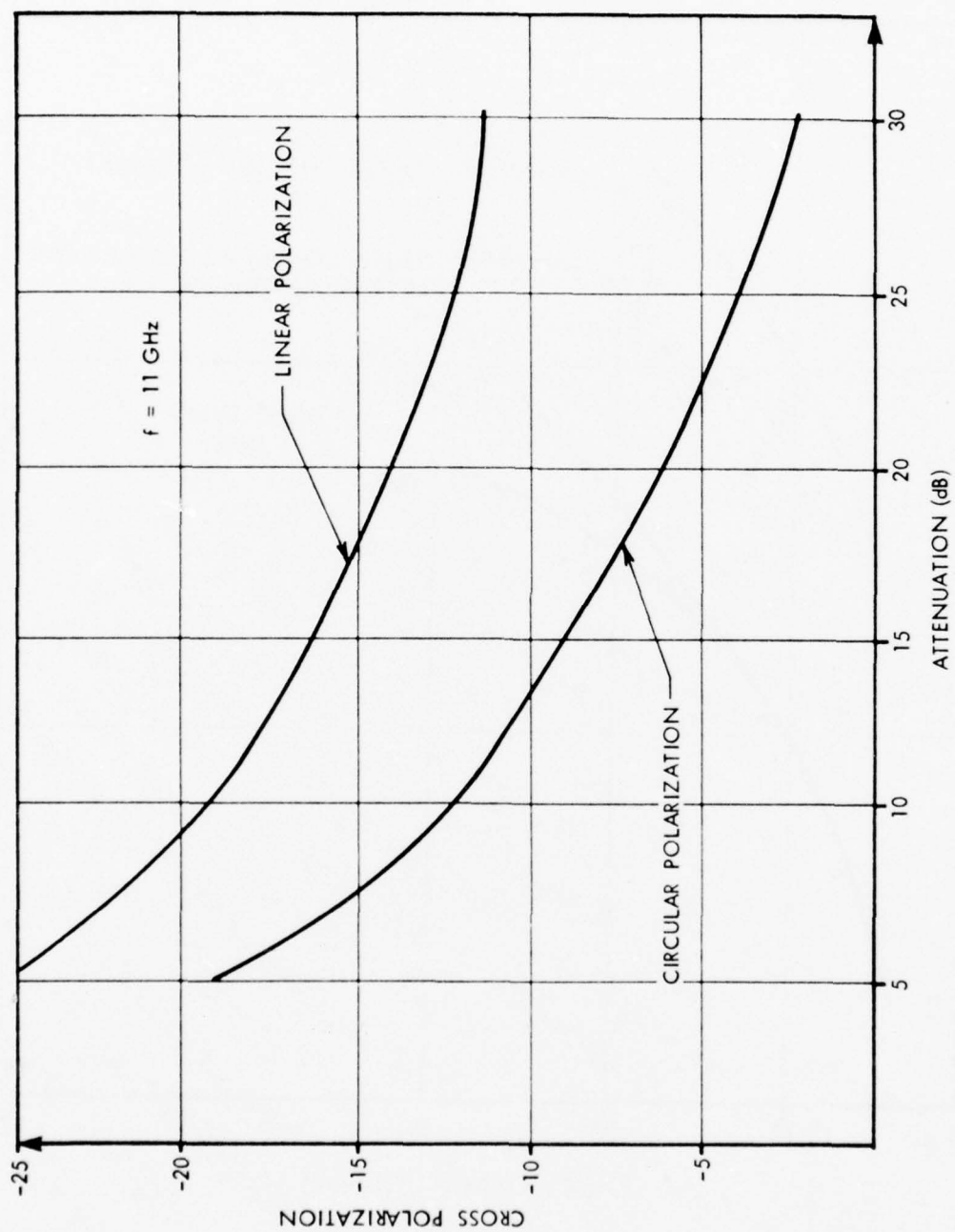
Figure D-2. Comparison of Rain Cross Polarization for Circular and Linear Polarizations

Relationship between rain attenuation and rain rate[21] is shown in Figure D-3. The figure shows the rate attenuation over a typical satellite-ground link of 5 kilometers, as a function of rainfall. For example, approximately a 10 dB attenuation results from approximately 50 mm per hour rainfall over the 5 kilometer path. As was seen from the last figures, at 11 GHz, attenuations approaching 10 dB are required to get significant depolarization such as -20 dB.

Such rainfalls only occur infrequently. Figure D-4 shows the frequency of occurrence of rainfall rates ar various locations in the country.[19a] A 50-millimeter per hour rain rate occurs only 100 to 300 minutes per year even in the worst locations such as Newark and New Orleans. In very dry areas, only several minutes per year are involved. For circular polarization, rainfalls less than 25 millimeters per hour can cause substantial cross polarization (-20 dB at 11 GHz) which involves greater than 30 minutes per year rainfall in Salt Lake City, but greater than 500 minutes per year in New Orleans.

In order to assess the relative effect of differential attenuation and differential phase shift of raindrops in causing cross polarization, Figure D-5 shows the effect of both differential attenuation and differential phase shift as a function of rain rate for several different frequencies.[16a] This plot is for circular polarization, whereas the effect for linear polarization is known to be at least 7 dB less, as has been discussed. A differential phase shift of rain causes the largest part of rain cross polarization. In most RF

[16a]DiFonzo, D., A. Williams, and W. Trachtman, "Adaptive Polarization Control for Satellite Frequency Reuse Systems," Internal Memo, COMSAT Laboratories, Clarksburg, Maryland, 1976.

[21]Ryde, J. W. and D. Ryde, "Attenuation of Centimeter Waves by Rain, Hail, and Clouds," General Electric Co., Research Labs Report No. 8516, 8670, Wembley, England, August 1944, and May 1945.

227
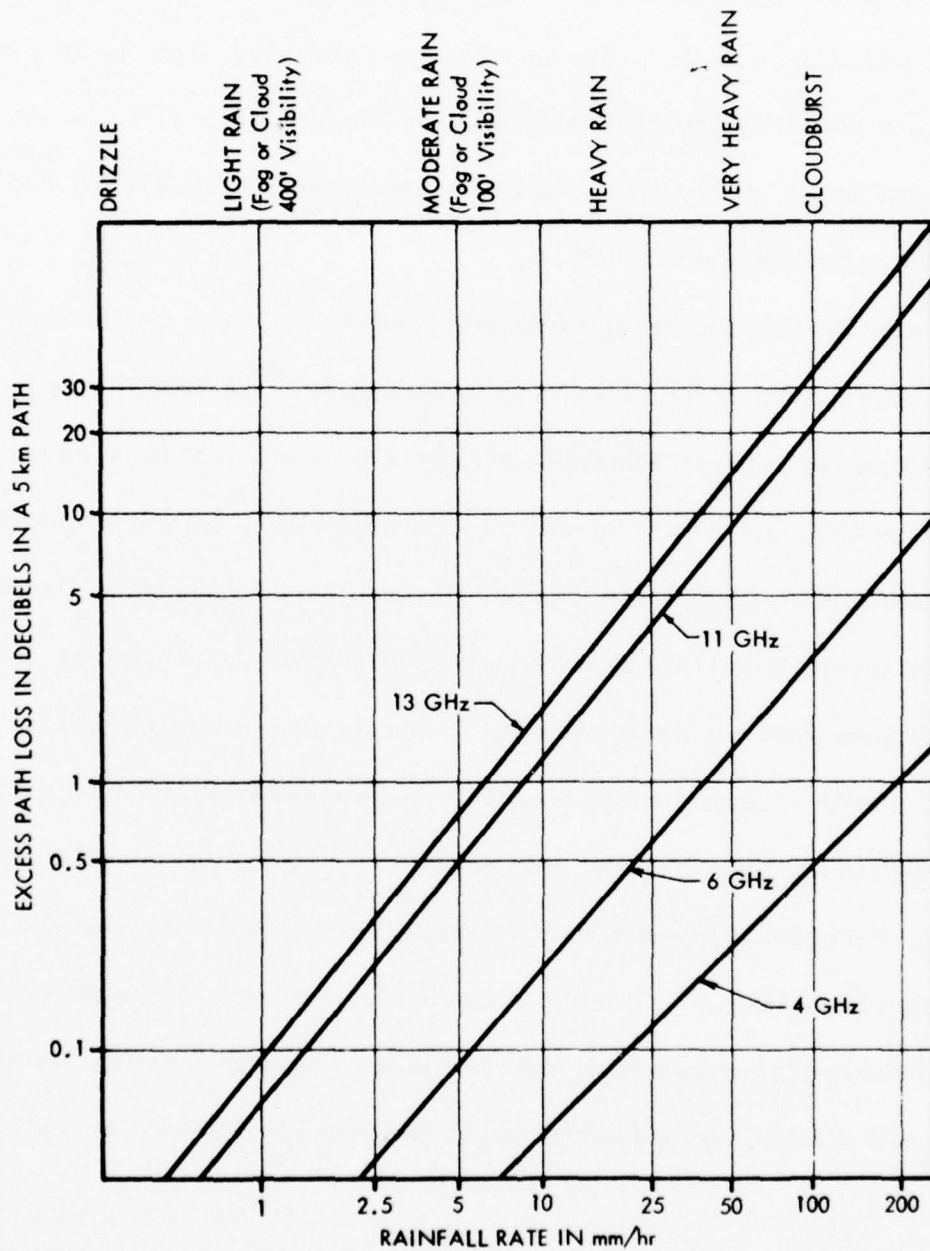
Figure D-3. Rain Attenuation vs Rainfall Rate (Theoretical, after Ryde and Ryde)

228
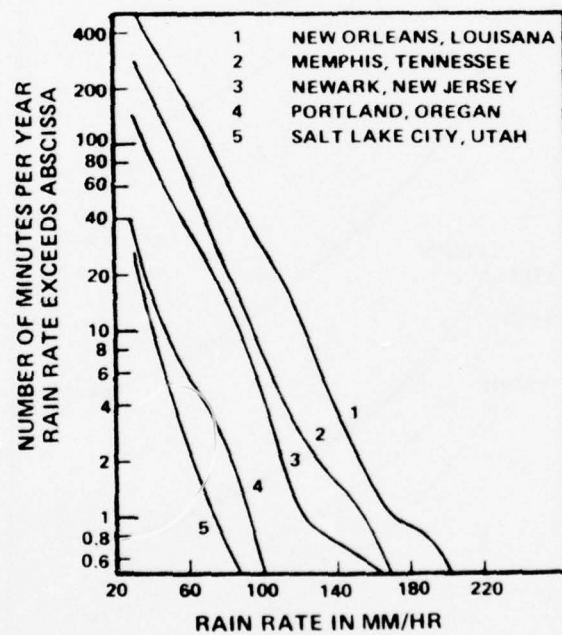
Figure D-4. One-Minute Rain Rate Distributions for a Five Year Period (1966-1970) Measured at Several Locations in the U. S. (From Hogg and Chu, 19a)

229
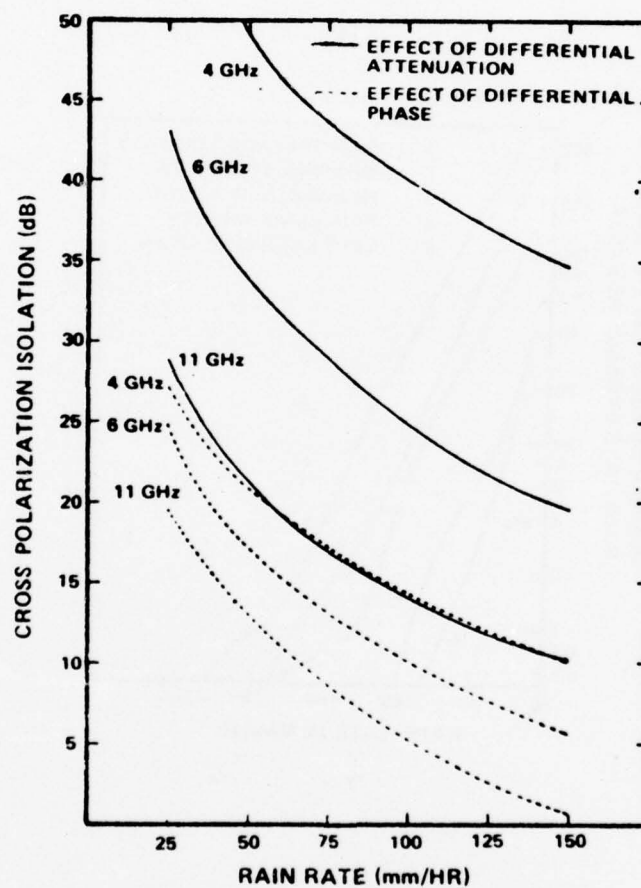
Figure D-5. Cross Polarization Isolation for Circular Polarizations
Vs. Rain Rate for 5 Km Path Length. (Reference, Difonzio, 16)

230

correction networks, this differential phase shift is removed by the first network of lossless phase shift operations. After the phase shift networks, the remaining cross polarization to be corrected is that caused by the differential rain attenuation only.

The effect of differential rain attenuation is to cause nonorthogonality of the two transmitted polarizations. This effect can be neglected below 4 GHz, and for most cases 6 GHz, so that in these cases the orthogonalization network may be unnecessary. However, at 11 GHz, significant nonorthogonality and cross polarizations can occur. For example, with a 5-mm/hr rain, Figure D-5 shows that -22 dB cross polarization is caused by differential rain attenuation for circular polarization. For linear polarizations, the figure would indicate that differential attenuation causes approximately 7 dB less (or -29 dB) cross polarization. However, other computations show an S_2 crosstalk of -22 dB or higher into our coupler network. To correct this nonorthogonality, correction networks involving cross coupling or attenuation are required, which in turn cause some loss in S/N even in an optimal network. In addition, the network is usually more complex than the initial phase shift network.

In summary, substantial rain cross polarization (-20 to -25 dB) occurs at 11 GHz for only a few tens to hundreds of minutes per year at rainy locations, only a few minutes per year in the desert. A link margin approaching 10 dB is required to communicate in this rain. The cost of any cross polarization correction system for this rain must be less than the cost of this loss in data, or the cost of additional power needed to overcome cross polarization without cancellation networks, when possible. Rain cross polarization

is at least 6–8 dB less for horizontal and vertical polarizations than for circular polarizations; thus, horizontal and vertical polarization should be used at frequencies of 11 GHz or higher.

D-1.1.2   Antennas

Well designed satellite antennas exhibit good polarization isolation at on-axis direction. Isolation in excess of 60 dB has been measured at 8 GHz. As the antenna is moved off the boresight null, cross polarization isolation rapidly decreases to -40 dB at 8 GHz and 35 dB at 15 GHz around the 3 dB point of the main beam. This is primarily due to a shift in the electromagnetic modes in the feed. A purely geometrical contribution is also made in that the polarization axes move with the antenna. It should be noted that these levels of cross polarization can be attained only if care is taken in the manufacture of the antenna.

In addition to these, there are other degradations. These include water on the antenna feed and reflector, and distortions caused by external interfering forces. The effects of wind loading have been extensively studied. Wind induced antenna rotation about the boresight axis has a very significant effect on linear polarizations. The effect of depolarization due to water on the surface of reflectors, radomes, and feed windows,[22] can be minimized by the proper design of the antenna system.

Severe antenna depolarization is, of course, possible; for example, with small antennas well off axis. Nevertheless, with high quality wideband links, it appears likely that good quality antennas will be used.

[22] See Reference Listing (22a, b) after Appendix E

D-1.1.3   Faraday Rotation

Faraday rotation affects linearly polarized waves passing through the iono-
sphere (50 kilometers to 400 kilometers). Therefore, Faraday rotation has no affect on
terrestrial links but does impact satellite links. Furthermore, circularly polarized waves
are not affected by Faraday rotation since both orthogonal linear components are rotated
equally. For the same reason, the orthogonality of dual-linear channels is not impacted
by Faraday rotation. Therefore, cross-channel coupling can be removed by rotation of
the receiving antenna feed, or rotation of the 180° (π-plate) phase shifter in the RF
correction network. The magnitude of the Faraday rotation is dependent on frequency as
well as time of day. The peak rotation is at noontime when the frequency dependency
approximated as rotation $R = 90^\circ/F^2$ where F is in GHz. The minimum rotation is at
dawn when the angular rotation is given approximately by $R = 18^\circ/F^2$ where F is in GHz.
Therefore, at 11 GHz the Faraday rotation varies from approximately 0.74° to 0.15°.
For perfectly aligned antennas, this results in a range of polarization isolations of 52 dB
at dawn to 38 dB at noontime. At 4 GHz, the rotation is much more severe varying from
5.6° at noon to 1.1° at dawn. These rotations correspond to isolations of 20 dB at noon
and 34 dB at dawn. An additional factor that is believed to impact the magnitude of
Faraday rotation is solar flares. Note that a period of increased solar flares is expected
in the late 70's and early 80's. However, no experimental results or theoretical predic-
tions appear to be available in the literature.

D-1.1.4   Multipath Fading

The third phenomena affecting the cross polarization ratio is polarization-selective fading. This appears to be a problem only in terrestrial links and not in satellite communication links. Narrow beamwidth antennas appear to remove the probability of multi-path fading due to reflections, which is the factor that causes deep polarization-selective fading. It is worthwhile to stress that fading causes degradation in the received cross polarization ratio, not because of cross polarization coupling, but because of reduction of the level of the desired signal at the receive antenna. Nevertheless, multi-path scattering can cause cross polarization coupling as well.

For applications to satellite-ground links, multi-path does not appear to be a major problem.

APPENDIX E

RAIN CROSS POLARIZATION ANALYSIS

E-1.   THEORETICAL MODELS OF RAIN

The basic theory and measurement data of rain depolarization has been studied by Chu, [19b,7,19a] Oguchi, [20] Ryde and Ryde, [4] Taur, [16e] and many others (references 2,5,8,9,11,16a,23-45). It is not intended to reiterate all the rain analysis here. However, some review will be given in order to;

        a.   Briefly summarize a rather complex literature

        b.   To present typical amplitude and phase cross-polarization voltages

        c.   To show the trade-off between linear and circular polarization

Most analyses of rain simulate the polarization effects via a single lossy phase shifter (i.e., or "rain-sheet" model), at some angle with respect to the horizontal axis. This model is used because the individual elliptical raindrops behave as a small lossy phase shifter at some angle from the horizontal. The value of the attenuation and phase shifter used in the single-plate simulation model result from theoretical and experimental data of rain.

The effect of a single phase shifter plate has been derived by Chu[19b] and Oguchi.[20] For an incident field with horizontal and vertical electric fields of E_H and E_V, respectively, acted on by a phase shifter whose effects are expressed by a matrix T, the resulting output fields, $E_H{}'$ and $E_V{}'$ are given by:

2,4,5,7,8,9,11,16a,e,19a,b,20,23-45 (See Reference Listing after Appendix E)

$$\begin{bmatrix} E_H' \\ E_V' \end{bmatrix} = \begin{bmatrix} T_{11} & T_{12} \\ T_{21} & T_{22} \end{bmatrix} \begin{bmatrix} E_H \\ E_V \end{bmatrix} \qquad\qquad (E-1)$$

where

$$T_{11} = \gamma_2 \cos^2 \theta + \gamma_1 \sin^2 \theta$$

$$T_{22} = \gamma_1 \cos^2 \theta + \gamma_2 \sin^2 \theta$$

$$T_{12} = T_{21} = \frac{\gamma_2 - \gamma_1}{2} \sin^2 \theta$$

$$\gamma_i = e^{-(\alpha_i - j\beta_i)L} \quad \text{for } i = 1, 2$$

α_i, β_i = total attenuation and phase shift constants per unit length for the

        major (1) and minor (2) axis of the raindrops, respectively.

L = path length through the rain

These equations show that cross-polarization can occur if $T_{12} \neq 0$, which occurs if the rain cant angle, $\theta \neq 0$, and γ_1 is not equal to γ_2 (i.e., the raindrops are oblate, so that the major and minor axis have different γ_i). Note the path length, L, must be known as well as the γ_i (a function of the rain rate) in order to calculate the fields.

The total attenuation and transmission phase shift (in the direction of the major rain axis) can be factored out, resulting in simplified equations involving simply the differential phase shift and differential transmission coefficients of the rain. The equations then become;

$$\begin{bmatrix} E_H' \\ E_V' \end{bmatrix} = \begin{bmatrix} T_{11} & T_{12} \\ T_{21} & T_{22} \end{bmatrix} \begin{bmatrix} E_H \\ E_V \end{bmatrix}$$

where

$$T_{11} = \gamma \cos^2 \theta + \sin^2 \theta$$

$$T_{22} = \cos^2 \theta + \gamma \sin^2 \theta$$

$$T_{12} = T_{21} = \left(\frac{\gamma - 1}{2}\right) \sin^2 \theta$$

$$\gamma = e^{-(\alpha - i\beta)}$$

$\alpha(\alpha_T)$, $\beta(\alpha_T)$ = the differential attenuation and phase shift, respectively,

between the major and minor axes of the rain sheet, over

a path length, which yields the total attenuation, α_T.

The resulting rain attenuation and phase (and the differential attenuations and phase shifts) versus the amount of rainfall (in millimeters per hour) is shown in Figure E-1 and E-2, respectively.[16e] Note that differential attenuation and phase between the major and minor axis of the raindrop, which indicates γ_1 is not equal to γ_2. The plot of rain attenuation shows that a rain of over 50 millimeters per hour produces a total attenuation of approximately 2 dB per kilometer, or 10 dB attenuation total over a typical satellite-to-ground link of 5 km. This case (10 dB fade) has been selected as the "worst-case" rain fade for our design; thus approximately 50 mm/hour of rain corresponds to our "worst-case" rain; i.e., the maximum rain that will still allow communication with the
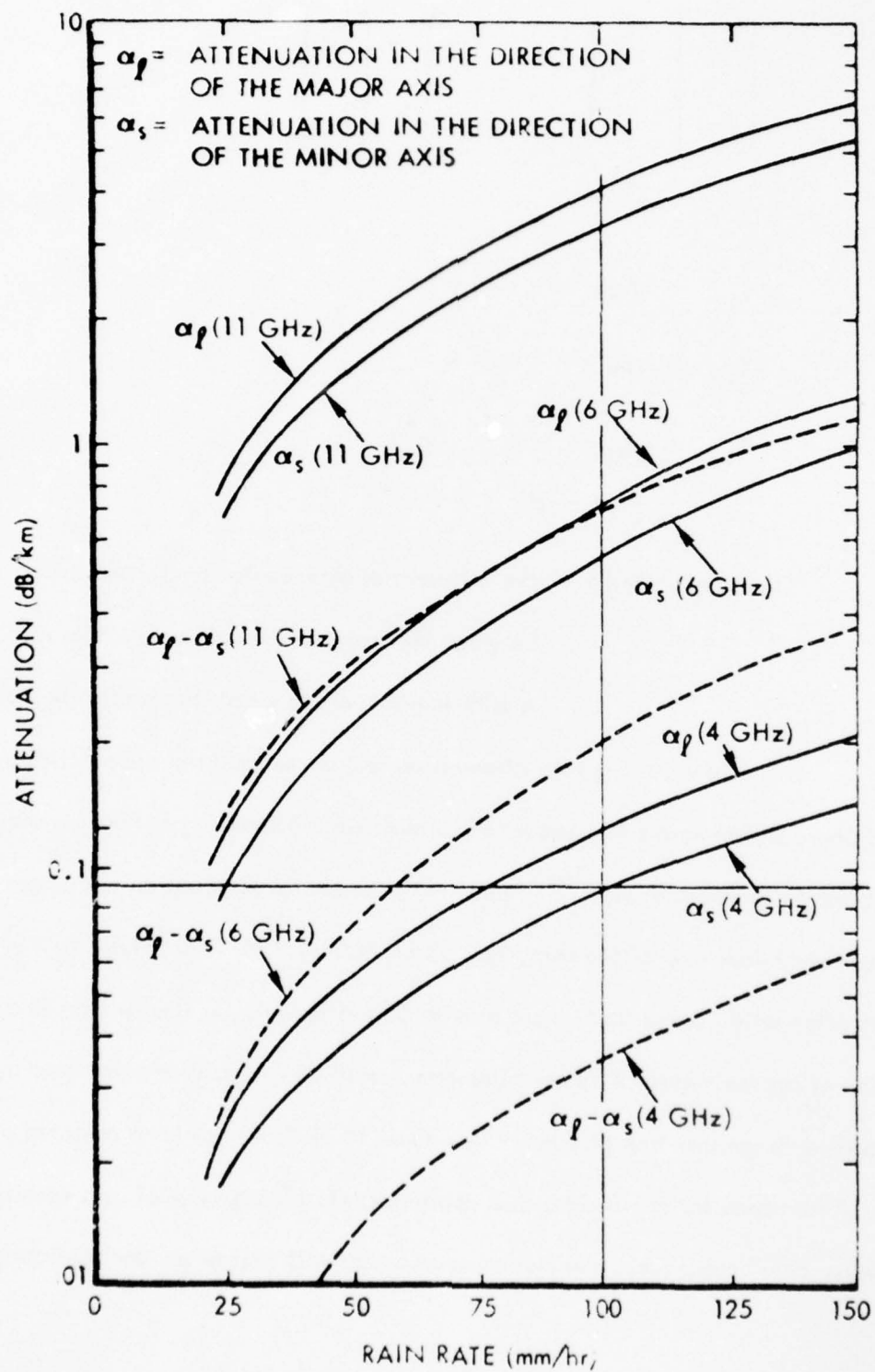
237

Figure E-1. Rain Attenuations. Average Path Length Through Rain ≈ 5 km

238
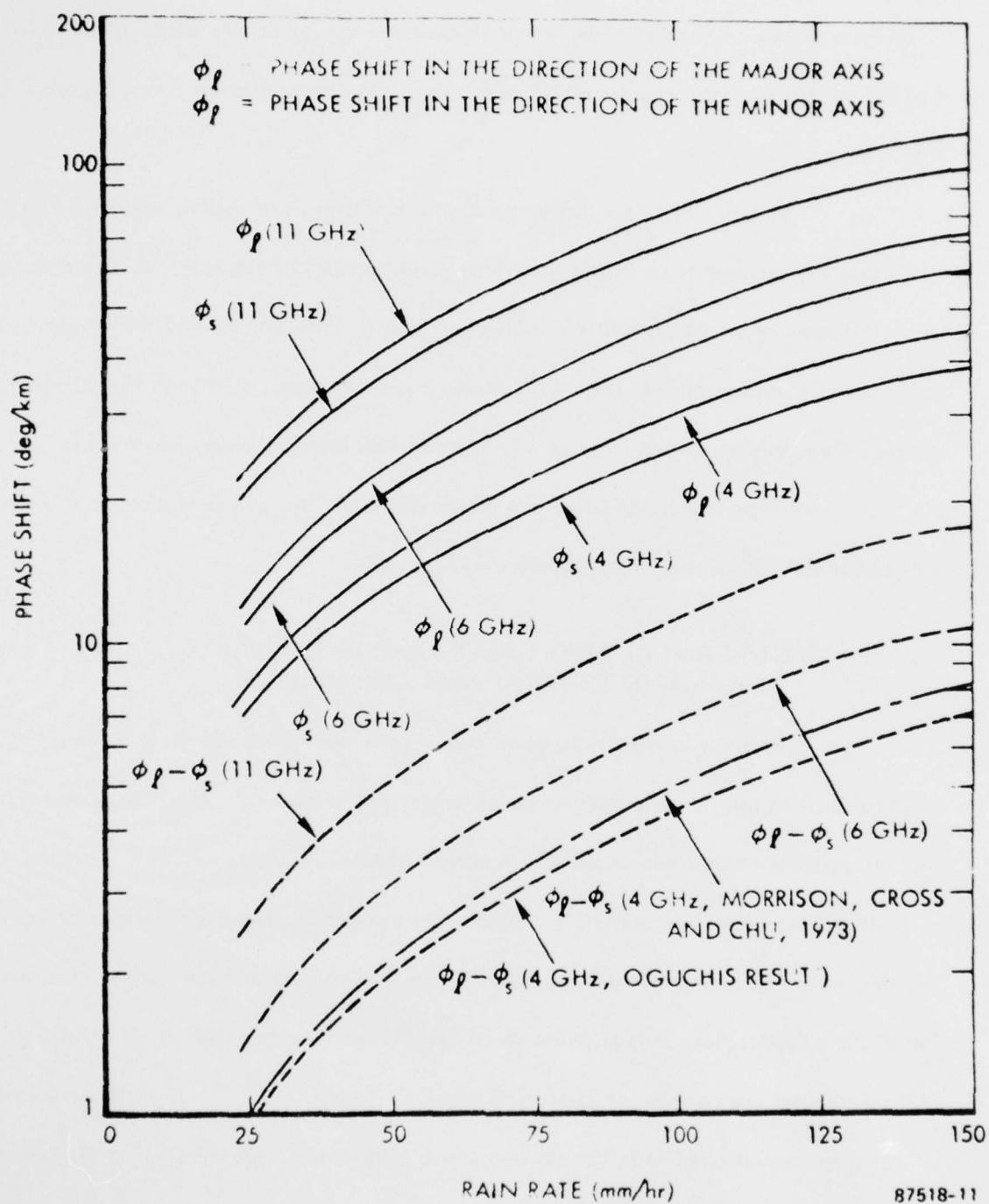
Figure E-2 Rain Phase Shift. Average Path Length Through Rain ~ 5 km

239

10 dB fade margin. Another older set of theoretical curves of rain attenuation[4] also show that 50 mm/hour of rain corresponds roughly to 10 dB attenuation in 5 km, Figure E-3. This is a very heavy rain.

In order to assess the frequency of occurrence of such a rainfall, Figure E-4 shows the number of hours per year of a given amount of rainfall. A 50 mm/hour rainfall occurs approximately 350 minutes per year in New Orleans at one extreme, or 6.5 minutes per year in Salt Lake City at the other extreme. Although the 50 mm/hour rainfall is roughly our worst-case on the basis of link margin, rain considerably less than this can cause cross-polarization at the 30-35 dB level; these rains and cross-polarizations will occur more frequently than the 50 mm/hour rains.

E-2. DIFFERENTIAL ATTENUATION AND PHASE SHIFT
NORMALIZED TO TOTAL RAIN ATTENUATION

In order to eliminate questions of how much path length is to be used, and what rainfall to use in computing cross-polarization, differential phase shift and differential attenuation can be expressed as a function of total rain attenuation. Thus the total rain attenuation can approximately measure the amount of rain present, and in addition the maximum allowable rain attenuation is usually specified as fade margin. For example, for 10 dB fade margins, it is possible to obtain the worst-case differential amplitude phase shifts expected from a rain. Figures E-5 and E-6 (from Chu[19b,7]) show the relationship of this differential amplitude (in dB) and phase (degrees), respectively, normalized to total attenuation, versus frequency. The various curves are for different rain amounts,

240

Figure E-3. Rain Attenuation vs Rainfall Rate (Theoretical, after Ryde and Ryde,
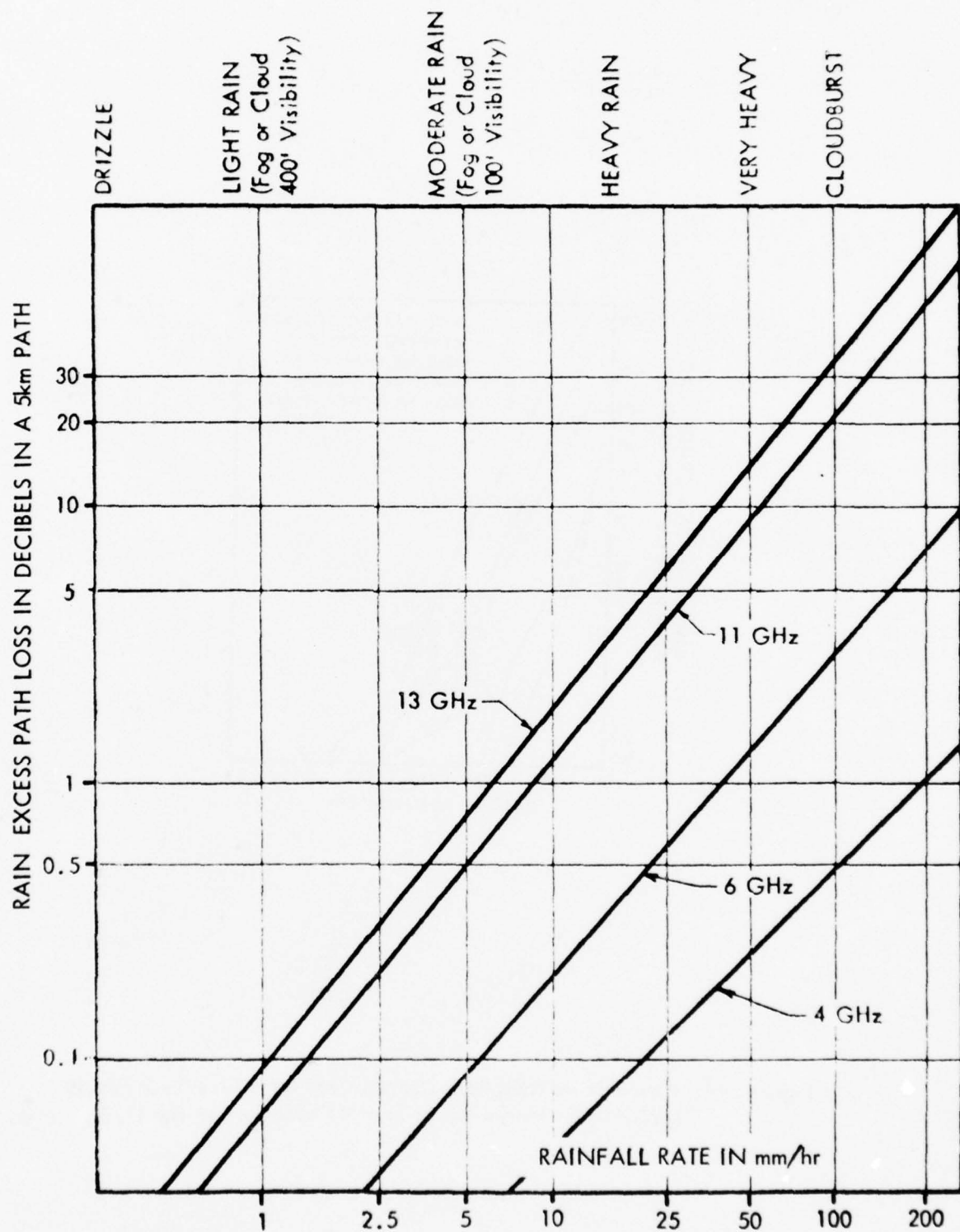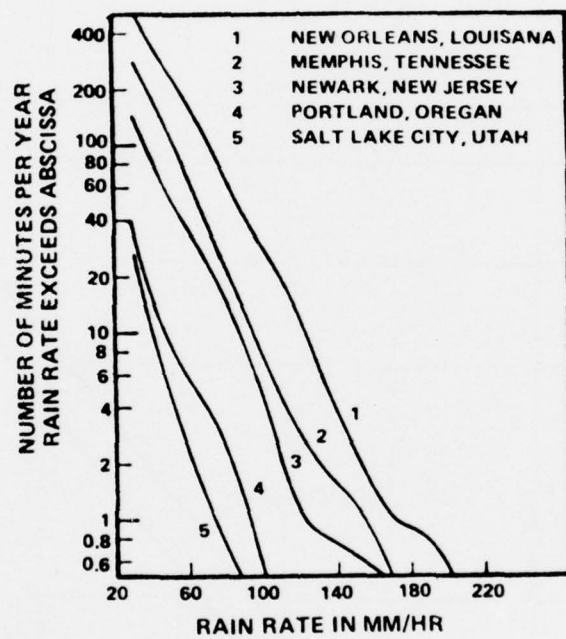
Figure E-4. One-minute Rain Rate Distributions for a Five Year Period (1966-1970) Measured at Several Locations in the U. S.

242
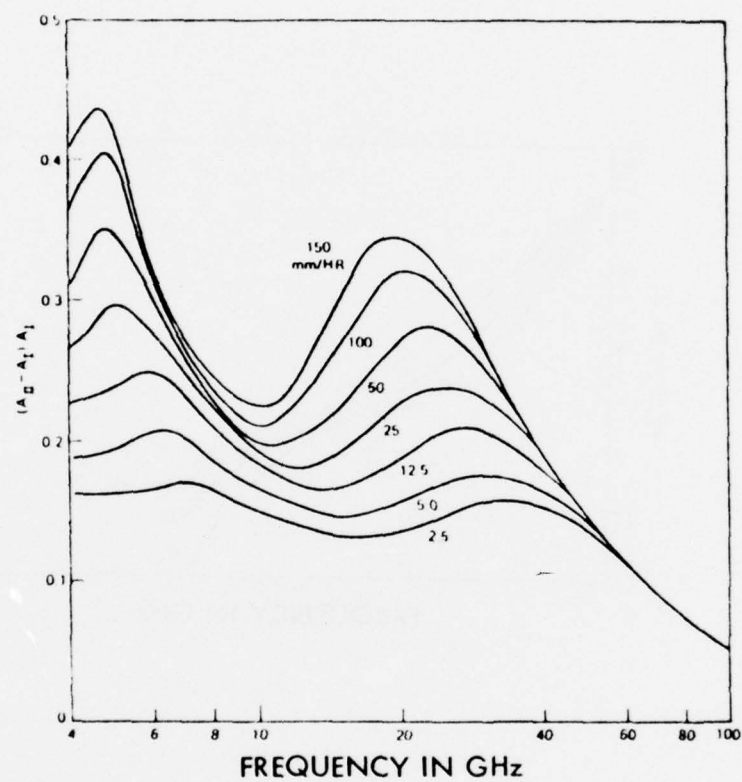
Figure E-5. Normalized Differential Attenuation with Respect to A_1

FREQUENCY IN GHz
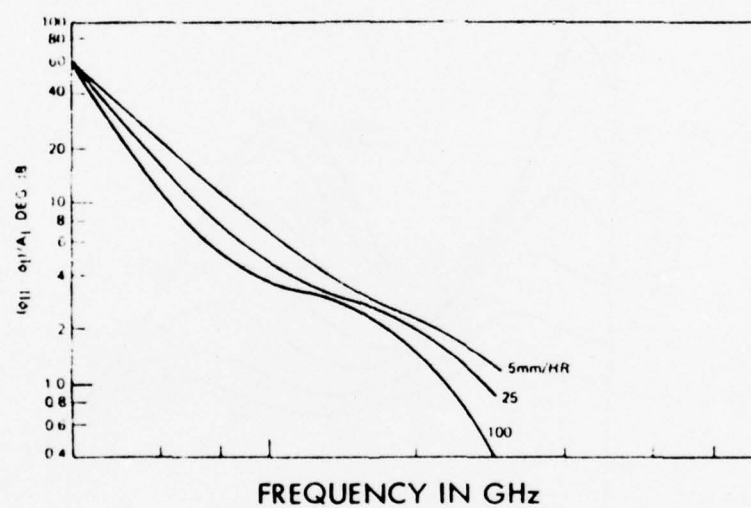
Figure E-6. Normalized Differential Phase Shift with Respect to A_l (4 to 30 GHz)

244

and the fact that they are close together shows that after normalization, the differential attenuation phase shifts are theoretically essentially independent of rainfall. At 11 GHz, and for the nominal 10 dB fade margin, the differential amplitude is found to be approximately 2 dB, and the differential phase shift is found to be approximately 30°. Other calculations have predicted somewhat less rain effects. The figures 1.5 dB and 25° have been used, respectively, to represent a 10 dB fade in the calculations of this appendix.

The absolute value of rain cant angle, θ, a measure of the average deviation of the raindrops from horizontal, can be evaluated from the rain data. The measured differential attenuation is compared with the theoretical formula available from the previous equations,

$$\left| \frac{\overline{T_{11}}}{\overline{T_{22}}} \right|^2 = \left| \frac{\gamma \cos^2 \theta + \sin^2 \theta}{\cos^2 \theta + \gamma \sin^2 \theta} \right|^2$$

in order to find the average θ. Note that T_{11} and T_{22} are independent of the sign of the cant angle, which allows the average absolute angle to be estimated from this data. Chu has found that the average absolute angle of the rain cant (a measure of deviation of the rain cant angle from horizontal) is approximately 25°. Others, using the rain cant angle to match measured cross-polarization, have used values of 15° for the rain cant angle.

RAIN CROSS POLARIZATION FOR LINEAR POLARIZATION

Even with the differential phase shift attenuation and rain cant angle, it is

still not possible to correctly compute the cross polarization of the rain for linear polariza-

tions. This is due to the fact that cross polarization due to large numbers of rain drops

having both positive and negative cant angles tend to cancel for linear incident polariza-

tion. This cancellation is due to the fact that the cross coupling term, $\sin^2 \theta$, is an odd

function, while the rain cant angles have a distribution of values between both positive

and negative cant angles. The factor ϵ has been introduced by Chu to account for the

average cant angle of the rain that actually causes cross polarization. This value of ϵ is

found from the measured rain cross polarization by the equation;

$$C_1 = \epsilon^2 \left| \frac{T_{12}}{T_{11}} \right|^2 \qquad (E-1)$$

Figure E-7 shows the calculations of the cross polarization versus rain attenuation for values

of $\epsilon = $ to 0.14 and 1.0. The curve for $\epsilon = 0.14$ is supported by considerable data,[19b,7]

but other rain data at 11 GHz as shown by the dark circles.[19a] It is clear that a range of

ϵ is required to match various rain data; i.e., that a given value of rain attenuation does

not imply a single value of polarization crosstalk. From the physical situation, polariza-

tion crosstalk can vary as the rain blows and tilts the given raindrops more or less with

respect to the horizontal axis. The value of $\epsilon \approx 1$ is used in this appendix for worst-case

calculations of the polarization decoupling networks.

Figure E-8 shows further theoretical curves for other frequencies,[19b] using

the value $\epsilon = 0.14$ in all the theoretical curves. Because of the small value of ϵ used,

7,19a,b (See Reference Listing after Appendix E)
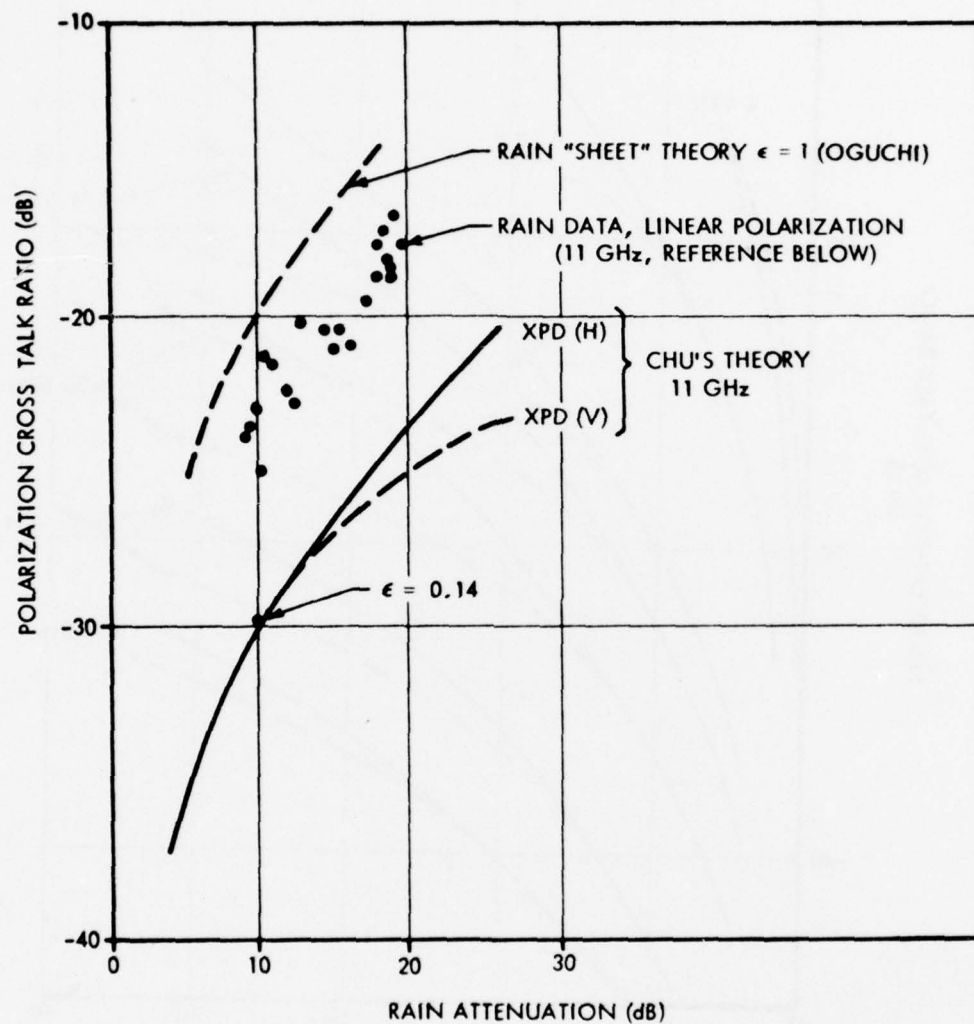
Figure E-7. Calculated vs Measured Cross Polarization
(Calculations and Data from Hogg and Chu)
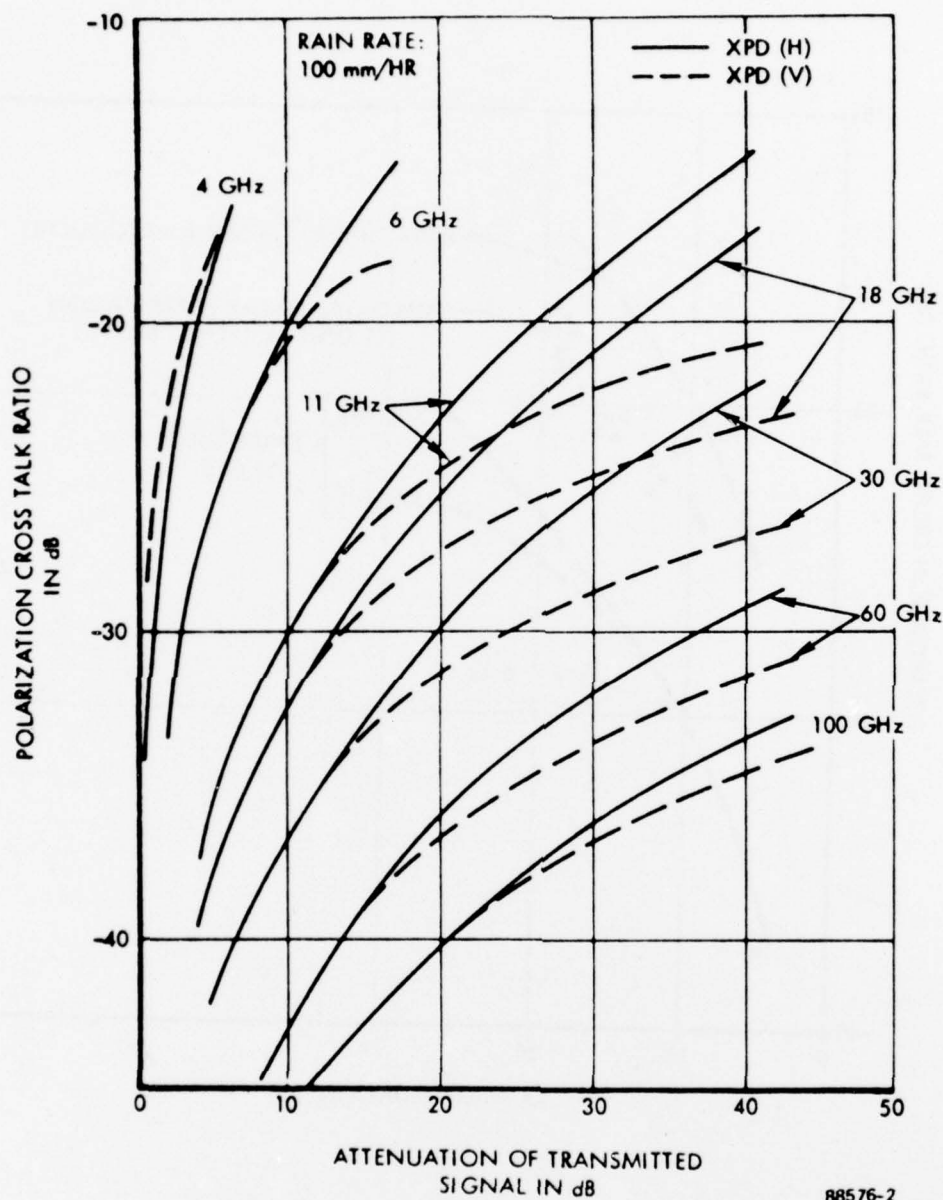
Figure E-8. Calculated Rain-Induced Cross Polarization of Horizontally and Vertically Polarized Waves. ε = 0.14, 5 km Link

248

these curves cannot be considered worst-case. For example, theoretical curves from Chu show that at 11 GHz, 10 dB path attenuation results in approximately 30 dB cross polarization, whereas data exists at −22 dB cross polarization.

The published rain curves show cross polarization, but do not give specific phase shifts of the horizontal and vertical components for use in simulations. Several specific rain cases were computed, as shown in Table E-1. In order to assure that calculations of the coupling network are essentially independent of specific rain model chosen, five rain cases were chosen, representing different cross polarizations, rain cant angles, and contributing rain fractions ϵ.

The first case is the worst possible case. Cases 2-4 are for smaller cant angles, where the total rain $\epsilon = 1$ is used in the calculation, and the rain cant angle determines the cross polarization. Case 3 is the nominal worst-case model to support the −22 dB worst-case rain data. Cases 5 and 6 use rain fractions, $\epsilon < 1$, with the 25° cant angle found by Chu. Case 7 indicates that for negative cant angles, the cross polarization phasor angles change by 180°. These cross polarization phasors are found from the formulas:

$$r_1 = T_{21}/T_{22}$$

$$r_2 = T_{12}/T_{11}$$

The value of the cross correlation, ρ, which measures the orthogonality of the polarizations, was then computed from the formulas in Appendix B. This orthogonality can be used, as in Appendix C, to compute "minimum loss" of correction circuits.

TABLE E-1 TYPICAL RAIN CASES

Rain Case No.	Cross Polarization			Differential Phase Shift ϕ	Cross Polarization Phasors		Correlation ρ
	Horizontal Channel (dB)	Vertical Channel (dB)	Cant Angle θ	Differential Attenuation (dB)	r_1 (amp/phase)	r_2	
1	12.5	12.5	45°	1.5	25°	$0.24/-112^\circ$	$0.24/-112^\circ$	0.17
2	14.4	15.3	23°	1.5	25°	$0.17/-120^\circ$	$0.19/-104^\circ$	0.13
3	21.3	22.5	10°	1.5	25°	$0.073/-123^\circ$	$0.086/-99.6^\circ$	0.059
4	27.0	28.5	5°	1.5	25°	$0.037/-123^\circ$	$0.044/-99^\circ$	0.030
5	24.8	24.6	25°	0.5	8°	$0.057/-115^\circ$	$0.059/-109^\circ$	0.043
6	28.5	28.5	45°	0.25	4°	$0.038/-112^\circ$	$0.038/-112^\circ$	0.028
7	12.5	12.5	-45°	1.5	25°	$0.24/68^\circ$	$0.24/68^\circ$	0.17

E-4.   CIRCULAR VERSUS LINEAR POLARIZATION

Using the equations in the previous sections, the cross polarization due to linear polarization may be compared with the cross polarization if circular polarization was used. In circular polarization, a rain cant angle of 45° is used to compute the cross polarization isolation. Note that this is the worst possible case for linear polarizations. Figure E-9 shows the calculation of cross polarization isolation, using the rain model with $\epsilon = 1$ rain cant angle $\theta = 15^{\circ}$ (similar to the rain Case 3).

The linear polarization is clearly better than circular polarization for all rain attenuations. This difference is sufficiently great so that there is little doubt that linear polarization is considerably superior to circular polarization for the 11 GHz frequency range and above. On the other hand, it is with much lower frequencies, such as 4 GHz, where Faraday rotation effects and increased phase shifts in the rain predominate, circular polarization may be superior, and is used by INTELSAT V and other 4-6 GHz satellites.

To provide quantitative examples of the cross polarization coupling effects of the transmission media comparing 4 and 11 GHz, and linear versus circular polarizations, two rain situations were hypothesized. The first case is a worst-case situation consisting of a cloudburst with a rain rate of 125 millimeters/hour. This rate of rain would be expected in an area such as New Jersey, 5 minutes/year. The second case is for a heavy rain with a rain rate of 25 millimeters/hour. This rate of rain would be expected to occur 1800 minutes/year. The quantitative results are tabulated in Table E-2.
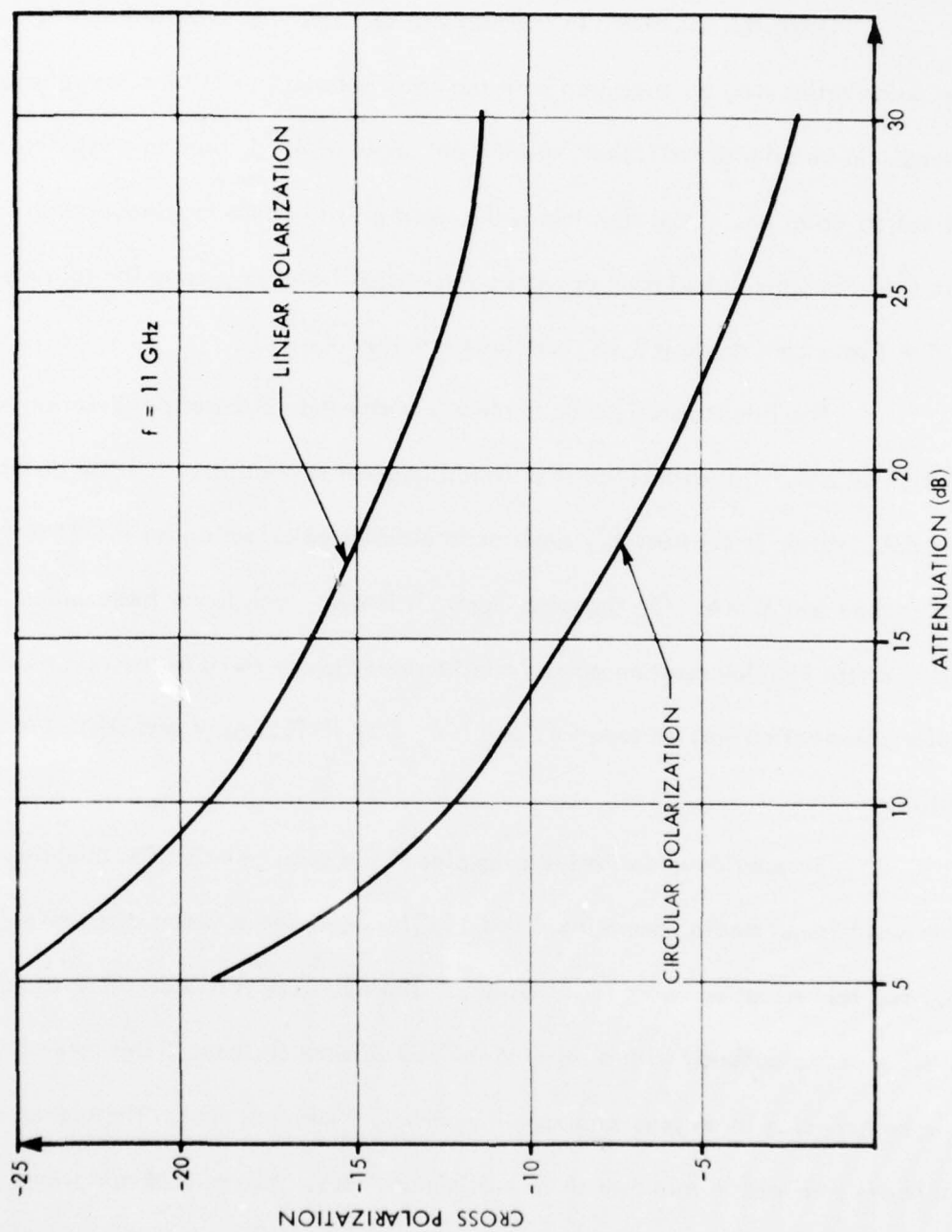
Figure E-9. Comparison of Rain Cross Polarization for Circular and Linear Polarization

TABLE E-2

Parameter	11 GHz Linear Polarization	11 GHz Circular Polarization	4 GHz Linear Polarization	4 GHz Circular Polarization
Worst-Case				
Cloudburst - Rain Rate 125 millimeters/hour 5 min/year 0.001% 5 kilometer path	-	-	-	-
Differential Attenuation	5 dB	5 dB	0.2 dB	0.2 dB
Differential Phase Shift	75°	75°	32.5°	32.5°
Polarization Coupling	-15 dB	-5 dB	-22 dB	-12 dB
Link Excess Attenuation	31 dB	31 dB	0.75 dB	0.75 dB
Normal Case				
Heavy Rain - Rain Rate 25 millimeters/hour 1800 min/year 0.36% 5 kilometer path				
Differential Attenuation	0.6 dB	0.6 dB	-	-
Differential Phase Shift	11.5°	11.5°	5°	5°
Polarization Coupling	-28 dB	-18 dB	-20 dB*	-28 dB
Link Excess Attenuation	4.5 dB	4.5 dB	0.13 dB	0.13 dB
Rate of Change	<5 Hz	<5 Hz	<5 Hz	<5 Hz
Variation with Frequency (10% bandwidth)	±0.5 dB	±0.5 dB	±0.5 dB	±0.5 dB

*Faraday rotation at noon

E-5.   EFFECT OF DIFFERENTIAL PHASE VERSUS ATTENUATION ON THE
            CROSS POLARIZATION TO CIRCULAR POLARIZATIONS

Although the previous rain models included both differential phase shift and

differential attenuation together, as actually occurs, the cross polarization due to either

the attenuation or phase shift can be computed separately. Figure E-10 shows the results

of such a calculation for circularly polarized incident signals.[6] The main use of these

calculations is to show that phase shift is the predominant cross polarization effect at all

frequencies shown, although differential attenuation can cause -22 dB cross polarization

with 50 mm/hour rain rate at 11 GHz (for circular polarization). This is the nonorthogon-

ality portion of the cross polarization. Therefore, phase shift networks alone can correct

rain cross polarization at 4 and 6 GHz, but not at 11 GHz, if -30 dB crosstalk minimum

is required.

For linear polarization, cross polarization is approximately 7 dB less, as

shown in Table E-2, so that differential attenuation will cause approximately -29 dB cross

polarization that will have to be corrected by an orthogonalization network, not by phase
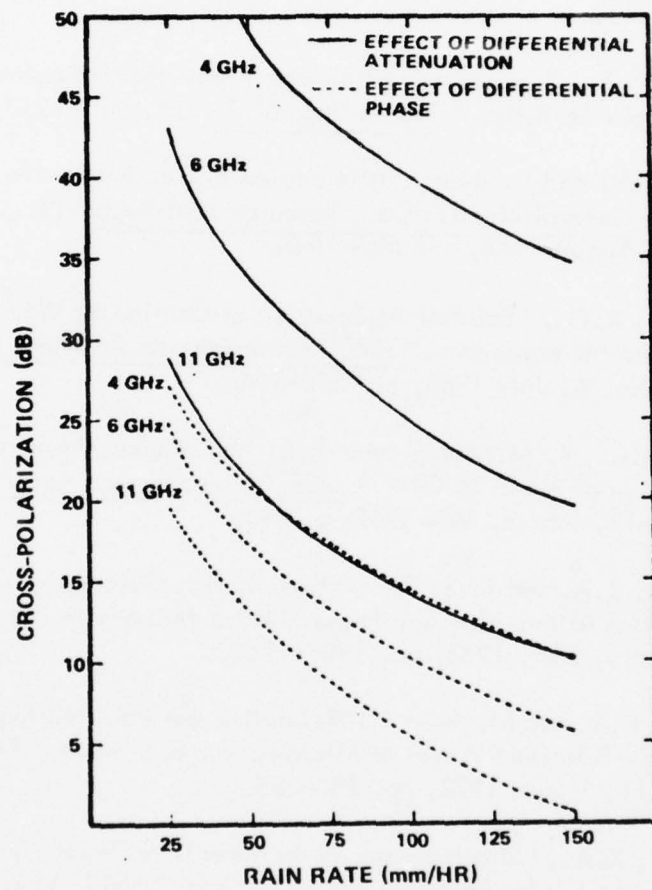
shift.

Figure E-10. Cross Polarization Isolation for Circular Polarizations vs Rain Rate for 5 km Path Lengths

REFERENCES

1. Norberry, J. R. and W. J. K. White, "Point Rainfall Rate Measurements at Slough, U. K.," IEEE Conference Publication No. 98.

2. Hogg, D.C., "Path Diversity in Propagation of Millimeter Waves Through Rain," IEEE Transactions on Antennas and Propagation, Vol. AP-15, No. 3, May 1967, pp. 410-415.

3. Bussey, H. E., "Microwave Attenuation Statistics Estimated from Rainfall and Water Vapor Statistics," Proceedings of the IRE, July 1950, pp. 781-785.

4. Ryde, J. W. and D. Ryde, "Attenuation of Centimeter Waves by Rain, Hail and Clouds," General Electric Co., Research Labs Report No. 8516, 8670, Wembley, England, August 1944, and May 1945.

5. Medhurst, R.G., "Rainfall Attenuation of Centimeter Waves: Comparison of Theory and Measurements," IEEE Transactions on Antennas and Propagation, Vol. AP-13, No. 4, July 1965, pp. 550-564.

6. Blevis, B.C., R. M. Dohoo and K. S. McCormick, "Measurements of Rainfall Attenuation at 8 and 15 GHz," IEEE Transactions on Antennas and Propagation, Vol. AP-15, No. 3, May 1967, p. 394.

7. Morrison, J.A. and T. S. Chu, "Perturbation Calculations of Rain-Induced Differential Attenuation and Phase Shift at Microwave Frequencies," BSTJ, Vol. 52, No. 10, Dec. 1973, pp. 1907-1913.

8. Watson, P.A. and M. Arbabi, "Rainfall Cross-Polarization of Linearly and Circularly Polarized Waves at Microwave Frequencies," Electronic Letters, Vol. 8, No. 11, 1 June 1972, pp. 283-385.

9. Semplak, R.A., "Simultaneous Measurements of Depolarization by Rain Using Linear and Circular Polarizations at 18 GHz," BSTJ, Vol. 53, No. 2, Feb. 1974, pp. 400-404.

10. Prabhu, V. K., "Error Rate Considerations for Coherent Phase-Shift Keyed Systems with Co-Channel Interference," BSTJ, March 1969, pp. 743-767.

11. Barnett, W.T., "Deterioration of Cross Polarization Discrimination During Rain and Multipath Fading at 4 GHz," Proceedings ICC, 1974, pp. 12D-1 to 12D-4.

12. Rassweiler, et. al., "Adaptive Polarization Separation Experiments," Final Report, NASA AAFE Contract NAS 1-13942, Harris ESD, Melbourne, Fla., Aug. 1976.

13. Papoulis, A., "Probability Random Variables and Stochastic Processes," McGraw-Hill, N. Y., 1965.

14. Davenport, W. B. and W. L. Root, "An Introduction to the Theory of Random Signals and Noise," McGraw-Hill, N. Y., 1958, pp. 256-257.

15. Chu, T. S., "Restoring the Orthogonality of Two Polarizations in Radio Communication Systems," Part I, BSTJ, Vol. 50, No. 9, Nov. 1971, pp. 3063-3069; Part II, BSTJ, Vol. 52, No. 3., March 1973, pp. 319-327.

16. a. DiFonzo, D., A. Williams, and W. Trachtman, "Adaptive Polarization Control for Satellite Frequency Reuse Systems," Internal Memo, COMSAT Laboratories, Clarksburg, Maryland, 1976.

    b. DiFonzo, D. and R. W. Kreutel, IEEE G-AP Symposium, 1971.

    c. DiFonzo, D., "Adaptive Antennas for Polarization Isolation in Frequency Reuse Systems," COMSAT Memorandum, TCLT/71-2085, July 15, 1971.'

    d. DiFonzo, D., "Interference Reduction Circuit," COMSAT Memorandum, TCLT/72-2018, March 2, 1972.

    e. Taur, R. R., "Rain Depolarization at 4, 6 and 11 GHz," COMSAT Technical Memo, CL-40-73, also COMSAT Technical Review, Vol. 4, No. 1., Spring 1974, pp. 187-190.

17. "System for Interference Signal Nulling by Polarization Adjustment," U. S. Patent 3,883,872 (to NASA), May 13, 1975.

18. a. Lu, H. S., "Polarization Separation by an Adaptive Filter," IEEE Transactions on Aerospace and Electronic Systems, Vol. 8, No. 6, pp. 954-956.

    b. Marshall, R. E. and C. W. Bostian, "An Adaptive Polarization Correction Scheme Using Circular Polarization," 1974, International IEEE/AP-S Symposium Digest, pp. 392-394.

19. a. Hogg, D. C. and T. S. Chu, "The Role of Rain in Satellite Communications," Proc. IEEE, Vol. 63, No. 9, September 1975, pp. 1308-1331.

    b.   Chu, T. S., "Rain-Induced Cross Polarization at Centimeter and Millimeter Wavelengths," BSTJ, Vol. 50, No. 8, Oct. 1974, pp. 1557-1579.

20.   Oguchi, T., "Attenuation of Electromagnetic Waves due to Rain with Distorted Raindrops," J. Radio Research Labs (Tokyo), Part 1 in Vol. 7 pp. 467-485, Sept. 1960; Part 2 in Vol. II, pp. 19-44, Jan. 1964; also Radio Science, Jan. 1973, pp. 31-38.

21.   Ryde, J. W. and D. Ryde, "Attenuation of Centimeter Waves by Rain, Hail, and Clouds," General Electric Co., Research Labs Report No. 8516, 8670, Wembley, England, August 1944, and May 1945.

22.   a.   Watson, P. A. and S. I. Ghobrial, "Cross Polarizing Effects of a Water Film on a Parabolic Reflector at Microwave Frequencies," IEEE Transactions on Antennas and Propagation, Vol. AP-20, No. 5., Sept. 1972, pp. 668-671.

    b.   Blevis, B. C., "Rain Effects on Radomes and Antenna Reflectors, "Proceedings IEEE Conference on Large Steerable Aerials (London), pp. 148-152.

23.   Watson, P. A., "Attenuation and Cross Polarization Measurements at 11 GHz," IEEE Transactions on Communications, Vol. COM-21, No. 4, April 1973, pp. 325-331.

24.   Watson, P. A., et al., "Mutual Interference Between Linear Cross-Polarized Radio Channels at 11 GHz," Electronic Letters, Vol. 7, No. 13, July 1971, pp. 375-376.

25.   Thomas, David T., "Cross Polarization Distortion in Microwave Radio Transmission Due to Rain," Radio Science, Vol. 6, No. 10, Oct. 1971, pp. 833-839.

26.   Saunders, Morton J., "Cross Polarization at 18 and 30 GHz Due to Rain," IEEE Transactions on Antennas and Propagation, Vol. AP-19, No. 2, March 1971, pp. 273-277.

27.   Lake, H. and J. F. Roche, "Reliability of an 11 GHz Communication System in a Tropical Environment," Telecommunications, Jan. 1969, pp. 15-19.

28.   Semplak, R. A., "The Effect of Rain on Circular Polarization at 18 GHz," BSTJ, Vol. 52, No. 6, July-Aug. 1973, pp. 1029-1030.

29.   Lin, S. H., "Statistical Behavior of Rain Attenuation," BSTJ, Vol. 52, No. 4 April 1973, pp. 557-581.

30. Barnett, W. T., "Multipath Propagation at 4, 6 and 11 GHz," BSTJ, Vol. 51, No. 2, Feb. 1972, pp. 321-360.

31. Babler, G. M., "A Study of Frequency Selected Fading for a Microwave Line-of-Sight Narrowband Radio Channel," BSTJ, Vol. 51, No. 3, March 1972, pp. 731-757.

32. Babler, G. M. "Selectively Faded Non-Diversity and Space Diversity Narrowband Microwave Radio Channels," BSTJ, Vol. 52, No. 2, Feb. 1973, pp. 239-261.

33. Subramanian, M., et al., "Phase Dispersion Characteristics During Fades in a Microwave Line-of-Site Radio Channel," BSTJ, Vol. 52, No. 10, Dec. 1973, pp. 1877-1902.

34. Barnett, W. T., "Microwave Line-of-Site Propagation With and Without Frequency Diversity," BSTJ, Vol. 49, No. 8, May 1970, pp. 1827-

35. Lin, S. H., "An Occurrence of Very Heavy Rain on a 42 Km Path," IEEE Transactions on Communications, Vol. 53, No. 5, May 1974, pp. 708-710.

36. Gill, W. and J. Byrne "2 GHz Digital Microwave Cross-Polarization Propagation Measurements," Telecommunications, June 1974, pp. 45-48.

37. Osborne, T. L., "Rain Outage Performance of Tandem and Path Diversity 18-GHz Short Hop Radio Systems," BSTJ, Vol. 50, No. 1, Jan. 1971, pp. 59-79.

38. Semplak, R. A., "Dual Frequency Measurements of Rain-Induced Microwave Attenuation on a 2.6 Kilometer Propagation Path," BSTJ, Vol. 50, No. 8, Oct. 1971, pp. 2599-2606.

39. Tillotson, L. C., "Use of Frequencies Above 10 GHz for Common Carrier Applications," BSTJ, Vol. 48, Nov. 6, July-Aug. 1969, pp. 1563-1576.

40. Lin, S. H., "Statistical Behavior of a Fading Signal," BSTJ, Vol. 50, No. 10, Dec. 1971, pp. 3211-3270.

41. Vigants, A., "Number and Duration of Fades at 6 and 4 GHz," BSTJ, Vol. 50, No. 3, March 1971, pp. 815-841.

42. Wulfsberg, Karl N. and E. E. Altschuler, "Rain Attenuation at 15 and 35 GHz," IEEE Transactions on Antennas and Propagation, Vol. AP-20, No. 2, March 1972, pp. 181-187.

43.	Stronhbehn, J. W. and S. F. Clifford, "Polarization and Angle-of-Arrival Fluctuations for a Plane Wave Propagated Through a Turbulent Media," IEEE Transactions on Antennas and Propagation, Vol. AP-15, No. 3, May 1967, pp. 416-421.

44.	Watson, P. A. and M. Arbabi, "Rainfall Cross Polarization at Microwave Frequencies," Proceedings IEEE (U.K.), Vol. 120, No. 4, April 1973, pp. 413-418.

45.	"Fluctuation of Cross Polarization Discrimination Ratio Due to Fading," Review of the Electrical Communications Laboratories, Vol. 19, No. 5-6, May-June 1971.

MISSION
of
Rome Air Development Center

RADC plans and conducts research, exploratory and advanced development programs in command, control, and communications (C^3) activities, and in the C^3 areas of information sciences and intelligence. The principal technical mission areas are communications, electromagnetic guidance and control, surveillance of ground and aerospace objects, intelligence data collection and handling, information system technology, ionospheric propagation, solid state sciences, microwave physics and electronic reliability, maintainability and compatibility.

AMERICAN REVOLUTION BICENTENNIAL
1776-1976